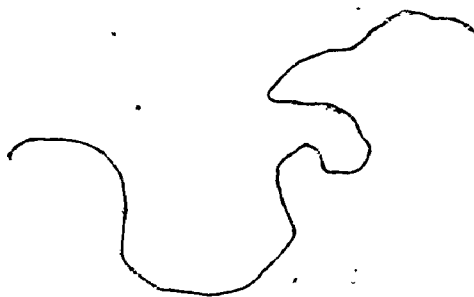


OXYGEN AND SULPHUR ISOTOPE GEOCHEMISTRY  
OF MARINE EVAPORITES



OXYGEN AND SULPHUR ISOTOPE GEOCHEMISTRY  
OF MARINE EVAPORITES

By

ERIC ROBERT OLSON, B.Sc. Eng.

A Thesis

Submitted to the School of Graduate Studies  
in Partial Fulfilment of the Requirements

for the Degree

Doctor of Philosophy

McMaster University

November, 1975



ERIC ROBERT OLSON 1977

DOCTOR OF PHILOSOPHY (1975)  
(Geology)

McMASTER UNIVERSITY  
Hamilton, Ontario.

TITLE: Oxygen and Sulphur Isotope Geochemistry  
of Marine Evaporites.

AUTHOR: ERIC ROBERT OLSON, B. Sc. Eng.  
(University of Saskatchewan)

SUPERVISOR: PROFESSOR H. P. SCHWARCZ

NUMBER OF PAGES: xviii, 254

## ABSTRACT

The variation in the ratio of oxygen isotopes in natural sulphate differs fundamentally from that of sulphur because it is linked to several geochemical cycles in addition to the sulphur cycle. Published results indicate that dissolved sulphate and water do not exchange oxygen isotopes to any measurable extent at low temperatures and near-neutral pH. In sulphate reduction however, the intermediate sulphite rapidly exchanges oxygen with water. Appreciable back oxidation of the intermediate sulphite confirms Rees' steady state model for bacterial sulphate reduction. Analogous indirect exchange with water may be effected by the cycling of sulphur by phytoplankton; crude calculations show that the flux of sulphur in the biomass may quantitatively dominate the processes that determine the oxygen  $\delta$  value of seawater sulphate.

The present formation of gypsum and anhydrite on the sabkhas of the Persian Gulf has led to several reinterpretations of the depositional environments of ancient evaporites. Sulphur and oxygen isotope analyses of the evaporite minerals and the interstitial brines from the Abu Dhabi sabkha strongly confirm Patterson's distinction between the seaward, mixed, and landward hydrological regimes. Isotopic equilibrium between

gypsum and dissolved sulphate with considerable exchange between early-formed gypsum and subsequent interstitial brines is demonstrated for the seaward zone. Bacterial reduction is significant in the mixed or central zone where little new deposition is occurring. The influx of continental brines in the landward zone is causing a marked shift to lighter sulphur  $\delta$  values. Gypsum-anhydrite transitions do not involve large isotope fractionations. The seaward and central zones constitute an analogue for shallow or subaerial evaporite mineral deposition and it is likely that a substantial range of variation would prevail on the much larger scale of ancient evaporites.

Isotopic studies on ancient evaporites have established that the sulphur  $\delta$  value of seawater sulphate has varied more than twenty per mille in the Phanerozoic. The narrow range of individual anhydrite beds like the Midale Evaporite that are considered to have a sabkha origin may be due to postdepositional homogenization. The very large range of sulphur  $\delta$  values, and to a lesser extent, oxygen  $\delta$  values of the Salina Formation is consistent with a sabkha origin on the flanks of the depositional basin. Two near surface gypsum mines in the Salina B Anhydrite had constant  $\delta$  values on a scale of hundreds of metres. Permian evaporites from geographically separate locations fall within a narrow range and coincidentally have the lightest sulphur and oxygen  $\delta$  values of any geological period. The sulphur isotope analyses reported here conform to the Phanerozoic pattern, and display comparable fluctuations in

the Precambrian. It is suggested that the noise on the curve may be primary depositional information. The oxygen isotope analyses do not support suggestions of significant variations over geological time, and limit the possible range of variation to less than three per mille.

Experiments on the exchange between gypsum crystals and dissolved sulphate have established an equilibrium isotope fractionation of about 3.5 per mille. Lower values found elsewhere are considered to be a kinetic isotope effect.

## ACKNOWLEDGEMENTS

I want to gratefully acknowledge here that I received considerable generous support and encouragement throughout this project from many individuals of whom only some are mentioned in the following.

Dr. H. P. Schwarcz suggested the project, advised on its analytical aspect, and thoughtfully criticized early versions of the manuscript. I thank him for supervising my progress from a total novice in isotope geochemistry.

Dr. H. G. Thode and Dr. J. R. Kramer, on my Ph. D. supervisory committee, made helpful suggestions for the analytical and experimental work, and in the interpretation of the data.

Mrs. J. Gleed taught me many of the laboratory procedures and Mrs. L. Binney carefully performed many of the isotopic analyses reported here.

Dr. C. E. Rees read early versions of the manuscript and discussions with him, particularly about process models, greatly improved the manuscript. Mr. J. Monster kindly provided me with samples and some sulphur isotope analyses. Mr. F. J. Longstaffe helped me to clarify several portions of the manuscript.

Dr. D. J. J. Kinsman and Dr. R. J. Patterson provided a suite

of evaporite minerals and interstitial brines from the sabkha at Abu Dhabi.

Core samples were obtained from the Ontario Ministry of Natural Resources Petroleum Resources Section Sample Repository at London, and visits and sampling were arranged by the Canadian Gypsum Company Mine at Hagersville, and the Domtar Construction Materials Limited Mine at Caledonia.

Mrs. L. Falkiner typed the manuscript with its author on the other side of the continent, and I thank her for avoiding many potential delays in its completion.

I especially want to thank Lindy and Amy Olson who patiently and supportively endured the long hours it took to complete this task - I dedicate this thesis to them.



## TABLE OF CONTENTS

	Page
INTRODUCTION	1
General	1
Marine Evaporites	2
Stable Isotopes	7
Research Goals	14
THE SULPHUR ISOTOPE GEOCHEMISTRY OF SULPHATE	17
Marine Evaporite Sulphur Isotope Geochemistry	25
THE OXYGEN ISOTOPE GEOCHEMISTRY OF SULPHATE	34
Marine Evaporite Oxygen Isotope Geochemistry	43
THE STABLE ISOTOPE GEOCHEMISTRY OF SALINE WATERS	48
Evaporite Processes	49
Hydration Water	52
GENERAL ANALYTICAL PROCEDURES	53
Mass Spectrometry	53
Sulphate Extraction on Anion Exchange Resin	53
Graphite Reduction of Barium Sulphate	55
Conversion from Barium to Sulphide to Silver Sulphide	60
Oxidation of the Silver Sulphide with Cupric Oxide	60
Water-Carbon Dioxide Exchange	63
THE SABKHA AT ABU DHABI	67
Introduction	67
The Persian Gulf	67
Abu Dhabi	69
Water Chemistry	79
Dolomite and Gypsum Formation	80
Gypsum-Anhydrite Equilibrium	85

	Page
STABLE ISOTOPE STUDIES, ABU DHABI SABKHA	89
Introduction	89
Crystallization	89
Gypsum-Anhydrite Transitions	90
Sulphate Reduction	90
Mixing	93
Evaporation	93
Secular Variation in Seawater	93
Summary of Possible Sabkha Processes	94
Samples	94
Isotopic Analyses of Dissolved Sulphate and Water	98
Isotopic Analyses of Evaporite Minerals	114
The Seaward Zone	129
The Landward Zone	131
The Mixed or Central Zone	133
Comparison with Butler <i>et al</i> (1973)	134
Application to Ancient Evaporites	137
Summary	139
STABLE ISOTOPE STUDIES, SOME ANCIENT EVAPORITES	143
Introduction	143
Models of Isotope Variation	145
The Midale Evaporite	149
Salina Formation	152
Permian Evaporites	165
Selected Other Evaporites	179
Genetic Significance of the Data	179
Secular Variation	185
CONCLUSIONS	224
Abu Dhabi Sabkha	224
Ancient Evaporites	225
Future Work	226
REFERENCES	227
APPENDIX	241
Exchange Experiments	241
Labelled Gypsum	251

## LIST OF TABLES

Table		Page
1-1	Salts laid down in Concentration of Seawater (Data of Usiglio, from Stewart, 1963)	3
2-1	Some Intermediate Steps in the Bacterial Reduction of Sulphate (from Kemp and Thode, 1968)	21
2-2	The Variable Rate of Change of $\delta^{34}\text{S}$ of Seawater Sulphate	31
3-1	The Flux of Sulphur in the Biomass	44
3-2	Literature values of Marine Evaporite Sulphate $\delta^{18}\text{O}$	46
5-1	Sulphate Oxygen Isotope Precision ( $2\sigma$ )	59
5-2	Sulphate Sulphur Isotope Precision ( $2\sigma$ , for an individual determination)	62
5-3	Brine Oxygen Isotope Precision ( $2\sigma$ , for single determination)	66
6-1	The Climate and Physiography of the Persian Gulf (from Purser and Seibold, 1973)	70
6-2	Stratigraphy of Sabkha Sediments Abu Dhabi (from Patterson, 1972)	74
6-3	Summary of Sabkha Evaporite Facies from Butler (1970)	78
6-4	Properties of the Dolomitizing Fluids (from Patterson, 1972)	84
7-1	Isotope Composition of Product (P) and Substrate (S) at Various extents of reaction for Constant Fractionation	91

Table		Page
7-2	Mechanisms that effect Isotope Shifts in the Sabkha Evaporite System	95
7-3	Isotopic Measurements, Density and Sulphate Concentration of Abu Dhabi Brines	99
7-4	Isotopic Determinations, Insoluble Content and Sulphate Content of Abu Dhabi Sediment Samples	103
7-5	Mean Isotopic Values for Abu Dhabi Brines grouped according to $m_{K^+}/m_{Br^-}$	109
7-6	Linear Correlation Coefficients within Groups for Abu Dhabi Brines	115
7-7	Mean Isotopic Values for Abu Dhabi Evaporite Minerals grouped according to $m_{K^+}/m_{Br^-}$ of associated brines	119
7-8	Linear Correlation Coefficients within groups for Abu Dhabi Evaporite Minerals	121
7-9	Isotopic Shifts that accompany Gypsum to Anhydrite and Anhydrite to Gypsum Transitions ( $\Delta_{G-A} = \delta_G - \delta_A$ )	123
8-1	Stratigraphy of the Salina Rocks (from Alling and Briggs, 1961)	159
8-2	The Zechstein Salt Sequence (from Braitsch, 1971)	176
8-3	Isotopic Analyses of the Mississippian Midale Evaporite	189
8-4	Isotopic Analyses of Upper Silurian Salina Rocks	194

Table		Page
8-5	Isotopic Analyses of some Permian Evaporites	210
8-6	Isotopic Analyses of Selected Other Evaporites	216
9-1	Isotopic Data on Saturated Solutions of Calcium Sulphate	244
9-2	<sup>18</sup> O-Labelled Gypsum via Sulphide/Water Exchange	253

## LIST OF FIGURES

Figure		Page
1-1	Salt Profiles (from Borchert and Muir, 1964)	4
1-2	Equilibrium Exchange Experiments	11
1-3	Rayleigh-type Kinetic Isotope Fractionation	13
2-1	Isotopic Geochemistry of Sulphur (from Holser and Kaplan, 1966)	18
2-2	Sulphate Reduction Rate Plot (from Kemp and Thode, 1968)	22
2-3	Reaction Scheme for <u>Desulfovibrio desulfuricans</u> (from Rees, 1973)	24
2-4	Sulphur Del Values versus Geological Time for Seawater Sulphate (from Thode and Monster, 1965)	27
2-5	Sulphur Del Values versus Geological Time for Seawater Sulphate (from Holser and Kaplan, 1966)	28
3-1	Steady State Model for Oxygen Del Value of Seawater Sulphate (from Lloyd, 1968)	40
3-2	Concentration and Oxygen Del Values of Sulphate dissolved in Interstitial Waters (from Lloyd, 1973)	42
3-3	Literature Values of Oxygen Del Values of Marine Evaporite Sulphate versus Geological Time	47

Table		Page
4-1	Oxygen Del Values of Water versus Salinity (from Lloyd, 1966)	50
5-1	Flow Scheme for Combined Oxygen and Sulphur Isotope Analysis of Sulphate	54
5-2	Successive Barium Sulphate Reduction by the Transmitted Light Method Testing Isotopic "Memory" in the Product Carbon Dioxide.	57
5-3	Flow Scheme for Oxygen Isotope Analysis of Brine	64
6-1	The Location of the Persian Gulf and Abu Dhabi	68
6-2	Sediment Distribution in the Persian Gulf (from Wagner and van der Togt, 1973)	71
6-3	Abu Dhabi Sabkha Sediment Profile (from Patterson, 1973)	73
6-4	Vertical Distribution of Sabkha Sedimentary Facies (from Butler, 1970)	75
6-5	Areal Distribution of Sabkha Sedimentary Facies (from Butler, 1970)	77
6-6	Areal Distribution of $m_{K^+}/m_{Br^-}$ - ratios of Abu Dhabi Brines (from Patterson, 1973)	81
6-7	General Hydrologic Framework of Sabkha (from Patterson, 1973)	82
6-8	Equilibrium Phase Relations for Gypsum and Anhydrite (from Kinsman, 1966)	88
7-1	Isotope Composition for Product (P) and Substrate (S) at various extents of reaction for $\alpha = 0.996$	92

Table		Page
7-2	Abu Dhabi Sample Stations (from Patterson, 1973)	97
7-3	Oxygen Del Values versus Concentration for Sulphate Dissolved in Abu Dhabi Brines	110
7-4	Sulphur Del Values versus Concentration for Sulphate Dissolved in Abu Dhabi Brines	111
7-5	Sulphur Del Values versus Oxygen Del Values for Sulphate Dissolved in Abu Dhabi Brines	112
7-6	Oxygen Del Values of Water versus Oxygen Del Values for Sulphate Dissolved in Abu Dhabi Brines	113
7-7	Areal Distribution of Oxygen Del Values of Water in Abu Dhabi Brines	116
7-8	Areal Distribution of Oxygen Del Values of Sulphate Dissolved in Abu Dhabi Brines	117
7-9	Areal Distribution of Sulphur Del Values of Sulphate Dissolved in Abu Dhabi Brines	118
7-10	Sulphur Del Values versus Oxygen Del Values for Abu Dhabi Evaporite Minerals	120
7-11	Areal Distribution of Oxygen Del Values for Abu Dhabi Evaporite Minerals	124
7-12	Areal Distribution of Sulphur Del Values for Abu Dhabi Evaporite Minerals	125
7-13	Sulphur Del Values versus Oxygen Del Values for Sulphate Dissolved in Brines and for Evaporite Minerals, Abu Dhabi Sabkha	126
7-14	Profile of Sulphur and Oxygen Isotope Variation normal to shoreline Abu Dhabi Sabkha - Data Only	127



Table		Page
7-15	Profile of Sulphur and Oxygen Isotope Variation normal to shoreline Abu Dhabi Sabkha - Trends Only	128
7-16	Depth Variation of Sulphur Isotope in Marine Supratidal Anhydrite cycle (from Butler <u>et al</u> 1973)	135
7-17	Sulphur and Oxygen $\delta$ Values versus Diameter for Gypsum of Seaward Zone, Abu Dhabi Sabkha	138
7-18	Schematic Summary of Isotope Variation at Abu Dhabi Sabkha	142
8-1	Model for Isotope Variation in Sulphate Minerals deposited in a Sabkha Environment	147
8-2	Midale Evaporite Sample Locations	151
8-3	Midale Evaporite Histograms of Isotopic Determinations	153
8-4	Sulphur $\delta$ Values versus Oxygen $\delta$ Values for Midale Evaporite Colour Groups	154
8-5	Areal Distribution of Midale Evaporite Colour Groups	155
8-6	Areal Distribution of Sulphur $\delta$ Values, Midale Evaporite	156
8-7	Areal Distribution of Oxygen $\delta$ Values, Midale Evaporite	157
8-8	Total Thickness of the Salina Evaporite (from Briggs, 1958)	160
8-9	Paleogeographic Map of the Michigan Basin and the Ohio-New York Basin during Salina time (from Briggs, 1958)	162
8-10	Generalised Cross Section of Niagara and Lower Salina carbonates and evaporites northern Michigan basin showing three basic lithologic successions (from Mesolella <u>et al</u> , 1975)	163

Table		Page
8-11	Salina Evaporite Sample Locations	166
8-12	Histogram of Sulphur Del Determinations of Salina Evaporite	167
8-13	Histogram of Oxygen Del Determinations of Salina Evaporite	168
8-14	Areal Distribution of Sulphur Del Values, A-1 Anhydrite, Salina Evaporite	169
8-15	Areal Distribution of Oxygen Del Values, A-1 Anhydrite, Salina Evaporite	170
8-16	Areal Distribution of Sulphur Del Values, A-2 Anhydrite, Salina Evaporite	171
8-17	Areal Distribution of Oxygen Del Values, A-2 Anhydrite, Salina Evaporite	172
8-18	Areal Distribution of Sulphur Del Values, B Anhydrite, Salina Evaporite	173
8-19	Areal Distribution of Oxygen Del Values, B Anhydrite, Salina Evaporite	174
8-20	Histogram of Sulphur Del Determinations, Permian Evaporites	177
8-21	Histogram of Oxygen Del Determinations, Permian Evaporites	178
8-22	Sample Locations, Permian Zechstein Formation	180
8-23	Areal Distribution of Sulphur Del Values, A-1 Anhydrite, Zechstein Formation	181
8-24	Areal Distribution of Oxygen Del Values, A-1 Anhydrite, Zechstein Formation	182

Table		Page
8-25	Sulphur Del Values versus Oxygen Del Values - Summary for Midale Evaporite, Salina Evaporite, and Permian Evaporites	183
8-26	Evaporite Sulphur Del Values versus Geological Time	186
8-27	Evaporite Oxygen Del Values versus Geological Time	187
8-28	Caledonia Mine Sample Sites	205
8-29	Caledonia Mine Geological Section and Sample Locations	206
8-30	Hagersville Mine Sample Sites	208
8-31	Hagersville Mine Geological Section and Sample Locations	209
9-1	Oxygen Del Values versus time exchange experiments	245
9-2	Northrop/Clayton Plot for Experiments 30 and 31, last 172 days	246
9-3	Northrop/Clayton Plot for Experiments 32 and 33, last 172 days	247
9-4	Northrop/Clayton Plot for Experiments 30 and 31, first 25 days	248
9-5	Northrop/Clayton Plot for Experiments 32 and 33, first 25 days	249
9-6	Oxygen-Labelled Sulphate from Sulphite Exchange with Oxygen-Labelled Water, at 25°C	252

## INTRODUCTION

### General

Sulphur and oxygen are elements that occur as more than one stable isotope, for example, sulphur of mass 32 and of mass 34. The heavy isotope,  $^{34}\text{S}$ , contains two more neutrons (18) but has the same number of protons (16) and the same extranuclear configuration as the light isotope,  $^{32}\text{S}$ . The proportions of the isotopes of the same element are not fixed; measurable differences in the  $^{34}\text{S}/^{32}\text{S}$  ratio have been found between, for example, the sulphate dissolved in seawater and the sulphide in the muds of the sea bottom. In general there is an isotope fractionation when part of some reservoir of an element is transferred to another reservoir in a geological cycle (in our example, the sulphide may have a  $^{34}\text{S}/^{32}\text{S}$  ratio smaller by five per cent than that of seawater sulphate).

In this work, oxygen and sulphur stable isotope ratio measurements on the evaporite minerals, gypsum ( $\text{CaSO}_4 \cdot 2\text{H}_2\text{O}$ ) and anhydrite ( $\text{CaSO}_4$ ) from diverse geological settings and on the products of laboratory experiments are presented. These measurements contribute to our knowledge of the systematic basis of isotope abundance variations.

They also add to our understanding of how evaporite rocks are formed, changed and preserved, and thus to our interpretation of the geological history of ancient evaporites.

### Marine Evaporites

Marine evaporite minerals form by precipitation from seawater concentrated by evaporation. This was demonstrated by Usiglio in 1849. His experiments also showed that there is a definite sequence of minerals that crystallize from seawater as evaporative concentration progresses (see Table 1-1). That characteristic sequence has been observed in many ancient evaporite formations. Nonetheless, there are several notable aspects of natural evaporite deposits that require more complex models than a straightforward total evaporation of a single batch of seawater.

As Figure 1-1 shows, the first formed minerals, calcite and gypsum, appear to be over-represented in the geological record. This may be due to subsequent solution of the more soluble last formed salts, but a more likely explanation can be found in the probable mode of formation of evaporite deposits.

The thickness of salt that would precipitate from a single batch of seawater is relatively small compared to the total thickness of salt in some evaporite formations, and to the probable volume of seawater initially in the basin. Therefore, it has been postulated that in an

Table 1-1: Salts laid down in concentration of seawater (Data of Usiglio, from Stewart, 1963)

Density <sup>1</sup>	Volume	Fe <sub>2</sub> O <sub>3</sub>	CaCO <sub>3</sub>	CaSO <sub>4</sub> ·2H <sub>2</sub> O	NaCl	MgSO <sub>4</sub>	MgCl <sub>2</sub>	NaBr	KCl
.0258	1.000	-----	-----	-----	-----	-----	-----	-----	-----
.0500	.533	0.0030	0.0642	-----	-----	-----	-----	-----	-----
.0836	.316	-----	Trace	-----	-----	-----	-----	-----	-----
.1037	.245	-----	Trace	-----	-----	-----	-----	-----	-----
1.1264	.190	-----	0.530	0.5600	-----	-----	-----	-----	-----
1.1604	.1445	-----	-----	.5620	-----	-----	-----	-----	-----
1.1732	.131	-----	-----	.1840	-----	-----	-----	-----	-----
1.2015	.112	-----	-----	.1600	-----	-----	-----	-----	-----
1.2138	.095	-----	-----	.0508	3.2614	0.0040	0.0078	-----	-----
1.2212	.064	-----	-----	.1476	9.6500	.0130	.0356	-----	-----
.2363	.039	-----	-----	.0700	7.8960	.0262	.0434	0.0728	-----
1.2570	.0302	-----	-----	.0144	2.6240	.0174	.0150	.0358	-----
1.2778	.023	-----	-----	-----	2.2720	.0254	.0240	.0518	-----
1.3069	.0162	-----	-----	-----	1.4040	.5382	.0274	.0620	-----
Total deposit	-----	0.0030	0.1172	1.7488	27.1074	0.6242	0.1532	0.2224	-----
Salts in last bittern	-----	-----	-----	-----	2.5885	1.8545	3.1640	.3300	0.5339
Sum	-----	.0030	0.1172	1.7488	29.6959	2.4787	3.3172	0.5524	0.5339

<sup>1</sup> Given by Usiglio in Baumé degrees. Restated here in specific gravities.

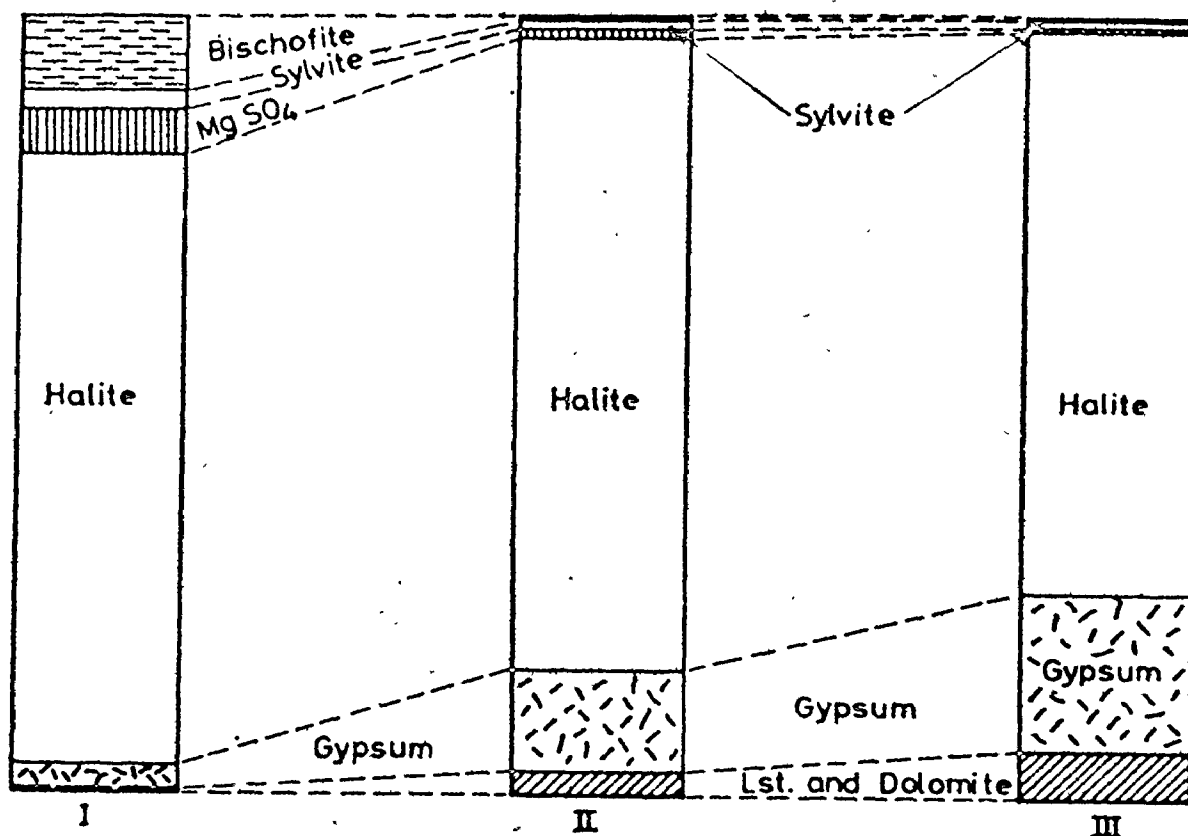


FIG. 6.5. COMPARATIVE PRECIPITATION PROFILES FROM EXPERIMENTAL EVAPORATION OF SEA WATER (I), FROM THE ZECHSTEIN EVAPORITES (II), AND FROM THE AVERAGE OF NUMEROUS OTHER MARINE SALT DEPOSITS (III)

Figure 1-1: Salt Profiles (from Borchert and Muir, 1964)

evaporite basin, continuous or intermittent replenishment of seawater took place across some restricting barrier. Such a process could well maintain the concentrated seawater in the calcite or gypsum precipitation range for prolonged periods, and consequently generate thick stratigraphic units of these minerals. This would result in large volumes of brine enriched in sodium chloride. In many cases, the chloride minerals do not follow the carbonate and sulphate minerals. One mechanism that has been suggested for the disposition of the sodium chloride and other residual components of seawater is reflux back to the open ocean. King (1947), in discussing the anhydrite-calcite laminae of the Permian Castile Formation raised the possibility that the dense chloride rich brines may have percolated back through the reef that partially closed the Castile basin to the open ocean.

This model of a barred basin with reflux - inferred in the absence of direct observations - dominated evaporite petrology until the fairly recent discovery of a modern analogue. Gypsum, anhydrite and halite are forming presently on the supratidal flats, or sabkhas, of the Persian Gulf. The textures of the sulphate minerals are similar to those seen in ancient evaporite rocks. The chemical mode of formation of the gypsum, namely precipitation concomitant with dolomitization of carbonate sediment, conforms with the common intimate association of dolomite and sulphate minerals. The Persian Gulf has received thorough scrutiny, of its hydrology, mineralogy, geochronology, and



other aspects, and it has inspired several reinterpretations of the depositional modes of many ancient evaporite formations. However, it is not at present clear what criteria can be applied to ancient evaporite rocks to determine conclusively whether they were deposited in deep water or shallow water or subaerially. The most persuasive evidence comes from the associated carbonate rocks because most gypsum and anhydrite rock fabrics have been shown to occur in both shallow and deep environments. Were some aspect of the geochemistry of gypsum and anhydrite shown to correlate with depositional water depth, then much of the dispute might be resolved.

The very recent discovery of the Mediterranean Evaporite has also provoked a reconsideration of earlier assumptions. Hsü (1972) and Hsü et al (1973) have amassed considerable detail to support their idea that the Mediterranean periodically dried up during the Miocene as the constriction at the Straits of Gibraltar cut off circulation with the open ocean. Their model is one of precipitation from shallow water in a deep basin. Hsu (1972) has discussed the possibility that this depositional mode may account for some ancient evaporites - notably those deposited in large continental basins. The universality of the desiccated basin model has not been established, but it has the character of a classic synthesis of (apparently) opposing hypotheses, namely deep basin versus shallow deposition.

## Stable Isotopes

Stable isotopes of an element have the same number of protons (atomic number) but different numbers of neutrons in the nucleus of the atom. Thus they differ in their atomic masses. In 1947, Harold Urey showed that stable isotopic molecules ought to have measurably different physical and thermodynamic properties. For this reason they should be fractionated in natural systems - for example, if sulphate is partly reduced to sulphide, the product sulphide should have less ~~34~~<sup>32</sup>S and the remaining sulphate should be reciprocally enriched.

The fundamental measuring instrument in stable isotope studies is the ratio mass spectrometer. Once samples have been prepared as pure gases, they are admitted into the evacuated mass spectrometer. At the source they are ionized and accelerated through a series of collimating slits. The ions then pass through a uniform magnetic field and describe circular trajectories, the radii of which are mass dependent. Heavier ions are deflected less, and the ion beam is separated into beams of equal mass ions. Two separate beams are collected and the ratio of their intensities is measured. This ratio can be transformed into the ratio of the stable isotopes involved. By a system of rapid switching, sample gas and standard gas are alternately admitted into the mass spectrometer. Comparison of their stable isotope ratios permits a precise determination of the relative stable isotope composition

of the sample gas relative to the standard without knowledge of the absolute isotope ratios.

The most commonly used expression for the stable isotope composition of a sample X is the del notation for the deviation in the isotope ratio of X from that of a standard.

$$\delta_X = \left[ \frac{R_X}{R_{STD}} - 1 \right] \cdot 10^3 \text{ (‰)} \quad 1-1$$

$$R_X = (\text{Heavy/Light})_X$$

The relative abundance of stable isotopes in two species, X and Y, is represented by the fractionation factor,  $a_{XY}$ .

$$a_{XY} = R_X / R_Y \quad 1-2$$

Alternatively, when comparing two samples, the delta notation is used.

$$\Delta_{XY} = \delta_X - \delta_Y \quad 1-3$$

Although the del values are ratio expressions, the ratios  $R_X/R_Y$  are very close to unity (for elements other than hydrogen,  $|\delta|$  is usually  $\ll 50\text{‰}$ ), and in the normal range, the following approximation is valid.

$$\delta_X - \delta_Y \approx 10^3 \ln a_{XY} \quad 1-4$$

The right hand side of Equation 1-4 is an exact formulation for

the fractionation factor or isotopic difference between two phases, X and Y.

There are two important types of standards used in stable isotope geochemistry. In the operation of the mass spectrometer, working standard gases are chosen on the basis of availability, isotopic uniformity and convenience. Analyses are ordinarily reported relative to international standards that have been analyzed in several laboratories. These global standards commonly are not widely available but are used because they represent the composition of a fundamentally important substance such as seawater or meteorites. Thus the scale of measurement attains real significance, more so than a totally arbitrary scale.

In considering the isotope composition of two or more substances that contain a common element, there are at least three mechanisms for effecting an isotope shift: equilibrium exchange, kinetic fractionation, and mixing.

Equilibrium isotopic exchange is the process of partitioning stable isotopes between two phases such that there is no tendency for further partitioning. Although the driving force in isotope exchange reactions is far less than for comparable chemical reactions, it is possible to write analogous expressions for such parameters as the free energy  $G$ ; at equilibrium the free energy must be at a minimum and  $\Delta G = 0$ . Because it is generally impossible to measure the heat absorbed or given off during an exchange reaction, the criteria for isotopic

equilibrium cannot be the same as those for chemical equilibrium. The two principal criteria are that chemical equilibrium must obtain in the system, and that the isotopic fractionation should be path and rate independent. For the second criterion, this is usually satisfied by approaching equilibrium from both directions, that is with the starting materials having an initial fractionation greater than the equilibrium fractionation in one case and less than it in another (see Figure 1-2).

Figure 1-2 was drawn assuming (1) that the two phases X and Y exchange a common isotope, and (2) that there is a great excess of Y so that exchange does not affect its composition. All intensive thermodynamic variables such as temperature and pressure are fixed. In all three exchange runs the composition of phase X proceeds from  $X_0$  and approaches the equilibrium value. The value is the same regardless of the composition of the starting materials, or the rate of exchange, but is dependent on temperature. Generally, the equilibrium fractionation factor decreases with increasing temperature.

Kinetic isotope fractionations accompany unidirectional chemical processes, such as the reduction of sulphate to sulphide without back oxidation, and reversible processes that do not achieve equilibrium. In such cases, the fractionations do depend on path and rate, and they are generally not the same for forward and backward steps. If a kinetic fractionation operates on a single batch, then the isotopic changes

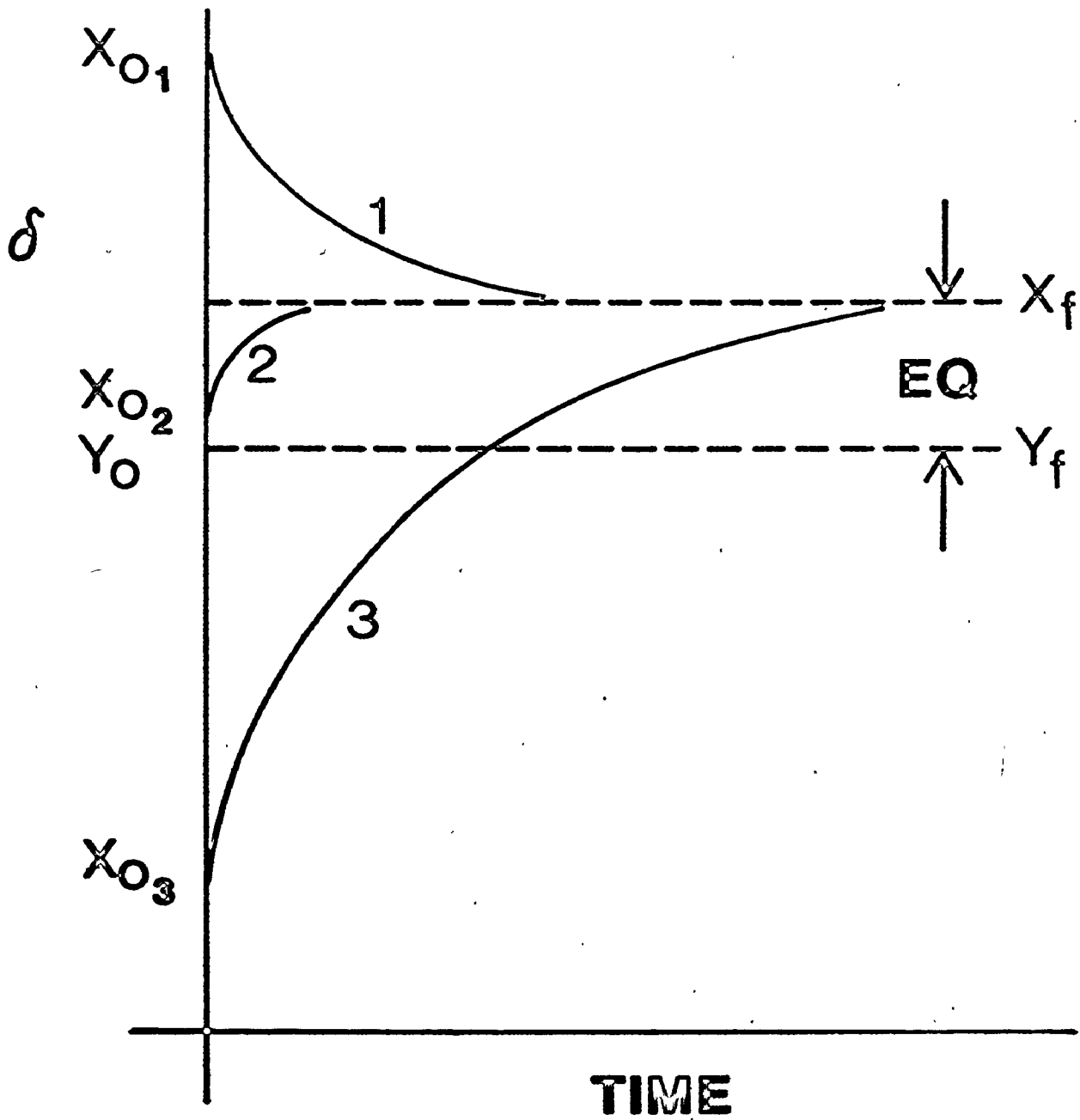


Figure 1-2: Equilibrium Exchange Experiments

follow Rayleigh distillation. This is shown in Figure 1-3, in which an initial mass of X reacts to form Y.

As shown,  $\delta(Y_0) > \delta(X_0)$  which for this example means that the heavy isotope reacts faster. Although the fractionation  $\delta(Y) - \delta(X)$  is constant throughout the reaction, a progressive change in the total or average composition of each phase results. As shown, the first product,  $Y_0$ , has the heaviest composition. The removal of heavy product causes the residual reactant X to be depleted and the progressive reaction causes X and Y to be successively lighter. Note that if the reaction proceeds to completion (100%),  $\delta(Y_f)$  will equal  $\delta(X_0)$  due to isotopic mass conservation. Equation 1-5 expresses the relationship between the isotopic composition of the product and the extent of the reaction expressed as a fraction, F.

$$\delta Y - \delta X_0 = [\delta Y_0 - \delta X_0] \ln F \quad 1-5$$

Thus it is clear that the kinetic isotope fractionations can only have a significant effect on the composition of the product materials if the reaction does not proceed to completion. This does happen if there is abundant reactant and only a negligible portion of it is consumed. In this case, the maximum net isotopic enrichment of the product will result.

A third isotope effect that may obtain in natural systems is mixing. In this case isotope mass balance requires that the mixed product simply

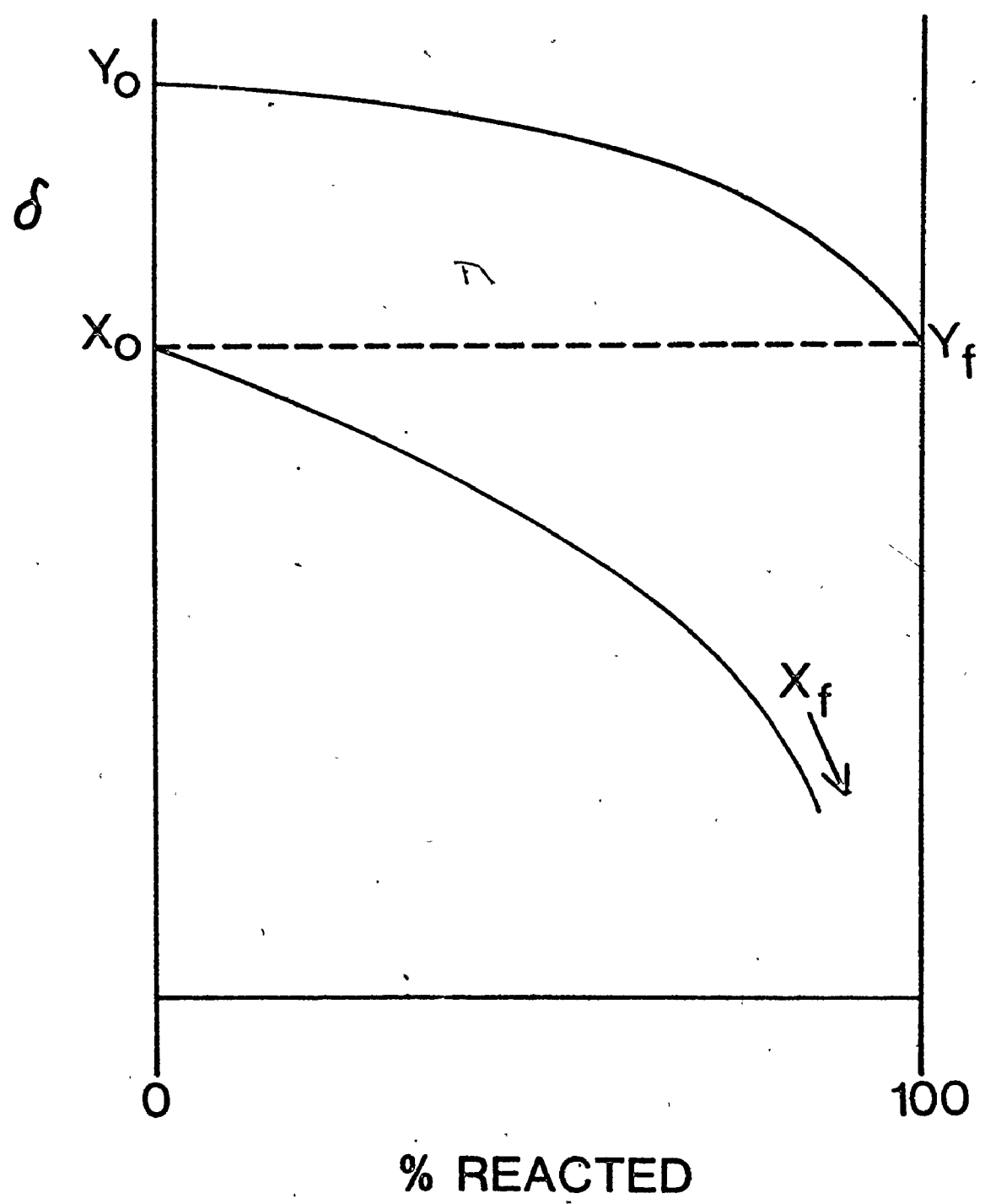


Figure 1-3: Rayleigh-type Kinetic Isotope Fractionation



have the weighted average isotope composition.

$$\delta_{X+Y} = \frac{X}{X+Y} \cdot \delta_X + \frac{Y}{X+Y} \cdot \delta_Y \quad 1-6$$

### Research Goals

At the inception of this study, little was known about the oxygen isotope composition of natural sulphates. It was considered that sulphate would readily exchange oxygen with water, in a manner comparable to that of carbonate. Laboratory experiments by Teis (1957) and Lloyd (1967, 1968) indicated that exchange takes place slowly but at rates that ought to effect total exchange and hence isotopic equilibrium of sulphate dissolved in seawater. Were that so, then the measurement of the oxygen isotope composition of an ancient evaporite sulphate would have to be interpreted in terms of the contemporaneous seawater oxygen and all waters with which the sulphate might have subsequently interacted. Such elaborate interpretations might be of limited value. However, it has been determined that present seawater sulphate is not in isotopic equilibrium with present seawater (Lloyd, 1968). Moreover, Lloyd's measurements on pore water sulphate from deep sea cores (Lloyd, 1973) indicate that exchange does not take place even over millions of years.

During the course of this study, at least two published studies have asserted that there is oxygen isotope variation in Phanerozoic evaporites comparable to that of the sulphur isotopes. In any attempt

to model such variation, it is necessary to fully establish the systematic nature of any isotopic fractionations.

Although several workers have measured the oxygen isotope composition of gypsum and the sulphate from which it precipitated - including some natural brine and mineral pairs - no measurements were made for conditions of unequivocal isotopic equilibrium. The measurements did however indicate that the fractionation factor ( $\Delta_{c-s} = \delta_{\text{crystal}} - \delta_{\text{dissolved sulphate}}$ ) was relatively large (up to 4‰). Thus the first goal of the research was to determine the equilibrium isotope fractionation between gypsum crystal and sulphate in solution.

The second goal was to measure the oxygen isotope composition of ancient evaporites to determine whether secular oxygen isotope variation comparable to that of sulphur could be demonstrated. Were such changes related to changes in the oxygen isotope composition of seawater, they would have profound implications for paleothermometry based on the calcite-water fractionation. Another possible outcome of the measurement of the oxygen isotope composition of evaporite sulphate is that it might complement the information provided by sulphur isotope analyses. The positive result that analysis of combined variation would yield more information than analysis of one or the other measured singly might be expected on the grounds that the oxygen in sulphate is not permanently linked to the sulphur cycle. The oxygen released by

the reduction of sulphate is in the form of carbon dioxide, and it enters the aqueous carbonate-carbon dioxide cycle. On the other hand, river sulphate, the major input to seawater sulphate, is largely produced by the oxidation of pyrite. The oxygen of that sulphate is newly incorporated and may contain atmospheric oxygen and meteoric water oxygen in some proportions, with or without some fractionation. Therefore the oxygen and sulphur isotope compositions of sulphate are generated in different ways. Thus it might be expected that this difference would be preserved in the evaporite record.

One of the most effective approaches to geological problems has been to study processes that are happening on the earth today and apply the principles that govern modern phenomena to ancient situations. This approach, known as actualism, assumes that although the rates of processes may have differed in the past, the kinds of processes were similar and the laws of science such as those of thermodynamics held then as they do today. The potential value of a modern analogue in this work is that it might bridge the gap between measurements on ancient rocks and inferences about contemporaneous seawater sulphate and other sulphate reservoirs. It is possible (and devoutly to be wished) that the study of a modern analogue might uncover some method for characterizing that particular depositional mode, and hence be applicable to the deep water versus shallow water controversy.

## THE SULPHUR ISOTOPE GEOCHEMISTRY OF SULPHATE

Although sulphur has four stable isotopes (mass 32, 33, 34, and 36), most results are reported in terms of the  $^{34}\text{S}/^{32}\text{S}$  ratio, using the  $\delta$  notation. The average abundance of each isotope is as follows:  $^{32}\text{S}$ , 95.02%;  $^{33}\text{S}$ , 0.75%;  $^{34}\text{S}$ , 4.21%;  $^{36}\text{S}$ , 0.02%. Thus the  $^{34}\text{S}/^{32}\text{S}$  ratio is about 1/20 and it is the most favourable for measurement. The international standard is meteoritic troilite, specifically Canyon Diablo Troilite (CDT). Meteoritic troilite is suitable as a sulphur isotope standard because it has an extremely uniform composition,\* and because it has fundamental geochemical significance in that it may represent the average sulphur isotope composition of the earth. As Figure 2-1 shows, mafic igneous sulphides have a value close to that of meteoritic troilite.

Marine evaporite sulphate (largely from anhydrite and gypsum) of Precambrian to Recent age lies between +9.6 and +35.8‰. Present seawater sulphate splits that range with a  $\delta^{34}\text{S}$  of about +20‰ and it

---

\*The isotopic uniformity of meteoritic troilite is being reinvestigated using the high precision sulphur hexafluoride method by C. E. Rees, McMaster University.

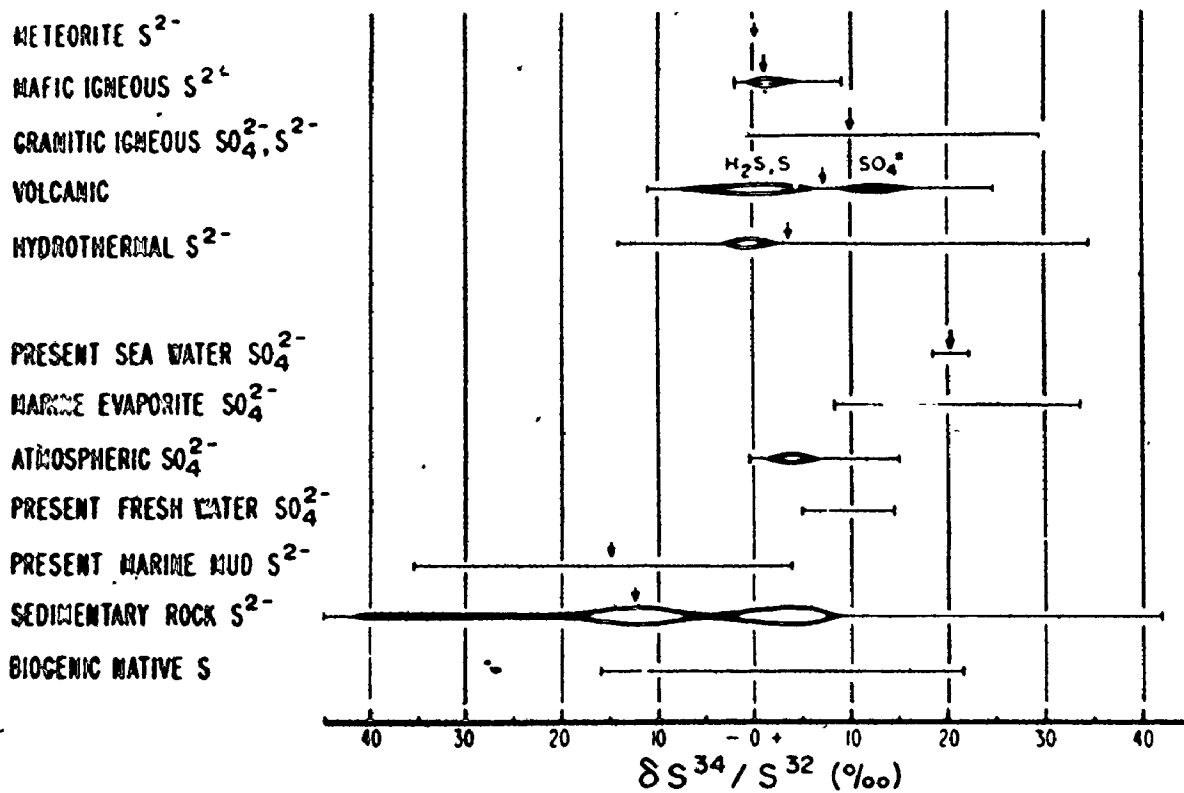


Fig.1. Isotopic geochemistry of sulfur. Arrows indicate mean values. Abstracted from all published data.

Figure 2-1: Isotopic Geochemistry of Sulphur (from Holser and Kaplan, 1966)

varies by less than one per mille throughout the whole ocean.

Sedimentary sulphides exhibit an extreme range of sulphur  $\delta$  values (see Figure 2-1). Like sulphide in modern marine mud, most ancient sedimentary sulphides have negative, highly variable, isotopic compositions. Atmospheric sulphate (0 to + 16‰) and present freshwater sulphate (-7.5 to + 15‰) are also substantially lighter than seawater sulphate.

Present freshwater sulphate, the major sulphate input to the world oceans, includes eroded evaporite sulphate, weathered and oxidized sedimentary and igneous sulphides, and sulphate from human activities. At its present composition it must tend to drive seawater sulphate to a lighter composition. There are two important ways of removing sulphate from the oceans: evaporite deposition and bacterial reduction with removal of the product sulphide.

The most effective agent for fractionating sulphur isotopes in the sedimentary sulphur cycle is bacterial reduction of sulphate to sulphide. Organisms such as Desulfovibrio desulfuricans preferentially metabolize <sup>32</sup>S, thereby creating isotopically light sulphide and heavier residual seawater sulphate. The overall extent of the fractionation depends on several factors - notably the rate of sulphate reduction, and whether or not the system is closed with respect to addition of seawater (Rees, 1973). D. desulfuricans is known to inhabit the anoxic parts of the sea; it is responsible for most reduction in reducing muds in sea

bottom trenches and deep landlocked sea basins (Goldhaber and Kaplan, 1974).

Experimental studies have shown that there are several steps in the bacterial reduction of sulphate. Kemp and Thode (1968) examined the effect of nutrient supply, electron donor, pH, temperature, bacterial cell walls (by using cell free extracts), and bacterial strain on the reduction of sulphate and of sulphite. They clearly established that sulphate reduction is a multistep process, and that the kinetic isotope fractionation (the composition of the product sulphide) is governed by the rates of all of the steps. Some possible intermediate steps are shown in Table 2-1.

Their experiments indicated that assimilation of sulphate by the cells would involve a small isotope effect (about - 2‰), whereas the actual reduction of sulphate in the cells (which involves the breaking of an S - O bond) creates a larger fractionation (up to -22‰). Although reduction of intermediate sulphite could result in a comparable large fractionation, Kemp and Thode concluded that the sulphide would be reduced extremely rapidly and therefore (normally) no fractionation would result in that step.

Rees (1973) has modelled the laboratory results of Kemp and Thode (1968), Kaplan and Rittenberg (1964), and Harrison and Thode (1958) in terms of a steady state model with zero order kinetics. The workers listed had observed that in their experiments, except at low

Table 2-1: Some Intermediate Steps in the Bacterial Reduction of Sulphate (from Kemp and Thode, 1968)

Step I	$H_2 + 2Fe^{3+}$	$\xrightarrow{\text{Hydrogenase}}$	$2Fe^{2+} + 2H^+$	(2)
Step II	$ATP + SO_4^{2-}$	$\xrightarrow{\text{ATP sulphurylase}}$	APS + Pyrophosphate	(3)
Step III	$APS + 2Fe^{2+} + 2H^+$	$\xrightarrow{\text{APS reductase}}$	$AMP + SO_3^{2-} + 2Fe^{3+} + H_2O$	(4)
Step IV	$X + SO_3^{2-}$	$\longrightarrow$	$H_2S$	(5)



sulphate concentrations, the bacteria quickly attained a constant rate of sulphate reduction; it follows that the intermediate steps achieved steady state. Figure 2-2, from Kemp and Thode (1968), provides an example of the constant rate of reduction.

During the period of constant reduction rate, the reactant sulphate would be depleted and the product sulphide generated at the same rate (moles/unit time), but the intermediate products would hold a level abundance. Zero order kinetics are appropriate because the number of moles reduced per unit time is constant and independent of sulphate concentration in the range (greater than  $10^{-2}$  M). Rees (1973) suggested that the overall fractionation depended on the relative magnitudes of the forward and backward flows between the internal bacterial sulphur reservoirs.

The very large fractionations (up to 46‰) occasionally observed in laboratory experiments, and commonly observed in nature (notably in the Black Sea) would result from significant back flow of sulphite to sulphate (in Figure 2-3, from D to C), and in this case the large fractionation in the reduction of sulphite is added to that for the reduction of sulphate. The interpretation is supported by the observation that the large fractionations correspond to very low production of hydrogen sulphide, and at these slow rates, the ratios of backward to forward flows for the intermediate steps approach unity. Thus Rees (1973) has modelled the total range of natural and laboratory

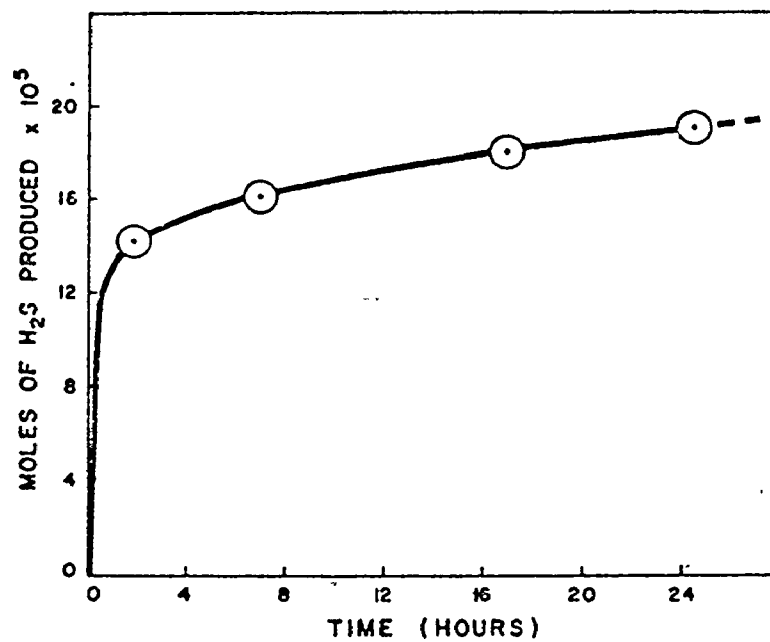


Fig. 3. Sulphate reduction by hydrogen with cell free extracts of *D. desulphuricans*, a typical rate plot. Temperature = 34.9°C; pH = 6.0; [SO<sub>4</sub><sup>2-</sup>] = 0.05 M; [ATP] = 2.8 mM; [methyl viologen] = 0.2 mM.

Figure 2-2: Sulphate Reduction Rate Plot (from Kemp and Thode, 1968)

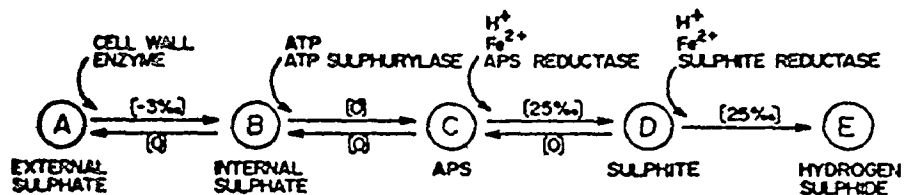


Fig. 2. Reaction scheme for *D. desulfuricans*. The various sulphur species are shown together with the enzymes and metabolites necessary to promote forward reaction steps. The numbers in brackets are the isotope effects assigned to the individual reaction steps.

Figure 2-3: Reaction Scheme for Desulfovibrio desulfuricans (from Rees, 1973)

observations in terms of the probable reaction steps in bacterial reduction. It is also apparent from the model that the fractionation may be highly variable; it is not surprising that irreproducible results have been generated in the laboratory. The point to be emphasized here is that under some circumstances, sulphate reduction is accompanied by a large fractionation that leaves seawater enriched in  $^{34}\text{S}$ .

### Marine Evaporite Sulphur Isotope Geochemistry

The traditional model of evaporite deposition has been the precipitation of gypsum from seawater concentrated by high net evaporation. Once the solubility product ( $\text{Ca}^{++}$ ). ( $\text{SO}_4^{--}$ ) of the saturated solution is exceeded, gypsum precipitation ensues. If the crystals are not subsequently redissolved, then sulphate is removed from the ocean. An isotope fractionation will occur if the sulphur isotope composition of the gypsum differs from that of the solution sulphate from which it precipitates. Thode and Monster (1965) have reported measurements of the sulphur isotope composition of gypsum crystals and of dissolved sulphate after the partial evaporation of a solutions of calcium sulphate. They determined that the crystals were 1.65‰ heavier than the dissolved sulphate. This may not be an equilibrium isotope fractionation because it is not demonstrably reversible, but it is the generally accepted estimate of the fractionation that accompanies evaporite deposition. Such an isotope shift would tend to decrease the  $\delta^{34}\text{S}$  value

of the remaining seawater sulphate, but the magnitude of the change would be very small. Holser and Kaplan (1966), using the 1.65‰ fractionation, have shown that in the evaporation of a single batch of seawater, the late stage sulphates would have substantially lighter sulphur isotope compositions (by 3 to 4‰). This then affords a test of that model for evaporite deposition; Holser and Kaplan's analyses and those of Nielsen (1965) of late stage sulphate bearing complex salts from Permian formations do exhibit a slight tendency to lighter values. On the other hand, Davies and Nassichuk (1975) note that individual anhydrite beds of the Carboniferous Otto Fiord Formation show "a gradient upward through the bed in  $\delta^{34}\text{S}$  from 16 to 12‰".

Marine evaporites of all geological ages have sulphur del values in the range +10 to +35‰. The composition of evaporites deposited in a single geological period or epoch falls within a much narrower range. For example Permian evaporites lie between +9 and +13‰ (Holser and Kaplan, 1966), whereas Middle Devonian evaporites range from +22 to +31‰ (Thode and Monster, 1965). On the basis of such results Thode and Monster (1965) drew the first curve of sulphur del value versus geological age. As Figure 2-4 and Figure 2-5 show, there is a clear maximum in the Cambrian and Ordovician, while the Permian evaporites present a distinct minimum. Subsequent versions have confirmed the general nature of the curve (Nielsen, 1965; Holser and Kaplan, 1966; Solomon et al, 1971; Yeremenko and Pankina, 1971;

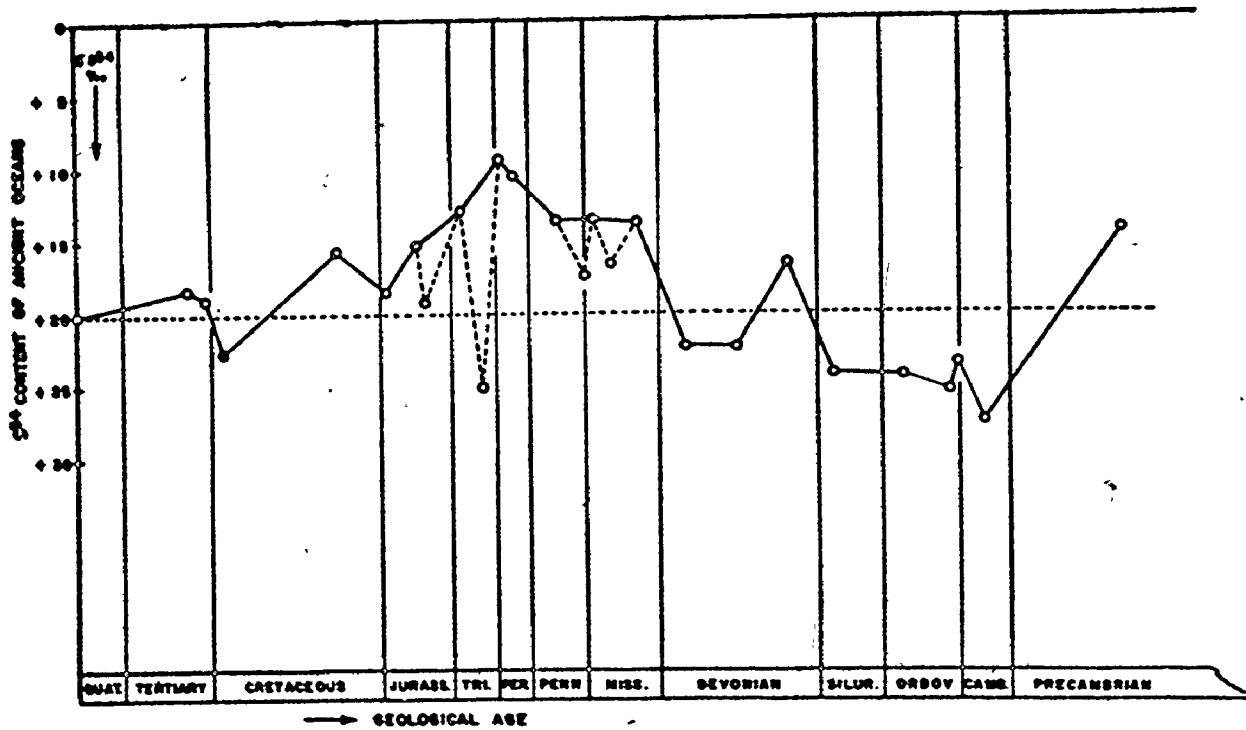


Figure 2-4: Sulphur Del Values versus Geological Time for Seawater Sulphate (from Thode and Monster, 1965).

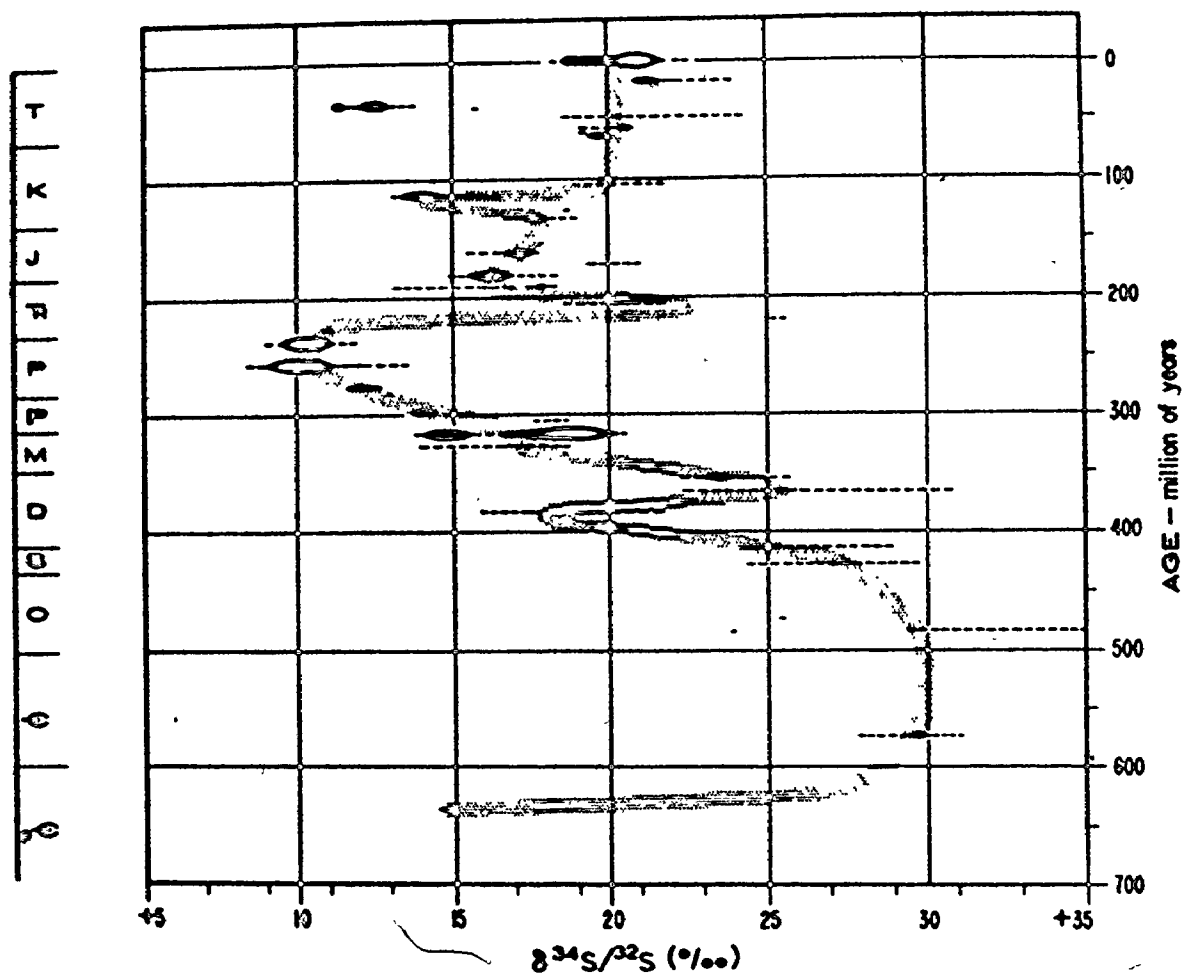


Fig.5. Sulfur-isotope age curve, from all present and previous data. Thickness of line suggests number of analyses, and dashed lines indicate ranges where only a few analyses or insufficient details have been published.

Figure 2-5: Sulphur Del Values versus Geological Time for Seawater Sulphate (from Holser and Kaplan, 1966)

Pilot et al , 1972; Claypool et al , 1972).

Thode and Monster (1965) suggested that these variations in the sulphur isotope composition of evaporites must be related to secular changes in the composition of contemporaneous seawater sulphate. They considered that the lightest measured  $\delta$  value for evaporites of any geological period would most closely approach the value of seawater sulphate at that time because the major fractionating agent, bacterial sulphate reduction, would drive the composition toward heavier values. They suggested that fractionation during crystallization could be ignored since its maximum effect is less than 2‰. Nielsen (1965), in discussing the relationship between evaporite composition and that of coeval seawater sulphate, pointed out counter trends (for evaporites to have lighter  $\delta$  values than seawater sulphate): fractionation in late stage evaporites, and the peculiar example of the Upper Oligocene evaporites of the Rhine Valley, to which correspond the Tertiary sulphur  $\delta$  values that are about 7‰ lighter than any others deposited since the Middle Cretaceous (see Figure 2-5). Holser and Kaplan (1966) concurred that fractionation during crystallization could be neglected, but they argued that the average composition for evaporites of any period would better estimate the composition of contemporaneous seawater sulphate. If deposition took place in oxygenated, ultrasaline, sterile waters with little bacterial reduction, and if the measured variation for a period or an epoch represents normally distributed scatter (due to depositional and post-



depositional effects), then the Holser and Kaplan average would be a superior estimate of the sulphur del value of coeval seawater sulphate. However, the preceding debate is resolved, there remains the firmly established net decrease of 20‰ in the Paleozoic, and the increase of 10‰ in the Mesozoic and Cenozoic.

Drawing a smooth curve of the secular change in seawater sulphate is complicated by the large range measured for some periods or epochs (for example, the Middle Devonian, +22 to +31‰ ) and by changes between succeeding periods and epochs that are counter to the general trend (although the Paleozoic values decrease from +30‰ in the Cambrian Period to +10‰ in the Permian, the Lower Devonian at +18‰ is followed by the Middle Devonian epochal average of +27‰ ). Inspection of Holser and Kaplan's (1966) curve shows several instances of these shorter term reversals.

In considering the relation between measurements on ancient evaporite rocks and contemporaneous seawater, and of the processes that cause the measured changes, it is well to bear in mind that shifts toward heavier and lighter sulphur isotope compositions appear to have taken place very rapidly (see Table 2-2).

Holser and Kaplan (1966) modelled these sulphur isotope variations in terms of isotopic mass balance and shifts of sulphur between shale and seawater. They considered that evaporite deposition could be neglected since the isotopic fractionation is likely to be very small.

Table 2-2: The Variable Rate of Change of  $\delta^{34}\text{S}$  of Seawater Sulphate

Cambrian to Permian	
(-20‰, $40 \times 10^7$ years)	-0.5‰/ $10^{+7}$ years
Silurian to Lower Devonian	
(-8‰, $2.5 \times 10^7$ years)	-3‰/ $10^{+7}$ years
Permian to Triassic	
(+11‰, $2.5 \times 10^7$ years)	+4‰/ $10^{+7}$ years
Lower to Middle Devonian	
(+7‰, $2 \times 10^7$ years)	+ 3.5‰/ $10^{+7}$ years
Cretaceous to Present	
(+3‰, $10 \times 10^7$ years)	+0.3‰/ $10^{+7}$ years

In their model, the tendency toward heavier  $\delta$  values corresponds to transfer to the sulphide reservoir (shale deposition) and the trend to lighter values results from the erosion of shales. Thus the sulphur is recycled and the rate of change of the sulphur  $\delta$  value is determined by rates of deposition and erosion that are in turn governed by tectonic and other factors. Naturally, the discovery of an indicator that appears to be sensitive to the most fundamental geological processes, and to the variability of at least the sulphate content of seawater provoked considerable attention.

Rees (1970) suggested that because evaporite deposition must influence the amount of sulphate in seawater, it must also affect the average isotopic composition of any outflow of sulphate from the oceans. In the special case of steady state (in which the isotope composition and the dissolved sulphate concentration are not changing), he showed that the sulphur isotope composition of seawater sulphate depends on the input composition, the weighted average bacterial reduction fractionation, and the ratio of evaporite deposition to sulphide formation rates.

Holland (1973) considered the question of changes in the partial pressure of oxygen in the atmosphere. He developed a more general model for the sulphur  $\delta$  value of seawater sulphate. Holland's Equation 10 (page 2607) may be rewritten as follows (Rees, personal communication):

$$\delta_o + \tau \frac{d\delta_o}{dt} = \delta_R - \Delta \cdot \frac{S}{R} \quad 2-1$$

$\delta_o$	= del seawater sulphate	(+20‰)
$\tau$	= residence time of sulphate in the ocean	(1 to 2 X 10 <sup>7</sup> years)
$\delta_R$	= del river sulphate	(+10‰)
S	= sulphide output	(= river input?)
R	= river input	(4 X 10 <sup>12</sup> moles/year)
$\Delta$	= fractionation during sulphate reduction	(-15, -29, -11‰)

Present values of the variables are included in parentheses. Note that evaporite deposition is implicitly incorporated in the expression. From this model, Holland related changes in the sulphur del value of seawater sulphate to the uptake and release of oxygen by the sulphur cycle. The broad pattern suggests gains in atmospheric oxygen during the lower Paleozoic and losses during the upper Paleozoic. Holland demonstrates that the estimates of the flux have wide error limits (they are notably sensitive to the average del value of evaporite being eroded; Holland has treated it as constant at +17‰). Moreover he demonstrates that the flux of oxygen in the carbon cycle is twice that of the sulphur cycle and it is possible for one cycle to buffer the other.

## THE OXYGEN ISOTOPE GEOCHEMISTRY OF SULPHATE

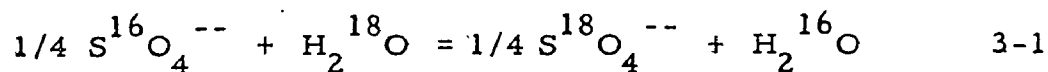
The three stable isotopes of oxygen have the following average abundance:  $^{16}\text{O}$ , 99.76%;  $^{17}\text{O}$ , 0.04%;  $^{18}\text{O}$ , 0.20%. Most analytical results are reported in terms of the variation of the  $^{18}\text{O}/^{16}\text{O}$  ratio, using the  $\delta$  notation. The most common international standard is SMOW (Standard Mean Ocean Water, Craig, 1961). Although suitable geochemically as a standard for  $^{18}\text{O}/^{16}\text{O}$  and D/H because seawater is a significant reservoir, SMOW itself is an artifact defined in terms of other standards (Craig, 1961). Another oxygen isotope scale used is PDB, a carbonate standard employed for paleotemperature work (Urey *et al.*, 1951). SMOW is used for all values of  $\delta^{18}\text{O}$  in this work.

Seawater sulphate has a uniform oxygen isotope composition of +9.5 to +10.0‰ (Longinelli and Craig, 1967; Rafter and Mizutani, 1967; Lloyd, 1968). Freshwater sulphate has oxygen  $\delta$  values from 0 to +11‰ (Cortecci and Longinelli, 1968; Schwarcz and Cortecci, 1973). Evaporite sulphate ranges from +11 to +18‰ (Solomon *et al.*, 1971; Sakai, 1972; Claypool *et al.*, 1972).

The factors controlling the oxygen isotope composition of sulphate are poorly understood. The oxygen that is temporarily fixed in sulphate also passes through other geochemical cycles - the carbon

cycle, the hydrological cycle, and others. Two implications of these interactions are that the oxygen isotope composition of sulphate may be affected by agents external to the sulphur cycle and that the oxygen composition can have information only back to the time of its incorporation into sulphate.

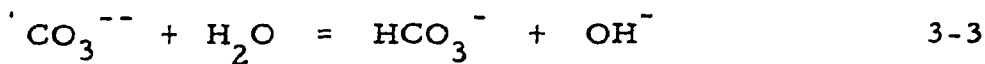
In principle, the most important aspect of sulphate oxygen systematics is isotopic exchange with water. An isotopic exchange reaction and the equilibrium constant for it are shown in Equations 3-1 and 3-2.



$$K_{EQUIL} = (S^{18}O_4^{--}) / (S^{16}O_4^{--}) \cdot 1/4 (H_2^{16}O) / (H_2^{18}O)$$

$$= (^{18}O/^{16}O)_{SO_4^{--}} / (^{18}O/^{16}O)_{H_2O} \quad 3-2$$

The other major natural oxyanion, carbonate, readily exchanges oxygen with water, and its composition reflects the water oxygen isotope composition and the water temperature (equilibrium isotope fractionations are temperature dependent). Epstein *et al* (1953) determined that calcite in equilibrium with water at 4°C should have an oxygen δ value 33‰ heavier than the water. Recent carbonate sediments have approximately that composition. The isotopic exchange is thought to take place through an intermediate species, bicarbonate ions.



At normal surface values of pH and temperature, analogous mechanisms for sulphate-water exchange are very slow.

Lloyd (1968) has reported the results of experiments intended to measure both the rate of exchange and the equilibrium exchange constant. Using solutions of sodium sulphate in water highly enriched in  $^{18}\text{O}$  (1.5%  $\text{H}_2^{18}\text{O}$ ), he determined the extent of exchange (change in sulphate oxygen) for a given time interval, at various conditions of pH and temperature. Exchange is more rapid in low pH solutions, but for a particular pH, the exchange can be modelled as a first order reaction according to the following expression:

$$\ln (1 - f) = -kt \quad 3-5$$

The extent of exchange is denoted by  $f$ , the exchange rate constant by  $k$ , and the exchange time by  $t$ . At  $4^\circ\text{C}$  (mean ocean temperature) the half time of exchange was  $10^4$  years for  $\text{pH} = 7$ , and  $5 \times 10^4$  years for  $\text{pH} = 8.2$ . These rates are very slow compared to those for carbonate, and are slower by about  $10^{-2}$  than the earlier experimental results of Teis (1957). The residence time of sulphate in the oceans has been estimated to be from 1 to  $2 \times 10^7$  years (see, for example, Holland, 1973); isotopic equilibrium ought to be established

unless other processes act more quickly to effect a steady state  $\delta^{18}\text{O}$  different from the equilibrium value.

Lloyd (1968) attempted to determine the equilibrium fractionation factor between dissolved sulphate and water, and between anhydrite and water. Because of the slow rates of exchange, he was obliged for the most part to use low pH and high temperatures to achieve measurable isotope shifts. The equilibrium fractionation factor was estimated (by Lloyd) by using the partial exchange technique of Northrop and Clayton (1966). The principle of the method is that isochemical isotope shifts at a given temperature proceed at the same rate. By varying the isotope compositions of the starting materials, equilibrium is approached in different directions, and can be determined by graphical interpolation.

Lloyd's (1968) results for the dissolved sulphate/water and for the anhydrite/water systems indicated (as they should have) that the logarithm of the fractionation is proportional to the inverse square of the absolute temperature. Extrapolation to  $4^{\circ}\text{C}$  indicates that dissolved sulphate in equilibrium with seawater should have an oxygen isotope composition of  $+38\text{‰}$ ; anhydrite would be about  $6\text{‰}$  heavier. Mizutani and Rafter (1969a) performed comparable experiments with sulphuric acid solutions, and their fractionation factors for bisulphate and water are in fair agreement with Lloyd's dissolved sulphate/water equilibrium. The oxygen  $\delta$  value of seawater sulphate is  $+9.7\text{‰}$



apparently almost 30‰ lighter than the equilibrium value! Urey (1947) calculated the equilibrium fractionation to be about 20‰ for sulphate and water at 4°C. This too suggests lack of equilibrium in the natural system, but it is significantly at variance with Lloyd's experimentally determined fractionation. Longinelli and Craig (1967), in work published before that of Lloyd, considered their value (+9.5‰) for seawater sulphate to represent long term average equilibrium, because the data of Teis (1957) indicated that equilibrium should occur. They ruled out rapid equilibrium because they found no correlation between  $\delta^{18}\text{O}$  of sulphate and  $\delta^{18}\text{O}$  of water for coexisting natural pairs.

Besides the problematical exchange with water, other processes can influence the oxygen del value of sulphate. Lloyd (1968) and Mizutani and Rafter (1969b, 1973) have reported the results of experiments on the bacterial reduction of sulphate. The earlier results did not supply enough data to estimate the kinetic fractionation for oxygen isotopes with the same degree of confidence that the analogous parameter has been determined for sulphur isotopes, although Lloyd's (1968) estimate of  $\Delta^{18}\text{O} = -4.5\text{‰}$  and Mizutani and Rafter's (1969b)  $\Delta^{18}\text{O} = -6.0\text{‰}$  are in good agreement.

Mizutani and Rafter's recent (1973) contribution provides a clearer understanding of the oxygen isotope fractionation in bacterial sulphate reduction. They showed that the fractionation depends on the oxygen del value of the water. Bacterial activity is clearly independent

of  $\delta^{18}\text{O}$  of water so exchange is implicit. Mizutani and Rafter (1973) consider that either an intermediate sulphate complex or intermediate sulphite may exchange (see Chapter 2); sulphite is known to exchange oxygen with water very rapidly. The fractionation factors determined by Mizutani and Rafter were highly variable even for the same temperature and  $\delta^{18}\text{O}$  of water. The largest fractionations (-12 and -25‰) occurred in the 'most natural' experiment, and are consistent with the observation for  $^{34}\text{S}/^{32}\text{S}$  that the maximum fractionations happen when the nutrient supply is limited.

Mizutani and Rafter (1969b) examined the reverse reaction, namely the bacterially mediated oxidation of sulphur to sulphate. The sulphate produced had the oxygen  $\delta$  value of the water in which it was oxidized. Lloyd's (1968) experiments on the oxidation of sulphide did not show such a simple relationship. Dissolved molecular oxygen (fractionated by -8.7‰) and water oxygen (with no fractionation) were apparently utilized in the ratio 1:2. The extremely rapid exchange between water and intermediate sulphite had a large influence on the ultimate composition of the sulphate.

Lloyd (1968) summarized his findings in the schematic diagram reproduced here as Figure 3-1. He postulates a steady state model in which light sulphate is enriched by bacterial reduction to its measured value, much lighter than equilibrium sulphate.

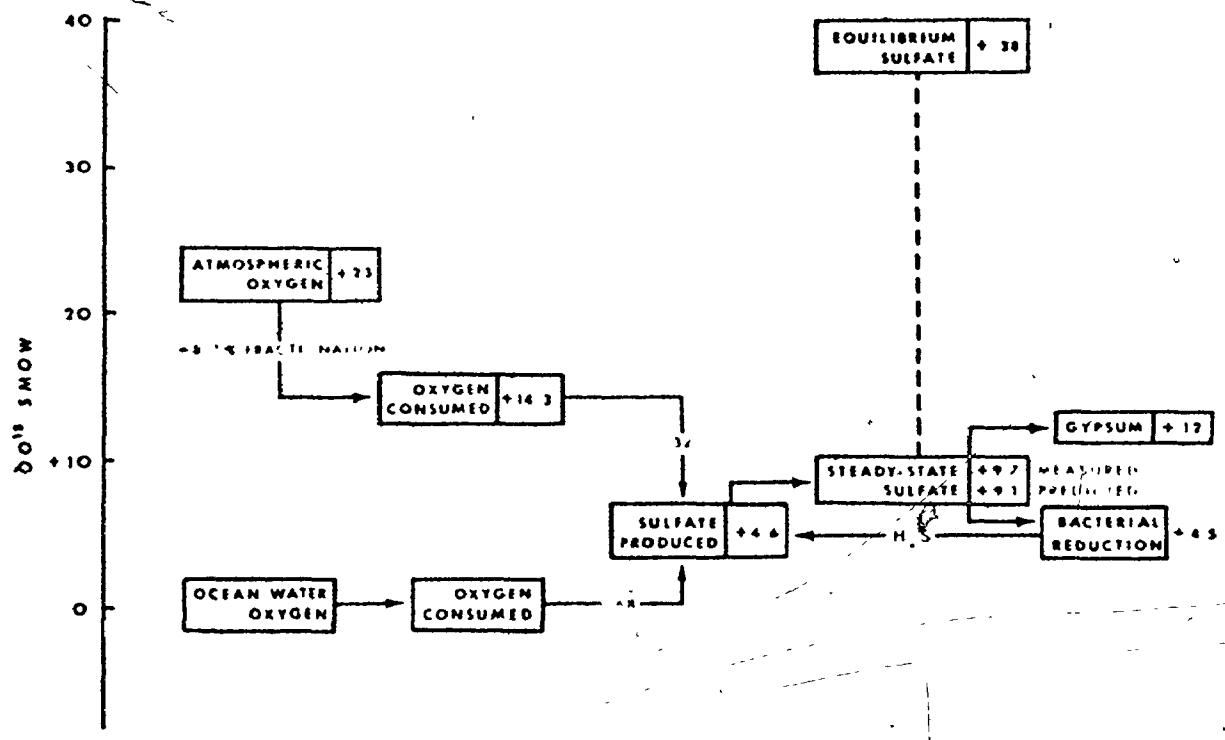


Figure 3-1: Steady State Model for Oxygen Del Value of Seawater Sulphate (from Lloyd, 1968)

Additional data relevant to these questions has come from analyses of interstitial waters obtained on Leg XV of the JOIDES project (Lloyd, 1973, in Volume XX of the Initial Reports). Waters extracted from intervals of core drilled in the Venezuelan Basin (Site 149) showed roughly constant sulphate concentration (2000 to 2500 ppm) and oxygen del value of sulphate (+9.7 to 11.9‰). This sediment section represents about 40 million years deposition. In the prevailing pH range (Geiskes, 1973), 6.9 to 7.8, the age of the oldest part of the core equals about 2500 half times of exchange. Site 148 (at the edge of the Aves Ridge) has more rapid deposition - the 250 metres cored represents about 6 million years accumulation. The sulphate concentration in this core decreases with depth, indicating progressive bacterial sulphate reduction. The oxygen isotope composition does not vary monotonically but increases from +13‰ to +26‰ in the first 50 metres, and decreases to +16‰ in the next 40 metres. The turnaround to lighter values with depth is puzzling. Lloyd's (1973) diagram showing sulphate concentration and  $\delta^{18}\text{O}$  of sulphate is reproduced here as Figure 3-2.

These results contradict the earlier experimental results of Lloyd (1968) in the following way. If exchange between sulphate and water does take place, then the equilibrium value for oceanic sulphate must be +9.5‰ to +10‰ (Site 149, Venezuelan Basin). Alternatively,

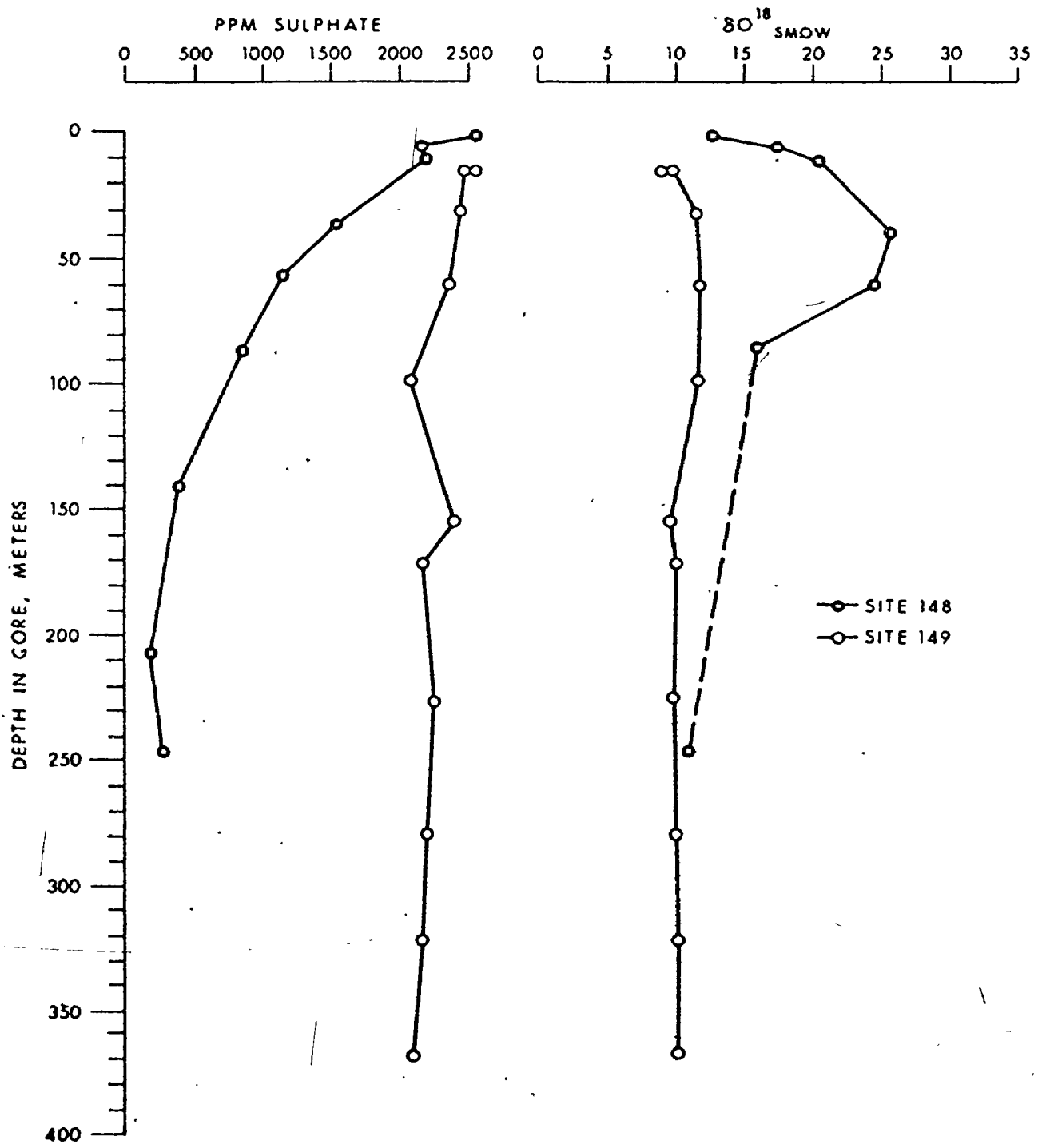


Figure 1. Sulfate concentration and  $\delta O^{18}$  values for interstitial waters, Sites 148 and 149.

Figure 3-2: Concentration and Oxygen Del Values of Sulphate Dissolved in Interstitial Waters (from Lloyd, 1973)

it may be concluded that exchange does not take place under these conditions. The latter possibility is supported by the data of Lawrence (1973) on the oxygen  $\delta^{18}\text{O}$  value of the porewaters. The  $\delta^{18}\text{O}$  of water varies by about 3‰, without correlative shifts in  $\delta^{18}\text{O}$  of sulphate.

One as yet unexamined process that may affect the oxygen isotope composition of sulphate is sulphate reduction during primary marine production. A crude calculation, outlined in Table 3-1, suggests that the flux of sulphur in the biomass is greater than the river flux. The large error inherent in this estimate does not permit a clear characterization of the quantitative importance of the plant flux. It is apparent that the plant flux is at least comparable to the river flux and may dominate it. It is not known what the composition of sulphate generated by this process is, nor are the mechanisms well defined. (Note that this flux will little affect the sulphur isotope composition; for sulphur it may be considered a closed loop.)

#### Marine Evaporite Oxygen Isotope Geochemistry

In the marine evaporite regime, the other important parameter in the sulphate system is the isotope fractionation in crystallization. Lloyd (1968) has reported  $\Delta^{18}\text{O}$  values of +2‰ (gypsum heavier than solution sulphate) for crystallization experiments and an average  $\Delta^{18}\text{O}$  of +3.6‰ for gypsum and brines from marine evaporating pans.

Table 3-1: The Flux of Sulphur in the Biomass

## (A) BIOMASS FLUX (consider only phytoplankton)

Net primary production (gross minus respiration)  
 =  $16 \times 10^9$  tons C/year ( $\pm 10\%$ )  
 (Koblentz-Mischke, et al 1970)  
 =  $1.33 \times 10^{15}$  moles C/year

Dry phytoplankton contains 50% C ( $\pm 10\%$ )  
 (Strickland, 1966)

Dry phytoplankton contains 1.15% S ( $\pm 10\%$ )  
 (Goldhaber and Kaplan, 1974)

Primary sulphur production  
 =  $1.15 \times 10^{13}$  moles S/year ( $\pm 40\%$ )

(B) RIVER FLUX =  $4 \times 10^{12}$  moles S/year ( $\pm 5\%$ )

(A/B) BIOMASS FLUX/RIVER FLUX

=  $2.9 \pm 1.3$   
 = 1.6 to 4.2

Analyses of the oxygen isotope composition of sulphate from marine evaporites have been published by Solomon et al (1971), Claypool et al (1972), Pilot et al (1972) and Sakai (1972). A summary of their results is presented in Table 3-2 and Figure 3-3.

Claypool et al (1972) have stated that the oxygen isotope composition of seawater sulphate is about 3.5% lighter than the values shown in Table 3-2 (second column). Although there is fair correlation between different workers, I would emphasize the paucity of data and the narrow total range of variation. There is some suggestion of characteristic compositions for each geological period, notably the Permian, but more data and a better systematic understanding are required to establish a pattern analogous to the secular variation of seawater sulphate sulphur.



Table 3-2: Literature Values of Marine Evaporite Sulphate  $\delta^{18}\text{O}$ 

<u>Geological Period</u>	<u>1</u>	<u>2</u>	<u>3</u>	<u>4</u>
(Holocene)		13		
Neogene	14	15	13	8-16
Paleogene				12
Cretaceous				9
Jurassic	11		13-17	3
Triassic			12-17	
Permian (U)	10-13	10	10-13	8-10
(M)	15-21		12-16	9-10
Pennsylvanian	15-21			
Mississippian	16-17			
Devonian (U)	17-21	17	14-16	15
(L + M)		12		15
Silurian				11
Ordovician				16
Cambrian	12-22	13	15	10-13
(Proterozoic)	12-23	14-17		13-25

1 - Solomon et al. (1971)3 - Pilot et al. (1972)2 - Claypool et al. (1972)

4 - Sakai (1972)

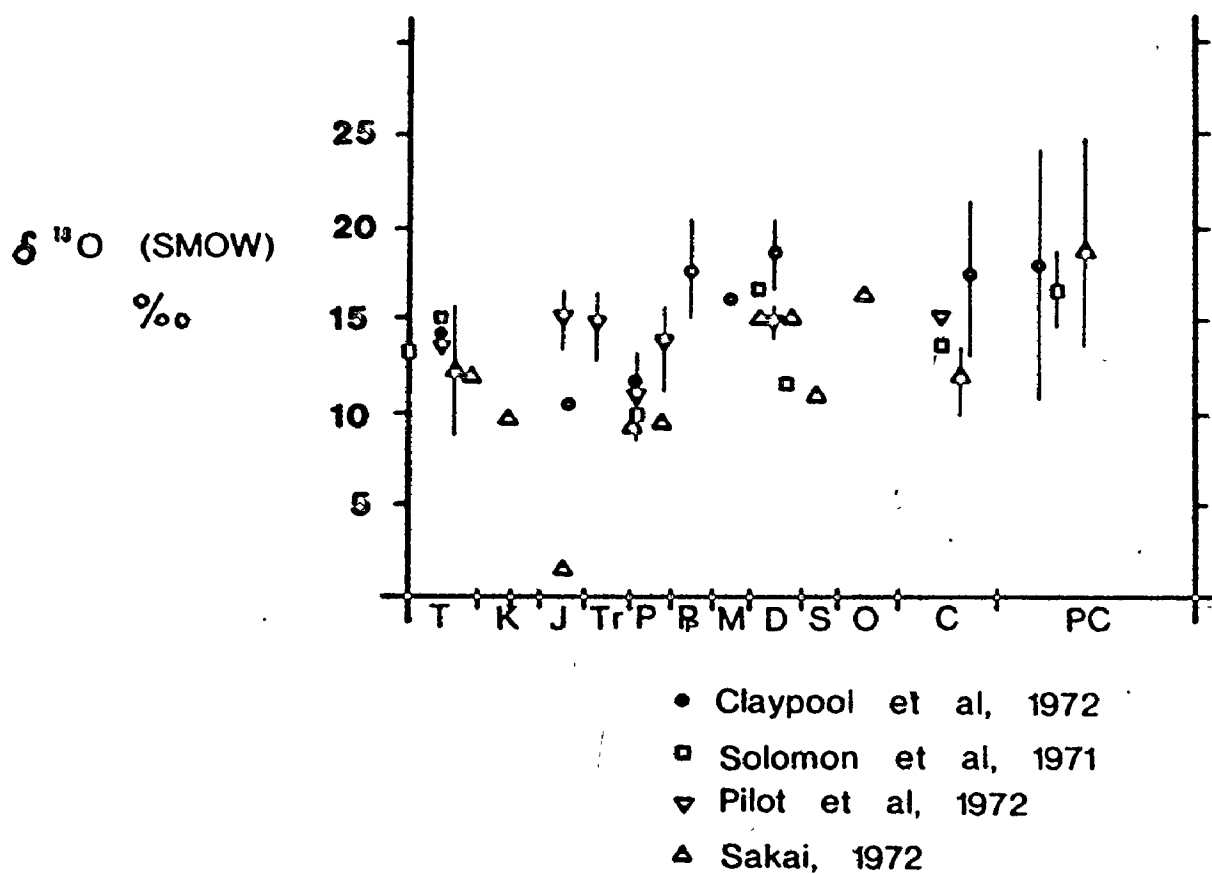


Figure 3-3: Literature Values of Oxygen Del Values of Marine Evaporite Sulphate versus Geological Time

## THE STABLE ISOTOPE GEOCHEMISTRY OF SALINE WATERS

The study of the oxygen isotope composition of sulphate is important in part because it may be possible to relate changes in  $\delta^{18}\text{O}$  of sulphate to changes in  $\delta^{18}\text{O}$  of water. If sulphate does equilibrate with water on a long term average (as suggested by Longinelli and Craig, 1967), and subsequently preserves a  $\delta^{18}\text{O}$  value determined by the equilibrium fractionation, then analyses of marine sulphate oxygen from ancient evaporites would give an independent estimate of the oxygen del value of seawater. Paleotemperature studies based on carbonate have assumed the constancy of seawater oxygen, but other studies, notably those on cherts (Perry and Tan, 1972; Chase and Perry, 1972; Knauth, 1972), suggest that the  $\delta^{18}\text{O}$  of seawater may have varied. Another possibility is that sulphate does not exchange with water at all under the prevailing conditions. In that case, if the mechanism of formation of sulphate involves seawater oxygen and is known, then  $\delta^{18}\text{O}$  of sulphate may furnish information about  $\delta^{18}\text{O}$  of the water present at the time of sulphate formation.

There are at least two important factors that affect the oxygen del value of water in brines: surface evaporative processes, and the removal of water of crystallization in such hydrated minerals as gypsum ( $\text{CaSO}_4 \cdot 2\text{H}_2\text{O}$ ).

## Evaporative Processes

Modern seawater has a composition close to that of SMOW (0‰). In the evaporation of water, the light species,  $H_2^{16}O$ , enters the vapour phase more rapidly than the heavy species,  $H_2^{18}O$  (in the same way,  $H_2O$  enters more rapidly than DHO), and will enrich the liquid in the heavier isotopic molecules. This process does occur; the vapour generated over the oceans is carried to the continents and is dumped as rainfall. Thus meteoric water is considerably lighter than SMOW; its isotopic composition depends on latitude, elevation, and temperature of precipitation (Dansgaard, 1964). The process of evaporation is approximately balanced by the return of light river water to the oceans. As the oceans themselves are mixed very rapidly (about 700 years), the present composition can be regarded as a steady state value.

There are areas that receive very little rainfall, and in them restricted bodies of water may experience high net evaporation with only intermittent replenishment from ocean water (for example, by unusually high tides, or storm-driven flooding). In such cases, it might be expected that the isotope composition would be driven toward heavier and heavier values as the salinity increases. Lloyd (1966) has shown that the oxygen isotope composition of saline waters does not in fact get heavier than about +6‰ (Figure 4-1). For some very saline brines, the oxygen  $\delta$  value of the water decreases with increasing salinity.

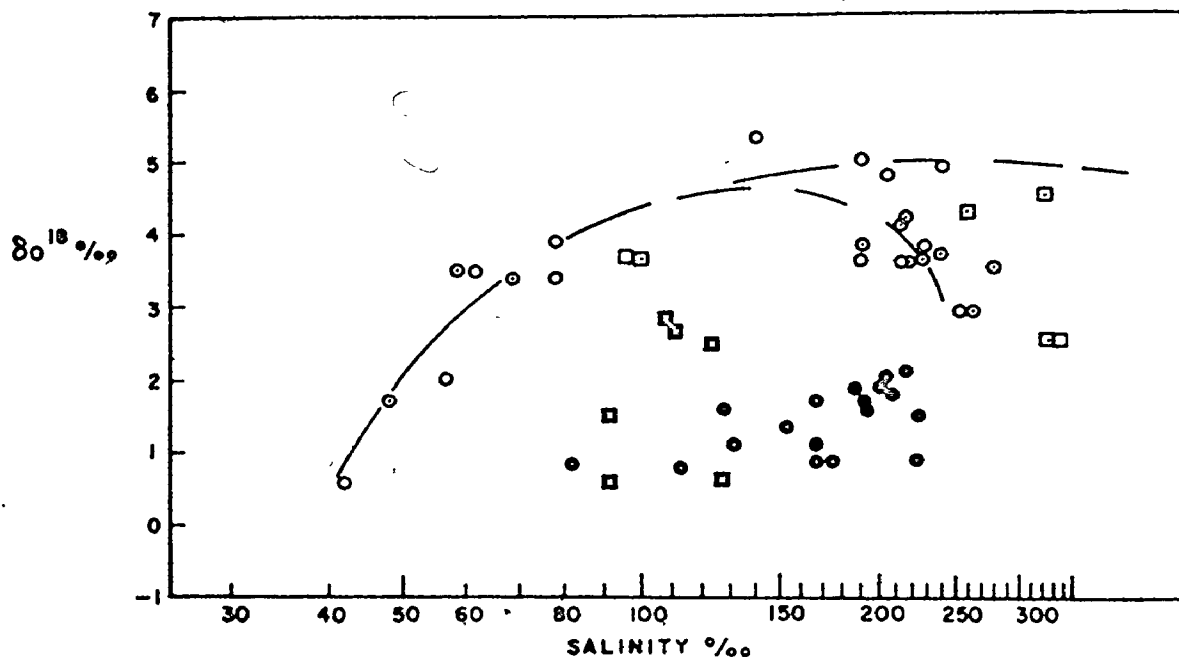


Fig. 6.  $\delta O^{18}$  versus salinity for natural brines: ○—Persian Gulf pit samples, ●—Bonaire samples, □—Inagua salt pond samples, ■—Inagua pit samples.

Figure 4-1: Oxygen Del Values of Water Versus Salinity  
(from Lloyd, 1966)

Lloyd (1966) interpreted these results in terms of competition between the kinetic effect that tends to enrich the brine (the forward flow), and atmospheric exchange that tends to lighten it (the back flow). He considered that these competing mechanisms are controlled by the salinity and by the atmospheric humidity.

Sofer and Gat (1973, and 1975) have confirmed the earlier results, and extended them to include deuterium/hydrogen variations as well. They distinguished between the isotope activity ratio and the isotope concentration ratio in a solution. Most water oxygen isotope analyses are performed by the method of equilibrating the unknown water with carbon dioxide (Epstein and Mayeda, 1953) and measuring the  $\delta$  value of the carbon dioxide. This provides a measurement of the activity ratio of  $\text{H}_2^{18}\text{O}/\text{H}_2^{16}\text{O}$ . Because certain dissolved species, such as  $\text{Mg}^{++}$ , acquire hydration spheres that preferentially incorporate  $\text{H}_2^{18}\text{O}$ , the activity ratio measured in this way is less than the concentration ratio of the two species. The hydrogen gas for D/H analyses is commonly prepared by total extraction in a uranium furnace and the D/H ratio is measured directly. These analyses are a measure of the isotope concentration ratio. Sofer and Gat (1973) have developed an empirical formula to convert oxygen activities to concentration ratios utilizing cation ( $\text{Mg}^{++}$ ,  $\text{Ca}^{++}$ ,  $\text{K}^+$ ,  $\text{Na}^+$ ) abundances, and Truesdell (1974) has extended our knowledge of these effects to higher temperatures ( $275^\circ\text{C}$ ). Sofer and Gat (1975) suggest that activity ratios best delineate surface

evaporative processes, but that concentration ratios facilitate the recognition of the origin of brines (their example: those formed by the solution of anhydrous evaporite deposits).

### Hydration Water

Fontes (1966), Gonfiantini and Fontes (1963), and Sofer (1975) have studied the isotopic composition of the water of crystallization of gypsum. Fontes (1966) reported that the hydration water oxygen  $\delta$  value was heavier than that of the solution water by 4‰. As Gonfiantini and Fontes (1963) pointed out, gypsum is readily dehydrated and most ancient gypsum may have experienced several hydration/dehydration cycles. The water of crystallization from this gypsum would reflect the last (meteoric) water with which the mineral had interacted. Fontes (1966) gives examples of Recent gypsum with heavy water of crystallization ( $\delta^{18}\text{O} = +7\text{‰}$ ) that he interprets to be primary (from heavy saline brines), and also examples of ancient gypsum with much lighter hydration waters that he considers to have originated from meteoric waters.

## GENERAL ANALYTICAL PROCEDURES

Three isotopic ratios were measured in the course of this study:  $S^{18}O_4^{--}/S^{16}O_4^{--}$ ,  $^{34}SO_4^{--}/^{32}SO_4^{--}$ , and  $H_2^{18}O/H_2^{16}O$ . Figure 5-1 illustrates the steps involved in the combined isotopic analysis of sulphate, and Figure 5-3 shows those for the oxygen isotope analysis of water or brine. The principles of these methods and their operating characteristics are briefly summarized in this chapter; details of the techniques may be found in unpublished Technical Memos of the Department of Geology, McMaster University (Olson, 1973; Coomer and Olson, 1974).

### Mass Spectrometry

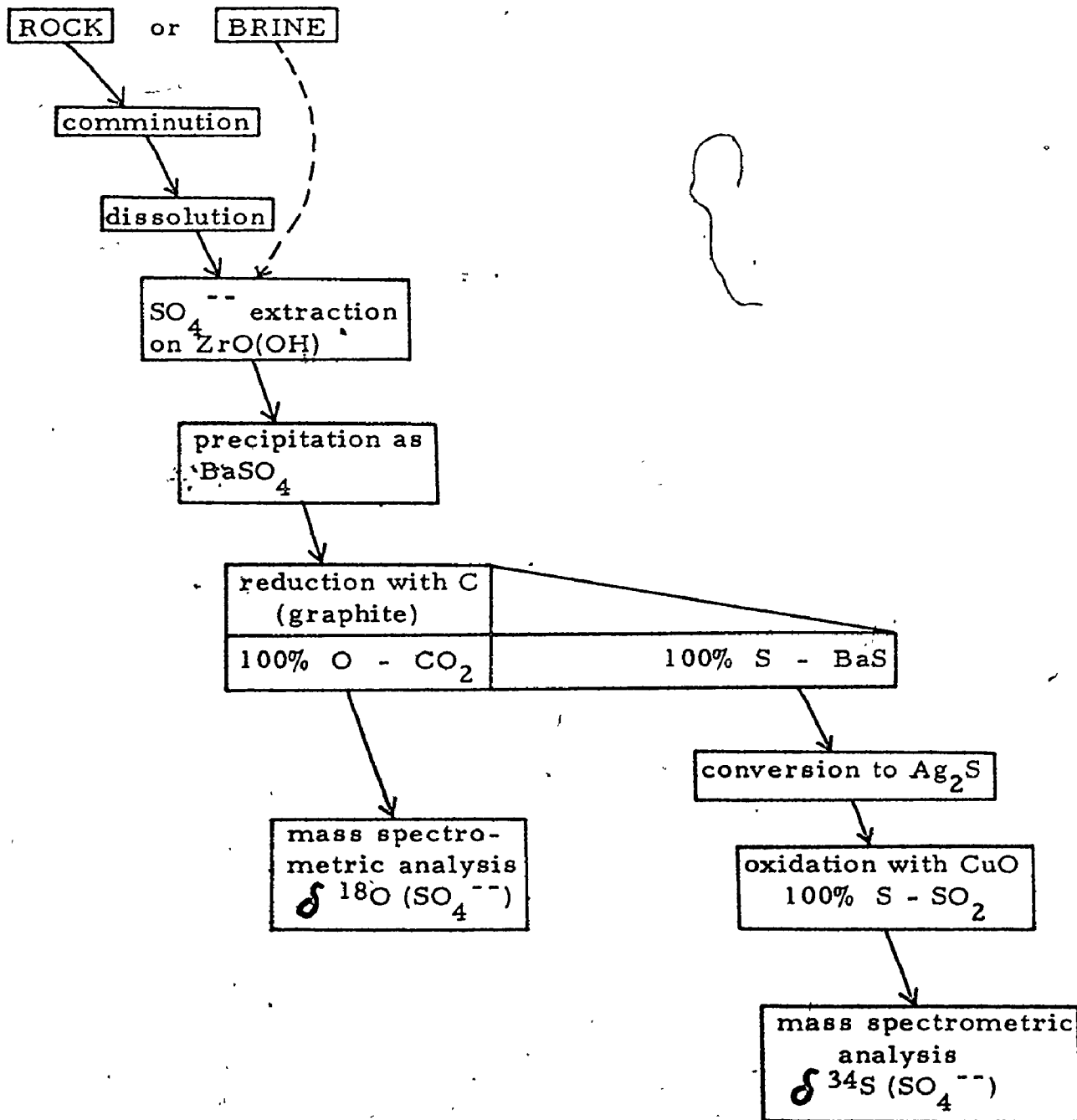
The mass spectrometer used for all of the stable isotope analyses in this study is a standard Nier-type gas source mass spectrometer. It is a  $90^\circ$  sector, 6 inch radius double collecting instrument with McKinney-type valves for rapid switching from sample gas to standard gas. A final correction to the ratio of sample to standard is made by comparing their respective traces on a strip chart recorder.

### Sulphate Extraction on Anion Exchange Resin

Gypsum or anhydrite is crushed and dissolved in distilled water,



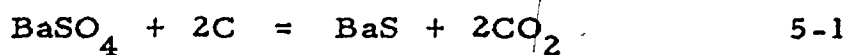
Figure 5-1: Flow Scheme for Combined Oxygen and Sulphur Isotope  
Analysis of Sulphate



after which the insoluble matter is filtered out. The sulphate anions are absorbed from the solution (or from a brine) onto a hydrous zirconium oxide ( $ZrO(OH)$ ) column at low pH. The column is then eluted with 1N NaOH and the sulphate is precipitated as barium sulphate. This method was developed by Cortecci and Longinelli (1968) for extracting sulphate from rainwater. It was applied here because it gives quantitative extraction and maximum purity. It has been found that the isotopic reproducibility is enhanced by the use of anion exchange instead of straight-forward precipitation of barium sulphate in the original filtered solution (Schwarcz, personal communication). Both the weight of insoluble matter and the weight of sulphate determined by this method are quantitative; precision is limited by sampling.

#### Graphite Reduction of Barium Sulphate

The barium sulphate is intimately mixed with a tenfold excess of spectrographic graphite, placed in a graphite crucible, and heated to greater than  $1000^{\circ}C$ . At that temperature, carbon dioxide forms by the following reaction:



The heat is supplied by transmitted light from four "focussed" projector bulbs (Olson, 1973). Earlier attempts to use a nichrome resistance furnace (Rafter, 1967) were suspect on the grounds of possible

oxygen isotope exchange between the hot silica and alumina walls and carbon monoxide (see Mizutani, 1971; and Sakai, 1971). Another method, not employed here, that avoids the possibility of exchange is passing an electric current directly through a platinum sample holder (Mizutani, 1971; Sakai, 1971). The present apparatus permits cooling of the walls of the evacuated pyrex tube by a cold air fan as the transmitted light is heating the graphite crucible. Successive reductions of barium sulphate of widely different compositions indicated no "memory effect" (see Figure 5-2).

About 15 to 25 milligrams of barium sulphate (120 to 200 micromoles  $\text{CO}_2$ ) is used for each reduction. The gas evolved is a mixture of carbon dioxide and carbon monoxide. The latter is converted to  $\text{CO}_2$  by glow discharge between two parallel platinum plates.



The gas is further purified by the removal of water vapour and any incondensable gases. The solid residue ( $\text{BaS} + \text{C}$ ) is sealed in a glass ampoule for subsequent sulphur isotope analysis. The net modal yield is 94% and is considered to represent quantitative extraction of oxygen from barium sulphate because about 3% is not transferred from the mortar, and because the manometer may be systematically indicating low yields.

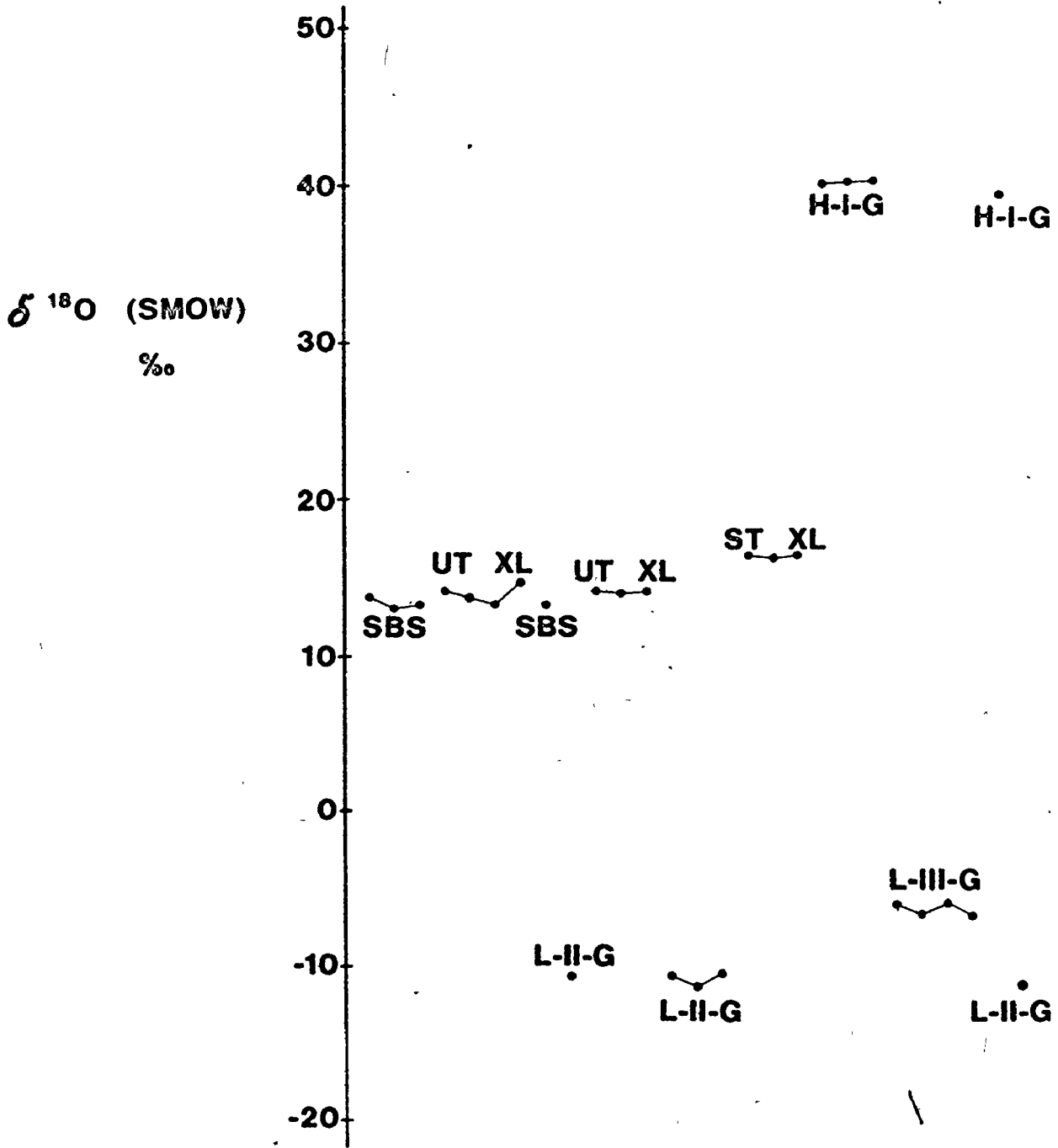


Figure 5-2: Successive Barium Sulphate Reduction by the Transmitted Light Method Testing Isotopic "Memory" in the Product Carbon Dioxide

In the course of the study, Standard Barium Sulphate (SBS), certified reagent grade barium sulphate purchased from Fisher Chemical Company, was analyzed many times to determine the precision of the method. As Table 5-1 shows, it became apparent that the precision on SBS was unacceptable. Isotope shifts originating in the mass spectrometer system were demonstrated (Olson, unpublished results). Accordingly, a 'double standard' system was adopted. The same aliquot of carbon dioxide was run each day, and all analyses on a given day were adjusted by a simple arithmetic correction that would give the second standard gas its accepted (mean) value. However, it is now clear, from comparing normalized and raw  $\delta$  values for different day duplicates, that the best (and acceptable) precision results from using uncorrected  $\delta$  values based on the working standard gas (GCS).

The last value listed in Table 5-1 ( $2\sigma = \pm 0.7$ ) is considered to be the best estimate of the precision of single oxygen isotope analyses of sulphate reported in this study. Comparisons of oxygen  $\delta$  values determined for the same sulphate in different labs gives a measure of the accuracy of the method. Longinelli found  $\delta^{18}\text{O} - \text{SBS} = -11.4\text{‰}$  (Schwarcz, personal communication), which is 1.1‰ lighter than the average shown in Table 5-2. Two isotopic analyses of sulphate extracted from Gulf of Mexico seawater averaged +10.3‰ which is 0.8‰ heavier than Longinelli and Craig's (1967) average of +9.5‰ and 0.6‰ heavier than Lloyd's (1968) average of +9.7‰. The comparability

Table 5-1: Sulphate Oxygen Isotope Precision ( $2\sigma$ )

SBS (70 samples, both methods)	$12.6 \pm 1.8\text{‰}$
SBS (39, resistance furnace)	$12.7 \pm 1.6\text{‰}$
SBS (31, transmitted light oven)	$12.5 \pm 2.1\text{‰}$
Same $\text{CO}_2$ aliquot (311 $\Sigma$ , 39)	$12.3 \pm 1.5\text{‰}$
Same $\text{CO}_2$ aliquot (448 $\Sigma$ , 63)	$13.1 \pm 1.7\text{‰}$
Same day duplicates (152 pairs)	$\pm 0.5\text{‰}^*$
Different day duplicates (normalized to second standard, 40)	$\pm 1.1\text{‰}^*$
Different day duplicates (uncorrected values, 43)	$\pm 0.7\text{‰}^*$

---

\* The variance and the standard deviation of a single analysis may be estimated for k pairs of analyses by the formula:

$$s^2 = \frac{d_i^2}{2k} \quad 5-3$$

In Equation 5-3,  $d_i$  is the duplicate difference for the  $i$ th pair (Bennett and Franklin, 1954).

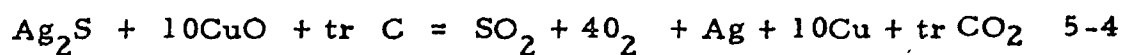
of oxygen del value analyses is further established in Chapters 7 and 8; the apparent tendency to heavier determinations is not seen there.

#### Conversion from Barium to Sulphide to Silver Sulphide

The BaS + C mixture is removed from the glass ampoule, and washed on a filter such that the soluble BaS drips into a solution of AgNO<sub>3</sub>. Silver sulphide (Ag<sub>2</sub>S) precipitates instantly; it is then boiled so that it coagulates. The precipitate is washed free of nitrate and dried in an air oven at 110°C overnight.

#### Oxidation of the Silver Sulphide with Cupric Oxide

The silver sulphide is mixed with a fourfold excess of cupric oxide (CuO) and put in a 6 mm (OD) quartz cylinder closed at one end. The cylinder is placed in one end of a 12 mm (OD) quartz tube which is then evacuated. The other end is heated to 950°C and the mixture is thrust into the hot end; at that temperature the oxidation is complete in 8 to 10 minutes. A mixture of gases is produced; a possible reaction scheme is shown in Equation 5-4.



The CO<sub>2</sub> forms by the oxidation of minor organic impurities. The SO<sub>2</sub> is purified and retained in break seal tubes for subsequent mass spectrometric analysis. The net modal yield is 94% and is considered to

represent quantitative extraction of sulphur from the silver sulphide. Details of the method are to be found in Coomer and Olson (1974); a published version of the technique is given by Fritz et al (1974). Monster (1974) has examined the relative efficacies of cuprous oxide and cupric oxide as oxidizing agents for sulphides.

The working standard gas used in the mass spectrometric determination reported here is tank sulphur dioxide. Although convenient because of its availability, this working standard gas has the drawback of having an unknown sulphur isotope composition. To solve this problem, that is, to develop an equation to convert values relative to the unknown tank gas to those relative to the international standard (CDT), an empirical method was adopted. Silver sulphide standards with a range of composition were obtained from Jan Monster (Chemistry Department, McMaster University). A plot of Monster's values (relative to CDT) versus the raw measurements yields a graphical solution for the conversion formula in the following form.

$$\delta^{34}\text{S (CDT)} = \delta^{66} \text{ (MEASURED)}. (\text{SLOPE}) + \text{INTERCEPT} \quad 5-5$$

The precision of the method is illustrated in Table 5-2. In it, raw measurements on the four silver sulphide standards and the standard deviation estimated by the duplicate difference method for silver sulphides from originally evaporite sulphate are summarized.



Table 5-2: Sulphate Sulphur Isotope Precision  
( $2\sigma$ , for an individual determination)

Standard No.	Number of Determinations	Precision $2\sigma$
2	11	$0.6 \pm 0.5\text{‰}$
6	11	$-7.4 \pm 0.4\text{‰}$
8	10	$5.5 \pm 0.4\text{‰}$
15	10	$18.7 \pm 0.6\text{‰}$
Duplicate difference (same day, 46)		$\pm 0.5\text{‰}^*$
Duplication difference (different days, 24)		$\pm 0.6\text{‰}^*$

---

\* The formula for calculating the standard deviation from pairs of analyses is given in Table 5-1.

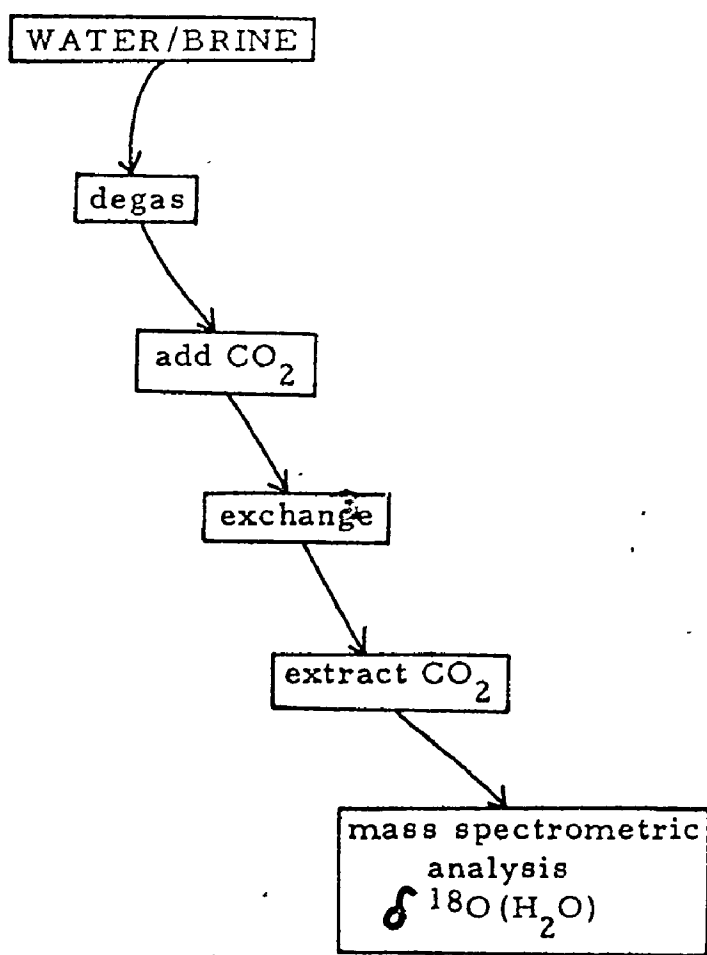
The accuracy of this method was established by analyzing 20 Mississippian evaporites that had been analyzed by Monster using a different sample preparation technique (a steady stream of oxygen oxidizes the sulphide) more than 10 years prior to this study. The mean of 20 analyses agreed to within less than 0.2‰ and almost two-thirds of the individual analyses were within 0.3‰. This excellent agreement attests to the comparability of the results reported here to those of Monster (a considerable portion of all reported measurements).

#### Water-Carbon Dioxide Exchange

This method for the oxygen isotope analysis of water is the standard one described by Epstein and Mayeda (1953). Two millilitres of acidified water or brine are degassed and then permitted to exchange with about half an atmosphere of carbon dioxide in an approximately two cubic centimetre vessel. The carbon dioxide is analyzed on the mass spectrometer after exchange at 25°C for two or more days.

Because the measurements reported here were done on brines with considerable concentrations of dissolved salts, there was some initial concern that isotopic exchange would be affected by hydration spheres, and that the composition measured would be systematically light (Sofer and Gat, 1973; Truesdell, 1974). Preliminary experiments with simple distillation apparatus for removing the dissolved salts resulted in extreme irreproducibility. Synthetic brines prepared with

Figure 5-3: Flow Scheme for Oxygen Isotope Analysis of Brines



water of known isotopic composition and dissolved salts in the appropriate concentration range were analyzed and yielded  $\delta^{18}\text{O}$  values close to that of the starting composition of the water. It was decided thereafter to exchange carbon dioxide with the raw brines containing their full complement of dissolved salts. As Sofer and Gat (1973) have demonstrated, this provides a measure of the activity of  $\text{H}_2^{18}\text{O}$  and  $\text{H}_2^{16}\text{O}$ , and they have presented an equation to convert to the concentration ratio. The isotopic analyses reported in this work have not been so converted (the maximum correction would have been about 0.5‰); they are activity ratios as measured.

The precision of these brine water analyses is given in Table 5-3. It is clear that the standard deviation for paired analyses is substantially less than for duplicates done on different days. It is considered that this deterioration of the precision is due to systematic changes in the mass spectrometer; normalizing these data to a second standard did give better precision. (These normalized  $\delta$  values have been rejected in order to be consistent with the procedures for  $\delta^{18}\text{O}$  of sulphate.)

2  
Table 5-3: Brine Oxygen Isotope Precision ( $2\sigma$ , for single determination)

○ Duplicate difference  
(same day, 29 pairs)  $\pm 0.7\text{‰}$  \*

Duplicate difference  
(different days, 23)  $\pm 2.0\text{‰}$  \*

---

\* The formula for calculating the standard deviation from pairs of analyses is given in Table 5-1.

## THE SABKHA AT ABU DHABI

### Introduction

Abu Dhabi is a sheikdom located along the southern (Trucial) Coast of the Persian Gulf (see Figure 6-1). In the last twenty years, the Persian Gulf has become a "type area" for carbonate sedimentology, and the coastal areas of the Persian Gulf have become "type areas" for carbonate diagenesis and the related formation of evaporite minerals. The coastal flat or sabkha at Abu Dhabi was the site of the first reported occurrence of extensive Holocene dolomite and of significant Holocene anhydrite in a surface environment and studies there have resulted in careful definition of the physical and chemical conditions that accompany the formation of these minerals. The specific applicability of genetic models developed at Abu Dhabi to ancient rocks has not been fully established. It is clear, however, that the coastal sabkha at Abu Dhabi constitutes a rare but important modern analogue for processes that may have occurred many times in the past.

### The Persian Gulf

The carbonate sedimentology and the carbonate diagenesis of the Persian Gulf have been summarized in a recent symposium volume

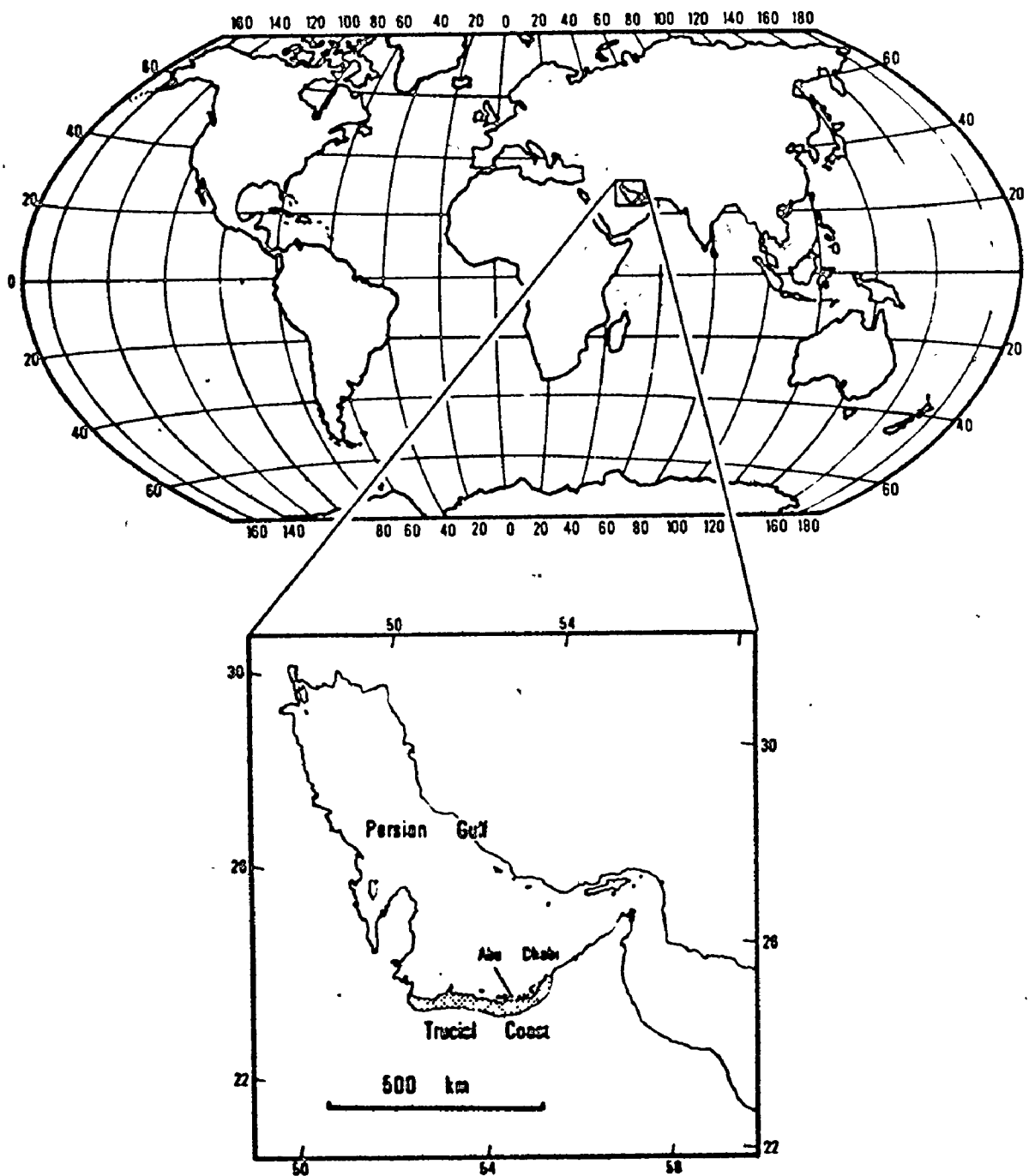


Figure 6-1: The Location of the Persian Gulf and Abu Dhabi

(The Persian Gulf, Purser (ed.), 1973). The following is a highlight summary taken from that source.

The Persian Gulf is large, shallow, and sufficiently restricted to cause elevated salinity (42‰ in the open Gulf; more than 60‰ in restricted lagoons). Some aspects of the climate and physiography of the Gulf are presented in Table 6-1.

The Holocene carbonate sediments of the Persian Gulf have been divided into twelve types by Wagner and van der Togt (1973). "Sands", 'muddy sands', and 'muds' are distinguished by the percentage,  $p$ , of  $< 63\mu$  particles ( $p < 10$ ,  $10 < p < 50$ ,  $p \geq 50$ ). The sediment types are further defined by the nature of the skeletal debris that constitutes the coarse portion of the sediment (for example, coral-algal sand, imperforate foraminiferal-gastropod sand). These sediments are not distributed symmetrically in the Gulf (see Figure 6-2). No rivers flow into its western half, which is very shallow and deepens only very gradually toward the basin axis. Called the Arabian Homocline (Kassler, 1973), its carbonate sediments are generally finer toward the basin axis, but coarsen locally over bathymetric highs. The eastern side contains considerable detrital material discharged by rivers flowing from the Zagros Mountains (see Seibold et al 1973).


#### Abu Dhabi

The sedimentology and the diagenesis of the carbonate sediments




Table 6-1: The Climate and Physiography of the Persian Gulf

(from Purser and Seibold, 1973)



RAINFALL:	less than 5cm/year
TEMPERATURE:	up to 40°C in summer, 15°C in winter
WIND:	NW <u>shamal</u> winds - winter 7 to 10 (Beaufort Scale) - summer about 0
LENGTH:	1000 km
WIDTH:	200 to 300 km
MEAN DEPTH:	35 m



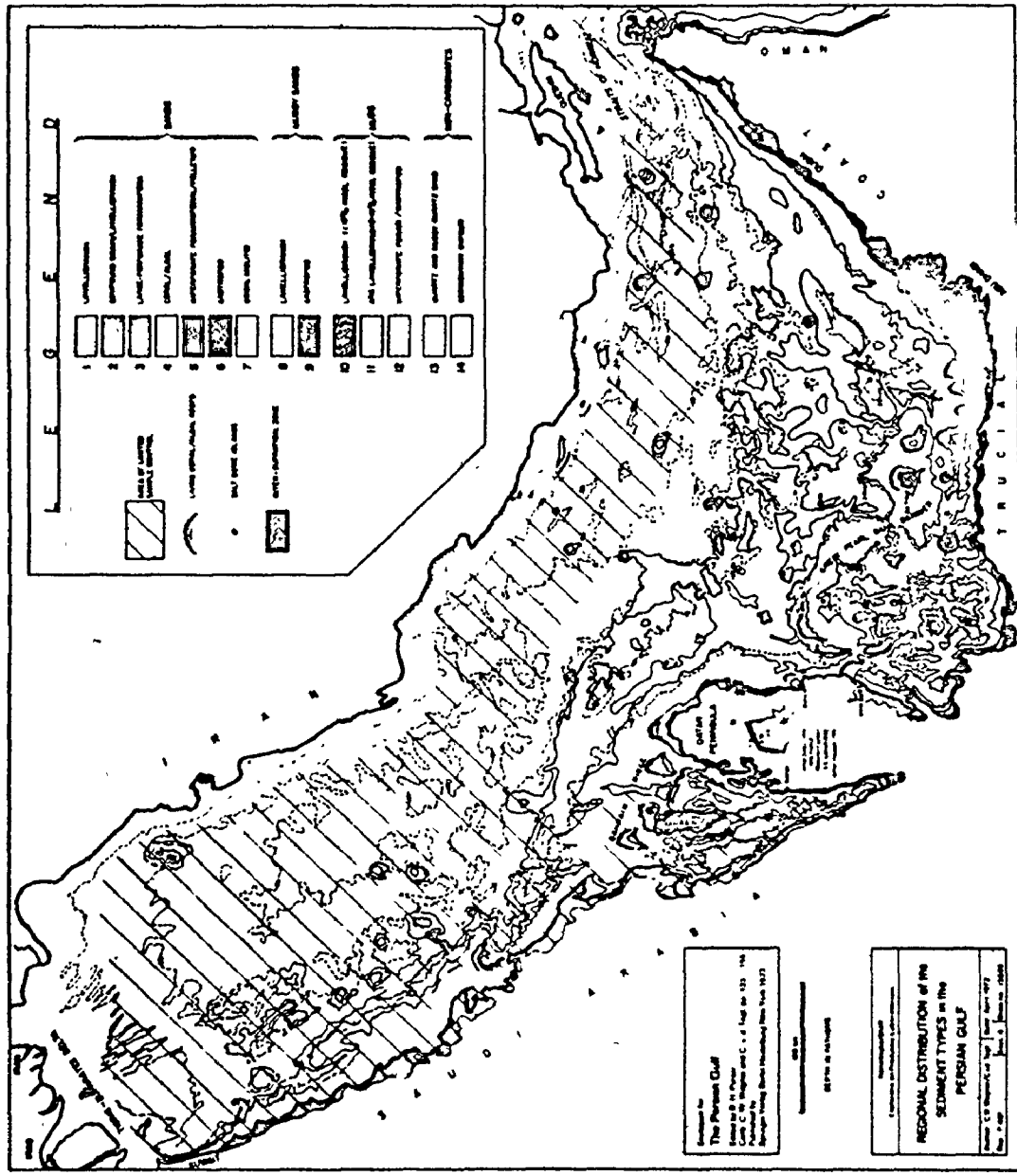


Figure 6-2: Sediment Distribution in the Persian Gulf (from Wagner and van der Togt, 1973)

at Abu Dhabi are a result of the interplay of many factors: the organic production of skeletal parts (as in the open Gulf), the offshore bathymetry, the topography of the coastal sabkha, the climate, and the slowly decreasing sea level. It should be emphasized that the processes seen at Abu Dhabi can be regarded as the extension of those processes prevalent in the Persian Gulf to the particular physiography of the offshore barrier complex and the coastal sabkha.

The Abu Dhabi coast faces the prevailing shamal winds, and might be expected to have relatively high wave energy levels and little deposition. This is the case for coastal parts east of Abu Dhabi (Purser and Evans, 1973), but an offshore partially submerged ridge called the Great Pearl Bank Barrier (Purser and Evans, 1973) shields the shoreline at Abu Dhabi. Where the Great Pearl Bank is emergent, coral-algal reefs have developed islands with downwind tails of coral-algal debris. In some cases, these tails have formed tombolos, further restricting circulation behind the Great Pearl Bank. As a result of this restriction and high net evaporation, the salinity in the lagoons may exceed 60‰, almost twice that of normal seawater.

The combination of the offshore barrier complex and the one metre drop in sea level (Patterson, 1972) have resulted in a prograding shoreline and a regressive sequence of intertidal and supratidal sediments. Radiocarbon dating of total carbon from carbonate sediments indicates that the highest Holocene shoreline occurred about 4000 to 5000 years

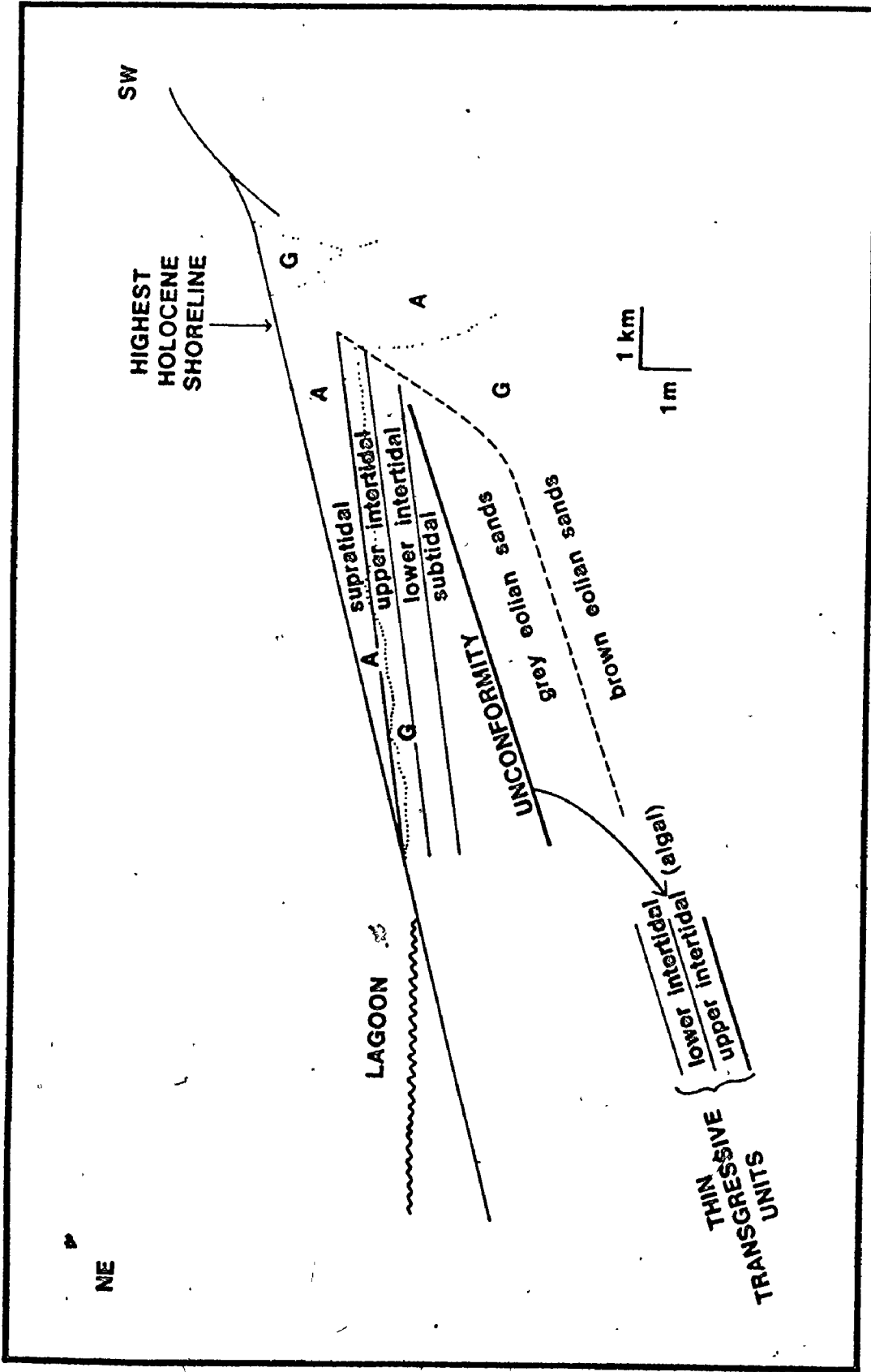


Figure 6-3: Abu Dhabi Sabkha Sediment Profile (from Patterson, 1973)

Table 6-2: Stratigraphy of Sabkha Sediments, Abu Dhabi  
(from Patterson, 1972)

Supratidal Facies:

0-100 cm, wedge of detrital sediments thickening inland from the shoreline. Dominated by anhydrite in inland areas; may be magnesite rich at base.

Upper Intertidal Facies:

60 cm, commonly an algal facies but coarse skeletal sands or gravels are high energy equivalent; anhydrite may be present in upper part; gypsum often abundant; intensively dolomitized in some areas. Full regressive development.

Lower Intertidal Facies:

60 cm, cream muddy pellet sands with abundant cerithids; large gypsum crystals common; fairly intensively dolomitized in some areas. Full regressive development.

Subtidal Facies:

0-3000 cm, grey-brown, peneroplid and lamellibranch rich muddy sands; thickens seaward. Minor dolomitization.

Upper Intertidal Facies:

2-5 cm, algal facies in some places, otherwise mixed pellet and detrital sands. Attenuated transgressive development.

UNCONFORMITY: generally fairly sharp, sometimes burrowed.

Grey Eolian Sands:

50-150 cm, grey, cross-bedded eolian sands, original iron oxide films around grains now present as iron sulphide minerals.

Brown Eolian Sands:

thickness unknown (probably about 5-10 m), brown, cross-bedded eolian sands with some gypsum.

UNCONFORMITY

Miocene Rocks

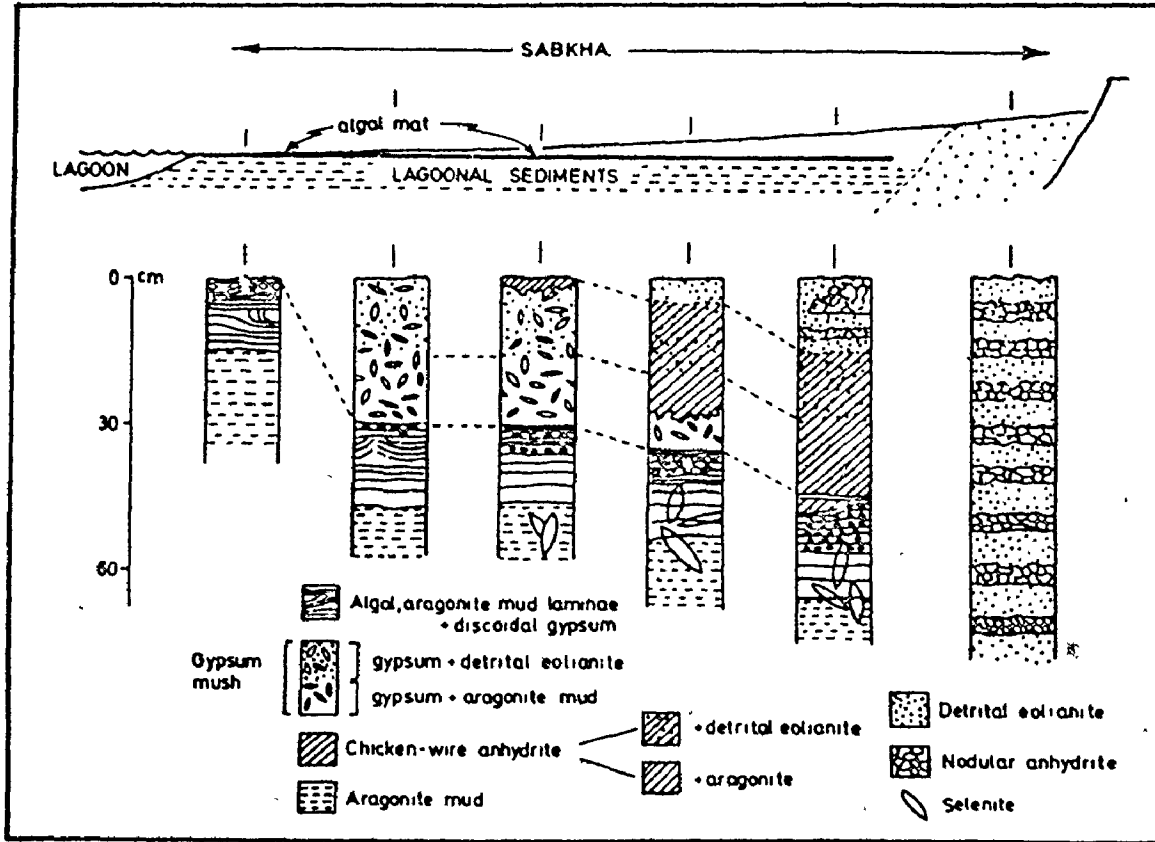


Figure 6-4: Vertical Distribution of Sabkha Sedimentary Facies  
(from Butler, 1970)

before present (Patterson, 1972). Thus a diachronous veneer of sediment, one to two metres thick, has developed on the sabkha (see Figure 6-3). Patterson's summary of the stratigraphy of the sabkha sediment is presented as Table 6-2.

Butler (1970) has also described the sediments of the coastal sabkha at Abu Dhabi. His summary lithological section is reproduced here as Figure 6-4. (Note the distribution of gypsum and anhydrite.)

Butler (1969, 1970) has carefully described not only the nodular aspect of the anhydrite, and the 'chicken-wire' appearance of closely packed anhydrite nodules, but also such structures as enterolithic diapirs that he suggests are diagnostic of the supratidal environment. Subsequent recognition of some comparable features in ancient evaporites that are intimately linked with deep water carbonate rocks, notably the Otto Fiord Evaporite (Davies and Nassichuk, 1975, Dean et al , 1975, Wardlaw and Christie, 1975) has undermined the diagnostic power of these textures.

Butler's (1970) facies map of the sabkha sediments is presented here as Figure 6-5; the facies descriptions in Table 6-3. In general, his facies conform to the pattern described. Butler suggests that the facies are controlled by the flooding frequency; higher numbered facies are flooded less frequently. The irregular, sinuous facies boundaries on Figure 6-5 are noteworthy; the complexity of the sabkha sediments and the importance of the flooding frequency will be apparent in the

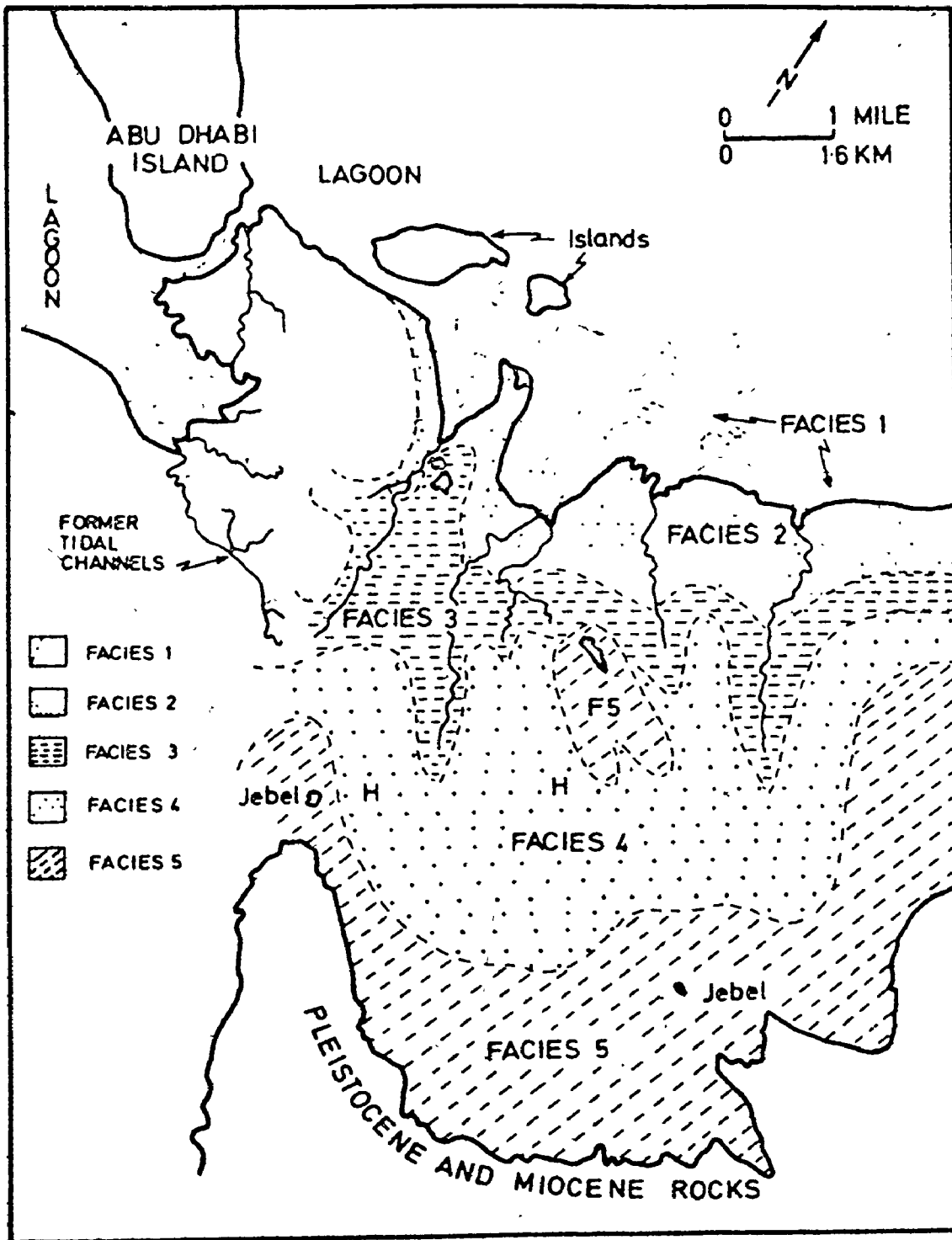


Figure 6-5: Areal Distribution of Sabkha Sedimentary Facies (from Butler, 1970)



Table 6-3: Summary of Sabkha Evaporite Facies from Butler (1970)

FACIES 1	upper intertidal zone laminated mats of blue-green algae, small (<1mm) gypsum crystals.
FACIES 2	surface mush of displacement gypsum (up to 2 cm long); some anhydrite flooding monthly or less frequently.
FACIES 3	extensive dolomitization; anhydrite replacing gypsum; flooding less than monthly.
FACIES 4	flooding as little as once every 5 years, chicken-wire anhydrite, anhydrite nodules diapir dike structures in anhydrite
FACIES 5	pleistocene aeolianites; no lagoonal or algal mat sediments; seams of anhydrite nodules; alteration to gypsum.

interpretation of the isotopic analyses presented in Chapter 7.

### Water Chemistry

The coastal sabkha is extremely flat, and even though it is sheltered, occasional wind-driven tides do flood large portions of its surface. This flood recharge (Butler, 1969) supplies concentrated brine that is subjected to further evaporation on the sabkha. It is sporadic, and is not distributed evenly, as it is controlled locally by relict tidal channels.

Patterson (1972) has made a thorough study of the hydrology and carbonate diagenesis of the sabkha at Abu Dhabi. He has measured the chemistry of the interstitial waters from the shoreline across the sabkha and extending to the groundwaters of the adjacent landward regime.

The chloride ion concentration increases sharply in the intertidal zone, reflecting increased salinity due to evaporation. The chloride ion concentration is roughly constant across most of the sabkha, this 'chloride plateau' being controlled by the solubility product of halite. In the landward portions of the sabkha, the chloride ion concentration decreases as dilute continental water seeps into the sabkha sediment.

The dissolved sulphate concentration trends are the opposite of the chloride ion concentration trends; the minimum ( $\text{SO}_4^{--}$ ) is in the centre of the sabkha. The concentration of calcium in solution varies reciprocally with sulphate so that the product  $(\text{Ca}^{++}) \cdot (\text{SO}_4^{--})$  is maintained at or near the solubility of gypsum and anhydrite. To some

extent the solubility of celestite ( $\text{SrSO}_4$ ) is also important.

Patterson (1972) has suggested that the origin of the brines may be distinguished by the  $\text{K}^+/\text{Br}^-$  ratio. He has shown potassium to be conservative across the sabkha, and that the original waters, seawater and continental water, differ greatly in their dissolved bromide concentration. A  $m_{\text{K}^+}/m_{\text{Br}^-}$  ratio of less than 25 corresponds to a marine derived groundwater, and Patterson considers that intermediate values delimit a zone of mixing of the two hydrological regimes (see Figure 6-6).

Patterson (1972) has presented a synthesis of the hydrological processes operating on the sabkha (Figure 6-7). Note that the landward regime is thought to be migrating toward the shoreline. The division of the seaward and landward hydrological regimes is considered further in the discussion of the isotopic analyses presented in Chapter 7.

#### Dolomite and Gypsum Formation

The concentration of sulphate dissolved in these interstitial waters increases sharply in the intertidal zone as a result of evaporation. Near the landward edge of the upper intertidal algal zone, the dissolved sulphate concentration decreases from about 200 moles per kilogram of solution to about 10 to 20 moles per kilogram. This decrease coincides with the precipitation of gypsum. Interstitial gypsum formation and the dolomitization of aragonitic sediment transpire simultaneously

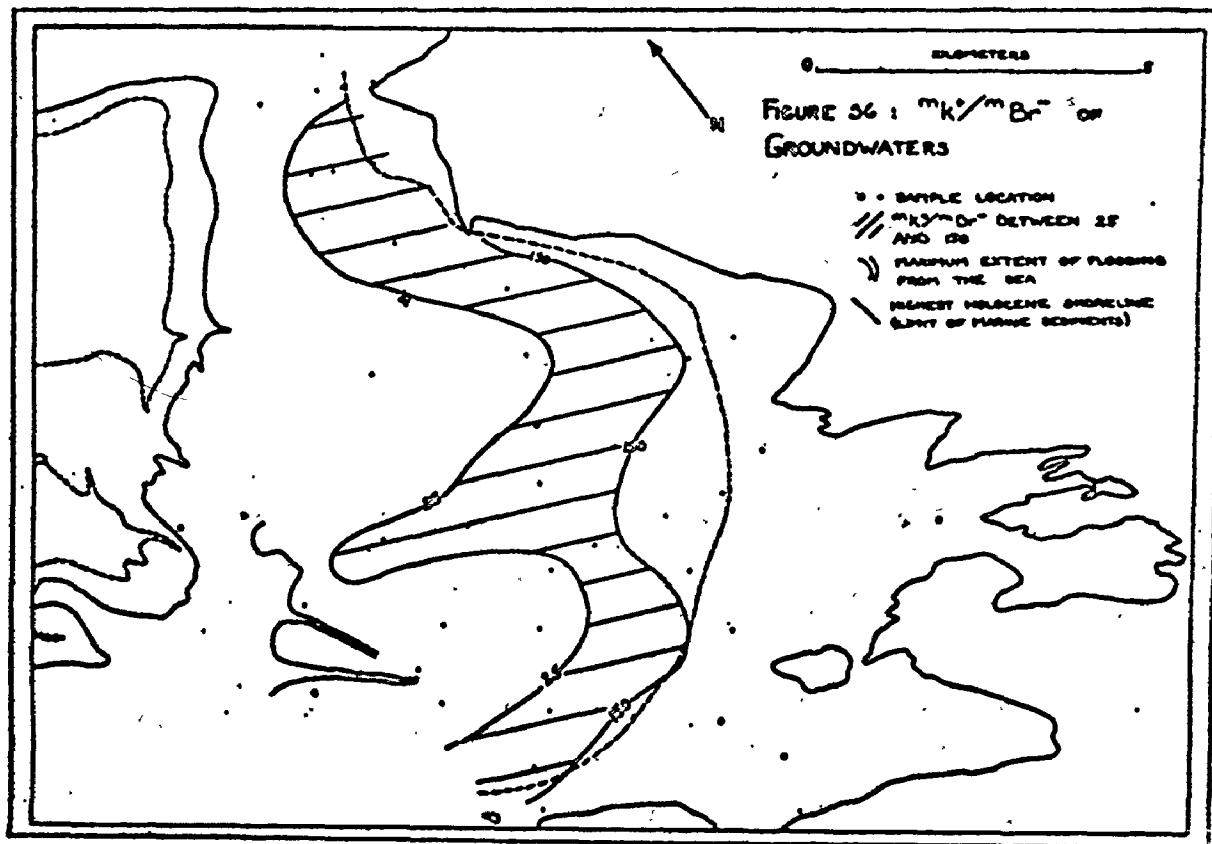


Figure 6-6: Areal Distribution of  $m_K + m_{Br^-}$  ratios of Abu Dhabi Brines (from Patterson, 1973)

# General Hydrologic Framework of Sabkha

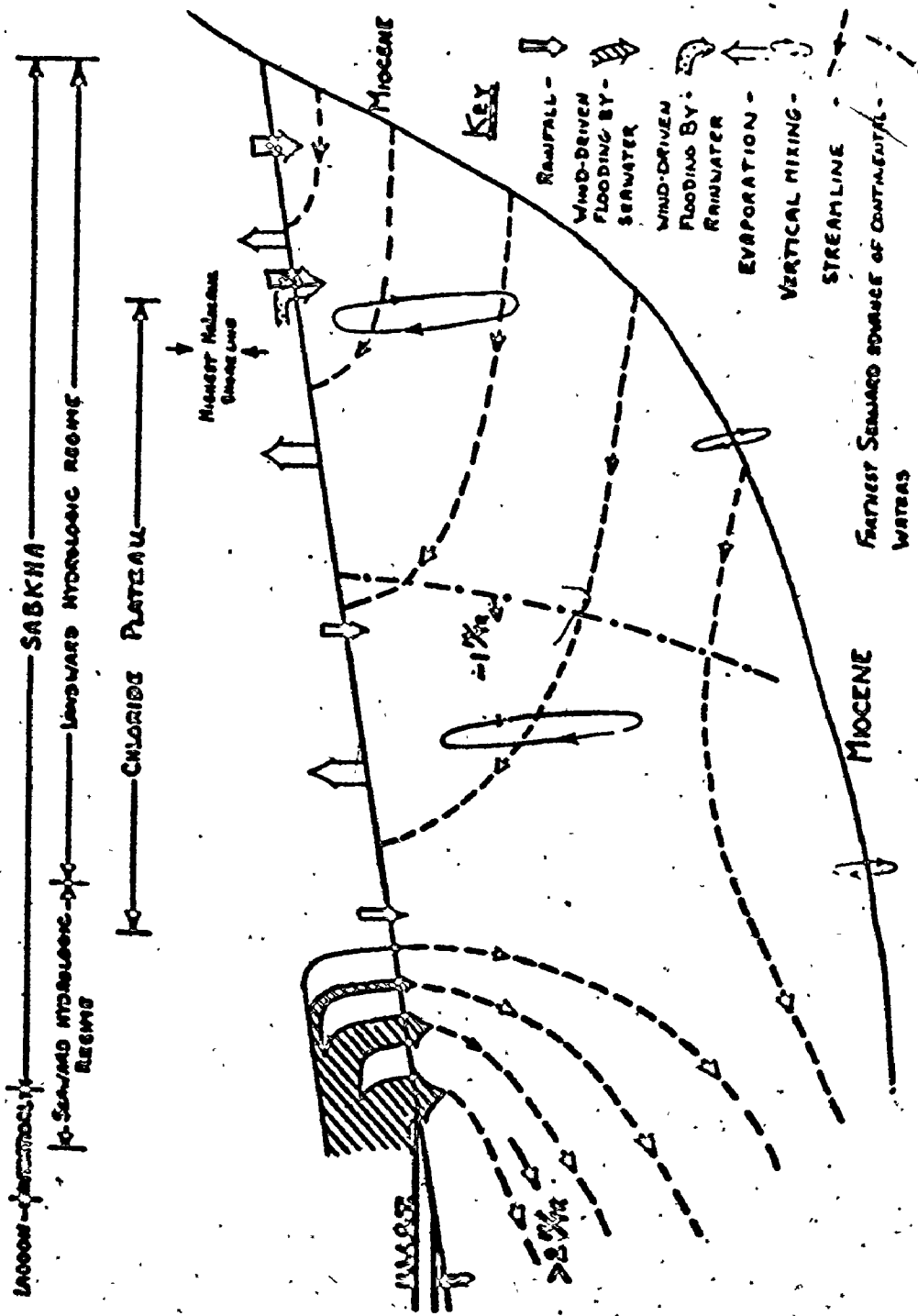


Figure 6-7: General Hydrologic Framework of Sabkha (from Patterson, 1973)

in this zone.

Patterson (1972) has measured the physical and chemical properties of the dolomitizing brines, and he has studied the mineralogy of the carbonate sediment in several detailed profiles at various locations on the sabkha. He has defined an optimum zone of dolomitization, and his summary of the attendant conditions is presented in Table 6-4.

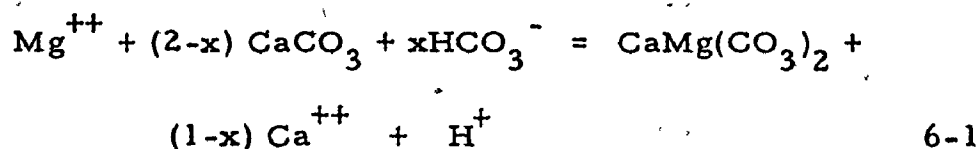
The dolomitization is occurring in a one kilometre wide strip that approximately coincides with the upper intertidal algal zone. The irregular sabkha topography is important in this process too; flood channels extend the zone several kilometres inland. Radio-carbon dating of the dolomite indicates that the dolomite nearest to the present shoreline has formed within the last 500 years (Patterson, 1972).

When aragonitic sediment is dolomitized,  $\text{Ca}^{++}$  is replaced by  $\text{Mg}^{++}$ , and the product  $(\text{Ca}^{++}) \cdot (\text{SO}_4^{--})$  increases. If the product reaches the saturation limit for gypsum at the ambient temperature, gypsum precipitates. This is the dominant mode of primary gypsum formation on the Abu Dhabi sabkha. This diagenetic gypsum formation is to be distinguished from the classical mode in which brines are simply evaporated to the saturation concentration, at which point gypsum precipitates.

Patterson has given the following dolomitization equation.

Table 6-4: Properties of the Dolomitizing Fluids (from Patterson, 1972)

$m_{\text{Cl}^-}/\text{kg}$	3.25 - 3.75
$m_{\text{Mg}^{++}}/m_{\text{Ca}^{++}}$	6 to 22
pH	6.3 to 6.9
Temperature	25 to 40°C
Eh	reducing



The quantity 'x' is the number of moles of bicarbonate supplied by the reduction of sulphate (one mole of sulphate produces two moles of bicarbonate). Patterson has determined that the reaction goes on in a reducing environment; the free oxygen may be depleted by decaying algal debris. He has reported a few measurements of the partial pressure of  $\text{H}_2\text{S}$ ; the values are low but they indicate that sulphate reduction is occurring in the zone of dolomitization.

Patterson attempted to calculate a mass balance for the quantities of dolomite and gypsum present in the sediment. Crude stoichiometry requires that 'x' be greater than zero and less than 0.1. Reduction on this scale might be expected to enrich the residual sulphate in  $^{34}\text{S}$ ; assuming a fractionation of 20‰ reduction of 10% of the sulphate would increase the sulphur del value by about 2‰.

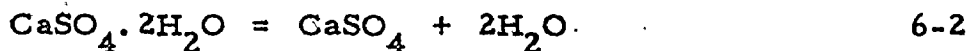
#### Gypsum-Anhydrite Equilibrium

The diachronous aspect of the sediment is reflected in the areal distribution of sulphate minerals on the sabkha. As noted, gypsum is found in the youngest sediment near the present high water strand line. From about one kilometre landward of the present shoreline across most of the sabkha, anhydrite is the dominant sulphate mineral in the



surface sediments. First reported by Kinsman (1966), this anhydrite forms by the dehydration of pre-existing gypsum; it subsequently receives a considerable addition of sulphate from interstitial waters (Patterson, 1972).

Gypsum-anhydrite equilibrium relations have been studied experimentally by several workers (Posnjak, 1940; MacDonald, 1953; Zen, 1965; Hardie, 1967; Blount and Dickson, 1973). Although disagreeing in detail, particularly on the transition temperature at one atmosphere, all of the foregoing concluded that anhydrite is the stable phase at relatively low temperatures (40 to 60°C), but were unable to effect the spontaneous nucleation of anhydrite in the laboratory. Kinsman (1966, 1969, 1974) has demonstrated that the gypsum to anhydrite transition and the reverse transition take place according to the temperature and water activity equilibrium relations suggested by the experimental results, notably those of Hardie (1967). The transition may be written as follows.



$$K_{\text{equil}} = (a_{\text{H}_2\text{O}})^2$$

Thus, reduced activity of water (usually taken as the vapour pressure of water in equilibrium with the solids) favours the formation of anhydrite. Kinsman (1970) has superimposed his field measurements

of temperature and brine concentration (which controls the water vapour pressure) on Holser's (unpublished) phase diagram. That figure, reproduced here as Figure 6-8, indicates that the mineralogical transition occurs under equilibrium conditions. The kinetic barriers to the formation of anhydrite as a primary precipitate are present at Abu Dhabi; all of the anhydrite has a gypsum precursor (Kinsman, 1969; Butler, 1969). In the most landward parts of the sabkha, continental groundwaters increase the water activity and the anhydrite reverts to gypsum.

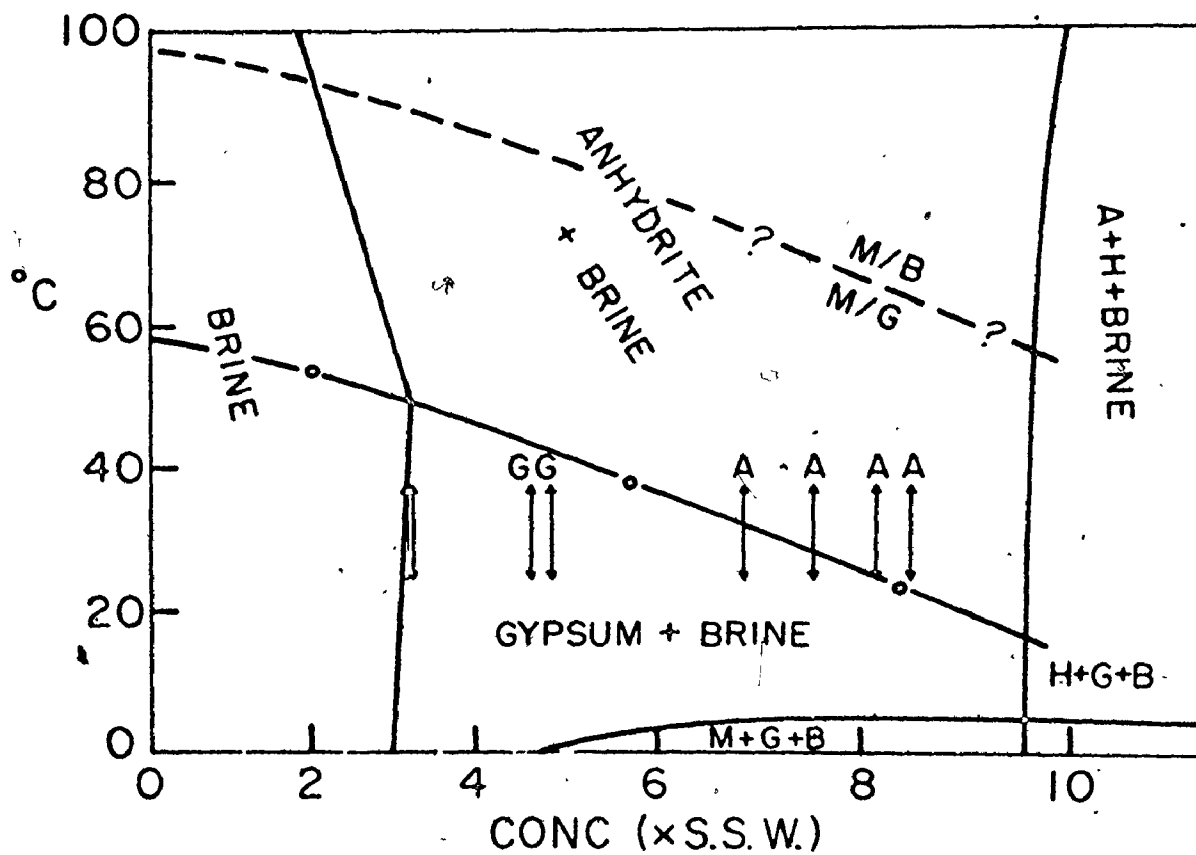


Figure 6-8: Equilibrium Phase Relations for Gypsum and Anhydrite (from Kinsman, 1966)

A = Anhydrite  
 B = Bassanite  
 G = Gypsum  
 H = Halite  
 M/B = Metastable Bassanite

Arrows denote annual temperature range

## STABLE ISOTOPE STUDIES, ABU DHABI SABKHA

### Introduction

Isotope ratio measurements on dissolved sulphate, brine water, and evaporite minerals are presented in this chapter. A general discussion of the nature and probable magnitude of the isotopic shifts caused by processes operating on the sabkha precedes consideration of the data. The following mechanisms are considered: gypsum crystallization, gypsum-anhydrite transitions, sulphate reduction, mixing, evaporation, and secular variation of the sulphate input.

### Crystallization

Isotope fractionations for the crystallization of gypsum have been reported as follows.

$\Delta^{18}\text{O} (\text{H}_2\text{O})$	(hydration water - water) (Fontes, 1966)	+4 to +6‰
$\Delta^{18}\text{O} (\text{SO}_4^{--})$	(crystal - dissolved sulphate) Lloyd, 1968)	+2 to 3.6‰
$\Delta^{34}\text{S} (\text{SO}_4^{--})$	(crystal - dissolved sulphate) (Thode and Monster, 1965)	+1.65‰

Such isotopic differences would be expected if the solid phase is forming

from a coexisting brine. If the fractionation is sustained throughout the depletion of a substantial portion of the initial brine, then the composition of the product crystal (P) and the residual substrate (S) will follow Rayleigh single batch curves. Table 7-1 lists the isotope composition of P and S at successive extents of reaction, for fractionations of 0.999, 0.998 and 0.996 (from Rees, unpublished tables). Figure 7-1 illustrates the change in  $\delta$  value of P and S for a fractionation of 0.996. Note that in each case both  $\delta$  (P) and  $\delta$  (S) decrease from their initial value.

#### Gypsum-Anhydrite Transitions

There are no published accounts of the isotope shifts in sulphate that accompany the mineralogical transitions between gypsum and anhydrite. It might be expected that the fractionations, if any, would be small.

#### Sulphate Reduction

Sulphate reduction is active in the sabkha sediments and it should be manifest as correlated shifts in  $\delta^{34}\text{S}$  and  $\delta^{18}\text{O}$  toward heavier values (Mizutani and Rafter, 1973). However the fractionation is elsewhere known to be highly variable (for both  $^{34}\text{S}/^{32}\text{S}$  and  $^{18}\text{O}/^{16}\text{O}$ ) and therefore difficult to predict. As there is decaying algal material nutrients may be plentiful; therefore small fractionations might be expected (Rees, 1973). Some of the  $\text{H}_2\text{S}$  produced may be oxidized in situ, diminishing the net measured shift in  $\delta^{34}\text{S}$ . The interstitial brines are

Table 7-1: Isotope Composition of Product (P) and Substrate (S) at various extents of reaction for constant fractionation (from Rees, unpublished tables)

% REACTION	Read $\delta(P)/\delta(S)$ (‰/‰)		
	$\alpha = 0.999$	$\alpha = 0.998$	$\alpha = 0.996$
0	-----/0.00	-----/0.00	-----/0.00
1	+1.00/-0.02	+1.99/-0.03	+3.97/-0.05
10	+0.95/-0.11	+1.90/-0.22	+3.78/-0.43
50	+0.70/-0.70	+1.39/-1.39	+2.77/-2.77
90	+0.26/-2.31	+0.52/-4.62	+1.02/-9.26
100	0.00/-----	0.00/-----	0.00/-----

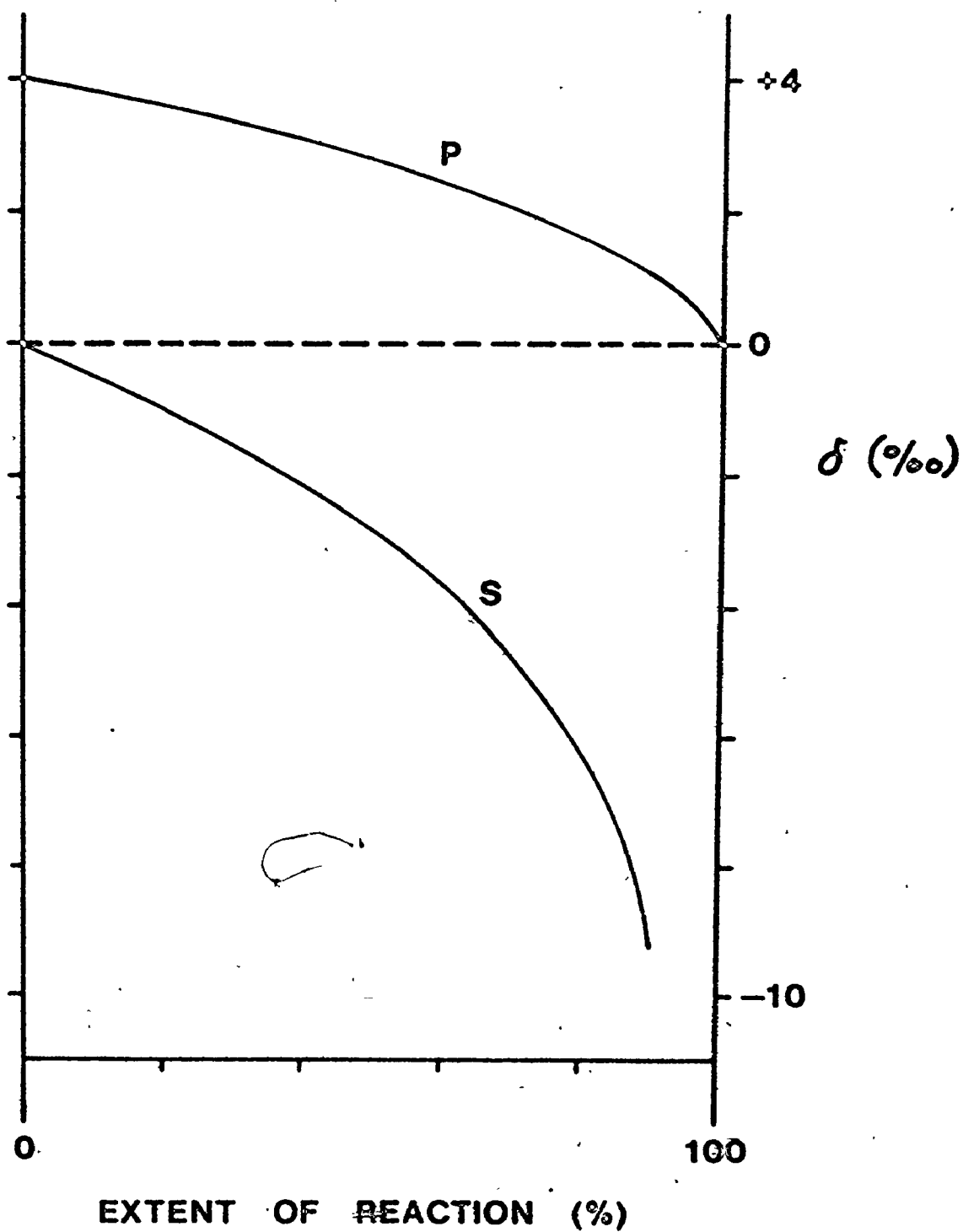


Figure 7-1: Average Isotope Composition for Product (P) and Substrate (S) at various extents of reaction for  $\alpha = 0.996$  (from Rees, unpublished tables)

mixed to some extent, and averaging would further obscure fractionations produced by sulphate reduction.

### Mixing

For the brines, in the absence of other effects, isotopic mixing should be observed in the boundary region between marine-derived brines and continental groundwaters. As will be seen, for the continental groundwaters,  $\delta^{34}\text{S}$  of the dissolved sulphate and  $\delta^{18}\text{O}$  of the water are light, and  $\delta^{18}\text{O}$  of the dissolved sulphate is heavy, relative to the respective parameters in marine brines. The relative masses will determine the actual isotopic shift, and in principle, the relative masses may be calculated from the observed shift. If the brines are in isotopic equilibrium with the solid phases, and if the brine isotope composition is changing due to such mixing processes, then the isotope composition of the coexisting solids ought to be shifting as the mixing and equilibration proceed.

### Evaporation

Evaporation tends to increase the oxygen  $\delta$  value of water up to a maximum of about +6‰ (Lloyd, 1966). It does not directly affect either the sulphur or the oxygen  $\delta$  value of dissolved sulphate.

### Secular Variation in Seawater

If the isotope composition of the sulphate minerals deposited



during the Holocene has not been altered by interactions with the changing hydrological regime, and if there has been secular variation of  $\delta^{34}\text{S}$  and  $\delta^{18}\text{O}$  of dissolved sulphate in Persian Gulf waters, then a profile normal to the shoreline might describe secular variation comparable in principle to the Phanerozoic seawater sulphate sulphur isotope curve but on a much shorter time scale. Patterson (1972) has calculated for a location in the present landward regime of the sabkha, that only one-sixth of the anhydrite in the sediment was primary gypsum from the seaward regime. That estimate is surprisingly low. If the landward regime continues to migrate across the sabkha toward the Gulf in step with the prograding seaward regime, and if the sulphate deposited as anhydrite is ultimately supplied in the proportions suggested by Patterson's estimate, it is clear that small secular changes in the sulphate of the Persian Gulf could not be distinguished with any confidence.

#### Summary of Possible Sabkha Processes

A qualitative summary of the isotopic shifts that may be effected by the processes operating on the sabkha is presented in Table 7-2.

#### Samples

The isotopic analyses reported here were done on samples provided by D. J. J. Kinsman of Princeton University. They were collected in the field in 1969 and 1970, and were obtained for this work at Princeton in 1973.

Table 7-2: Mechanisms that effect Isotope Shifts in the Sabkha Evaporite System

	$\delta^{34}\text{S}$ dissolved sulphate	$\delta^{18}\text{O}$ dissolved sulphate	$\delta^{18}\text{O}$ brine
CRYSTALLIZATION	↓	↓	↓
SULPHATE REDUCTION	↑	↑	—
MIXING WITH LANDWARD REGIME	↓	↑	↓
EVAPORATION	—	—	↑
SECULAR VARIATION	?	?	?

(The arrows show the qualitative change in isotope composition that should result for each process, based in part on experimentally determined fractionations.)

The suite of interstitial brines and groundwaters gives complete lateral coverage of the sabkha from the intertidal zone across the sabkha extending to the groundwaters of the landward continental regime. The brines were stored at Princeton in sealed, full or almost full, glass bottles. Our subsamples were placed in full, watertight 60 ml plastic bottles. They were not opened until they were analyzed for their water oxygen isotope composition. In a few instances, minor amounts of halite had precipitated between the bottle and its screw cap. Although no substantial loss of brine was apparent, there were fears initially that evaporative loss of water had altered the water oxygen isotope composition of the brines. The results presented here encourage the conclusion that such effects were absent or minimal; comparable values for the oxygen isotope composition of Abu Dhabi brines have been reported by McKenzie (1974). Details of the water chemistry may be found in Patterson's (1972) thesis. The sample names correspond to the Kinsman-Patterson levelled grid (Figure 7-2); the stations on a traverse are 200 metres apart.

The solid samples represent all of the major sulphate mineral parageneses: diagenetic interstitial gypsum of the intertidal zone; anhydrite after gypsum of the central sabkha; and gypsum after anhydrite of the landward parts of the sabkha. For heterogeneous samples, phases were separated by hand picking. The mineralogy of fine grained samples was determined by peak measurements on an X-ray diffractometer trace;

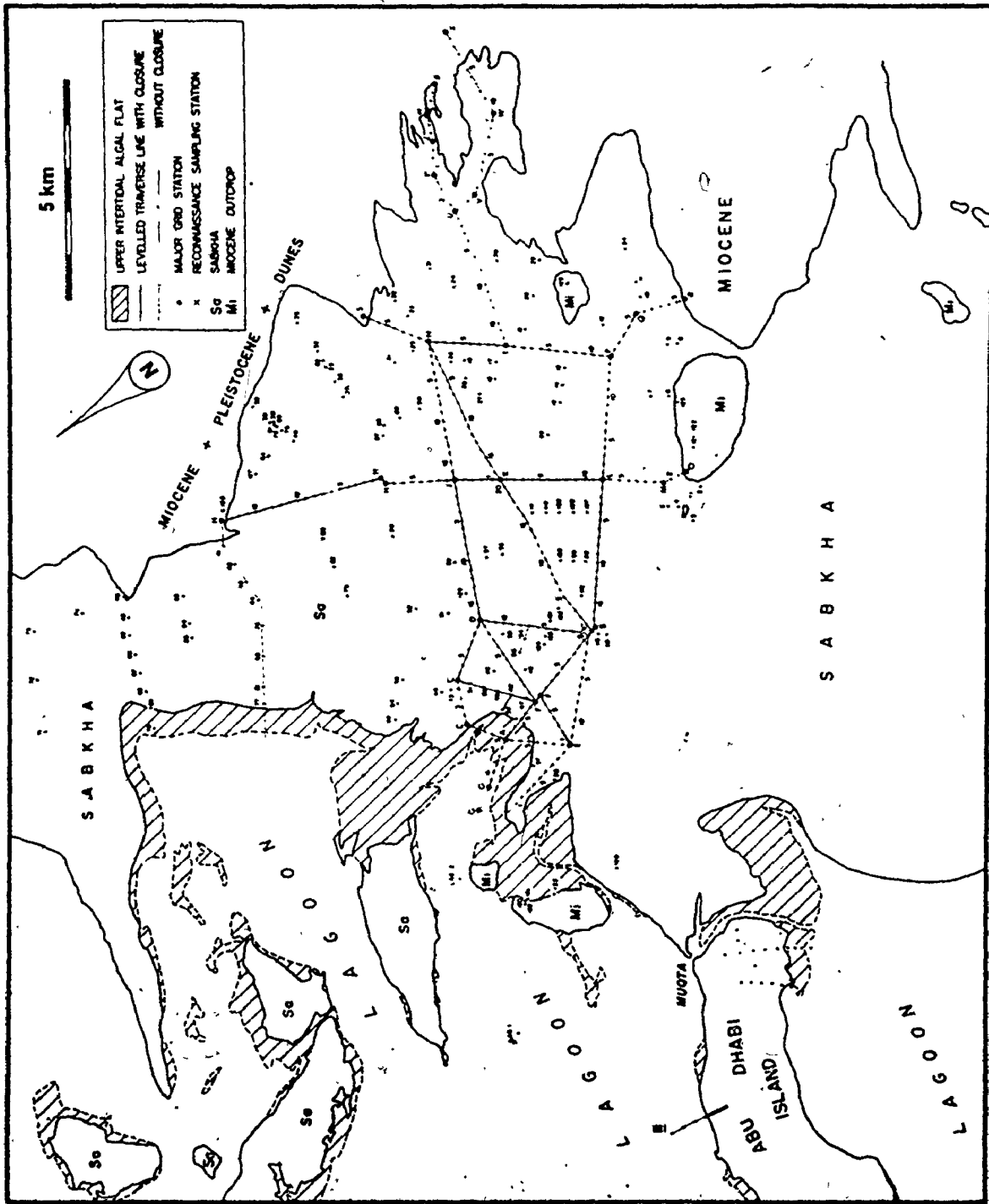


Figure 7-2: Abu Dhabi Sample Stations (from Patterson, 1973)

this was done for all anhydrites for which isotope analyses are reported.

The isotopic analyses of the brines are reported in Table 7-3 and of the solids in Table 7-4. The number of determinations of any parameter is indicated by the figures in parentheses, and the value listed is the mean. The standard deviation of a single analysis, estimated from pooled duplicates, is listed at the end of each column.

#### Isotopic Analyses of Dissolved Sulphate and Water

Using Patterson's (1972)  $m_K + /m_{Br}$  - discriminator for water origin (indirectly, from location of samples with respect to zones on Figure 6-6), the brines analyzed here were grouped into seaward, landward, and mixed regimes. The mean  $\delta$  values for each regime, and those of seawater (from the literature) and the regional groundwater system (from Table 7-3) are presented in Table 7-5. It is clear that the sulphur and oxygen  $\delta$  values for sulphate in the seaward regime are very close to those for seawater. In the landward regime, the sulphur  $\delta$  is very close to (about +16 ‰) but the oxygen  $\delta$  is considerably lighter than that of the continental groundwater system.

The relationships between these isotopic parameters and dissolved sulphate concentration are shown in Figures 7-3, 7-4, 7-5 and 7-6. On all of these diagrams, the grouping according to Patterson's criterion is valid; that is, the groups occupy more or less distinct areas. The correlation between variables within groups was tested, and the

TABLE 7-3: Isotopic Measurements, Density, and Sulphate Concentration of Abu Dhabi Brines

(EA6 reads 6th station from E toward A etc. on Figure 7-2.)

NAME (Kinsman)	DENSITY gm/ml	(SO <sub>4</sub> <sup>--</sup> ) moles kg <sup>-1</sup> x10 <sup>3</sup>	δ <sup>18</sup> O (SMOW) Water	δ <sup>18</sup> O (SMOW) SO <sub>4</sub> <sup>--</sup>	δ <sup>34</sup> S (CDT) SO <sub>4</sub> <sup>--</sup>	
EA6(SW) 3/69	1.10 (2)	81.3	4.8 (2)	10.7 (3)	19.7 (3)	
EA5 3/69	1.13	121.9	4.8 (3)	10.8 (2)	19.6 (2)	
EA3+400'	1.20	175.0	2.9 (2)	9.0 (7)	19.8 (3)	
G'E2	1.16	116.7	3.3 (2)	10.4 (3)	20.3 (2)	
G'E6	1.18	113.5	1.9 (2)	9.9 (2)	19.7 (2)	
G'E8	1.20	134.4	1.3 (2)	9.9 (2)	20.0 (2)	
JD13	1.20	7.9	0.8 (2)	9.3 (3)	16.9 (2)	
JD9	1.19	9.7	0.3 (2)	10.3 (3)	16.9 (2)	
JD6	1.19	10.4	2.1 (2)	12.1 (3)	18.8 (1)	
JD3	1.20	17.7	1.8 (2)	14.6 (3)	18.6 (2)	
J	1.20	10.4	0.5 (2)	14.8 (2)	16.6 (2)	

NAME (Kinsman)	DENSITY gm/ml	(SO <sub>4</sub> <sup>--</sup> ) moles kg <sup>-1</sup> x10 <sup>3</sup>	δ <sup>18</sup> O (SMOW) Water	δ <sup>18</sup> O (SMOW) SO <sub>4</sub> <sup>--</sup>	δ <sup>34</sup> S (CDT) SO <sub>4</sub> <sup>--</sup>
KJ3	1.19	14.6	3.3 (2)	14.0 (2)	18.4 (2)
NJ14	1.19	17.7	2.8 (3)	16.5 (2)	18.1 (1)
NJ11	1.18	15.6	3.2 (2)	13.7 (2)	17.2 (2)
NJ9	1.19	14.6	3.5 (1)	12.6 (2)	17.5 (2)
NJ6	1.19	12.5	5.2 (2)	13.4 (2)	17.4 (2)
NJ3	1.18	22.9	2.6 (2)	13.4 (2)	14.7 (2)
NS2	1.15	35.4	6.2 (2)	12.3 (2)	14.6 (1)
NS3	1.15	37.5	5.5 (2)	12.9 (2)	15.8 (1)
NS6	1.15	41.7	6.4 (2)	12.7 (2)	15.8 (1)
WV5	1.10	45.8	5.7 (2)	13.1 (2)	15.9 (2)
XW5	1.06	52.1	4.8 (2)	14.0 (2)	16.0 (2)
H'H'18	1.13	41.7	5.5 (2)	13.1 (2)	16.8 (2)
H'H'15	1.18	21.9	3.2 (2)	14.0 (2)	17.7 (2)

NAME (Kinsman)	DENSITY gm/ml	(SO <sub>4</sub> <sup>--</sup> ) moles kg <sup>-1</sup> <sub>3</sub> x10 <sup>3</sup>	δ <sup>18</sup> O (SMOW) Water	δ <sup>18</sup> O (SMOW) SO <sub>4</sub> <sup>--</sup>	δ <sup>34</sup> S (CDT) SO <sub>4</sub> <sup>--</sup>
H'H"12	1.19	11.5	1.9 (2)	14.7 (2)	18.8 (3)
H'H"8	1.19	13.5	2.3 (2)	14.7 (2)	18.4 (2)
H	1.17	21.9	2.8 (2)	12.6 (2)	19.4 (2)
H (res)	1.17	21.9	2.3 (2)	12.4 (2)	19.1 (2)
JH6	n. d.	n. d.	1.8 (2)	12.9 (2)	17.0 (2)
JH3	1.19	20.8	2.9 (2)	12.4 (4)	17.5 (1)
KJ3	1.19	14.6	3.3 (2)	14.0 (2)	18.4 (2)
KL4	1.19	36.5	0.3 (2)	10.3 (2)	18.5 (2)
KL9	1.19	13.5	-0.3 (2)	9.0 (2)	17.9 (2)
ML2	1.18	15.6	4.7 (2)	9.0 (2)	15.9 (1)
OM2	1.12	28.1	5.5 (2)	11.6 (2)	16.0 (2)



NAME (Kinsman)	DENSITY gm/ml	(SO <sub>4</sub> <sup>--</sup> ) moles kg <sup>-1</sup> x10 <sup>3</sup>	δ <sup>18</sup> O (SMOW) Water	δ <sup>18</sup> O (SMOW) SO <sub>4</sub> <sup>--</sup>	δ <sup>34</sup> S (CDT) SO <sub>4</sub> <sup>--</sup>
AA8 38 Km	1.0	36.5	1.4 (2)	16.5 (2)	16.2 (2)
AA9 77 Km	0.99	9.4	-0.5 (2)	16.1 (2)	15.8 (2)
AA11 115 Km	0.99 (2)	0.6	-0.3 (2)	14.6 (1)	n.d.
FLOOD4	1.15	85.4	0.2 (2)	9.0 (2)	19.2 (2)
FLOOD6	1.16	91.7	n.d.	8.7 (2)	19.7 (2)
			1.0	0.7	0.6

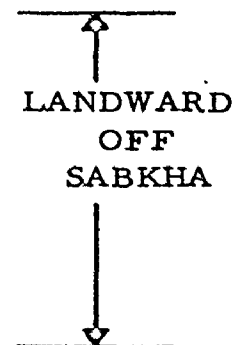


Table 7-4: Isotopic Determinations, Insoluble Content and Sulphate Content of Abu Dhabi Sediment Samples

NAME (Kinsman)	DESCRIPTION	%INS	(SO <sub>4</sub> <sup>--</sup> ) moles kg <sup>-1</sup>	δ <sup>18</sup> O (SMOW)	δ <sup>34</sup> S (CDT)
C'A1PB1	GYPSUM: discs, (3 cm diam)	5.2	5.35	15.2 (2)	21.9 (2)
	ARAGONITE: mud, white (XRD: AR)	78.8	0.06		
EA5+400' Algal mat	GYPSUM: euhedral platelets (1-3 mm); brown, lamin. algal mat; clean subsample	9.2	6.26	13.9 (2)	21.3 (2)
EA5+400' 0-10cm	GYPSUM: euhedral platelets (0.5-3 mm)	13.7	5.26	13.6 (2)	21.0 (2)
	GYPSUM: discs, (1 cm diam)	9.8	5.18	13.2 (2)	21.1 (2)
	ARAGONITE: mud, white (2 mm grains)	87.0	0.07		
EA3 10 cm	GYPSUM: discoidal platelets; (3 mm diam)	8.6	4.79	12.4 (4)	21.4 (2)
	GYPSUM: discoidal platelets (0.1 - 3 mm)		3.76	12.5 (2)	21.3 (2)
AD1152	GYPSUM: subhedral crystals (1 cm)	9.1	5.19	12.5 (2)	20.8 (2)
	ANHYDRITE: white, friable, powder (XRD: AN)	18.6	4.65	12.5 (2)	21.3 (2)

NAME (Kinsman)	DESCRIPTION	%INS	(SO <sub>4</sub> <sup>--</sup> ) moles kg <sup>-1</sup>	δ 18 <sub>O</sub> (SMOW)	δ 34 <sub>S</sub> (CDT)
C'ICIPB2	GYPSUM: selenite	30.4	3.49	14.8 (2)	22.2 (2)
	GYPSUM: aragonite mud, greenish brown, (XRD: AR)	68.1	0.65	15.2 (2)	21.2 (2)
AD886	GYPSUM: crystals, (to 1 cm); swallow- tail twinning	7.9	4.87	12.0 (2)	19.8 (2)
	ANHYDRITE: white, sugary, friable (XRD: AN)	11.0	5.99	12.9 (2)	20.7 (2)
	ANHYDRITE: in cal- cite mud; buff; (XRD: CT, AN)	67.0	0.85	12.9 (2)	20.1 (2)
AD888	GYPSUM: selenite; (1 cm diam)	2.4	4.43	12.1 (5)	20.5 (2)
	BASSANITE: white, sugary, elongate grains; (XRD: BA)	2.9	4.27	11.9 (2)	20.0 (2)
AD893	GYPSUM: euhedral selenite; (1 cm diam)		3.85	12.6 (2)	20.5 (2)
	BASSANITE: white (XRD: BA)	2.5	6.15	12.2 (3)	20.8 (2)

NAME (Kinsman)	DESCRIPTION	%INS	(SO <sub>4</sub> <sup>--</sup> ) moles kg <sup>-1</sup>	δ 18 <sub>O</sub> (SMOW)	δ 34 <sub>S</sub> (CDT)
BD6+350' a	ANHYDRITE: mud; dark buff, friable, aggregates (XRD: AN, CT)	71.7	1.13	14.4 (2)	21.1 (2)
BD6+350' b	HALITE: (XRD: HA)	21.5	0.34		
	CALCITE: brown mud (XRD: CT)	86.2	0.46		
BD6+350' c	ANHYDRITE: gray- white mud (XRD: AN)	48.5	2.76	14.4 (2)	20.7 (2)
H'H"2	ANHYDRITE: opaque white aggregate; with 20% translucent plates & prisms (XRD: AN)	18.6	4.60	13.8 (3)	20.8 (2)
NJ14 20-25 cm	ANHYDRITE: white, friable lumps; (2 cm) (XRD: AN)	12.3	4.62	16.8 (3)	20.2 (2)
NJ14 25 cm squeeze	ANHYDRITE: friable, mixture of white & clear; (XRD: AN)	32.4	3.99	16.8 (2)	19.7 (2)
	CALCITE: friable mud; creamy brown	80.3	0.13		
BK20 47-54 cm	GYPSUM: subhedral discoidal platelets; sized (0.5-4 mm diam) (2500 yr - C14)	7.2	5.10	13.7 (3)	21.1 (2)

NAME (Kinsman)	DESCRIPTION	%INS	(SO <sub>4</sub> <sup>2-</sup> ) moles kg <sup>-1</sup>	δ <sup>18</sup> O (SMOW)	δ <sup>34</sup> S (CDT)
M squeeze	GYPSUM: selenite crystals (to 1 cm)	17.6	4.04	14.1 (3)	17.3 (2)
	carbonate mud: brown, sugary	88.6	0.01		
M 35-40 cm	GYPSUM: selenite, corroded	6.6	4.71	14.2 (2)	17.7 (2)
	carbonate mud: brown, sugary	79.9	0.16		
M+200' 50-54 cm	ANHYDRITE: white, crystalline (XRD: AN)	12.9	4.92	13.2 (2)	17.5 (2)
LP3	GYPSUM: disc (6 cm diam); green inclusions in clear gypsum; subsample (010) cleavage fragment	9.5	5.01	16.4 (2)	21.8 (2)
LP7 3-13 cm	ANHYDRITE: white, friable, crystal- line; replacing discs; some secondary (?) gypsum (XRD: AN)	28.9	3.77	12.0 (3)	19.9 (2)
R82	GYPSUM: elongate, multicrystal aggre- gate (2 cm long); corroded; with inclusions	9.2	4.92	16.7 (2)	17.9 (2)
	carbonate mud: brown	81.7	0.19		

NAME (Kinsman)	DESCRIPTION	%INS	(SO <sub>4</sub> <sup>--</sup> ) moles kg <sup>-1</sup>	δ <sup>18</sup> O (SMOW)	δ <sup>34</sup> S (CDT)
AD1134	ANHYDRITE: white nodule (5 cm diam) (XRD: AN)	29.9	3.82	14.1 (2)	17.7 (2)
AD1119	ANHYDRITE: friable, buff mud (XRD: AN, CT, HA)	38.4	3.32	13.6 (2)	16.4 (2)
	ANHYDRITE/GYPSUM: mixture; sugary halite(?) 60% anhydrite mud 30% gypsum prisms 10%	22.3	0.92	12.0 (1)	16.0 (1)
	ANHYDRITE/GYPSUM: whole sample	38.4	1.48	13.2 (2)	16.3 (2)
AD1121 (1)	GYPSUM: selenite, corroded (to 1.5 cm)	10.9	5.10	14.4 (3)	17.2 (2)
	ANHYDRITE: white mud (XRD: AN)	34.7	3.86	13.1 (4)	16.5 (1)
AD1121 (4)	GYPSUM: selenite, clear (>1 cm)	5.0	5.03	13.9 (2)	17.2 (2)
	ANHYDRITE: white mud (XRD: AN)	41.4	3.16	15.9 (1)	16.9 (2)
	GYPSUM/ANHYDRITE: whole sample	31.8	2.82	14.6 (3)	16.7 (2)
GGC4	GYPSUM: selenite, twinned (2 cm x 0.7 cm) multi- generation gypsum	1.0	5.29	14.9 (2)	16.7 (2)

NAME (Kinsman)	DESCRIPTION	%INS	(SO <sub>4</sub> <sup>2-</sup> ) moles kg <sup>-1</sup>	δ <sup>18</sup> O (SMOW)	δ <sup>34</sup> S (CDT)
GGC4	GYPSUM: euohedral selenite (1 cm x 2 mm); gypsum from continental water grown in pit	0.8	5.54	14.7 (3)	17.4 (3)
	Miocene GYPSUM: after anhydrite (Kinsman)	5.2	5.35	15.8 (2)	21.2 (1)
			<hr/>		
			2 σ	±0.7	±0.6

Table 7-5: Mean Isotopic Values for Abu Dhabi Brines, grouped according to  $m_{K^+}/m_{Br^-}$

	$\delta^{18}O(SMOW)$ WATER (‰)	$\delta^{18}O(SMOW)$ SULPHATE (‰)	$\delta^{34}S(CDT)$ SULPHATE (‰)
SEAWARD	2.4	10.0	19.5
MIXED	2.0	13.3	18.1
LANDWARD	4.9	12.7	16.1
SEAWATER	0.0	9.7	20.0
REGIONAL CONTINENTAL GROUNDWATER	1.4	16.5	16.2



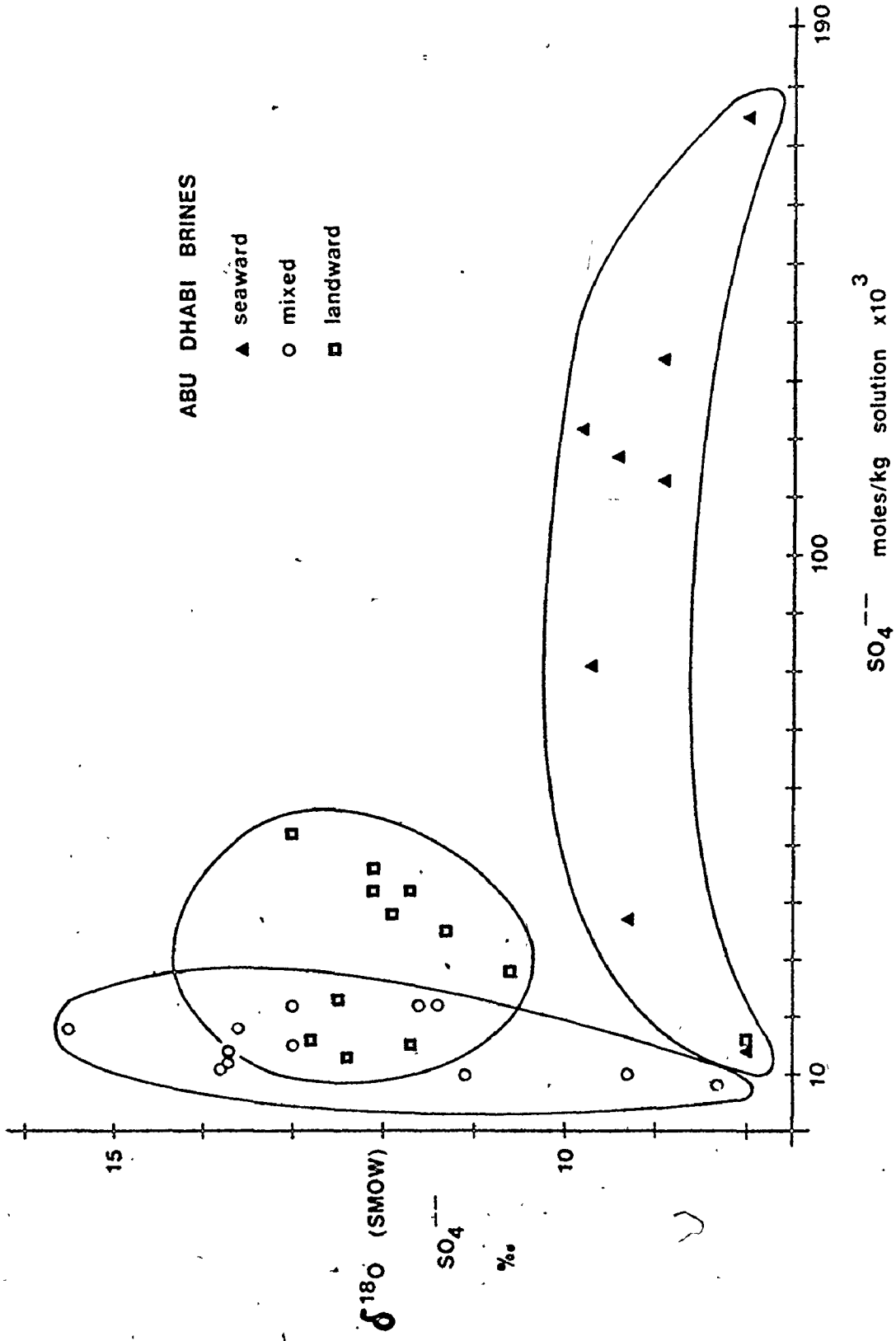


Figure 7-3: Oxygen Del Values versus concentration for Sulphate Dissolved in Abu Dhabi Brines

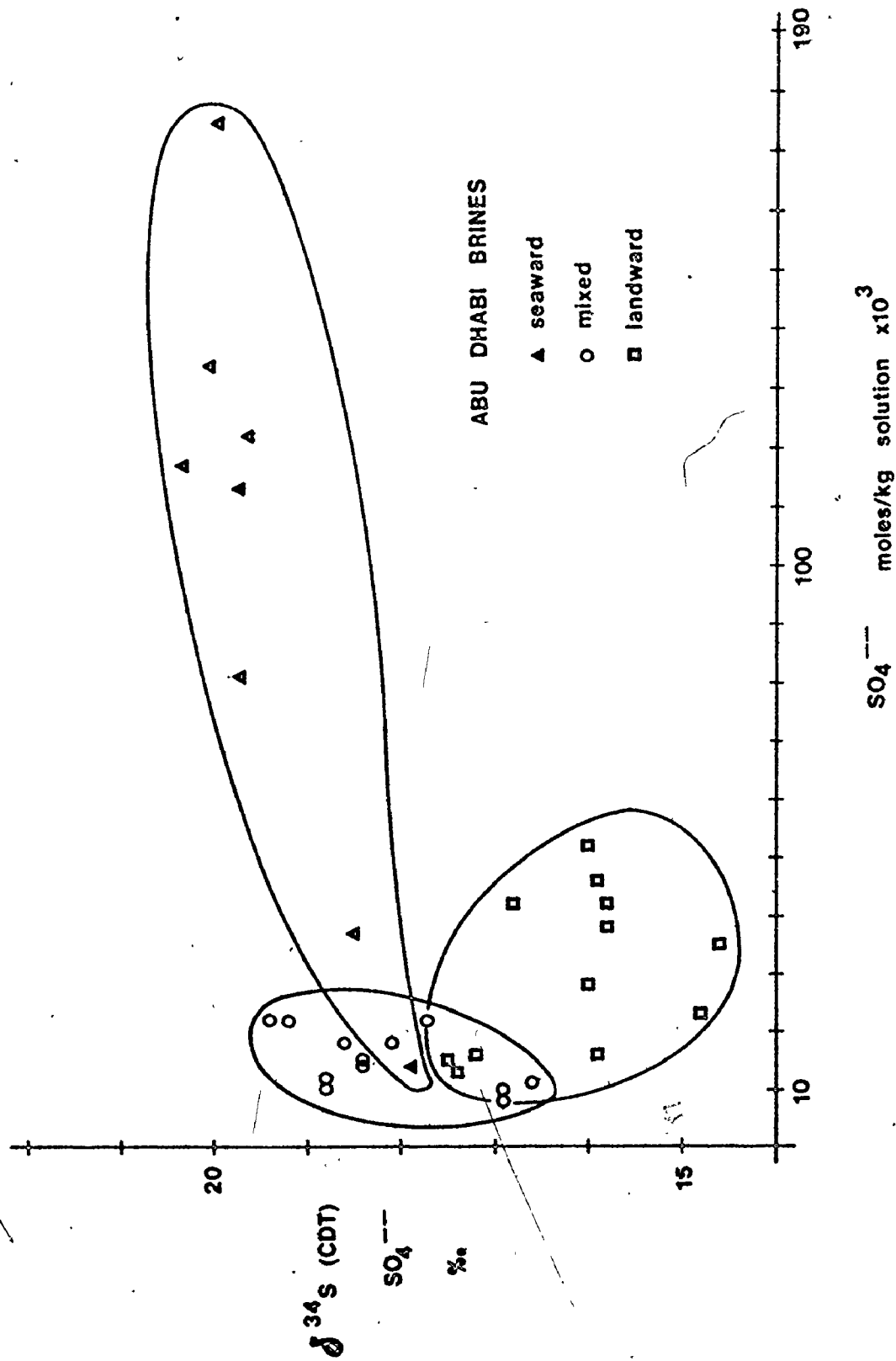


Figure 7-4: Sulphur Del Values versus Concentration for Sulphate Dissolved in Abu Dhabi Brines

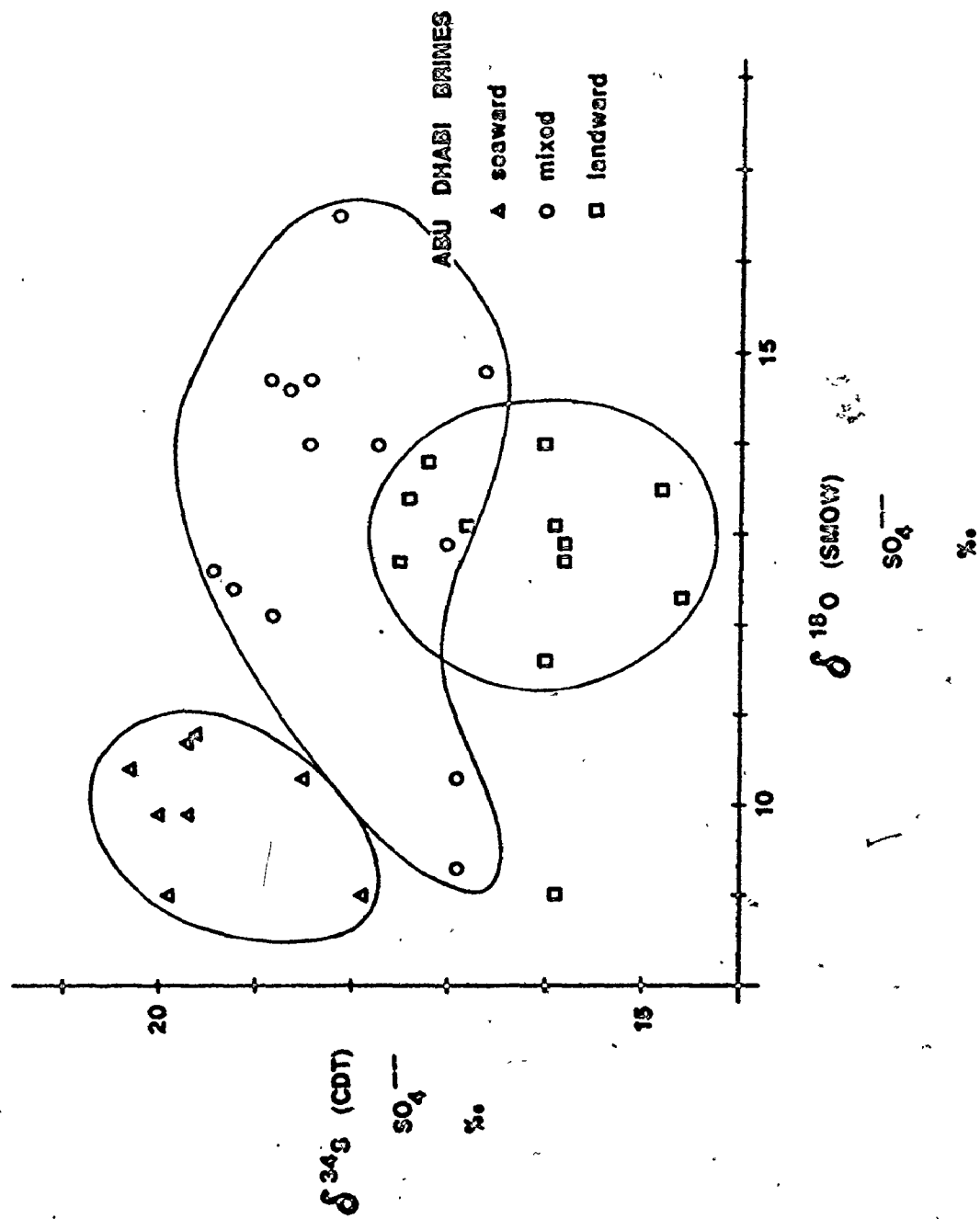


Figure 7-5: Sulphur Del Values versus Oxygen Del Values for Sulphate Dissolved in Abu Dhabi Brines

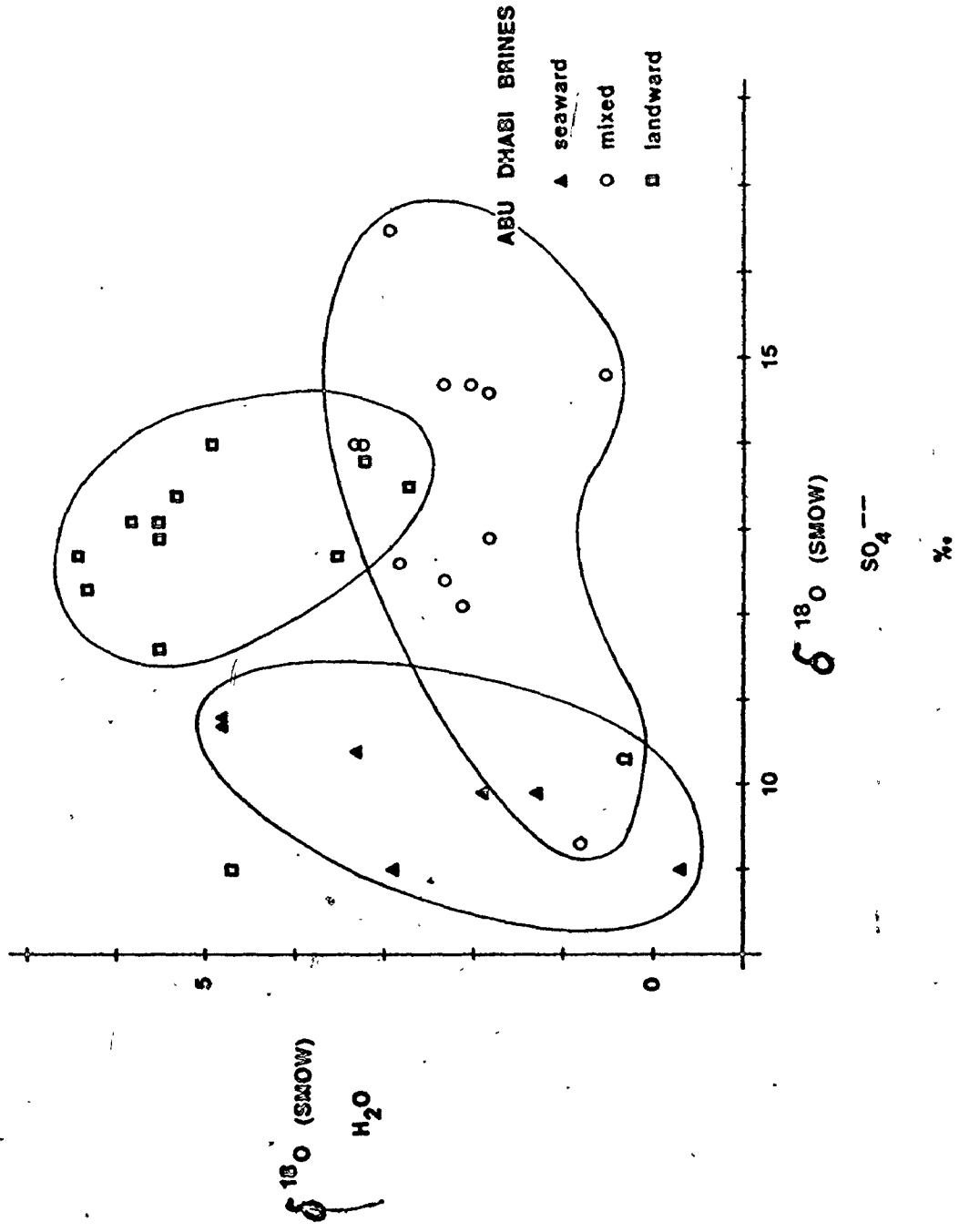


Figure 7-6: Oxygen Del Values of Water versus Oxygen Del Values for Sulphate Dissolved in Abu Dhabi Brines

linear correlation coefficient (l. c. c.) was found to be significant at the 0.02 confidence level only for  $\delta^{34}\text{S}$  versus dissolved sulphate concentration. The linear correlation coefficients are listed in Table 7-6. There are weaker correlations between  $\delta^{18}\text{O}(\text{SO}_4^{--})$  and  $\delta^{18}\text{O}(\text{H}_2\text{O})$  for both the seaward and mixed groups.

The lateral variation of  $\delta^{18}\text{O}(\text{SMOW})$  of water,  $\delta^{18}\text{O}(\text{SMOW})$  of dissolved sulphate, and the  $\delta^{34}\text{S}(\text{CDT})$  of dissolved sulphate is not random; there is regular variation both parallel and perpendicular to the shoreline. These isotopic parameters are plotted on maps of the sabkha in Figures 7-7, 7-8 and 7-9.

#### Isotopic Analyses of Evaporite Minerals

Although it was developed for the interstitial brines, Patterson's (1972)  $m_{\text{K}^+}/m_{\text{Br}^-}$  - discriminator was used (indirectly, from the location of the samples with respect to the zones on Figure 6-6) to group the evaporite mineral samples into seaward, landward and mixed regimes. The mean  $\delta$  values for each regime are presented in Table 7-7.

The relationship between  $\delta^{34}\text{S}$  and  $\delta^{18}\text{O}$  for the Abu Dhabi evaporite minerals is shown in Figure 7-10. The seaward and landward groups are well separated on that plot; the separation is largely due to the difference in  $\delta^{34}\text{S}$ . Only the seaward group  $\delta$  values showed significant correlation at the 0.02 level (see Table 7-8).

The sulphur and oxygen  $\delta$  values of gypsum and anhydrite

Table 7-6: Linear Correlation Coefficients within Groups for Abu Dhabi Brines (number of observations in parentheses)

	SEAWARD	MIXED	LANDWARD
$\delta^{18}\text{O}(\text{H}_2\text{O})/\delta^{18}\text{O}(\text{SO}_4^{--})$	0.608(8)	0.499(13)	0.176(12)
$\delta^{34}\text{S}(\text{SO}_4^{--})/\delta^{18}\text{O}(\text{SO}_4^{--})$	0.343(8)	0.259(13)	0.187(12)
$\delta^{18}\text{O}(\text{SO}_4^{--})/(\text{diss SO}_4^{--})$	0.006(8)	0.382(12)	0.292(12)
$\delta^{34}\text{S}(\text{SO}_4^{--})/(\text{diss SO}_4^{--})$	0.868(8)*	0.568(12)	0.406(12)

\* The linear correlation coefficient was found to be significant at the 0.02 level for the following relationship:

$$\delta^{34}\text{S}(\text{SO}_4^{--}) = 0.00135 (\text{diss SO}_4^{--}) + 18.12\text{‰}$$

where dissolved sulphate concentration is expressed in moles per kilogram of solution.

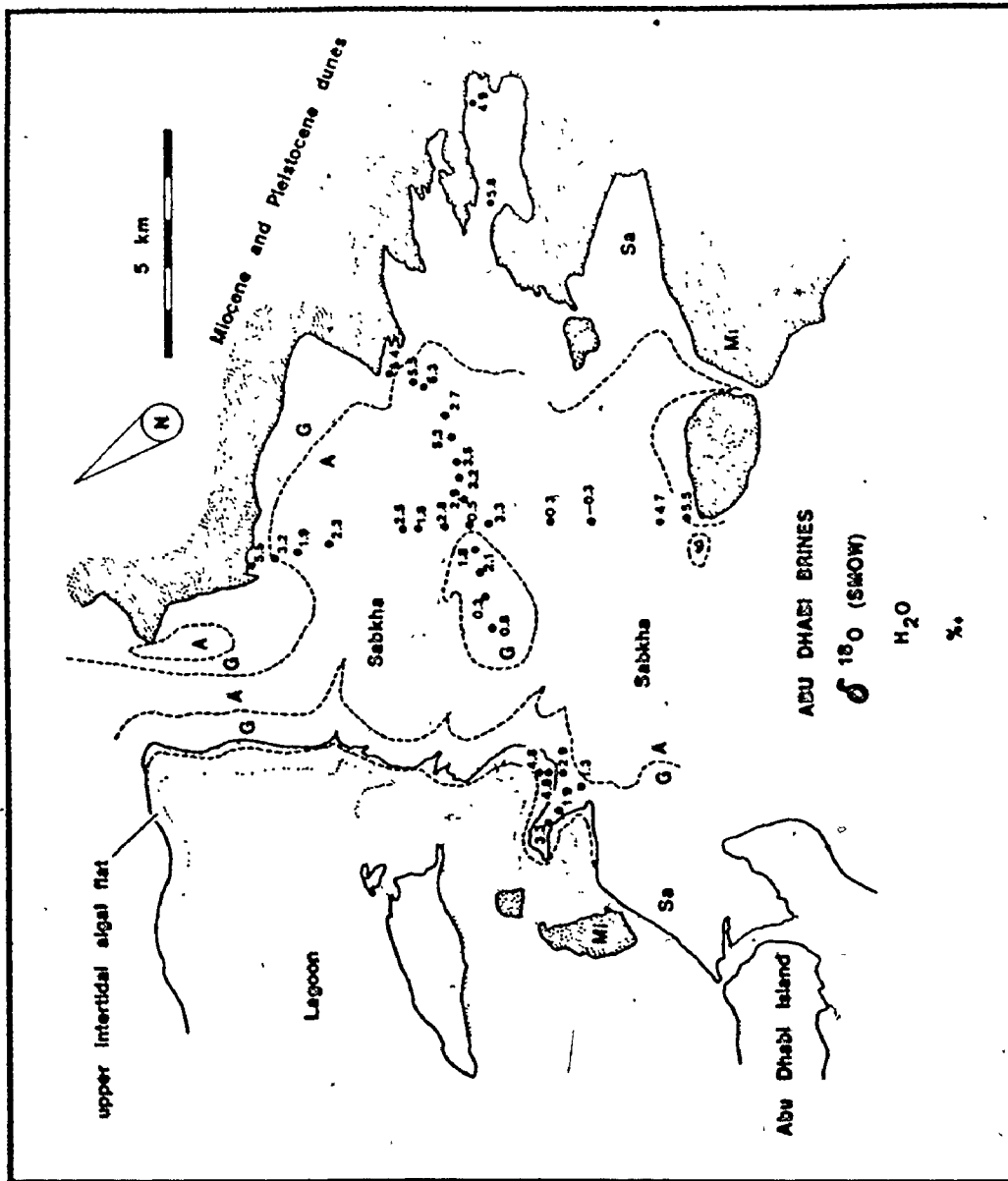


Figure 7-7: Areal Distribution of Oxygen Del Values of Water in Abu Dhabi Brines

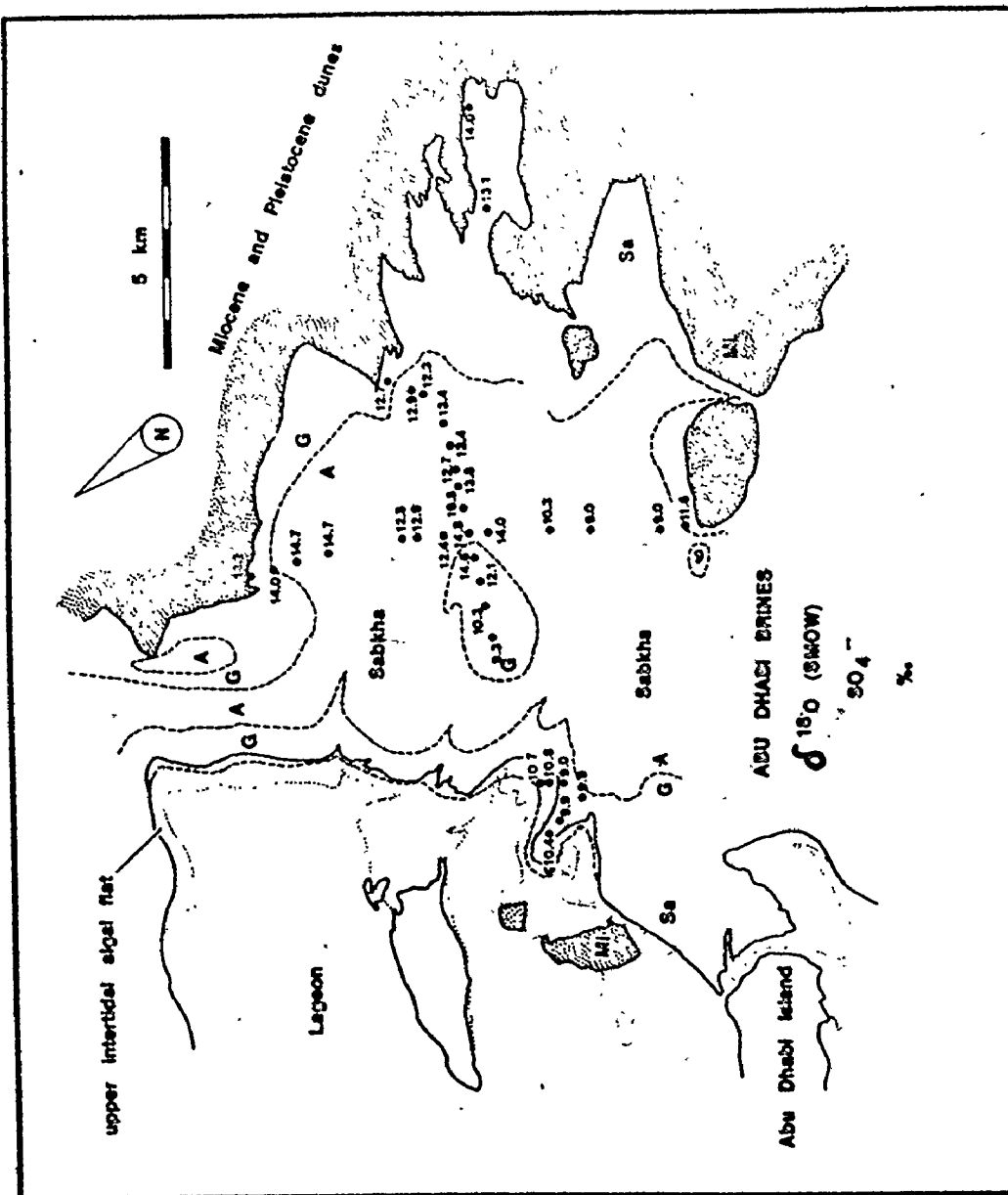


Figure 7-8: Areal Distribution of Oxygen Del Values of Sulphate in Abu Dhabi Brines



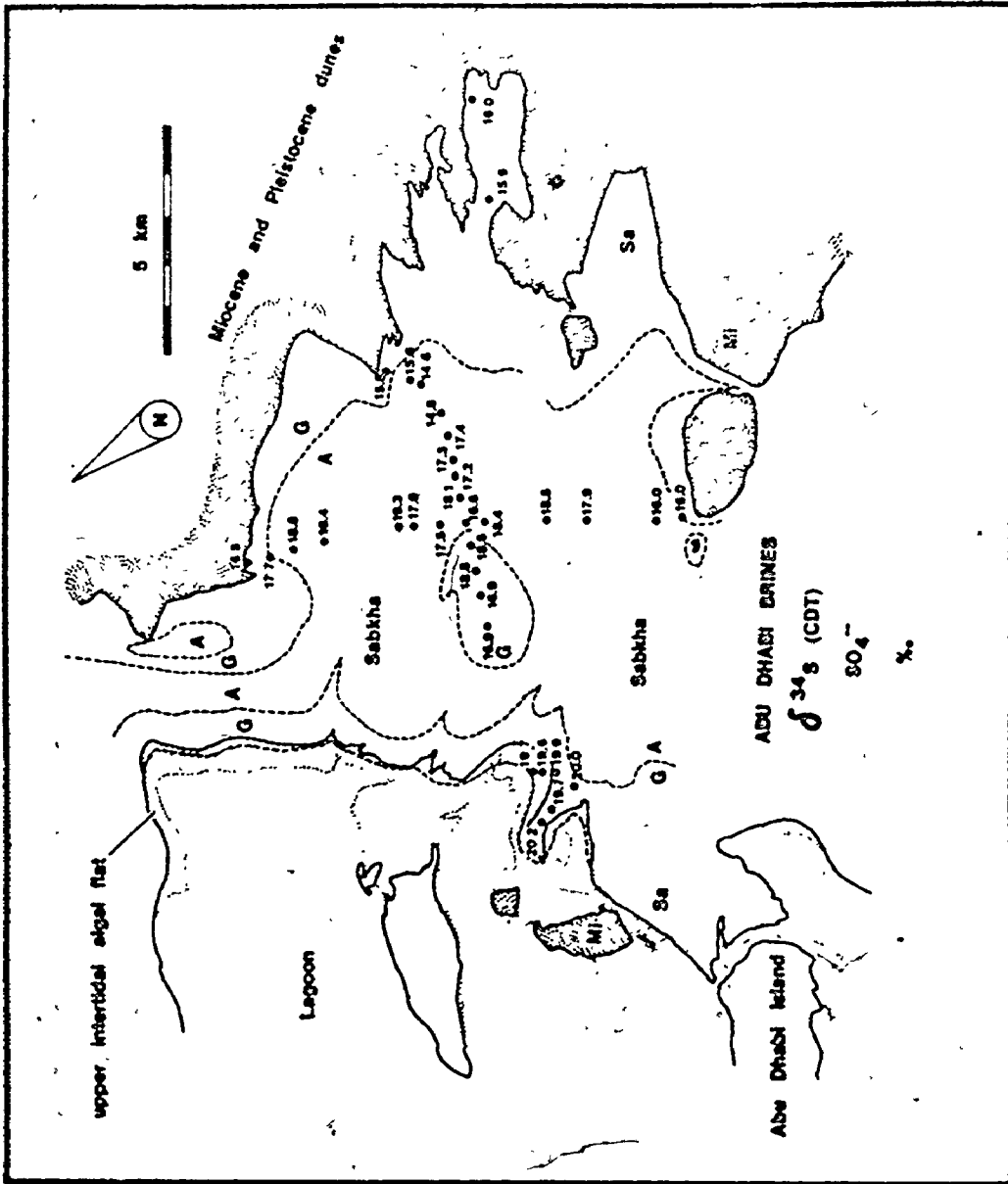


Figure 7-9: Areal Distribution of Sulphur Del Values of Sulphate Dissolved in Abu Dhabi Brines

Table 7-7: Mean Isotopic Values for Abu Dhabi Evaporite Minerals,  
grouped according to  $m_K/m_{Br}$  - of associated brines

	$\delta^{18}O$ (SMOW) SULPHATE (‰)	$\delta^{34}S$ (CDT) SULPHATE (‰)
SEAWARD	13.5	21.0
MIXED	15.5	20.4
LANDWARD	14.3	17.2

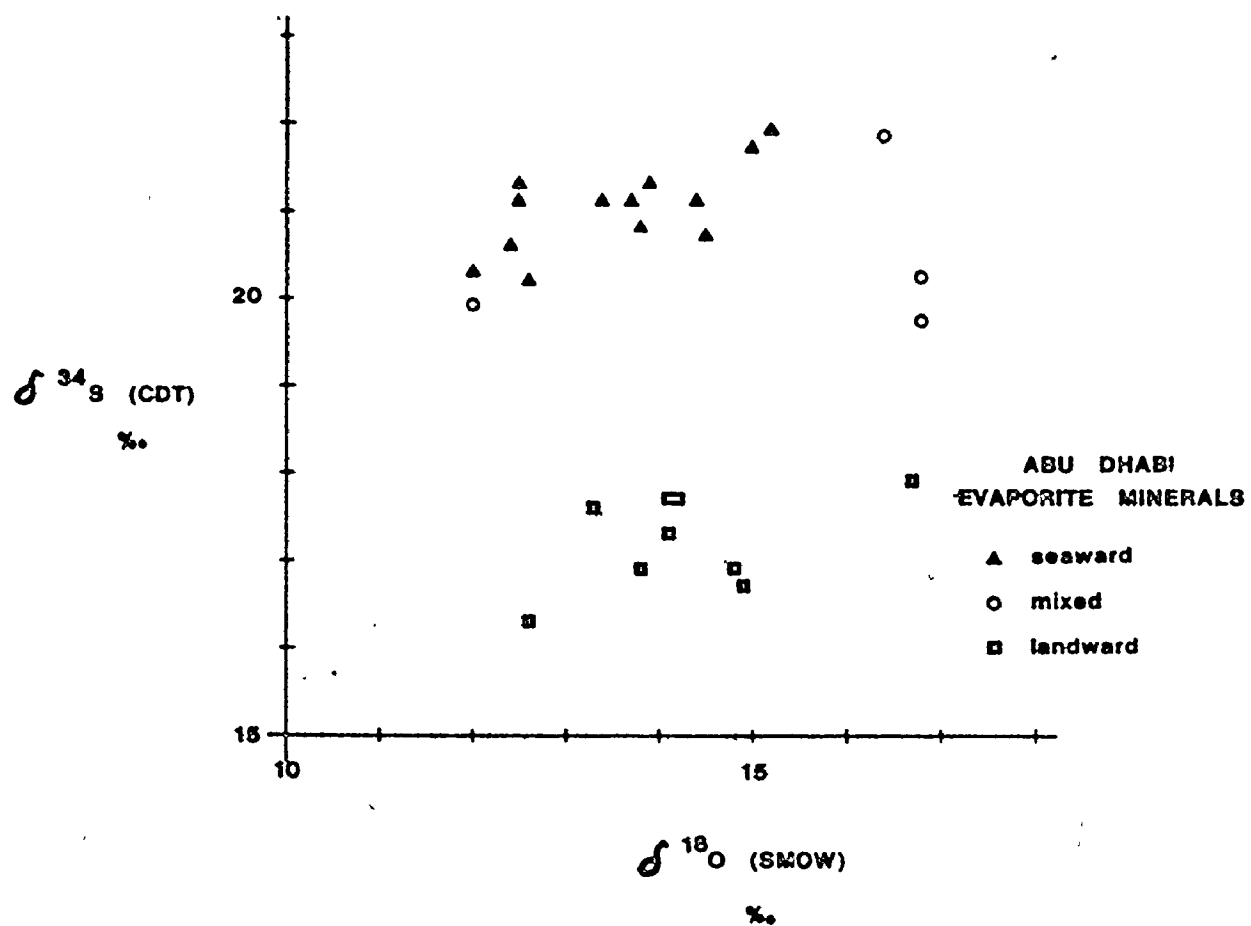


Figure 7-10: Sulphur Del Values versus Oxygen Del Values for Abu Dhabi Evaporite Minerals

Table 7-8: Linear Correlation Coefficients within groups for Abu Dhabi Evaporite Minerals (number of observations in parentheses)

	SEAWARD	MIXED	LANDWARD
$\delta^{34}\text{S}(\text{SO}_4^{--})/\delta^{18}\text{O}(\text{SO}_4^{--})$	0.674(13)*	0.274(4)	0.465(9)

\* The linear correlation coefficient was found to be significant at the 0.02 level for the following relationship:

$$\delta^{34}\text{S}(\text{SO}_4^{--}) = 0.314 \delta^{18}\text{O}(\text{SO}_4^{--}) + 16.76\text{‰}$$

separated from the same samples or from adjacent samples were used to determine the isotope shifts that accompany the mineralogical transitions ( $\Delta = \delta_{\text{gypsum}} - \delta_{\text{anhydrite}}$ ). The mean isotopic shifts shown in Table 7-9 are very close to zero ( $\Delta^{34}\text{S} = 0.02\text{‰}$  and  $\Delta^{18}\text{O} = 0.01\text{‰}$ ). Two bassanite subsamples have been treated as anhydrite in the foregoing.

The oxygen and sulphur  $\delta$  values for these minerals have been plotted on maps of the Abu Dhabi sabkha in Figures 7-11 and 7-12 respectively. For those locations at which both gypsum and anhydrite are present and their  $\delta$  values have been determined, the  $\delta$  values have been averaged to simplify the figures. Inspection of Figures 7-11 and 7-12 shows that the variation of these isotopic parameters has spatial regularity that is better defined for  $\delta^{34}\text{S}$  than for  $\delta^{18}\text{O}$ .

The sulphur and oxygen  $\delta$  values for the evaporite minerals and the brines of both the seaward and the landward regimes are shown in Figure 7-13.

In order to facilitate interpretation of the following data the isotope compositions of the brines and the evaporite minerals have been plotted together on a profile normal to the shoreline (Figures 7-14 and 7-15). The line of the profile is approximately ADJN on the Kinsman/Patterson levelled grid (Figure 7-2). The horizontal scale is in kilometres measured from the present high water strand line and may be regarded as a crude time scale from the present high water strand line

Table 7-9: Isotopic Shifts that accompany Gypsum to Anhydrite and Anhydrite to Gypsum Transitions ( $\Delta_{G-A} = \delta_G - \delta_A$ )

	$\Delta^{34}\text{S}$	$\Delta^{18}\text{O}$
AD1152 (G to A)	-0.44	-0.04
AD886 (G to A)	-0.88	-0.90
AD888 (G to B)	+0.48	+0.23
AD893 (G to B)	-0.28	+0.46
M, M+200' (A to G)	-0.36	+0.92
AD1121(1) (A to G)	+0.63	+1.32
AD1121(4) (A to G)	+0.27	-1.94
mean $\pm 1\sigma$	0.02 $\pm 0.56\text{‰}$	0.01 $\pm 1.11\text{‰}$

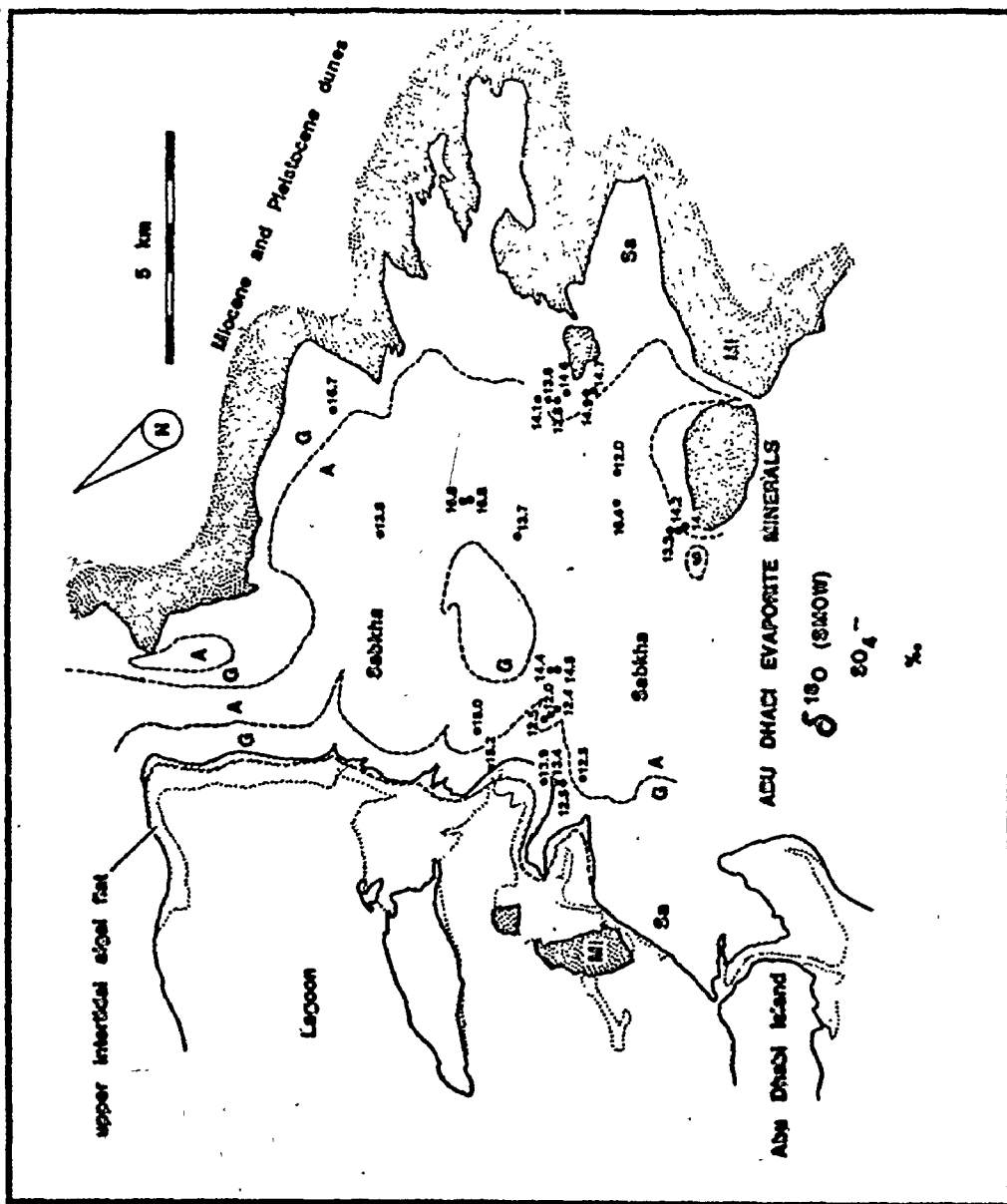


Figure 7-11: Areal Distribution of Oxygen Del Values for Abu Dhabi Evaporite Minerals

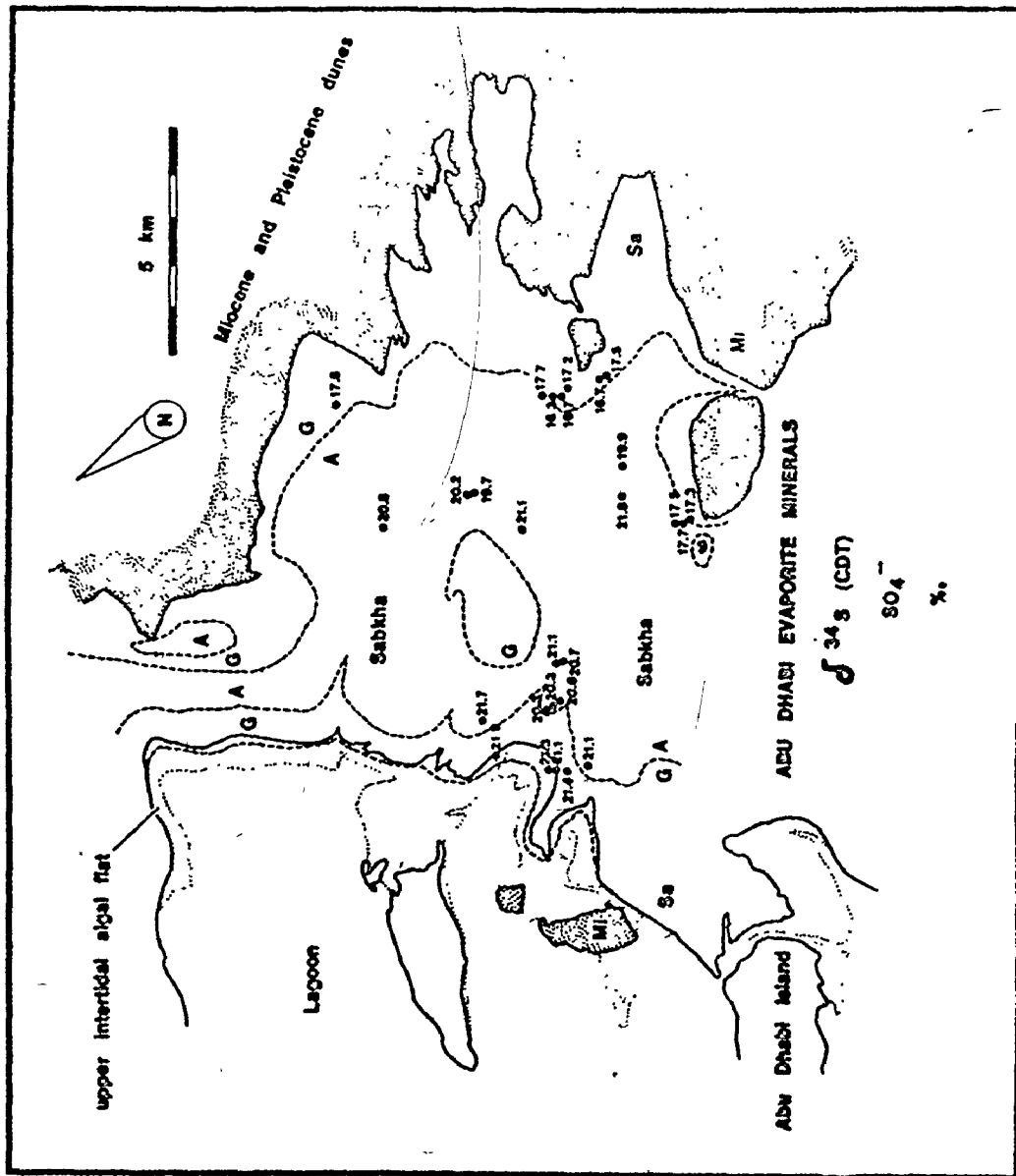


Figure 7-12: Areal Distribution of Sulphur Del Values for Abu Dhabi Evaporite Minerals



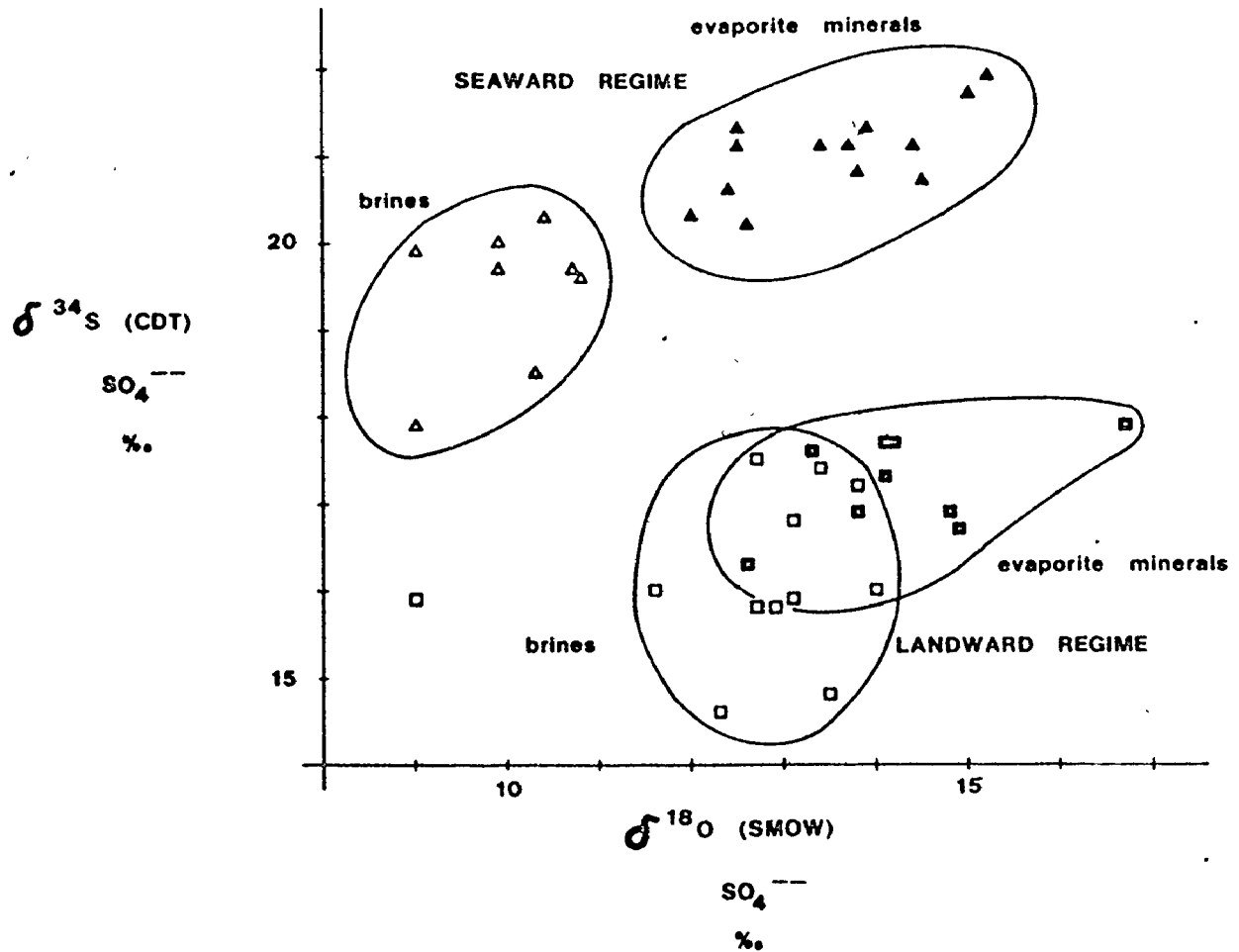


Figure 7-13: Sulphur Del Values versus Oxygen Del Values for Sulphate Dissolved in Brines and for Evaporite Minerals, Abu Dhabi Sabkha

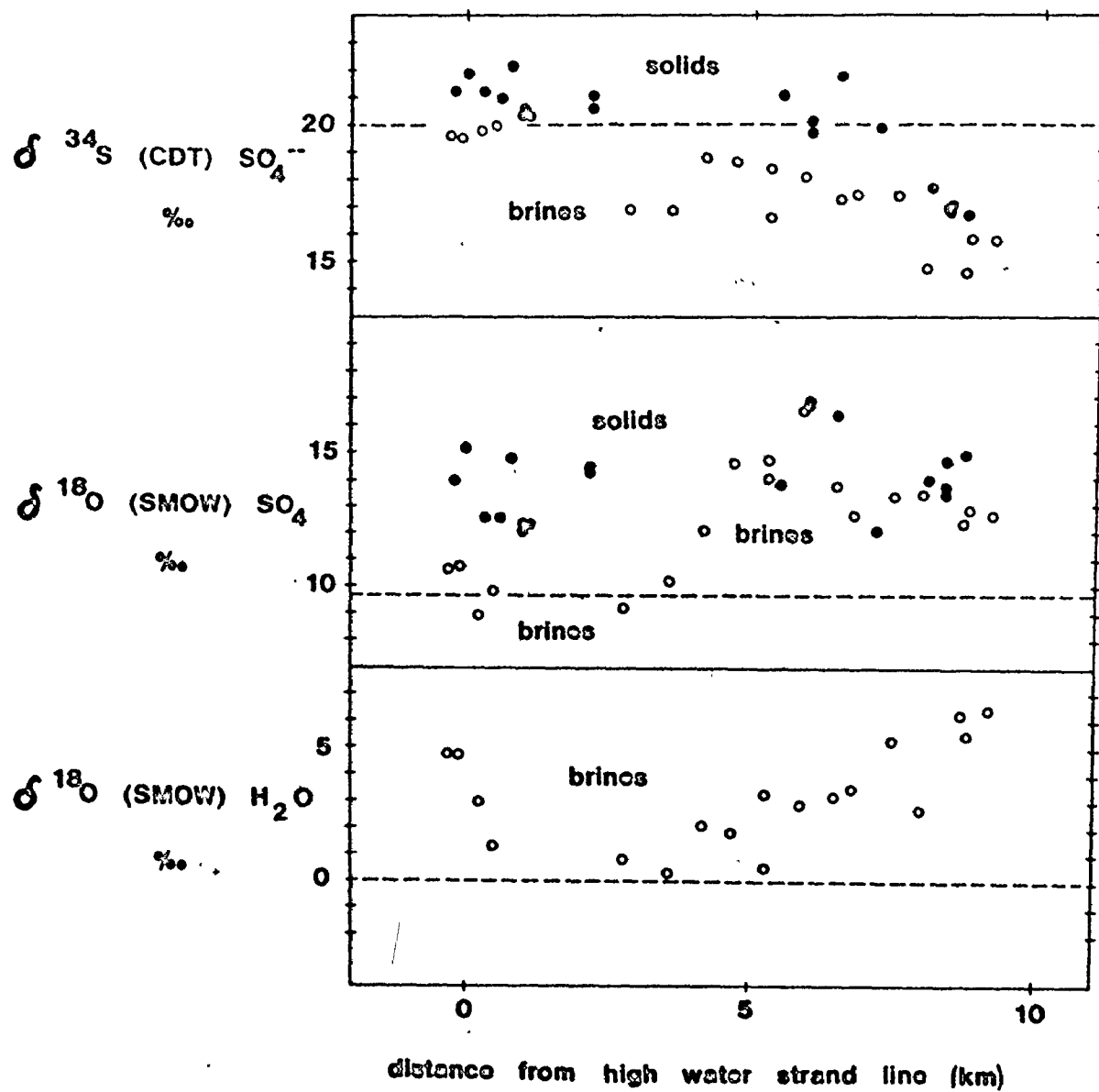


Figure 7-14: Profile of Sulphur and Oxygen Isotope Variation normal to shoreline Abu Dhabi Sabkha - Data Only

(dashed lines are values for modern seawater)

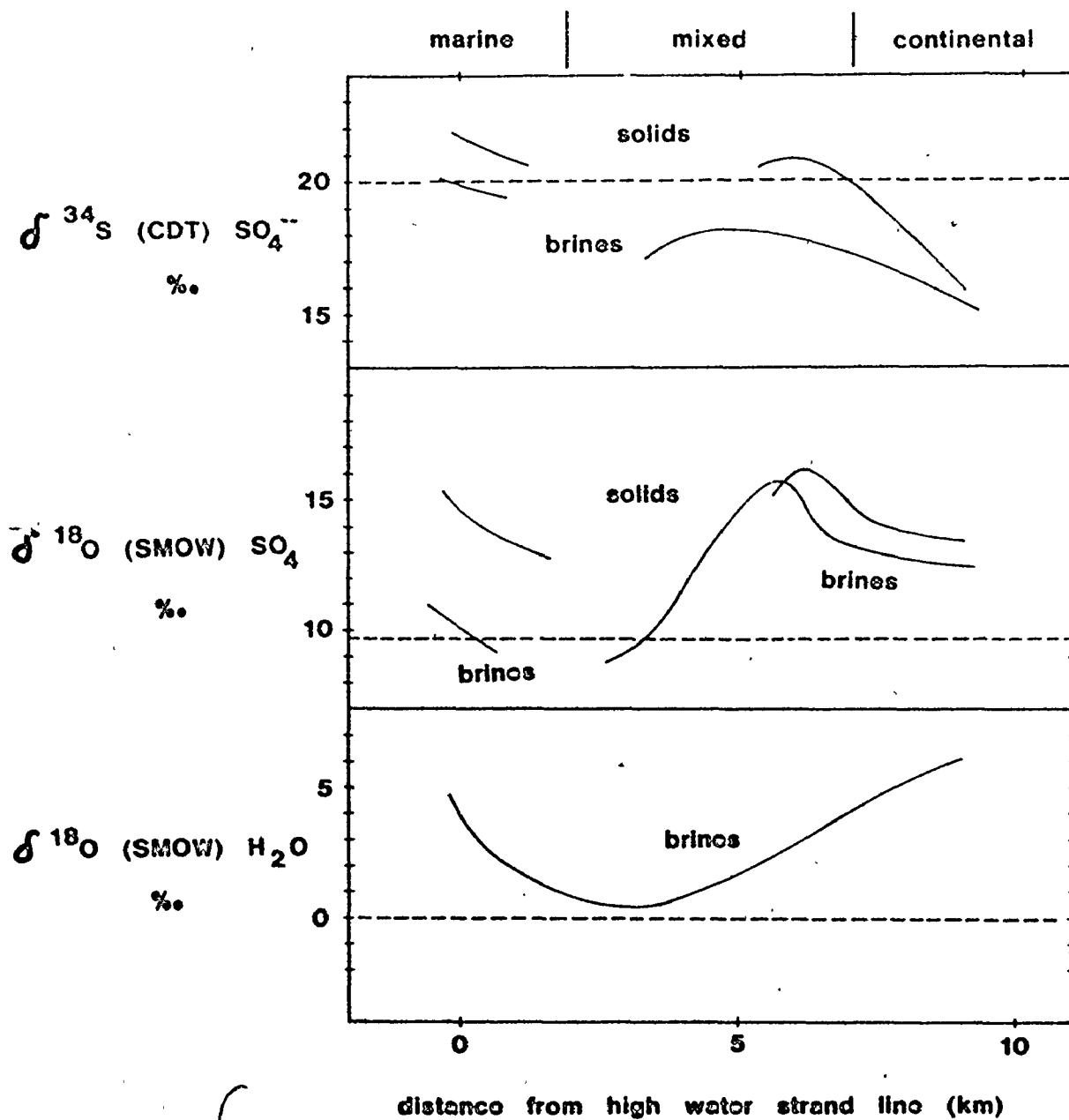


Figure 7-15: Profile of Sulphur and Oxygen Isotope Variation normal to shoreline Abu Dhabi Sabkha - Trends Only

(0 years) to the highest Holocene shoreline (4000 to 5000 years).

Analysis of Figure 7-9 suggests the action of several of the mechanisms proposed above.

### The Seaward Zone

In the seaward zone, the isotopic composition of the solid phase is uniformly heavier than that of the coexisting brine ( $\Delta^{34}\text{S} = 1.5\text{‰}$  and  $\Delta^{18}\text{O} = 3.5\text{‰}$ ); this may be interpreted as the equilibrium isotope fractionation between gypsum crystals and dissolved sulphate. Although Lloyd (1968) and Schwarcz (1974) found  $\Delta^{18}\text{O} = 2\text{‰}$  for gypsum precipitation in the laboratory, they also found larger fractionations (3 to 5‰) for natural gypsum-brine pairs. The results of experiments reported in the Appendix indicate that the larger fractionation is the equilibrium fractionation and that the smaller shift is a kinetic effect.

Although the landward decrease in sulphate concentration (Chapter 6) seems to correspond to progressive crystallization caused by evaporative concentration in a closed system, the isotopic data do not conform to that model. After 95% of a finite batch of dissolved sulphate has been removed as gypsum, with an oxygen isotope fractionation of 3.5‰, the dissolved sulphate remaining would be depleted in  $^{18}\text{O}$  by as much as 10‰ with respect to its initial composition (see Figure 7-1). In fact, a decrease in the oxygen  $\delta$  value of less than two per mille is observed for the brine and the crystals. The decrease for the sulphur  $\delta$  value is less than one per mille. The problem then is to

explain how isotopically heavy sulphate can be removed as gypsum without the commensurate depletion of the residual sulphate. Two mechanisms could explain the observed trends: rapid re-equilibration between crystals and liquid in the interstitial brine and isotopic enrichment due to bacterial sulphate reduction.

The expected 10‰ shift in  $\delta^{18}\text{O}$  of crystalline sulphate noted above is calculated under the assumption that there is no back-exchange between crystals and liquid after precipitation has occurred. This, however, is very unlikely since both phases stay in intimate contact long after precipitation. This could result in extensive isotopic exchange between these phases, and in considerable reduction in the shift in isotopic composition of each phase. If exchange were carried to completion, then even at 99% precipitation of sulphate, no apparent shift in  $\delta^{18}\text{O}$  of the crystals (beyond the original 3.5‰ crystal-liquid fractionation) would be observed.

Bacterial sulphate reduction results in heavier sulphur and oxygen  $\delta$  values in the remaining sulphate. It is known to occur in sabkha sediments, particularly where algal material is decaying. Mizutani and Rafter (1969b, 1973) have shown that such shifts would be correlated; significant linear correlation has been demonstrated between  $\delta^{34}\text{S}$  and  $\delta^{18}\text{O}$  for the evaporite minerals of the seaward zone.

However the slope of the best-fit line to the  $\delta^{34}\text{S}$  vs  $\delta^{18}\text{O}$  plot of evaporite minerals from the seaward zone is 0.313. This is far from the values observed by Mizutani and Rafter ( $\sim 4$ ) and is

quite close to the ratio of the sulphur and oxygen fractionations actually observed between crystals and brine ( $\sim 0.43$ ). This strongly suggests that variation in both parameters is principally controlled by crystal-liquid fractionation, for example during re-equilibration of crystals and liquid in the interstitial brine. Thus, at least in the seaward zone, bacterial reduction does not appear to have been a controlling factor on isotopic composition.

The oxygen  $\delta$  values of the brines in the seaward regime are heavy (mean  $\delta^{18}\text{O}(\text{H}_2\text{O}) = +2.4\text{‰}$ , maximum =  $4.8\text{‰}$ ) conforming with models of enrichment in  $^{18}\text{O}$  due to evaporation. The tendency to lighter values toward the centre of the sabkha away from the intertidal zone is discussed in a subsequent section.

### The Landward Zone

The isotopic trends seen in the landward zone of the sabkha (see Figure 7-15) cannot be modelled solely in terms of precipitation of gypsum or anhydrite from the interstitial brines. It can be seen in Figure 7-15) that the sulphur and oxygen  $\delta$  curves for the evaporite minerals and the brines in this regime converge. The difference between the mean  $\delta^{34}\text{S}$  for the minerals and that of the brines is  $1.1\text{‰}$ ; for  $\delta^{18}\text{O}$  the difference between the means is  $1.6\text{‰}$  (see Figure 7-13). In both cases, the minerals are isotopically heavier than the brines. By itself, such precipitation would drive the isotopic composition of both

phases to lighter values as the brine migrates toward the centre of the sabkha (note that the dissolved sulphate concentration decreases across the landward zone toward the centre of the sabkha). In fact, the sulphur and oxygen  $\delta$  values of the minerals and brines of the landward zone increase toward the centre of the sabkha.

The brines in the landward zone are concentrated by evaporation without dolomitization, and it might be expected that the smaller kinetic isotope fractionations would obtain there. Even so, a trend to lighter, not heavier, isotopic values in the centre of the sabkha should be observed.

As has been pointed out, the influx of continental groundwaters into the landward zone of the sabkha must result in the mixing of masses of sulphate of different isotopic composition. This can be clearly seen in Figure 7-15, as the most landward brines contain sulphate with  $\delta^{34}\text{S} = +15\text{‰}$  and those closer to the sabkha centre have progressively heavier sulphur  $\delta$  values. A similar trend is observed for  $\delta^{18}\text{O}$ , but the most landward values (about  $+12\text{‰}$ ) are considerably lighter than those measured for the continental groundwater system (about  $+16\text{‰}$ , see Table 7-5). Patterson (1972) has noted that the continental groundwaters sampled (the AA series) may not represent a single continuous hydrological system; it is clear that the oxygen  $\delta$  value of the landward sulphate input is not the same as that of the continental samples measured.

Nevertheless, it is apparent that mixing of masses of sulphate

of different isotopic composition controls the sulphur and oxygen  $\delta$  values of brines in the landward regime. Any isotope fractionations effected by precipitation of gypsum or anhydrite are obscured. It is likely that the brines and minerals are not in isotopic equilibrium because the fractionations are smaller than those of the seaward regime. This might be expected because the equilibration may proceed slowly; however, some of the mineral samples were taken from above the water table, and therefore should not be considered as coexisting with the brines.

Isotopic mixing cannot account for the heavy oxygen  $\delta$  values of water in the landward brines, because the input is light (1‰ see Table 7-5). However, just as evaporative processes can be invoked to explain the high values observed in the seaward regime, so might near surface evaporative processes increase the oxygen  $\delta$  value of land-derived water. The tendency to lighter values toward the centre of the sabkha away from the landward zone is discussed in the next section.

#### The Mixed or Central Zone

The brines of the mixed or central zone contain little sulphate, and almost no gypsum or anhydrite accumulation occurs in it. It is in this zone that the effects of bacterial sulphate reduction should be most apparent, and the evaporite minerals sampled here have the heaviest sulphur and oxygen  $\delta$  values measured (see Figure 7-15). Also, the isotopic composition of the brines of the mixed zones is displaced from a



line joining the seaward and landward regimes on a  $\delta^{34}\text{S} / \delta^{18}\text{O}$  plot toward heavier values (see Figure 7-5). These two trends are best explained by bacterial sulphate reduction, and roughly conform with Patterson's calculations on the stoichiometry of dolomitization and sulphate reduction (see Chapter 6).

The light oxygen  $\delta^{18}\text{O}$  values of water of the central sabkha are problematical because there is no quantitatively significant process for removing  $^{18}\text{O}$  faster than  $^{16}\text{O}$ . As noted, the landward brines do not have the lightest  $\delta^{18}\text{O}(\text{H}_2\text{O})$ , so mixing cannot be invoked, at least not with continental groundwaters. One possibility is the local channelling of rainwater that would supply water depleted in  $^{18}\text{O}$ .

#### Comparison with Butler et al (1973)

Butler et al (1973) have also measured sulphur  $\delta^{34}\text{S}$  values for brines and evaporite minerals of the Abu Dhabi sabkha. Their results are in general agreement with those presented here. They find that  $\delta^{34}\text{S}$  of marine-derived brines is about 4‰ heavier than  $\delta^{34}\text{S}$  of continental-derived brines. Their measurements of  $\delta^{34}\text{S}$  variation with depth show lighter sulphur  $\delta^{34}\text{S}$  values for deeper (older) samples (see Figure 7-16); this vertical trend conforms to the lateral trend to lighter  $\delta^{34}\text{S}$  toward the sabkha centre in the seaward zone.

There is an apparent systematic difference in the measurement of  $\delta^{34}\text{S}$  between the two studies. Butler et al (1973) indicate that the

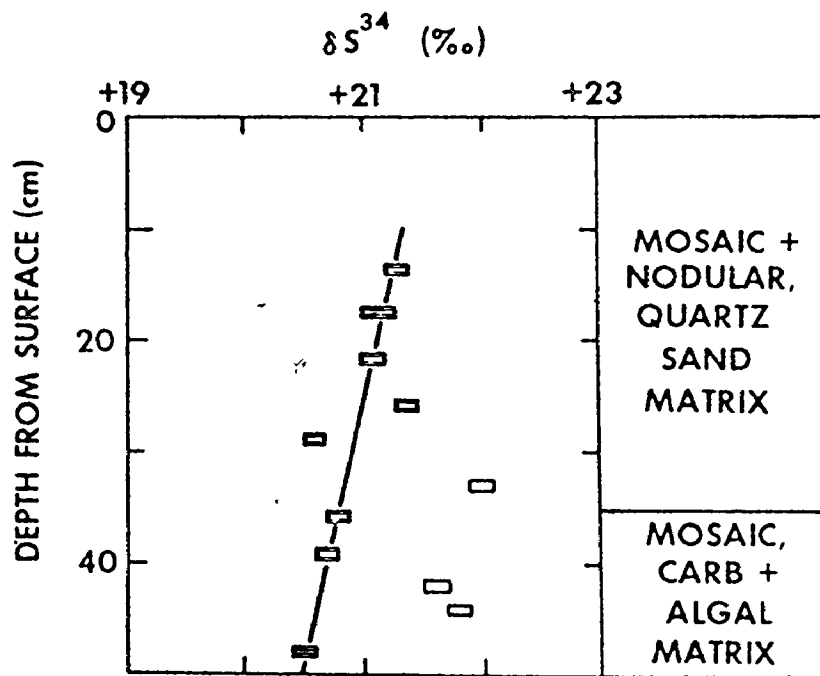


Fig. 7. Depth variation of sulphur isotope in marine supratidal anhydrite cycle. Solid data points = no bacterial action; open = bacterial action. Note core description

Figure 7-16: Depth variation of sulphur isotope in marine supratidal anhydrite cycle (from Butler et al 1973) Solid Data points = no bacterial action; open = bacterial action. Note core description

source marine brines have a  $\delta^{34}\text{S} = +23\text{‰}$ , more than three per mille heavier than the measurements here for the seaward regime. Their determinations for continental brines are likewise heavier by about 2‰. I can offer no explanation for this systematic difference; I would emphasize the excellent agreement for  $\delta^{34}\text{S}$  and  $\delta^{18}\text{O}$  between the published values for seawater and the seaward regime brines (this work). It should be noted that Butler et al (1973) have separated their samples according to whether or not they were taken from sediment in which sulphate reduction was indicated by the smell of  $\text{H}_2\text{S}$ ; this distinction is not made here.

Butler et al. (1973) have found a range of  $\delta^{34}\text{S}$  of gypsum from +26 to +19‰. They attribute this range to fractionation by gypsum precipitation; they consider that source marine brine has  $\delta^{34}\text{S} = +23\text{‰}$ , that first-formed crystals would be 1.65‰ heavier, and that after 95% of the dissolved sulphate is used up, the last-formed gypsum has  $\delta^{34}\text{S} = +19\text{‰}$ . I have found a shift of less than 1‰ in the seaward regime, and unlike Butler et al (1973), have demonstrated the lateral variation (decreasing toward the sabkha centre). For gypsum, Butler et al (1973) have shown that the sulphur  $\delta$  values correlate with crystal grain size. They suggest that a "possible explanation is that one is seeing the effect of continued crystal precipitation from a brine constantly changing in isotopic composition combined with crystal zonation" and that the large crystals "have small cores which are isotopically lighter than the

surrounding gypsum! I would expect that gypsum growing in a brine that is progressively becoming isotopically lighter to acquire lighter outer shells. However, my data for gypsum from the seaward zone shows no significant correlation between the gypsum grains and either  $\delta^{34}\text{S}$  or  $\delta^{18}\text{O}$  (see Figure 7-17).

As mentioned, Butler et al (1973) observe that  $\delta^{34}\text{S}$  of marine supratidal anhydrite decreases from 21.2‰ at 15 cm below the surface to about 20.5‰ at about 50 cm and this shift may be analogous to the lateral trend for  $\delta^{34}\text{S}$  in the seaward regime (this work). They also find for supratidal anhydrites crystallized from continental-derived brines that  $\delta^{34}\text{S}$  decreases from about +20‰ at 5 cm depth to about +17‰ at 60 cm depth. This variation may be comparable to the mixing effects observed in the landward regime. Similarly, mixing in the landward regime may account for their observation that the "hydration of marine anhydrite to gypsum via a solution phase in a continental brine regime results in the gypsum being isotopically lighter than the 'parent' anhydrite".

#### Applicability to Ancient Evaporites

From the foregoing, it is clear that ~~no~~ simple isotopic characteristic can be used to indicate a sabkha-type depositional environment of an ancient evaporite. A large range of  $\delta^{34}\text{S}$  and  $\delta^{18}\text{O}$  might be expected especially in those cases in which sulphate reduction was extensive.

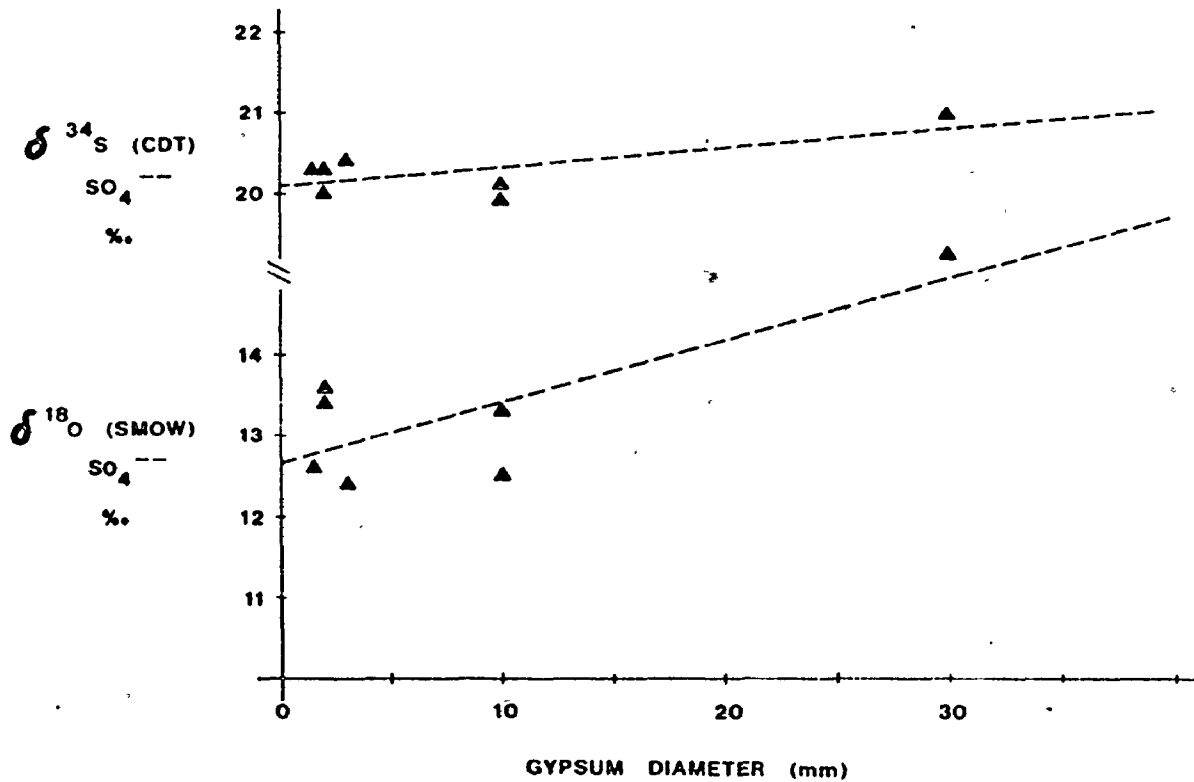


Figure 7-17: Sulphur and Oxygen Del Values versus Diameter of Gypsum of Seaward Zone, Abu Dhabi Sabkha

(I. C. C. of straight lines shown not significant at 0.02 level)

The  $\delta^{34}\text{S}$  and  $\delta^{18}\text{O}$  values might be correlated, due either to crystal-liquid fractionation or bacterial reduction. However, Mizutani and Rafter (1973) have shown that some intermediates in the bacterial reduction scheme can exchange oxygen isotopes with water, and this process might obscure the latter correlation. Isotopic variation with depth at a single location (as shown by Butler et al, 1973) might be expected, but Davies and Nassichuk (1975) have apparently found such vertical variation in the Otto Fiord Formation which they (and others) argue formed in deep water.

Consistent lateral variation would not be expected. The sinuous nature of the facies boundaries, and the irregularity of the sabkha topography result in considerable isotopic variability along strike.

The significance of the landward regime is difficult to estimate. It is conceivable that sabkha evaporite deposition could proceed with negligible landward inputs, depending on the paleogeography of the depositional site.

### Summary

It has been shown that the brine origin discriminator developed by Patterson (the  $m_{\text{K}^+}/m_{\text{Br}^-}$  ratio) has validity for the sulphur and oxygen isotope compositions of the sulphate dissolved in those brines. Furthermore, the evaporite minerals from those zones also have distinctive  $\delta^{34}\text{S}$  and  $\delta^{18}\text{O}$ . It is considered that the stable isotope

ratios are in fact more sensitive to such processes as mixing than the  $m_{K^+}/m_{Br^-}$  ratio.

Gypsum is precipitating in the interstices of the seaward regime in isotopic equilibrium with the dissolved sulphate. The failure of the residual sulphate to be depleted in  $^{34}S$  by an amount that corresponds to the fraction removed (the decrease in dissolved sulphate concentration) may be explained by isotopic exchange between the early-formed crystals and later-stage solutions.

Mixing of brines of different isotopic composition dominates the lateral isotopic variation seen in the landward regime. It appears that the evaporite minerals and brines are not in isotopic equilibrium, but the sample coverage in this work presents some uncertainty in this matter. It is clear that a wave of sulphate that is lighter than the seaward regime ( $\delta^{34}S = +16\%$ ) may significantly decrease the ultimate composition of evaporite minerals in these sediments.

In the central zone, the sulphur and oxygen  $\delta$  values of the evaporite minerals are heavier than elsewhere, having been enriched by sulphate reduction. The brines of the mixed regime are likewise anomalously heavy.

The oxygen  $\delta$  values of the brine water are heavy in both the seaward and landward regimes, probably because of extensive evaporation. The relatively light values of the central sabkha are problematical.

Secular variation of Persian Gulf sulphate on the Holocene time

scale is not required to model these data.

It is considered that ancient evaporites deposited in a sabkha environment would have a wide range of  $\delta^{34}\text{S}$  and  $\delta^{18}\text{O}$  and that they might be correlated, but that constant  $\delta$  values along strike would not be found.

The foregoing summary is illustrated in Figure 7-18.



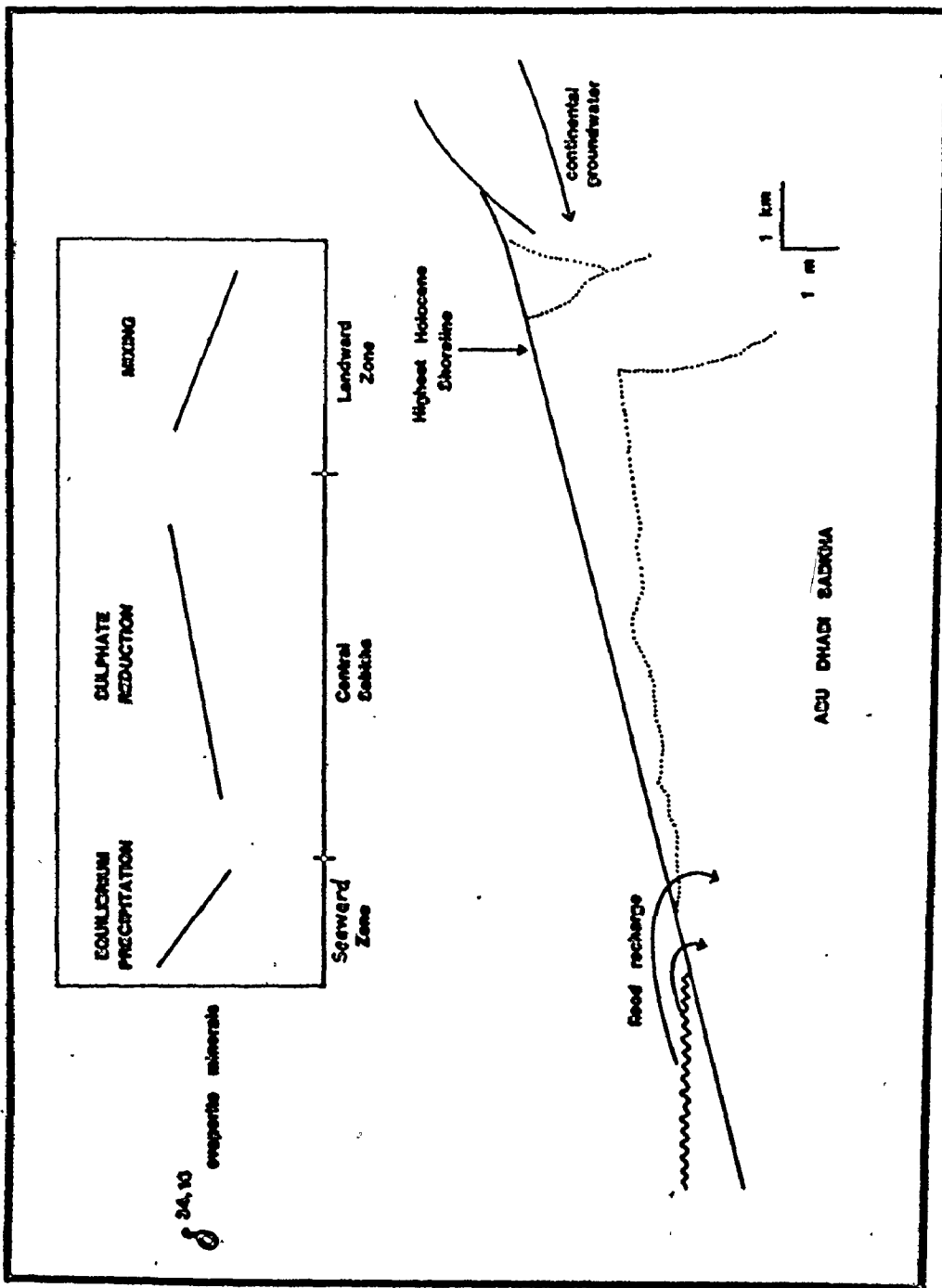


Figure 7-18: Schematic Summary of Isotope Variation at Abu Dhabi Sabkha

## STABLE ISOTOPE STUDIES, SOME ANCIENT EVAPORITES

### Introduction

It has been established that the sulphur  $\delta$  values of ancient evaporites can be related to the sulphur  $\delta$  values of contemporaneous seawater sulphate (Thode and Monster, 1965; Holser and Kaplan, 1966). The secular variation apparent in graphs of  $\delta^{34}\text{S}$  versus time has been attributed to changes in the rates of the major mechanisms of sulphate addition to or removal from the ocean (see, for example, Rees, 1970; Holland, 1973).

Although the secular variation in  $\delta^{34}\text{S}$  of evaporites and seawater sulphate is now well established, it is appropriate to review the empirical method by which it was first established. After analyzing more than 500 samples from evaporites of diverse geological age (mainly Phanerozoic) and wide geographic spread, Thode and Monster (1965) found the following: some individual beds of wide lateral extent have a range of  $\delta^{34}\text{S}$  of about two per mille (e. g. Lower Ratcliffe: 18.5 to 20.6‰); evaporites deposited over much wider geographic spread in the same geological period or epoch also have a narrow range (e. g. Permian: 9.6 to 12.6‰); the total range of  $\delta^{34}\text{S}$  values in

---

\* This unit, now known as the Midale Evaporite (Fuzesy, 1960) is discussed in detail in the next section.

Phanerozoic and late Precambrian evaporites is greater than twenty per mille. These three conditions were necessary and sufficient evidence of secular variation in  $\delta^{34}\text{S}$  of seawater sulphate.

Some determinations of  $\delta^{18}\text{O}$  of sulphate in ancient evaporites have been published by Solomon et al (1971), Claypool et al (1972), Pilot et al (1972) and Sakai (1972). Claypool et al (1972) have suggested that  $\delta^{18}\text{O}$  of seawater sulphate was always 3.5‰ lighter than the values of coeval evaporites (their data range from  $\delta^{18}\text{O} = 10$  to  $\delta^{18}\text{O} = 17$ ‰). However, there has not been published any account of the isotopic homogeneity of single beds, or formation, or of evaporites deposited in the same period in different basins.

In the preceding chapter, it has been shown that evaporite minerals deposited in a Holocene sabkha environment have  $\delta^{34}\text{S}$  and  $\delta^{18}\text{O}$  that can be related to  $\delta^{34}\text{S}$  and  $\delta^{18}\text{O}$  of present seawater sulphate only in a very complicated way. Moreover, there is no simple pattern of isotope variation across the sabkha (even neglecting the isotopic influence of the landward regime). Nonetheless, it is possible that depositional environments have isotopic signatures - for example, the shallow and subaerial processes of the sabkha may result in a wide range of isotopic variation, whereas deposition in deep water might have fostered greater isotopic homogeneity.

In this chapter, sulphur and oxygen isotopic analyses of some ancient marine evaporites are presented. The geological units are

presented in order of increasing complexity. The Midale Evaporite is a single thin, laterally extensive, anhydrite bed. The Salina Formation is a well known intracratonic cyclical evaporite formation. A third group of samples represents the extensive evaporite formations of the Permian System deposited in basins in Germany, the United States and elsewhere. The fourth grouping lumps diverse evaporites for which the data are too few for depositional environment characterization but are sufficient to contribute to the growing body of data on sulphur and oxygen isotope variation in evaporites.

#### Models of Isotope Variation

The models described below set out possible patterns of variation of  $\delta^{34}\text{S}$  and  $\delta^{18}\text{O}$  for evaporite minerals deposited in a sabkha environment and for those deposited in deep water. These models are based in part on the results described in the preceding chapter, and in part on inferences from hypothetical models proposed for deep water deposition (see, for example, Schmalz, 1969). Geological criteria for distinguishing evaporites deposited in these environments are included, but it should be emphasized at the outset that there is not universal acceptance of any of these criteria. Wardlaw and Christie (1975), in proposing a deep water origin for the Pennsylvanian Otto Fiord Formation, suggest that no single criterion is conclusive, but that several together are required to be convincing.

Evaporite minerals deposited on a sabkha should be closely

related to carbonate units containing shallow water fauna and particularly evidence of an algal facies. The gypsum or anhydrite should be intimately associated with dolomite because gypsum precipitation and dolomitization transpire concomitantly in sabkha sediment. Some features that may be seen are mud cracks, armoured mud balls, ripple marks, flat pebble conglomerates, and cross bedding. The sulphate facies sediments may be more or less confined to the basin margin. A large range of  $\delta^{34}\text{S}$  and  $\delta^{18}\text{O}$  would be expected. Although the range seen in Abu Dhabi sabkha sediments is not too large (for  $\delta^{34}\text{S}$ : 2.4‰ ; for  $\delta^{18}\text{O}$ : 3.2‰ ), it is likely that the same processes (especially bacterial sulphate reduction) would generate a greater range operating on a larger scale. Sabkha sediments are diachronous; concentric progressive lateral variation as shown in Figure 8-1 might be expected for a single regressive unit. The same variation would be observed in a vertical section through the regressive unit, but would not be diagnostic of sabkha deposition (this vertical variation has been observed in the Otto Fiord Formation by Davies and Nassichuk, 1975). The lateral variation might be very irregular; at Abu Dhabi, the sediment facies contacts are very sinuous, and relict tidal channels locally control such processes as dolomitization.

The sulphate minerals deposited in deep water do so uniformly over the whole basin floor whenever evaporative concentration causes the solubility product of gypsum to be exceeded. The strongest criterion

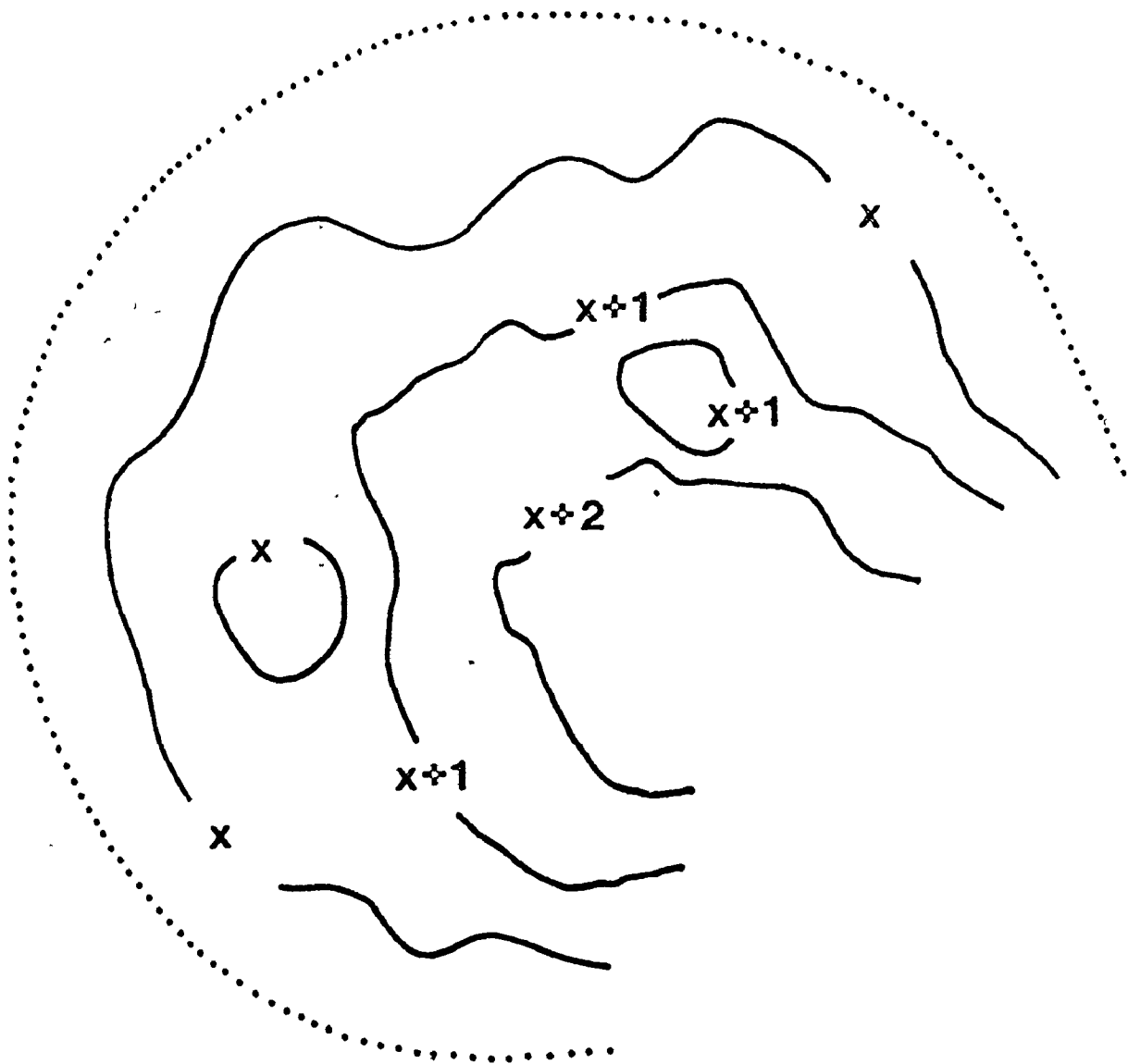


Figure 8-1: Model for Isotope Variation in Sulphate Minerals deposited in a Sabkha Environment  
(X = sulphur or oxygen del value)

for the recognition of such deposition is the existence of even parallel laminae of alternating anhydrite and calcite (dolomite) that are traceable over long distances. The anhydrite may be confined to a central portion of the basin, or may be thicker there. The associated carbonate rocks should contain deep water fauna. The sulphate and carbonate facies rocks may be fairly separate as their deposition is not as closely linked as it is in the sabkha environment. Close vertical proximity to the more concentrated salt facies, such as sylvite, may also be indicative of deep water deposition. A narrow range of  $\delta^{34}\text{S}$  and  $\delta^{18}\text{O}$  would be expected in individual evaporite beds. If sulphate reduction took place, it would not be local and thus the expected lateral isotopic uniformity would not be affected. The sulphur isotope measurements noted by Davies and Nassichuk (1975) may be of fundamental importance here. They found for individual anhydrite beds of the Otto Fiord Formation, "a gradient upward through the bed in  $\delta^{34}\text{S}$  from 16 to 12‰". These trends seem to correspond to that expected for progressive crystallization of single batches of seawater (see preceding chapter). These results are an apparent exception to the established uniformity of individual beds, and they may indicate a unique depositional mode for the Otto Fiord Evaporite. Clearly, a fuller account of the results of Davies and Nassichuk (1975) is required to establish their significance.

In both of the models postulated above, only the variation expected for primary deposition is described. It is possible that

subsequent diagenesis could affect the variation that is finally observed. Gypsum-anhydrite transitions in sabkha sediments have little effect on either  $\delta^{34}\text{S}$  or  $\delta^{18}\text{O}$  (see previous chapter). Murray (1964) has described the transition of gypsum to anhydrite caused by increased temperature after burial to a certain depth and the transition from anhydrite to gypsum if the anhydrite subsequently comes in contact with groundwater. In either case there may be a pervasive fluid phase, and in that case, extensive recrystallization and isotopic homogenization might take place.

#### The Midale Evaporite

The Midale Evaporite is the basal unit of the Ratcliffe Beds of the Madison Group (Mississippian) of southeastern Saskatchewan (Fuzesy, 1960). It has been referred to previously as the evaporite of the Lower Ratcliffe Beds, and was so described in the work of Thode and Monster (1965). As all of the Mississippian rock units of southeastern Saskatchewan are markedly time-transgressive, the Mississippian Names and Correlations Committee of the Saskatchewan Geological Society has chosen to call them beds, that are defined on the basis of marker beds, but stratigraphically they are considered neither time units nor rock units (Fuzesy, 1960).

The Midale Evaporite does not crop out; its nature and extent have been determined entirely from drill cores. The areal distribution of the Midale Evaporite and the location of the samples used in this



study are shown in Figure 8-2. The Midale Evaporite has maximum thickness of 39 feet, and an average thickness of 26 feet. Fuzesy (1960) has described the Midale Evaporite as consisting "mainly of massive, brittle, anhydrite having a conchoidal fracture, with dolomitic anhydrite, evaporitic and anhydritic dolomite beds."

Fuzesy (1960) and Fuller (1956) considered that the Midale Evaporite and all of the other similar Mississippian evaporites were formed in restricted marine lagoonal environments of the Williston Basin. Besides the Midale, there are five other distinct areally extensive anhydrite beds in the Madison Group (Fuzesy, 1960). Fuller (1956) has emphasized the cyclical nature of these evaporites; he suggests that the marine regime alternately advanced and retreated, and that the anhydrite beds were deposited during successive withdrawals. Fuzesy (1973) has recently suggested a sabkha origin for these rocks. Amongst the evidence for this origin is a) the restriction of anhydrite occurrences to near the margin of the basin; and b) the intimate association of dolomite and anhydrite, so that in some hand specimens they cannot be distinguished.

The Midale Evaporite samples were obtained from Jan Monster of McMaster University. All are anhydrite from drill cores and all appear to be fresh. There is considerable variety in the appearance of the samples, especially in their colour, but all are massive anhydrite; there is no suggestion of fine laminations. The isotopic analyses are

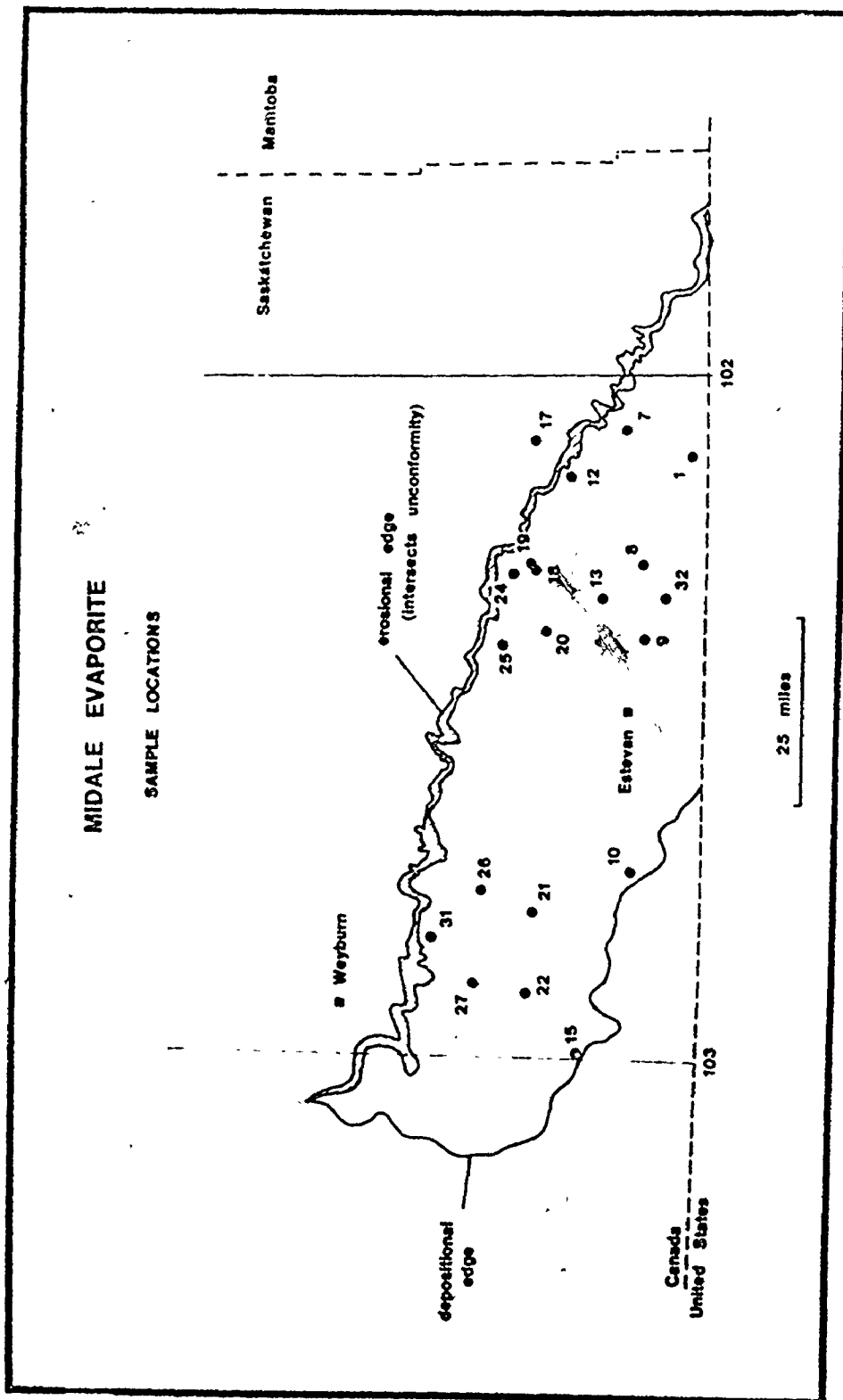


Figure 8-2: Midale Evaporite Samples Locations (base map after Fuzesy, 1960)

presented at the end of this chapter (Table 8-3). Histograms of  $\delta^{34}\text{S}$  and  $\delta^{18}\text{O}$  for all of the samples are shown in Figure 8-3. They display a very narrow range of variation for both parameters.

The very narrow range of isotopic variation is further evident on a plot of  $\delta^{34}\text{S}$  versus  $\delta^{18}\text{O}$ . The samples were grouped according to colour for such a graph of isotopic analyses (see Figure 8-4). No significant grouping is seen on that plot, that is, the groups based on colour do not occupy different areas on a graph of  $\delta^{34}\text{S}$  versus  $\delta^{18}\text{O}$ , even though they do occupy more or less distinct areas on a map (Figure 8-5).

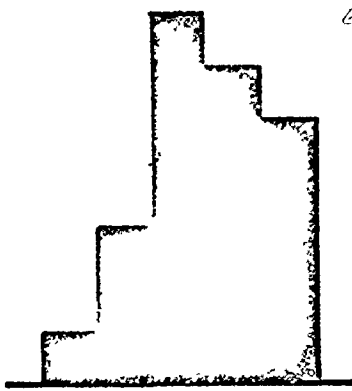
The spatial distribution of  $\delta^{34}\text{S}$  and  $\delta^{18}\text{O}$  is shown in Figures 8-6 and 8-7; contours of equal  $\delta$  values are drawn on those figures.

Discussion of these data is deferred to a subsequent section, in which the data for the Salina Formation and for the Permian evaporites are also treated.

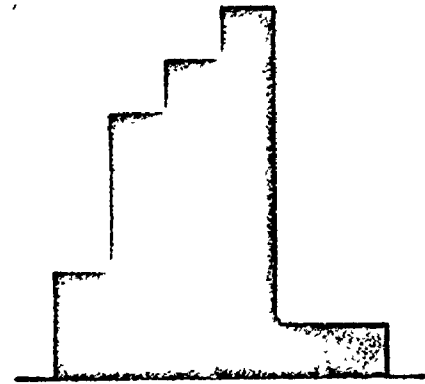
### Salina Formation

The Upper Silurian Salina rocks of southern Ontario, Michigan New York and elsewhere in the United States are a well known example of an intracratonic evaporite sequence. Despite their familiarity, the Salina rocks are a major focal point for the ongoing debate about evaporite depositional environments. Within the last year, workers studying

## MIDALE EVAPORITE

 $\delta^{18}\text{O}$  (SMOW)  
‰


15.4	—	15.0
15.9	—	15.5
16.4	—	16.0
16.9	—	16.5
17.4	—	17.0

 $\delta^{34}\text{S}$  (CDT)  
‰


18.4	—	18.0
18.9	—	18.5
19.4	—	19.0
19.9	—	19.5
20.4	—	20.0
20.9	—	20.5



1 analysis

Figure 8-3: Midale Evaporite Histograms of Isotopic Determinations

## MIDALE EVAPORITE

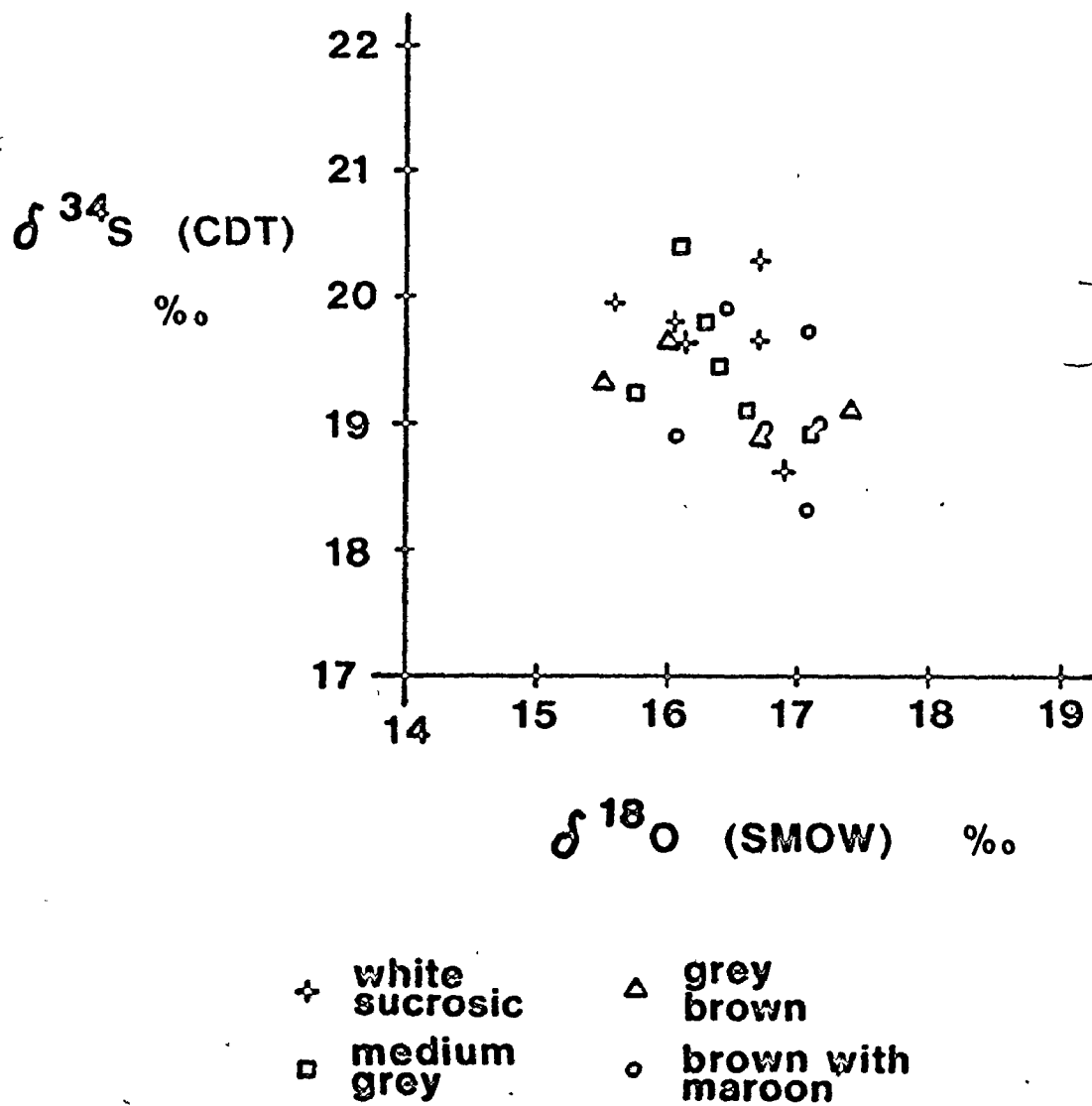


Figure 8-4: Sulphur Del Values versus Oxygen Del Values for Midale Evaporite Colour Groups

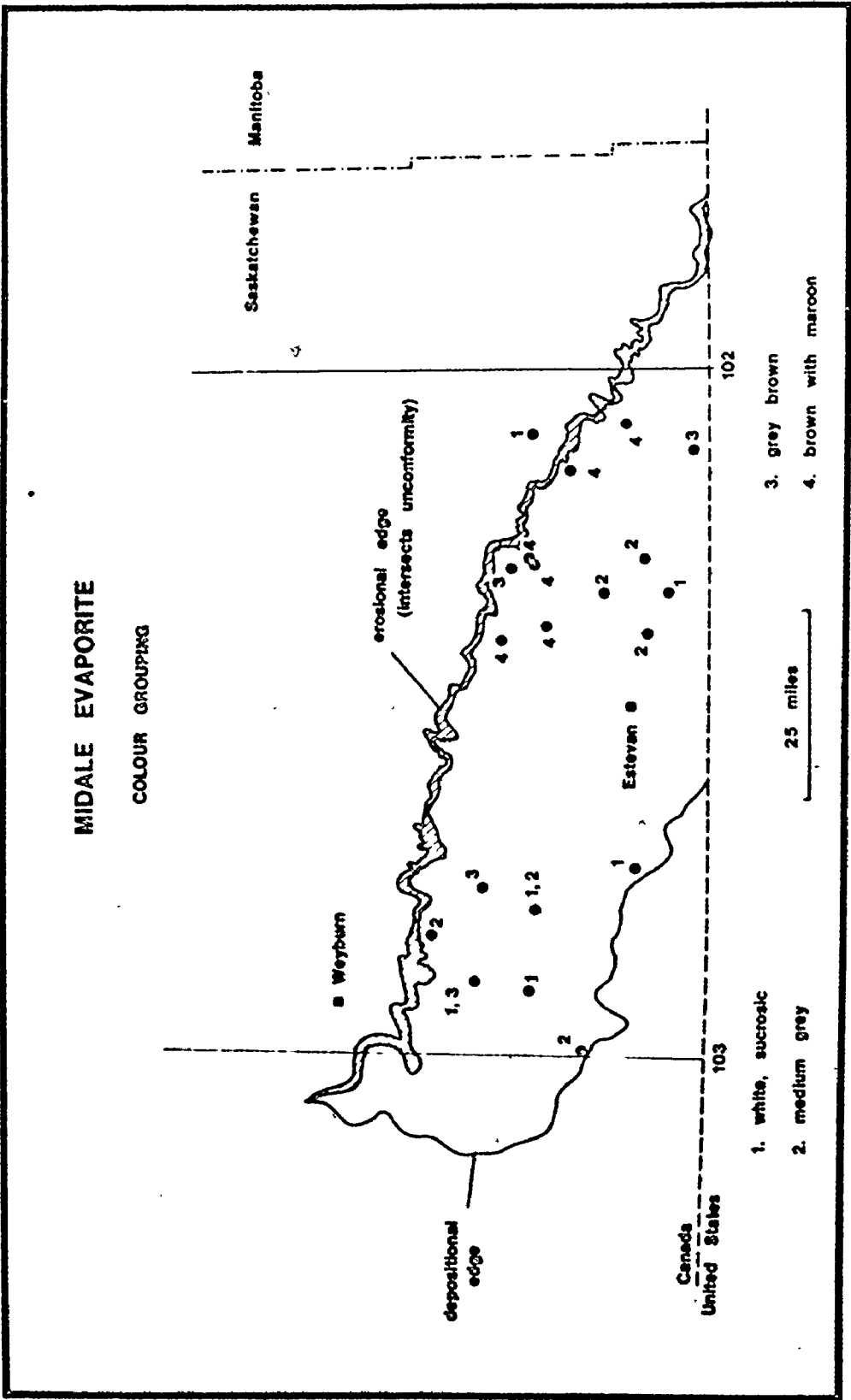


Figure 8-5: Areal Distribution of Midale Evaporite Colour Groups

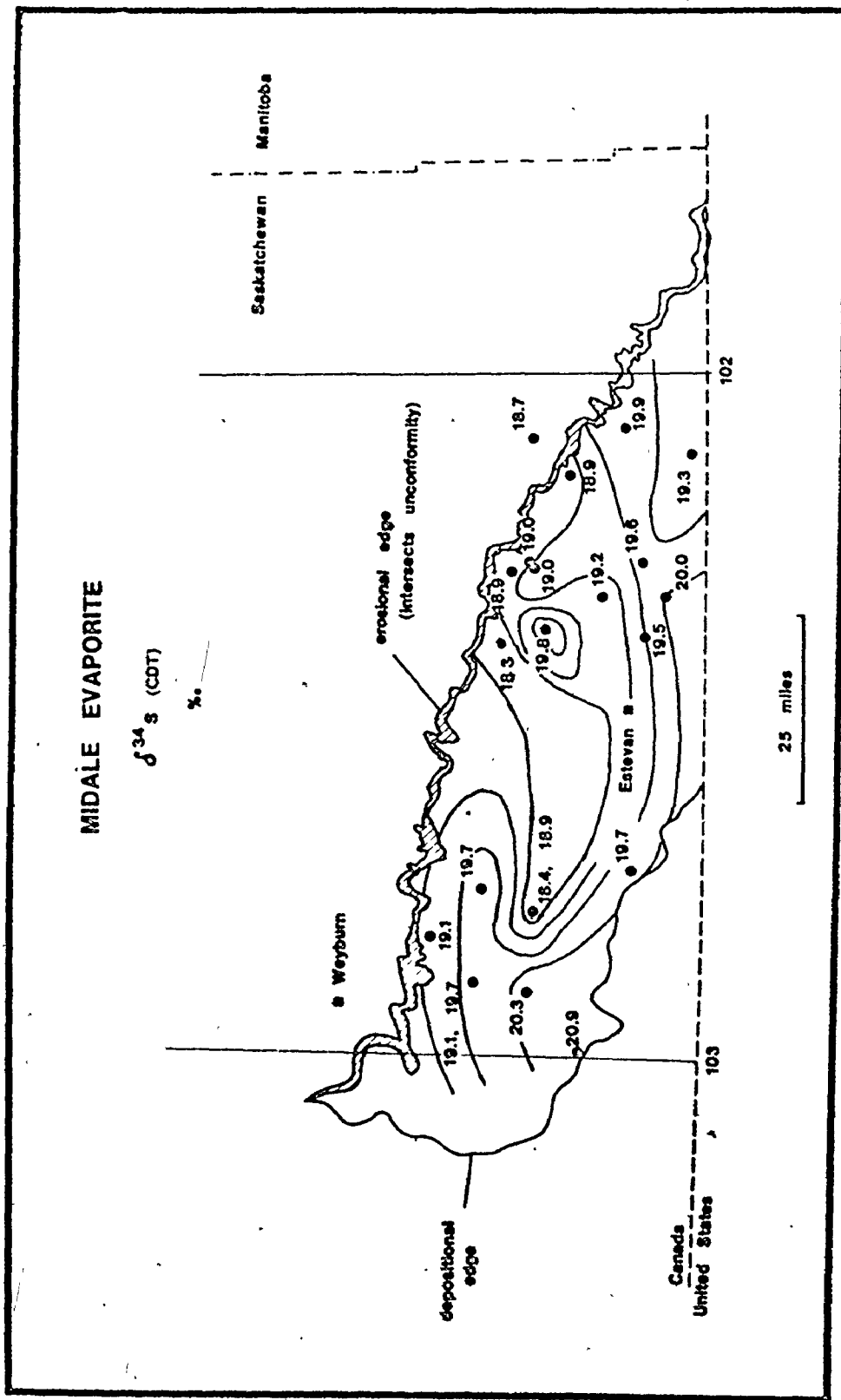


Figure 8-6: Areal Distribution of Sulphur Del Valúes, Midale Evaporite (contour interval: 0.5‰)

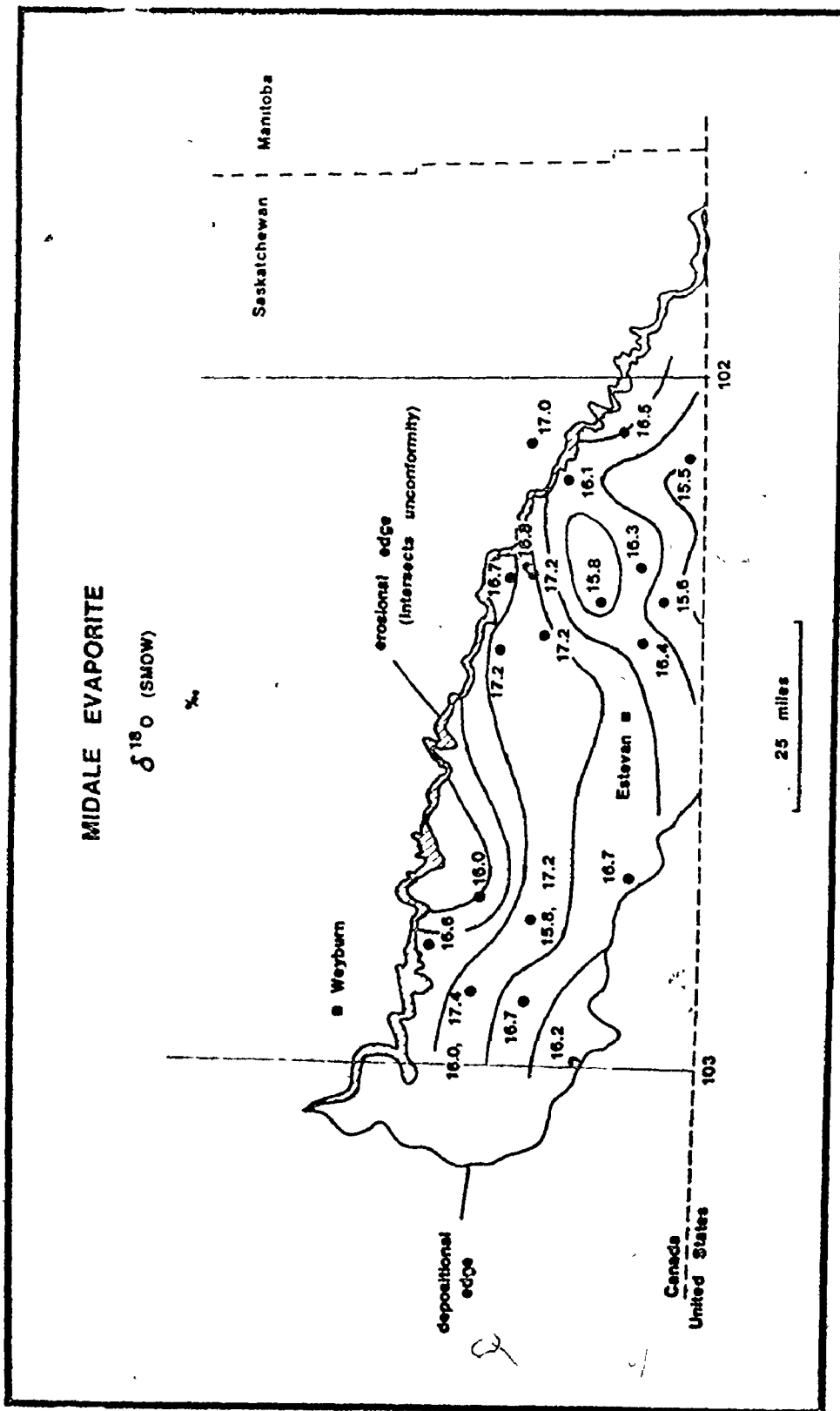


Figure 8-7: Areal Distribution of Oxygen Del Values Midale Evaporite (contour interval: 0.05‰)



different units of the Salina sequence have proposed three opposing genetic models. My intention here is to first to outline the lithology and areal extent of the Salina rocks and second to summarize the petrological and sedimentological arguments. A full synthesis of the Salina depositional environments is beyond the scope of this work, but some speculation about the probable resolution is included.

The stratigraphic nomenclature of the Salina is not entirely uniform. In southern Ontario, the Salina Formation includes all rocks between the Guelph Formation and the Bass Island Formation. In Michigan, the Salina rocks have group status, and the Salina Group lies between the Niagara Group and the Bass Island Group. In New York, the Salina Group occurs between the Lockport Group and the Cobleskill Formation. These rocks, here referred to as the Salina rocks, are continuous across the political borders and the letter subdivisions (A, B . . . G) proposed by Landes in 1945 (see Table 8-1) are recognized everywhere and commonly used in Ontario (Beards, 1967) and in Michigan (Alling and Briggs, 1961). All of the Salina rocks were deposited in Late Silurian time (the Cayugan Epoch) (Alling and Briggs, 1961; Berry and Boucot, 1970). The Salina rocks in total and most of the subdivisions are thickest in the basin centre (see Figure 8-8).

In the vertical sequence, successive layers conform to the Usiglio (1849) pattern, in that, for example, halite overlies and is overlain by anhydrite. In this context, the subdivisions of Landes (1945) are

Table 8-1: Stratigraphy of the Salina Rocks (from Alling and Briggs, 1961)

Unit II (Bass Island dolomite):

175-570 feet thick, largely buff dolomite near base,  
anhydrite and salt beds near center of basin

Unit G:

Uppermost Salina formation, 4-100 feet thick, characteristically  
grey shaly dolomite, green and red shales near Mackinac  
Straits.

Unit F:

Uppermost salt in the Salina section 0- 1230 feet thick.  
Thick beds of salt separated by shale, shaly dolomite,  
dolomite and anhydrite.

Unit E:

30-122 feet of gray or red shale with some dolomite,  
shaly dolomite and anhydrite.

Unit D:

25-65 feet, nearly pure salts, with thin partings of  
buff dolomite.

Unit C:

60-160 feet, largely shale or shaly dolomite with anhydrite  
and buff dolomite in places.

Unit B:

240-400 feet thick, almost pure salt with minor dolomite

Unit A:

30-1105 feet thick, limestone, dolomite, salt and  
anhydrite. This unit was subdivided (Evans, 1950, p. 59):

A<sub>2</sub>: Buff to brown dolomite  
or limestone.  
Dark gray dolomite  
Salt or Anhydrite

A<sub>1</sub>: Fine brown to grayish  
brown dolomite or limestone  
Fine gray dolomite or limestone  
Salt or anhydrite

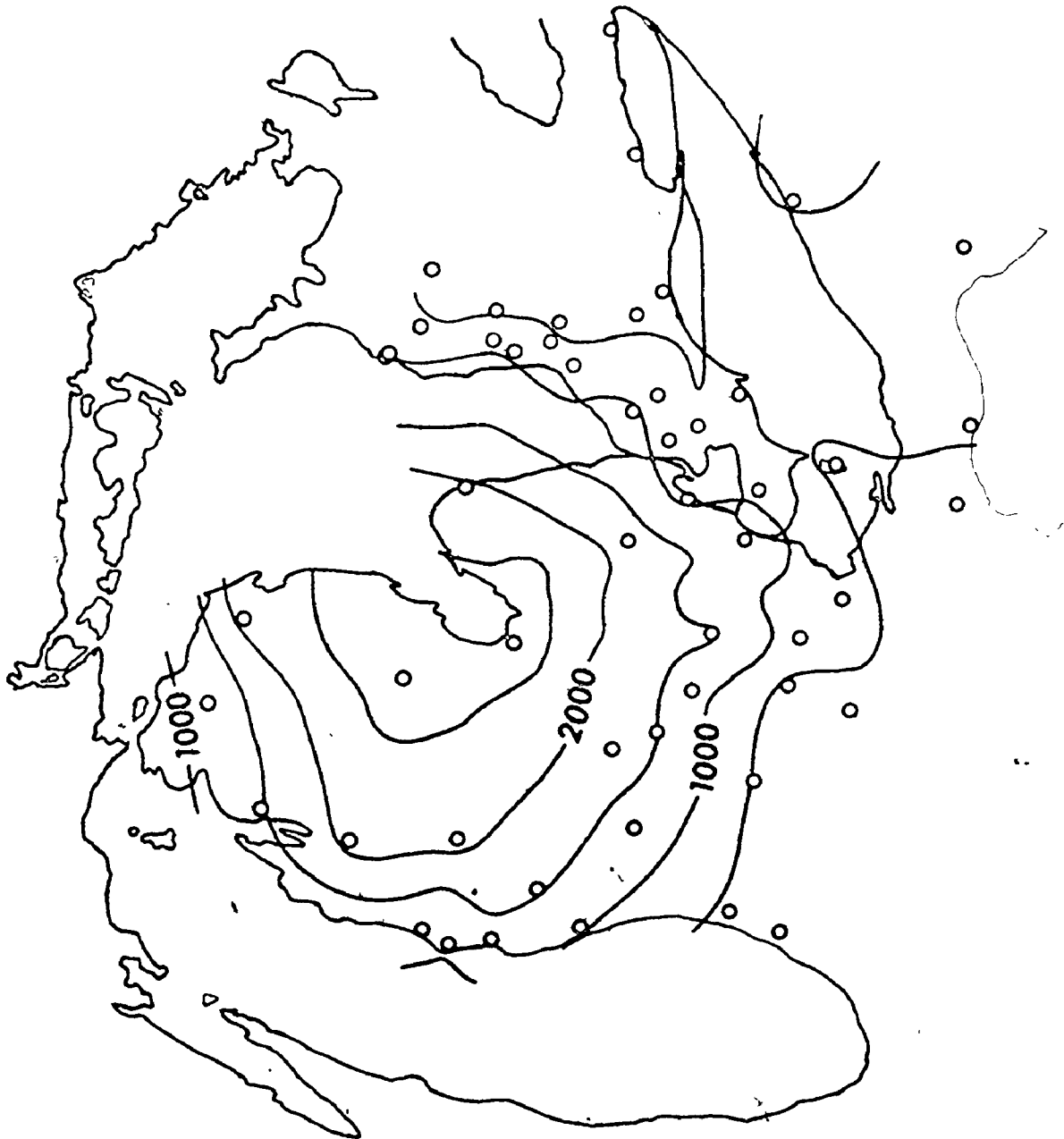


Table 8-8: Total Thickness of the Salina Evaporite (from Briggs, 1958)

lithologically cyclical, but the full progression is not developed in all of the units. The gross lateral distribution of these facies is a pattern of concentric circles with central halite surrounded by anhydrite, etc. (Briggs, 1958). Briggs (1958) has shown that the facies are locally displaced toward the centre of the basin, and he suggests that these localities mark the channelways for the influx of replacement brine (see Figure 8-9).

The margin of the Michigan Basin was a locus of reef development during the Cayuga Epoch. Both barrier reefs and pinnacle reefs have been recognized along most of the circumference of the basin (Mesolella et al 1974) (see Figure 8-10).

Several basins were active in the Late Silurian on the North American craton. Figure 8-10 shows two, but there were at least two to the north in the Arctic seaway as well. Thus the Silurian is an example of multiple basin evaporite deposition; Branson (1915) has postulated that forebasins may concentrate the inflow to a terminal basin, accelerating the rate of evaporation.

Three opposing models for Salina deposition have been postulated: deepbasin/deep water (Sloss, 1969; Mathews and Egleson, 1974), deep basin/shallow water (Dellwig, 1955; Mesolella et al 1974), and shallow basin/subaerial (Treesh and Friedman, 1974; Gill, 1974). In general, the models seem to account for the features of the specific aspect of lithological division of the Salina for which they were designed, but they

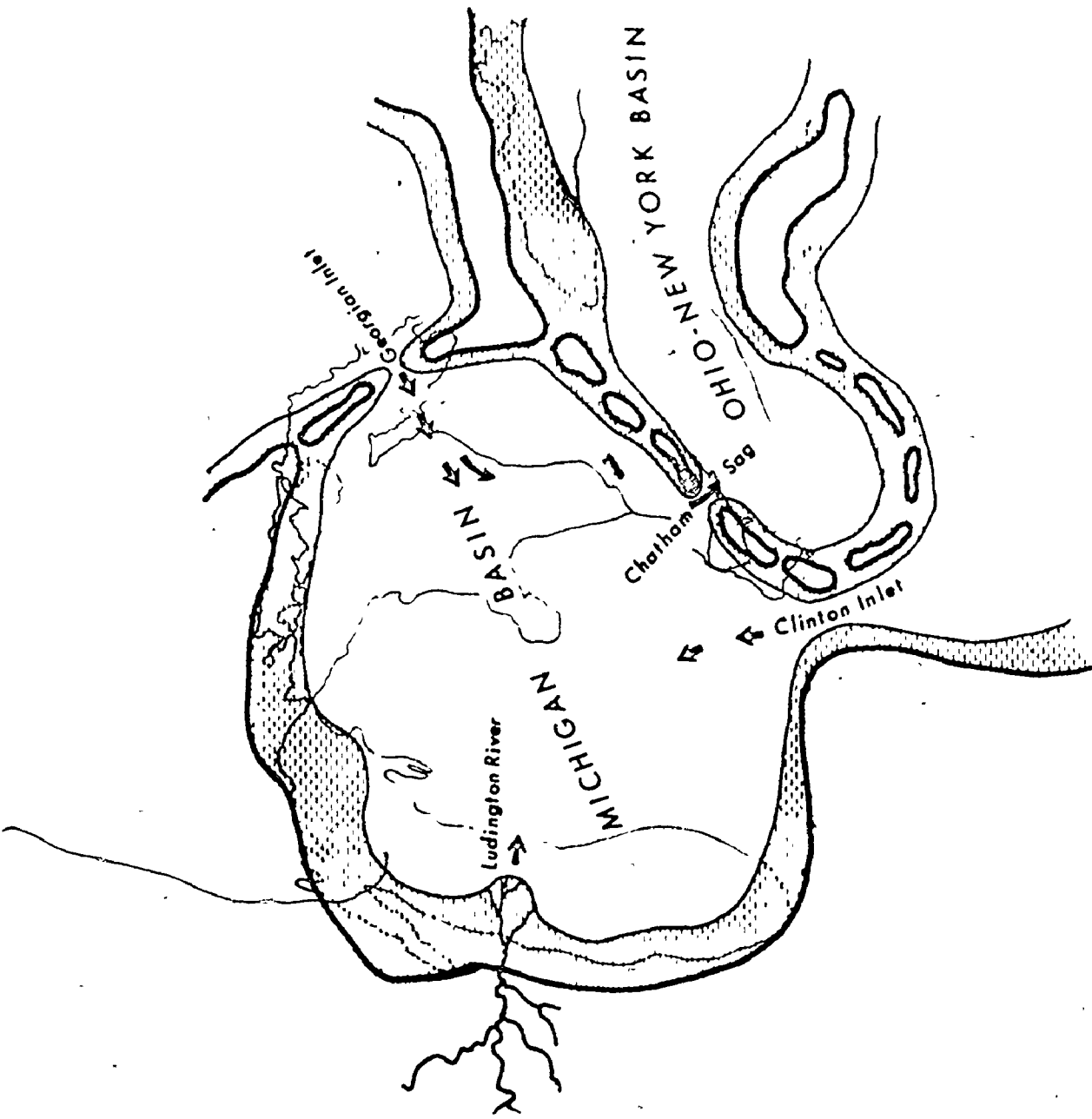


Figure 8-9: Paleogeographic Map of the Michigan Basin and the Ohio-New York Basin during Salina time (from Briggs, 1958)

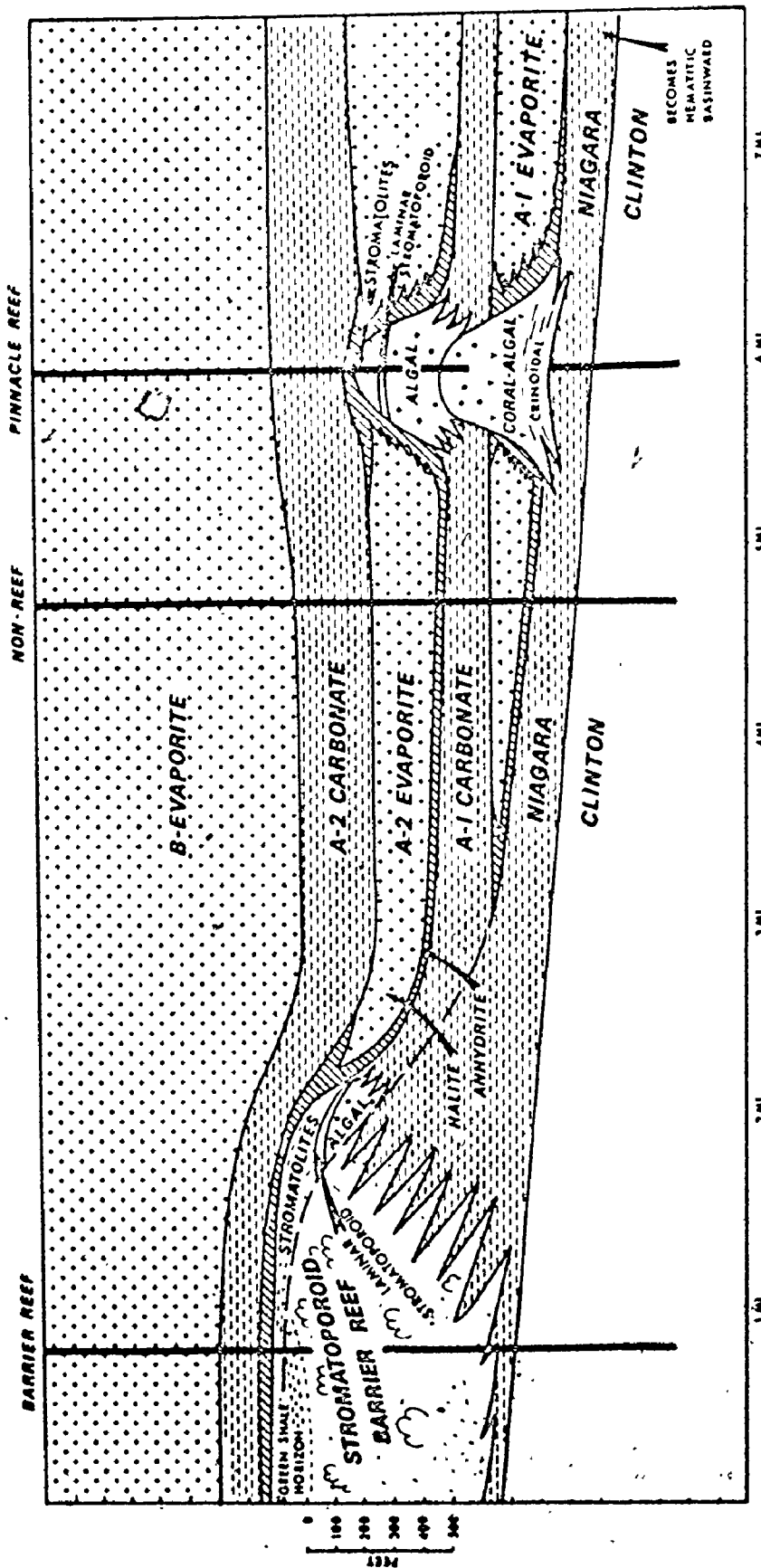


Figure 8-10: Generalised cross section of Niagara and lower Salina carbonates and evaporites northern Michigan basin showing three basic lithologic successions (from Mesolella et al, 1975)

are not convincing when applied to the entire sequence. It is impossible that all models so far advanced are correct but it is improbable that one of them alone can account for the great diversity of the Salina rocks. It is worth noting that some of the models are not mutually exclusive. Jacka and Franco (1974) model shelf deposition in the Permian Delaware Basin in terms of seven environments that are comparable to the present Trucial Coast; it is reasonable to suppose that sabkha deposition could take place on a mature cratonic peneplain simultaneously with the deposition of the more soluble salts in local depressions. As Mathews and Egleson (1974) have emphasized, the paleoslopes of the basin were probably extremely gentle. As such, great areas would be inundated by the influx of relatively small amounts of water.

The samples studied here are splits taken from drill cores stored at the Sample Repository of the Ministry of Natural Resources of Ontario at London, and samples obtained underground at the gypsum mines at Caledonia, Ontario and Hagersville, Ontario. Most of the cores at the London Repository have well cards already logged for them in a standardized format (Beards, 1967). In the case of the Norfolk County well (SAL15) and the two mines, correlation was made by the writer in accordance with the same scheme. The core samples are anhydrite rather than gypsum; most have a white gypsum rind that formed during the drilling. In all cases it was possible to avoid the gypsiferous rim. The samples from the gypsum mines are all alabastine gypsum; only

traces of anhydrite can be seen in thin section. Few of the anhydrite core samples showed the nodular form that is supposed to be diagnostic of supratidal deposition. Many of the anhydrites have clearly been recrystallized - these show solution contacts and coarser crystal size. Some of the carbonate in the core samples does show the wavy irregular laminae that are common in reef and other shallow environments. The only samples with parallel, even laminae are the anhydrite/dolomite laminae of the basin centre.

The isotopic analyses of the Salina samples are presented in Table 8-4 at the end of this chapter. The sample locations are shown in Figure 8-11.

Histograms of  $\delta^{34}\text{S}$  and  $\delta^{18}\text{O}$  are presented in Figures 8-12 and 8-13; a wide range of each is evident.

The lateral variation of  $\delta^{34}\text{S}$  and  $\delta^{18}\text{O}$  for the A-1 Anhydrite, the A-2 Anhydrite, and the B Anhydrite is shown in Figures 8-14 to 8-19.

### Permian Evaporites

Several famous evaporite formations were deposited during the Permian. The German Zechstein is the most studied evaporite sequence in the world, and German salt geologists have accorded it implicit status as the "type evaporite". The exotic chloride facies salts of the Zechstein were modelled in terms of equilibrium parageneses by van't Hoff (1912).



### SALINA EVAPORITE SAMPLE LOCATIONS

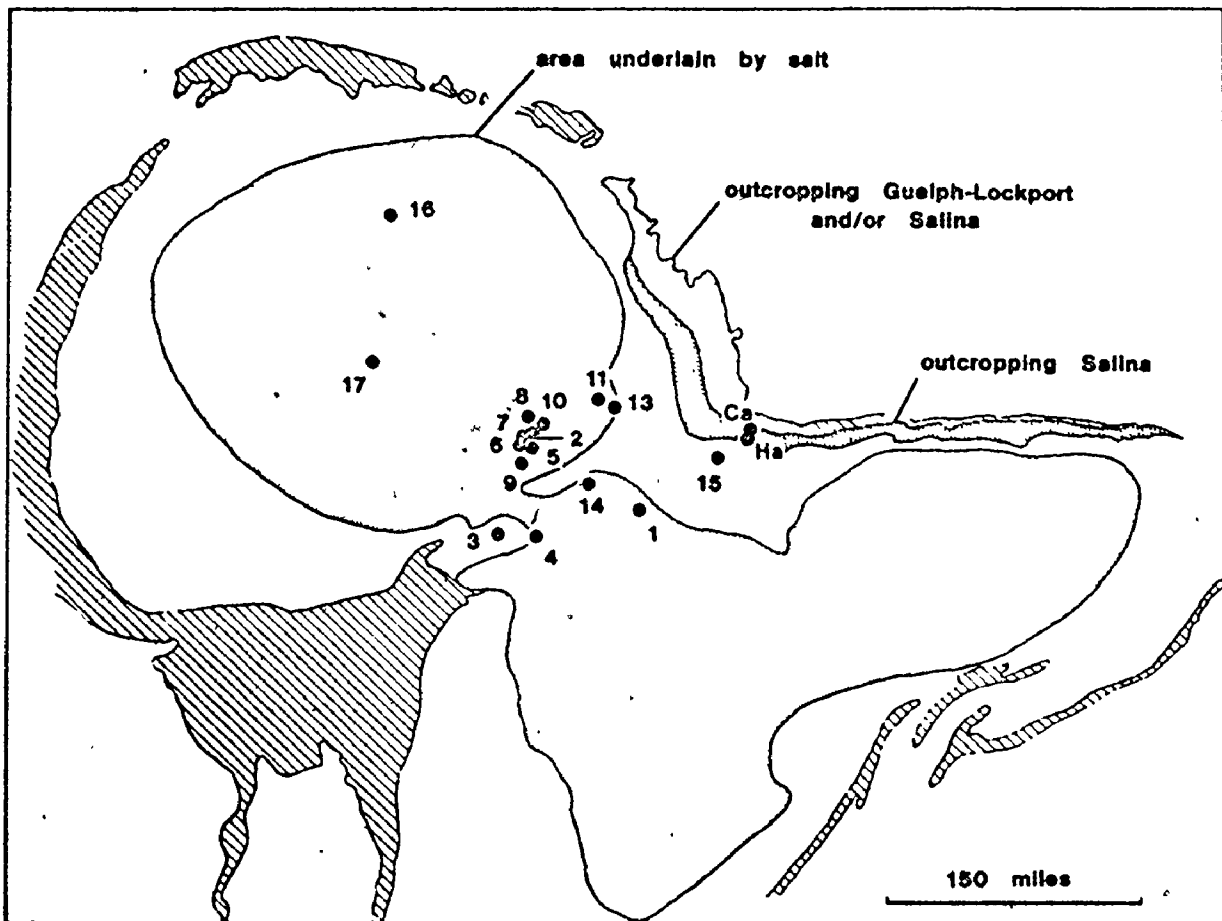


Figure 8-11: Salina Evaporite Sample Locations (map from Guillet (1964) based on Roliff (1949) and Alling and Briggs, 1968)

SALINA EVAPORITE

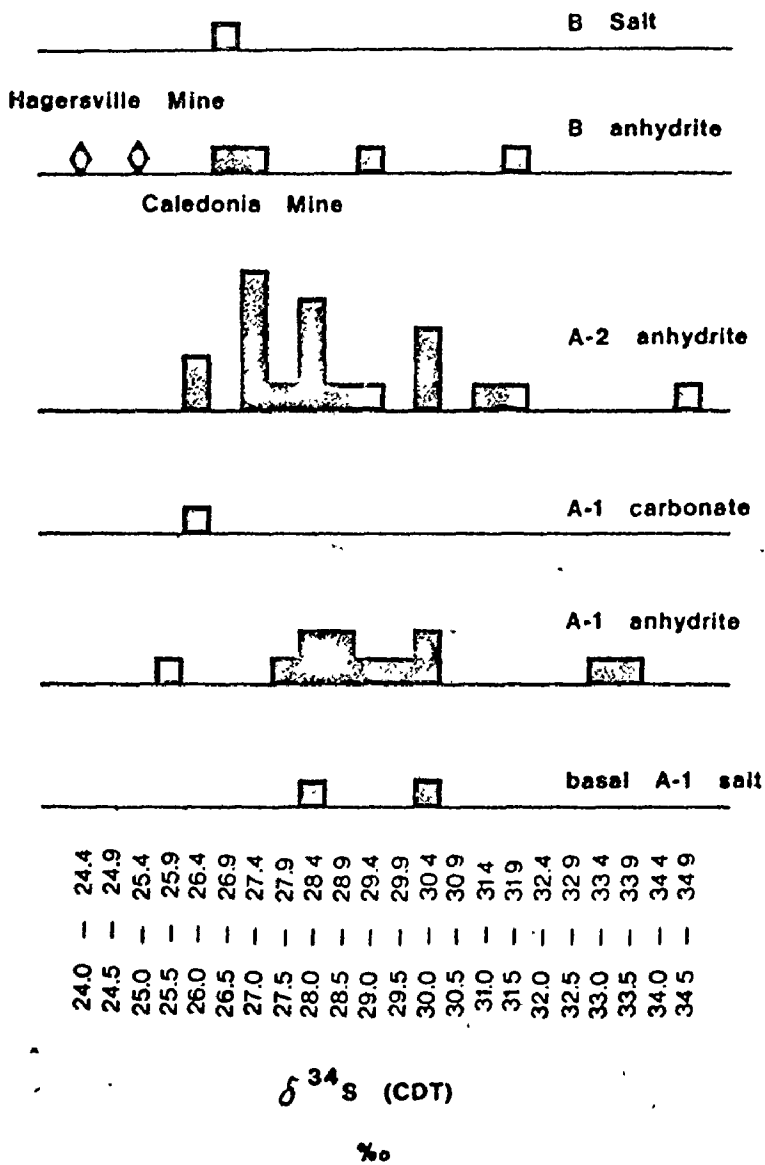


Figure 8-12: Histogram of Sulphur Del Determinations of Salina Evaporite

SALINA EVAPORITE

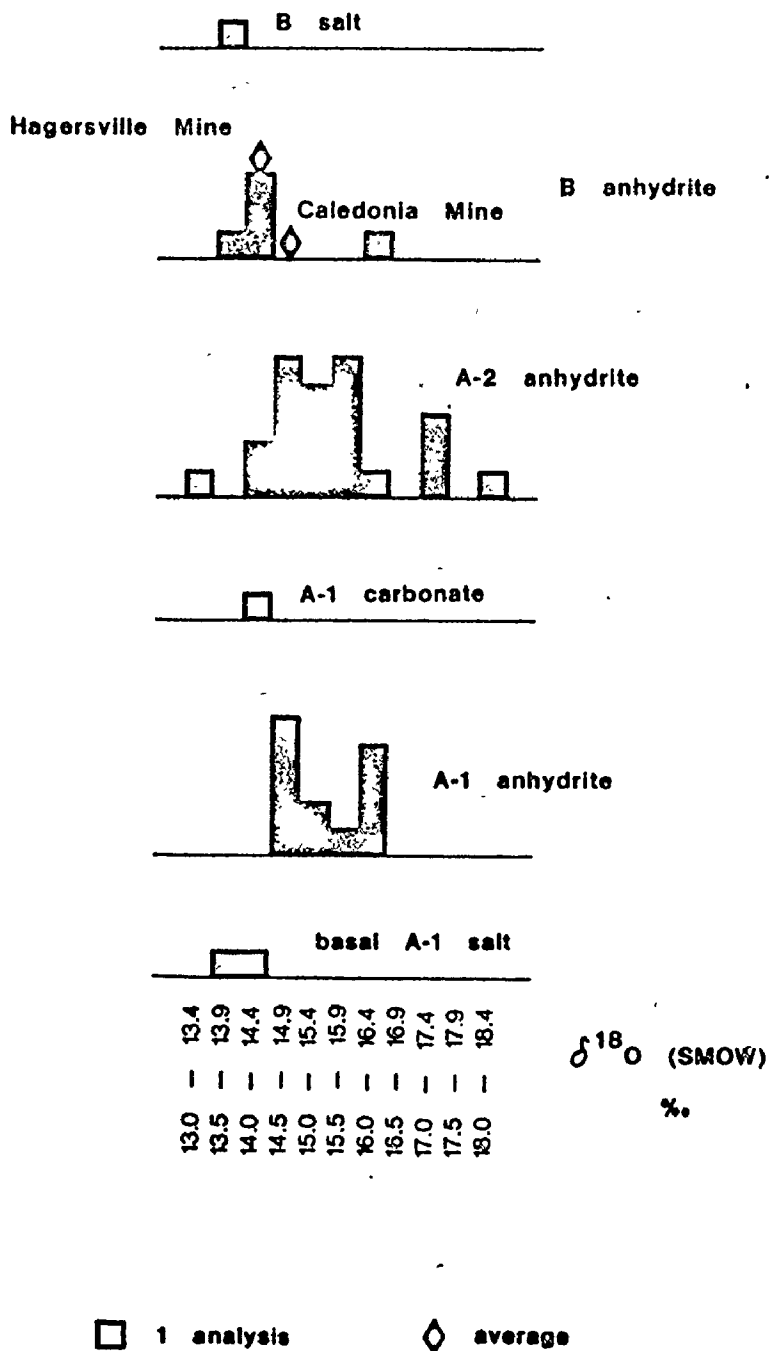


Figure 8-13: Histogram of Oxygen Del Determinations of Salina Evaporite

## SALINA EVAPORITE

A-1 Anhydrite

$\delta^{34}\text{S}$  (CDT) ‰

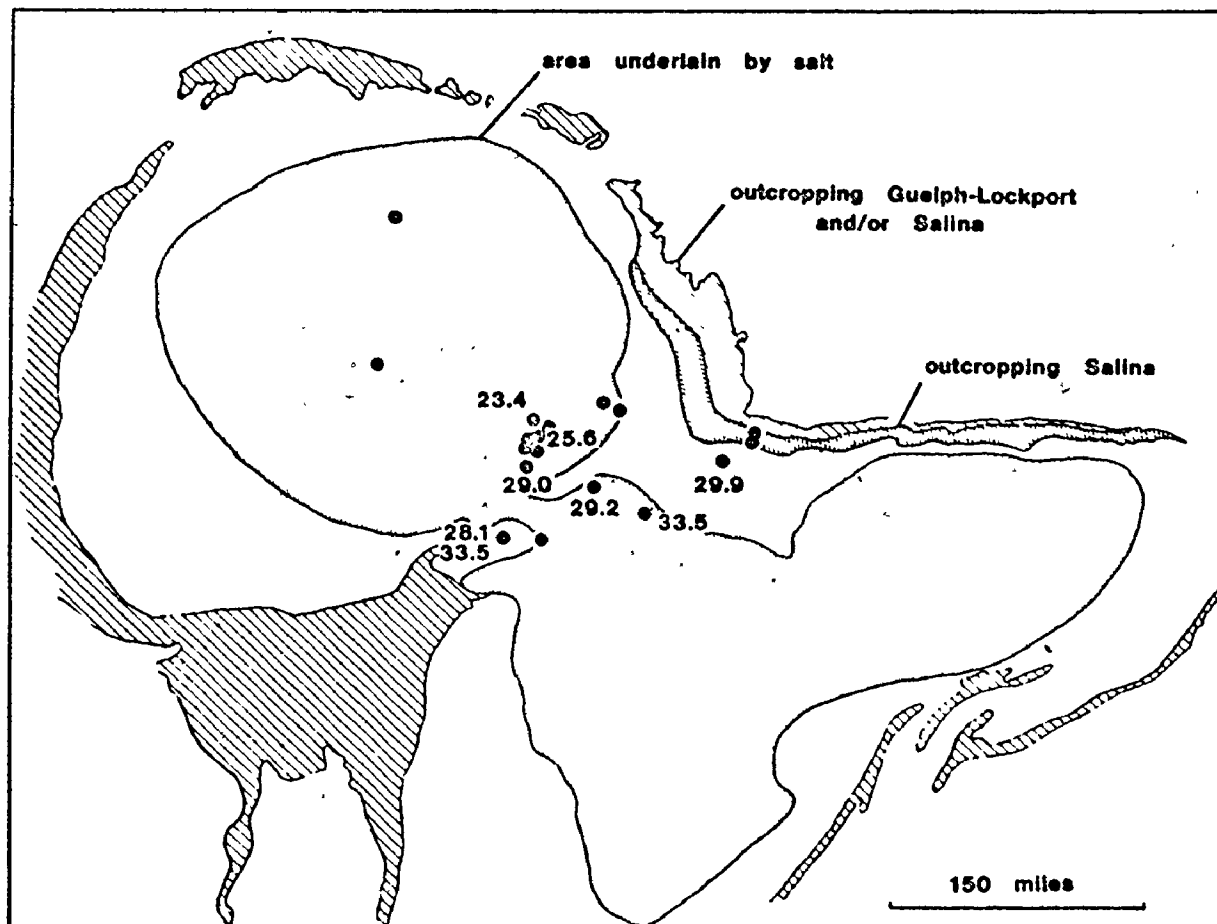


Figure 8-14: Areal Distribution of Sulphur Del Values,  
A-1 Anhydrite, Salina Evaporite

**SALINA EVAPORITE**

A-1 Anhydrite

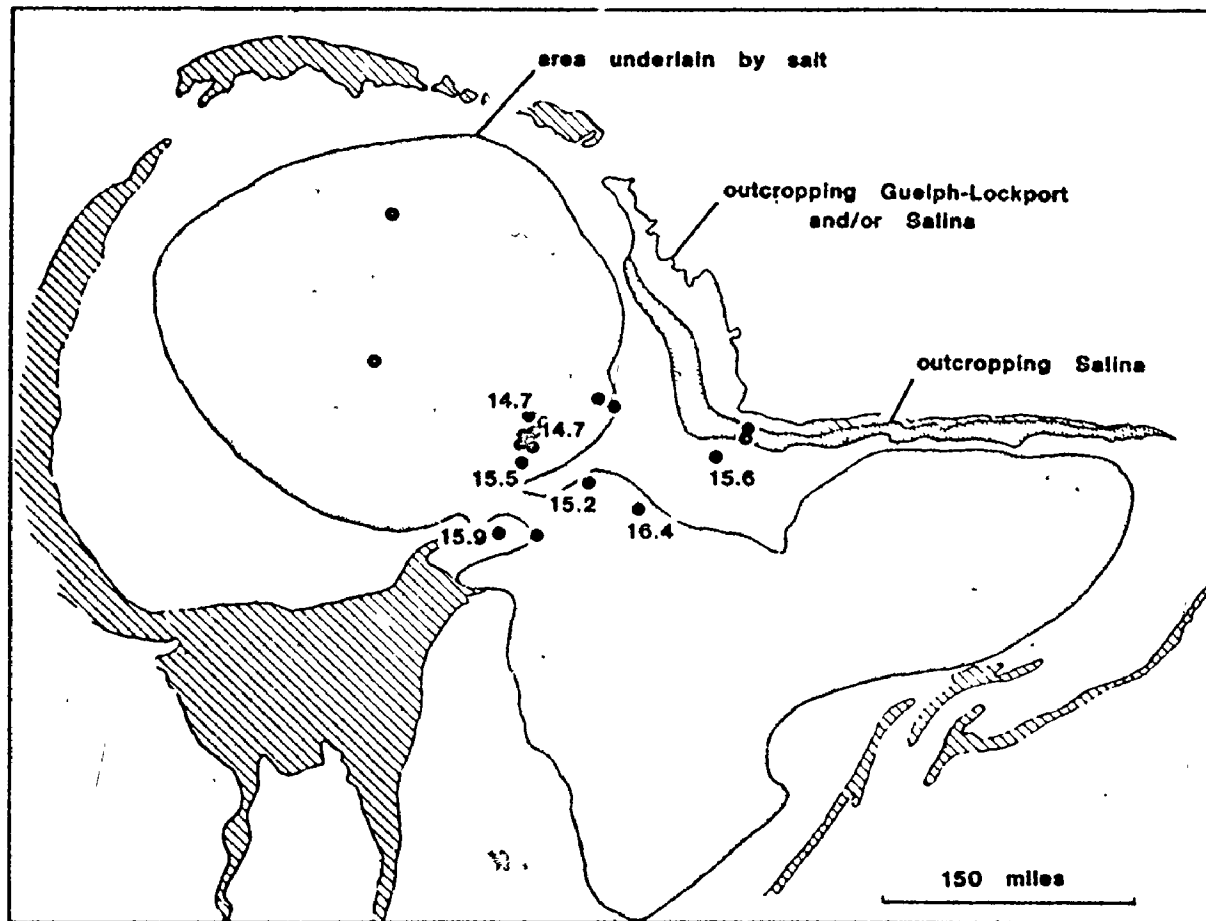
 $\delta^{18}\text{O}$  (SMOW) ‰

Figure 8-15: Areal Distribution of Oxygen Del Values, A-1 Anhydrite, Salina Evaporite

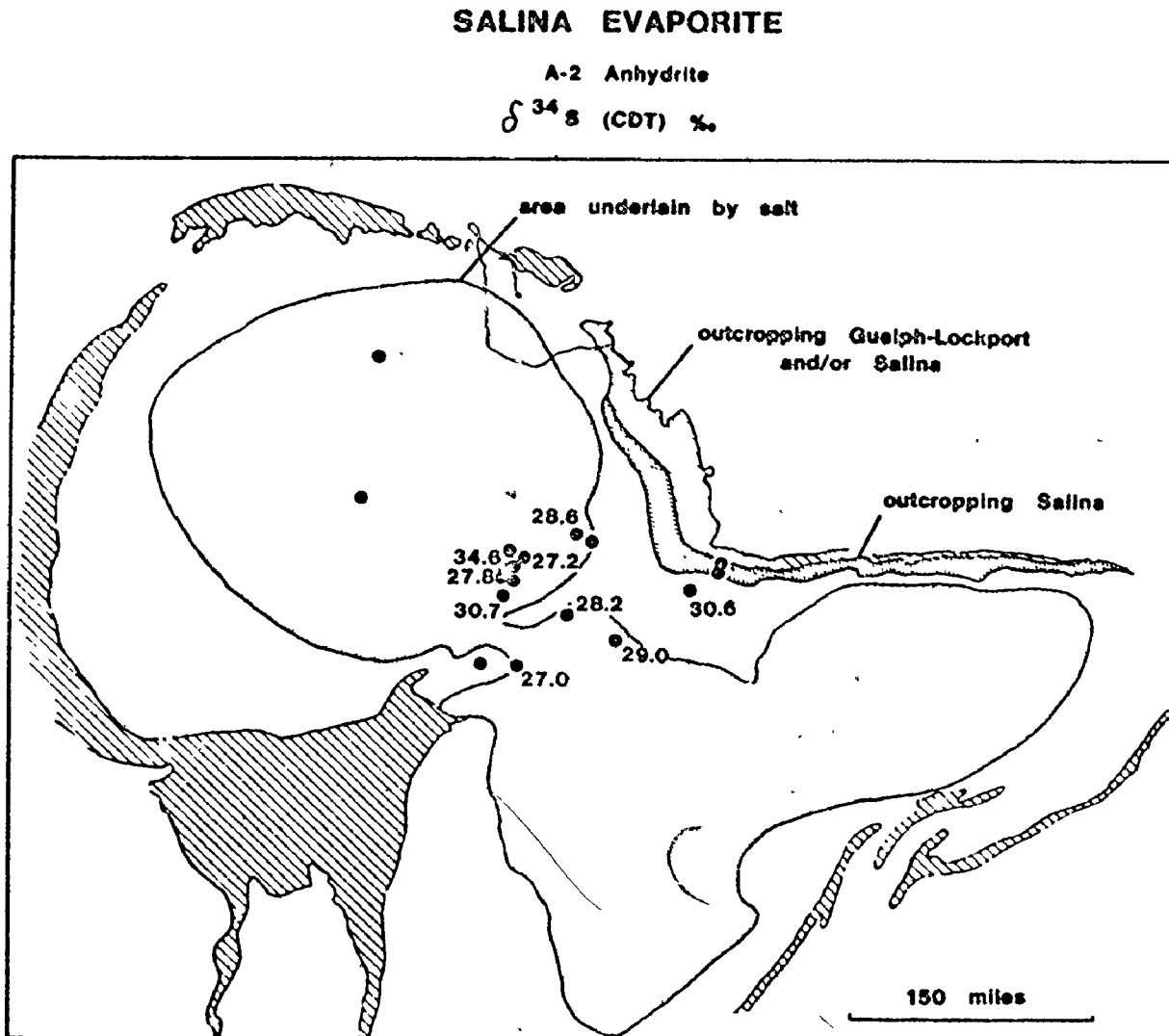


Figure 8-16: Areal Distribution of Sulphur Delt Values A-2.  
 Anhydrite, Salina Evaporite

## SALINA EVAPORITE

A-2 Anhydrite

$\delta^{18}\text{O}$  (SMOW) ‰

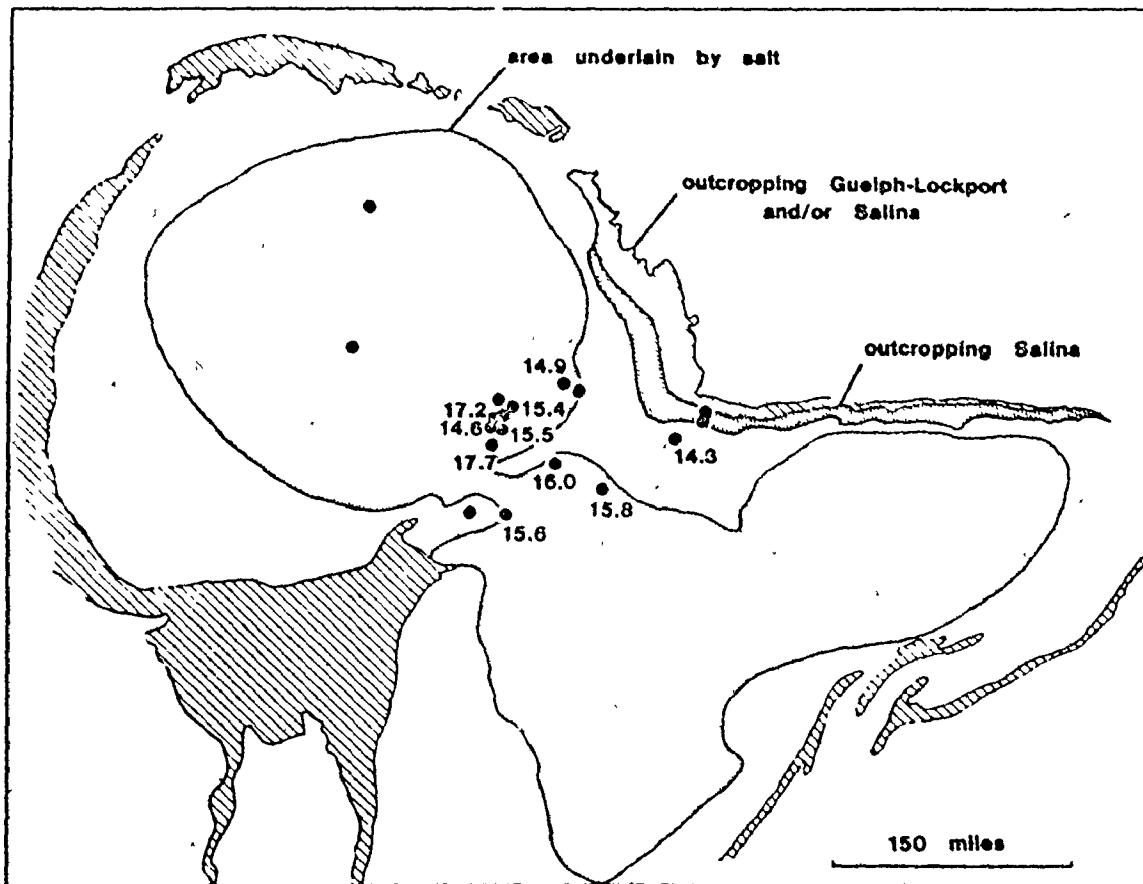


Figure 8-17: Areal Distribution of Oxygen Del Values A-2 Anhydrite, Salina Evaporite

## SALINA EVAPORITE

B Anhydrite

$\delta^{34}\text{S}$  (CDT) ‰

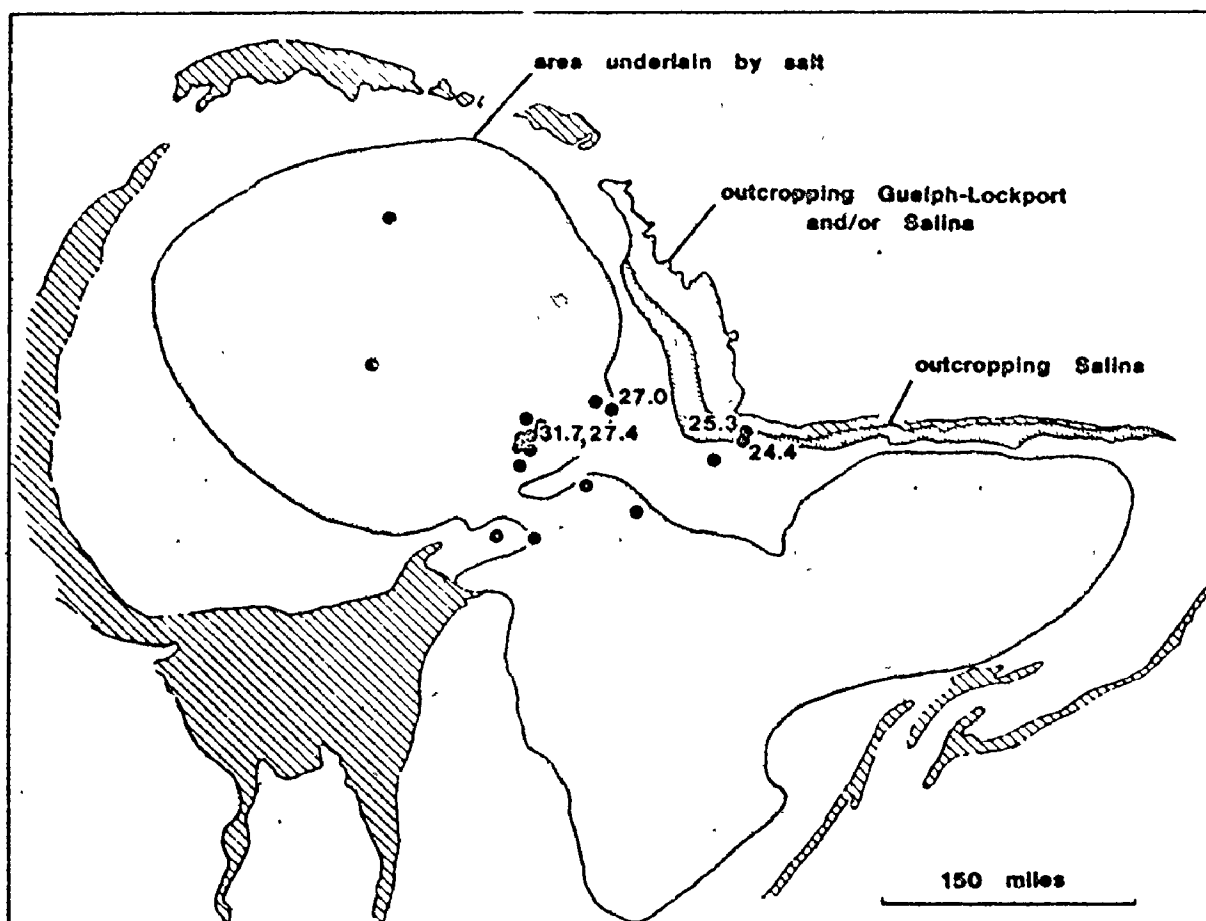


Figure 8-18: Areal Distribution of Sulphur Delta Values B Anhydrite, Salina Evaporite



## SALINA EVAPORITE

B Anhydrite

$\delta^{18}\text{O}$  (SMOW) ‰

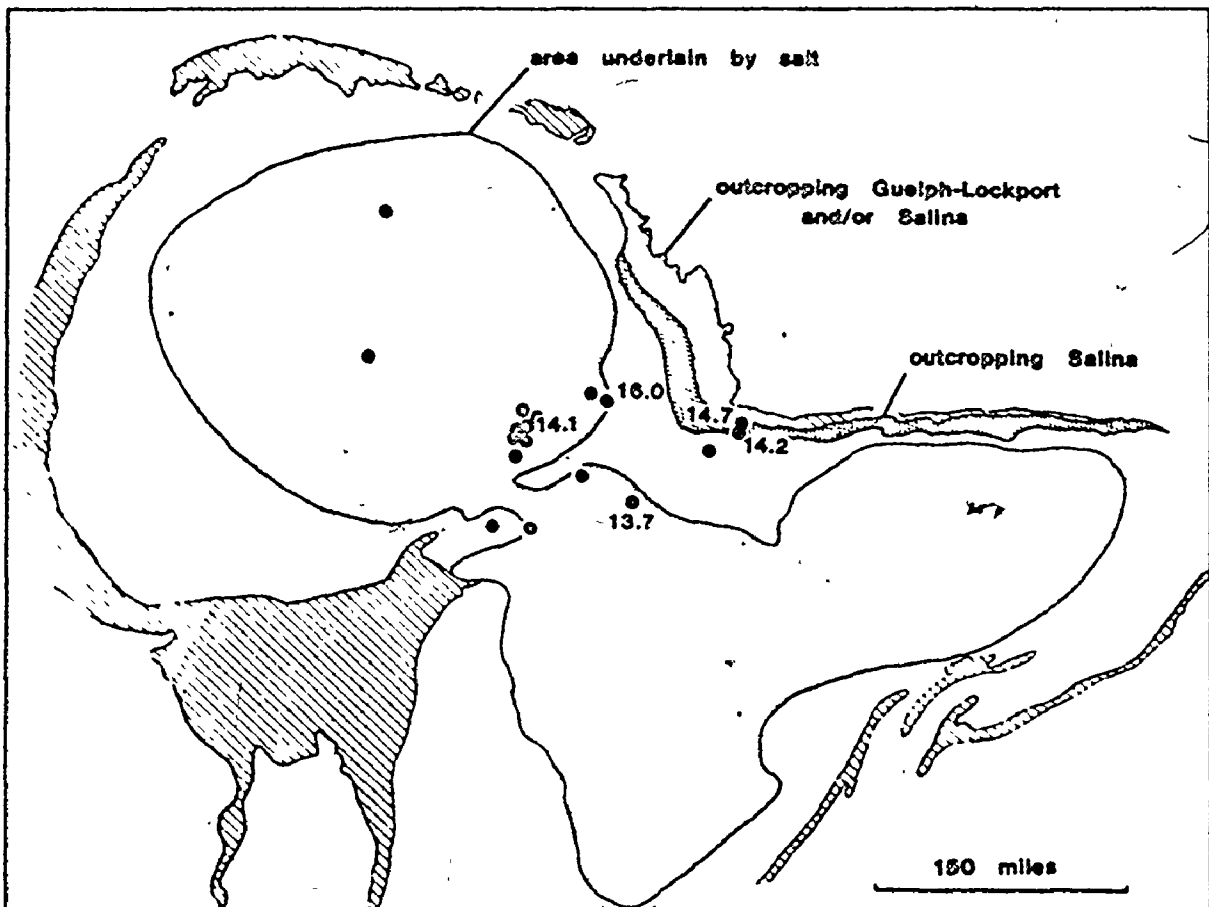


Figure 8-19: Areal Distribution of Oxygen Del Values B Anhydrite, Salina Evaporite

The cyclicity of the Zechstein is apparent in the table reproduced from Braitsch (1971) (Table 8-2).

Richter-Bernburg (1955) has correlated Zechstein anhydrite-carbonate laminae over great distances; he attributes their formation to seasonal differences in basin inflow. Comparable laminae in the Permian Castile have also been correlated over great distances (Anderson and Kirkland, 1966). It was for these laminae that King (1947) invoked the mechanism of reflux: the absence of halite that ought to accompany the deposition of substantial carbonate and anhydrite is explained by reflux of the NaCl-rich brines through the permeable reefs that apparently regulated the restriction of the Castile, back to the open ocean.

The samples analyzed in this study were obtained from Jan Monster, McMaster University. Although the geological units are nominally anhydrite, both gypsum and anhydrite are found in the samples. All the samples except those from the Castile Formation are either hand specimens or large core splits. The Castile samples are drill cuttings - a gypsiferous sand.

Histograms of  $\delta^{34}\text{S}$  and  $\delta^{18}\text{O}$  for the Permian samples are presented in Figures 8-20 and 8-21. The values of  $\delta^{34}\text{S}$  were determined by Jan Monster, and have previously been published in summary form (Thode and Monster, 1965). The isotopic analyses are listed at the end of this chapter in Table 8-5.

Table 8-2: The Zechstein Salt Sequence (from Braitsch, 1971)

Cycle	Name	Symbol	Stratigraphic Description
<u>Overlying beds</u>			Trias (Bundsandstein)
Z4	Aller Series <sup>a</sup>	A4r Na4  A4 T4	Grenzanhydrit (boundary anhydrite) Aller rock salt ("Youngest" rock salt)  Pegmatitanhydrit Red Salzton
Z3	Leine Series	Na3 { K3 Ri  K3 Ro A3 Ca3 T3	with Riedel potash seam Leine rock salt ("Youngest" rock salt)  with Ronnenberg potash seam Hauptanhydrit Plattendolomit Gray Salzton <sup>b</sup>
Z2	Stassfurt Series	K2 Na2 (K) Na2  A2 Ca2  T2	Stassfurt seam Kieseritic transition beds Stassfurt rock salt ("Older" rock salt)  Basalanhydrit Hauptdolomit (Ca2d=Hauptdolomit Ca2st=Stinkschiefer) Brownish red "Salzton" <sup>ib</sup>
Z1	Werra Series	Alβ Na1 { K1 H  K1 Th Alα  Ca1 T1	Upper Werra anhydrite with Hesse potash seam Werra rock salt ("Oldest" rock salt)  with Thuringia potash seam Lower Werra anhydrite (= Anhydrit-Knotenschiefer) Zechstein limestone Kupferschiefer
<u>Underlying beds</u>			Lower Permian (Rotliegendes)

<sup>a</sup> The Aller and Leine Series are sometimes together referred to as the Niedersachsen Series.

<sup>b</sup> Salzton = salt clay, but here the term has a stratigraphical significance and the is . . . . .)

PERMIAN EVAPORITES

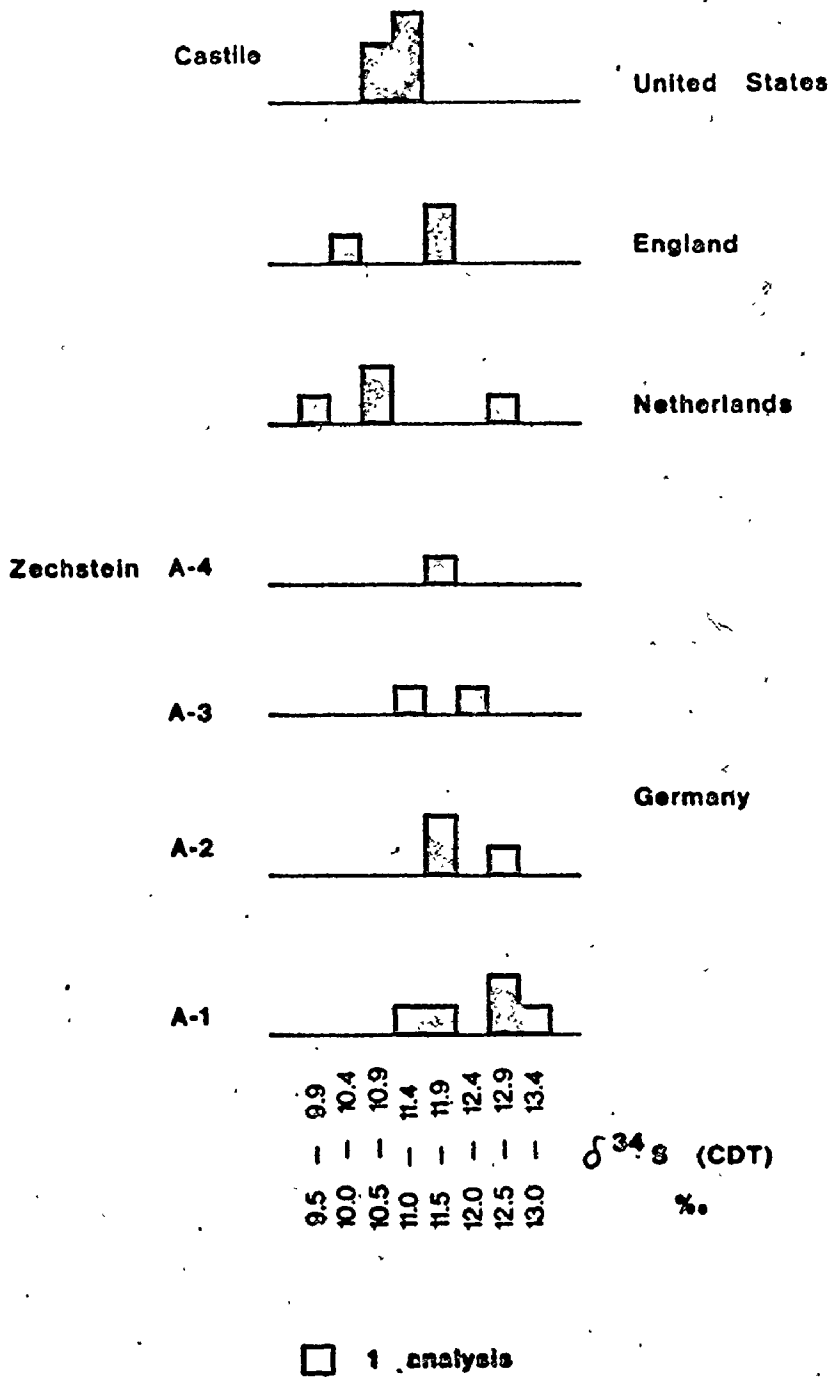


Figure 8-20: Histogram of Sulphur Del Determinations, Permian Evaporites (analyses by Jan Monster, McMaster University)

PERMIAN EVAPORITES

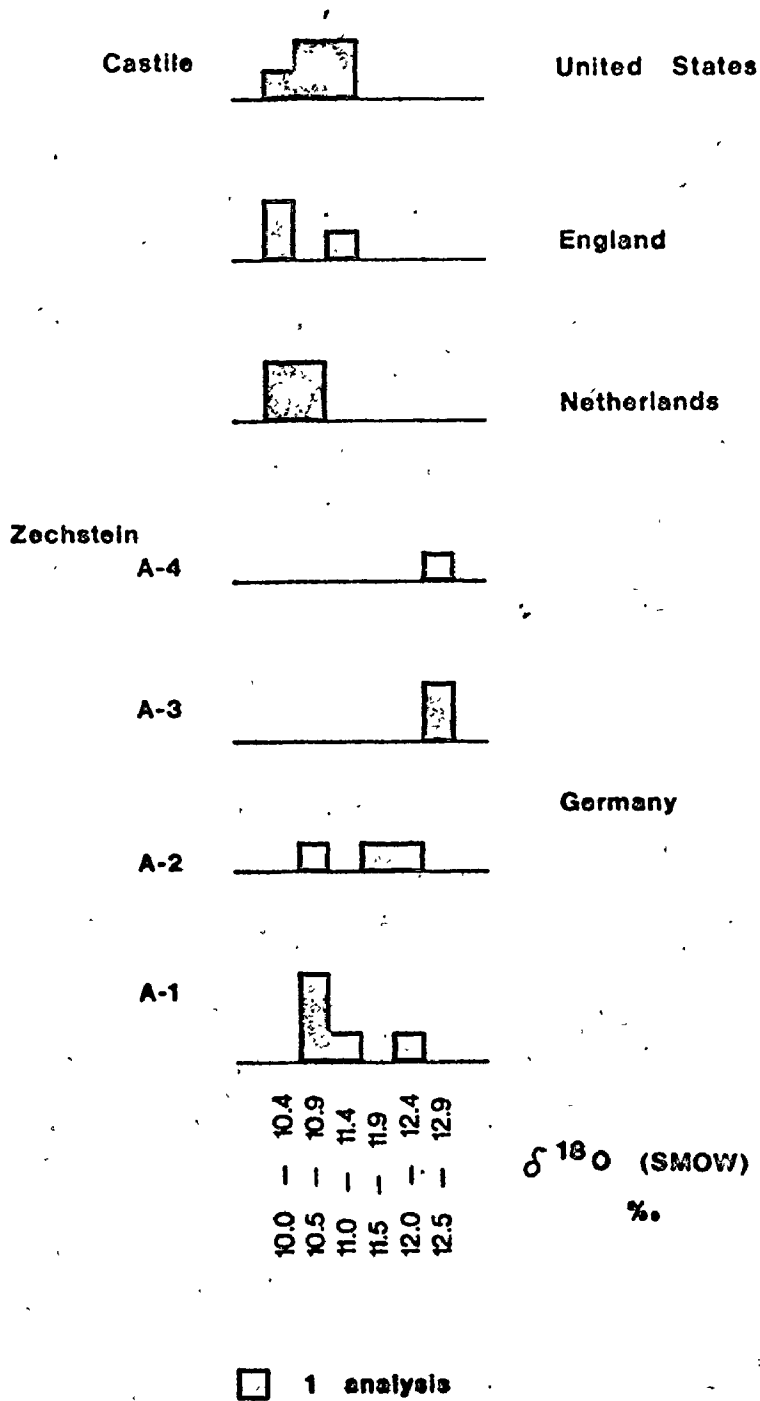


Figure 8-21: Histogram of Oxygen-18 Determinations Permian Evaporites

The sample locations and the areal variation of  $\delta^{34}\text{S}$  and  $\delta^{18}\text{O}$  in the A-1 (the Werra Anhydrite) are shown in Figures 8-22, 8-23 and 8-24.

#### Selected Other Evaporites

The isotopic analyses of selected other evaporites are presented in Table 8-6.

#### Genetic Significance of the Data

The Midale Evaporite has a very uniform sulphur and oxygen isotope composition over its appreciable areal extent. Neither  $\delta^{34}\text{S}$  nor  $\delta^{18}\text{O}$  has significant correlation with insoluble content, sulphate content, nor do they correlate significantly with each other. The lateral variation of  $\delta^{34}\text{S}$  and  $\delta^{18}\text{O}$  is not entirely random; it is possible to draw contours of equal  $\delta$  values that are parallel or subparallel to the depositional edge. These isotopic measurements conform better to the variation proposed for deposition in deep water (the narrow range, particularly for  $\delta^{34}\text{S}$ , is evident in Figure 8-25), except for the weakly defined lateral variation (see Figures 8-6 and 8-7). However the geological evidence better supports a sabkha origin. If such an origin is accepted for the Midale Evaporite, then the narrow range of isotope variation may be a result of postdepositional homogenization.

The Salina rocks have a very large range of  $\delta^{34}\text{S}$  (10‰) and

### ZECHSTEIN FORMATION SAMPLE LOCATIONS

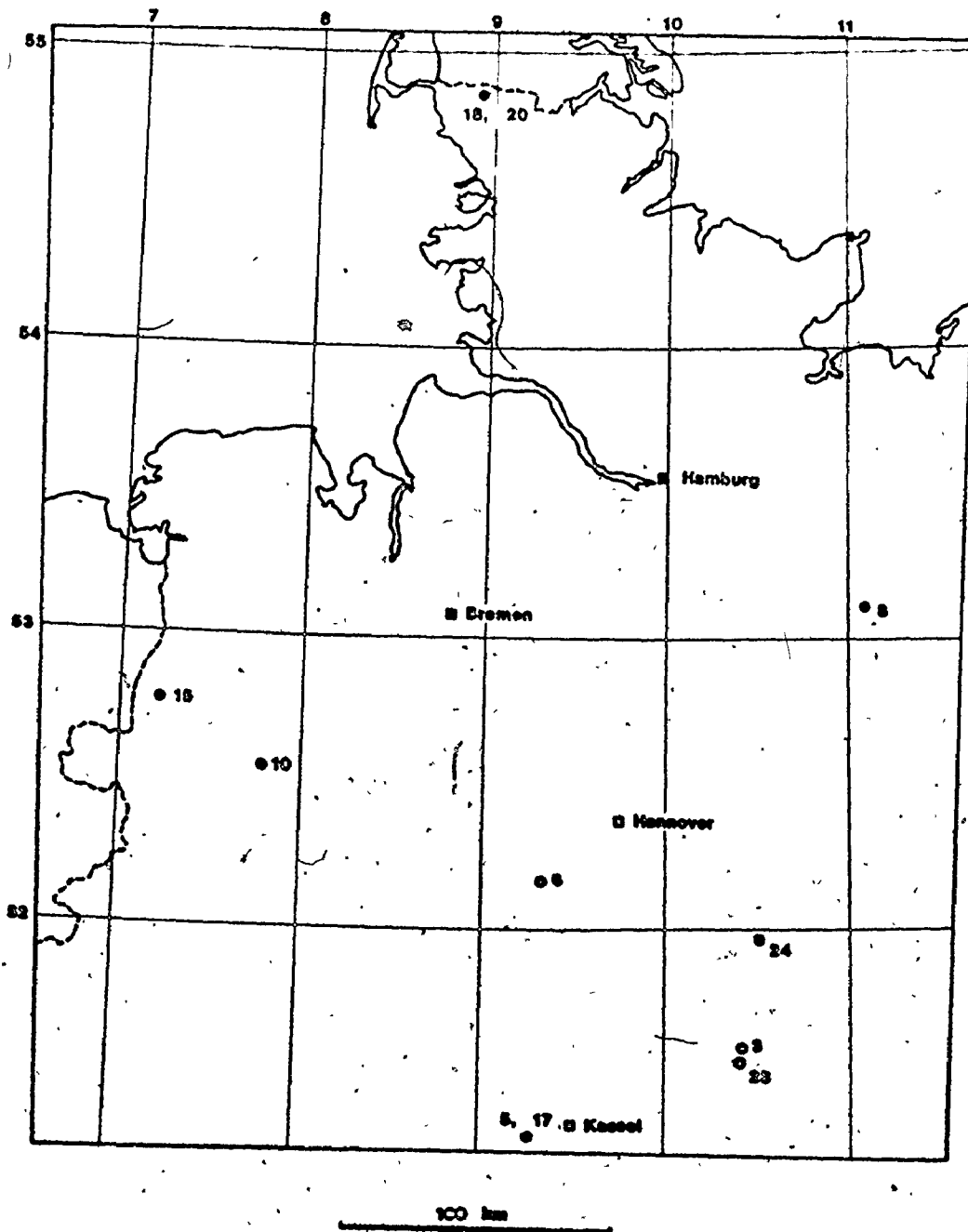


Figure 8-22: Sample Locations, Permian Zechstein Formation (supplied to Jan Monster by G.

ZECHSTEIN FORMATION

$\delta^{34}\text{S}$  (CDT) ‰

A-1

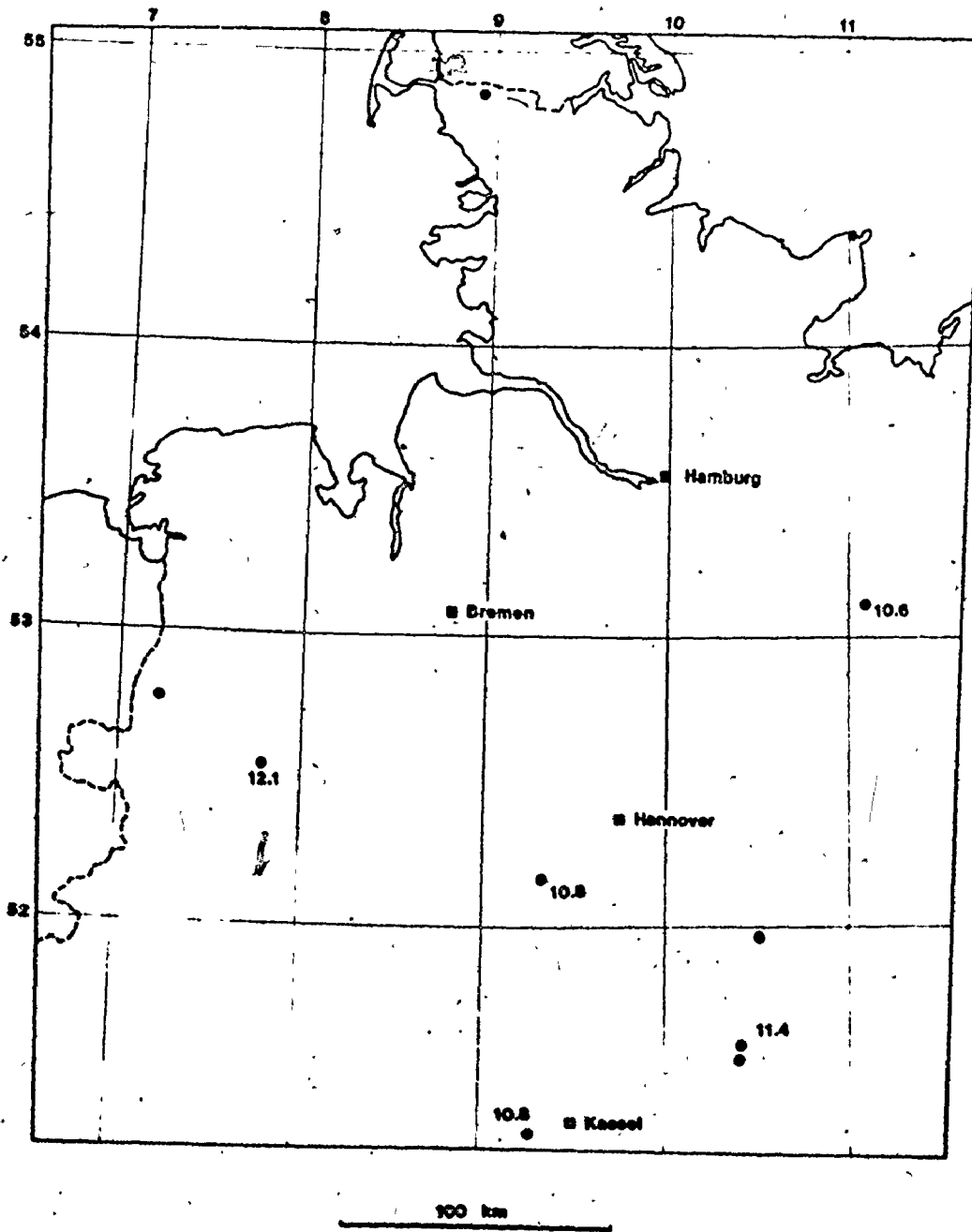


Figure 8-23: Areal Distribution of Sulphur Del Values  
A-1 Anhydrite, Zechstein Formation



## ZECHSTEIN FORMATION

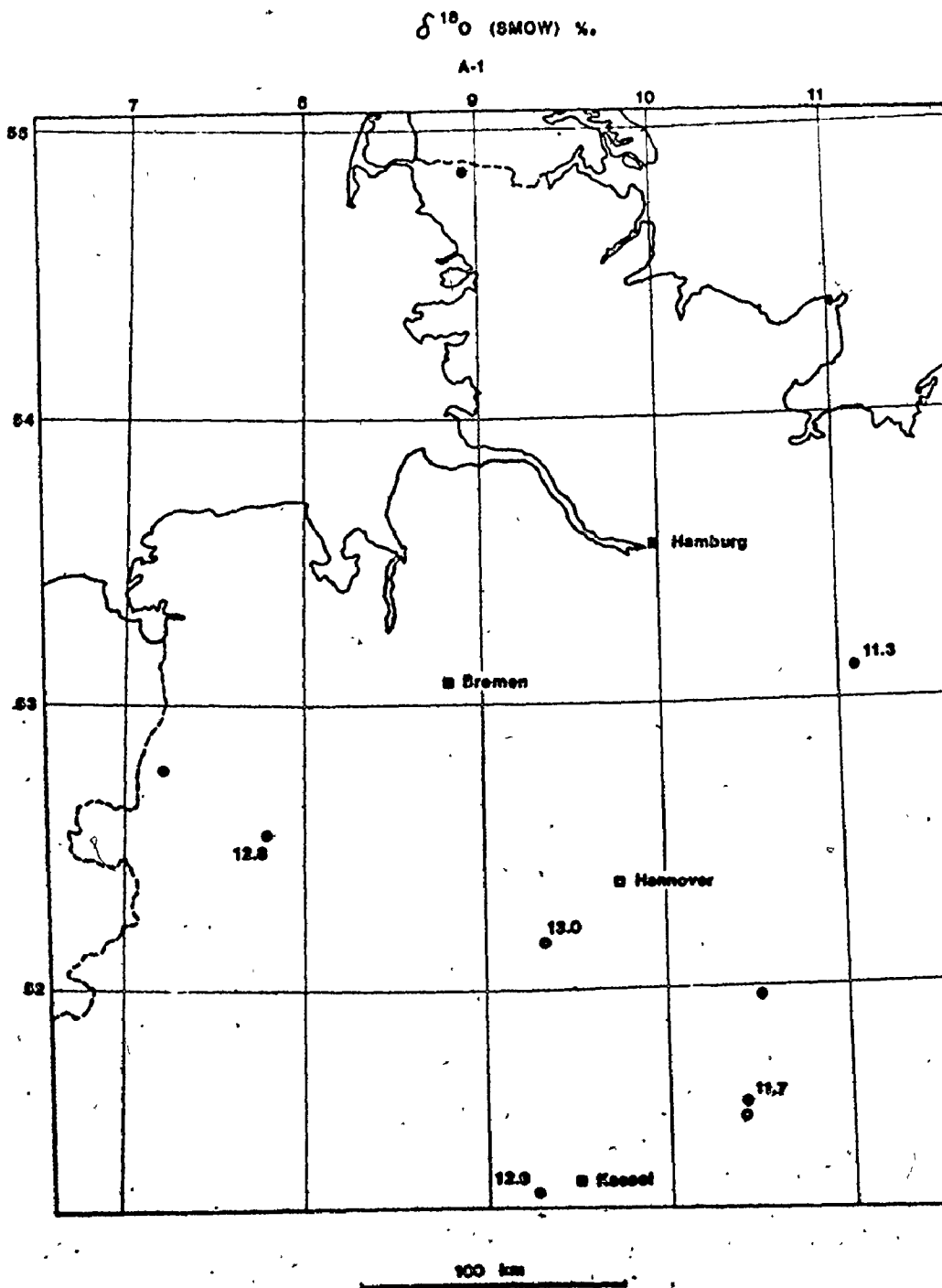


Figure 8-24: Areal Distribution of Oxygen Del Values, A-1 Anhydrite, Zechstein Formation

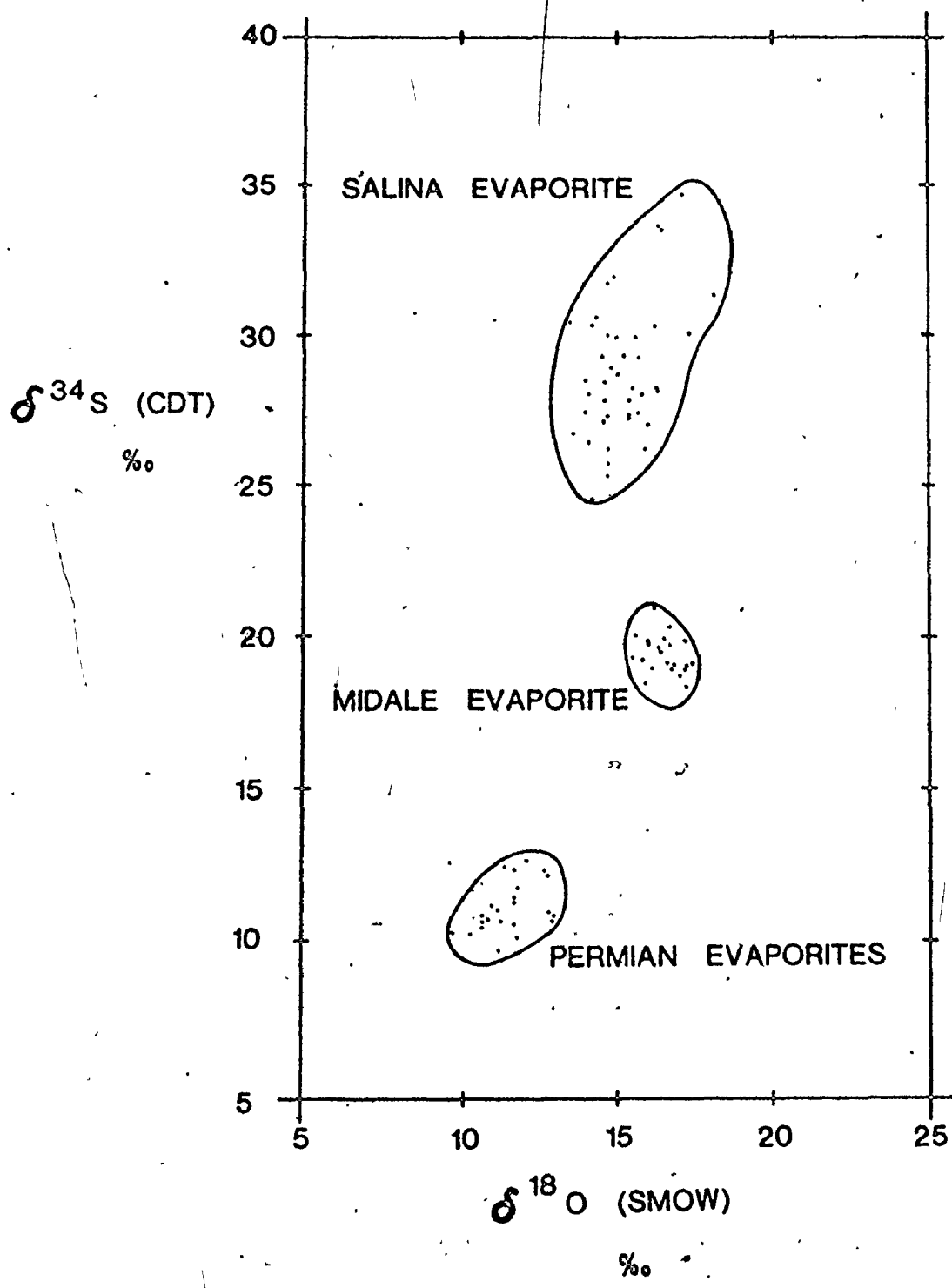


Figure 8-25: Sulphur Del Values versus Oxygen Del Values - Summary for Midale Evaporite, Salina Evaporite and Permian Evaporite

$\delta^{18}\text{O}$  (5‰).  $\delta^{34}\text{S}$  and  $\delta^{18}\text{O}$  show a weak positive correlation, with a slope of about  $\Delta^{34}\text{S}/\Delta^{18}\text{O} = 3.2$ , close to the range of values observed by Mizutani and Rafter (1969, 1973) for bacterial reduction of sulphate. This suggests that bacterial reduction was responsible for much of the isotopic variation observed in these rocks, which is in marked contrast to the results from the Abu Dhabi sabkha. There is no systematic lateral variation in  $\delta^{34}\text{S}$  or  $\delta^{18}\text{O}$ . Although the sample distribution does not permit a strong test of the spatial variation, there is no suggestion whatever of concentric variation. The wide range of isotopic variation suggests subaerial deposition. For these samples, recrystallization appears to have been local, and the primary (?) isotopic differences have been preserved. The geological evidence supports a sabkha origin for these rocks except for those deposited in the immediate basin centre. The basin centre samples show even, parallel laminae and sylvite is present in the immediately overlying sequence. Away from the basin centre, the samples do not show such laminations, and some are associated with stromatolitic carbonate rocks. Treesh and Friedman (1974) have described other features such as mud cracks and armoured mud balls that indicate a sabkha origin for Salina rocks of the Appalachian Basin. The samples obtained from the underground mines have extremely uniform isotopic compositions (the variance of the samples from the Caledonia Mine is less than the stated precision for both  $\delta^{34}\text{S}$  and  $\delta^{18}\text{O}$ ). The sample spacing is much closer than for the rest of the rocks, and the

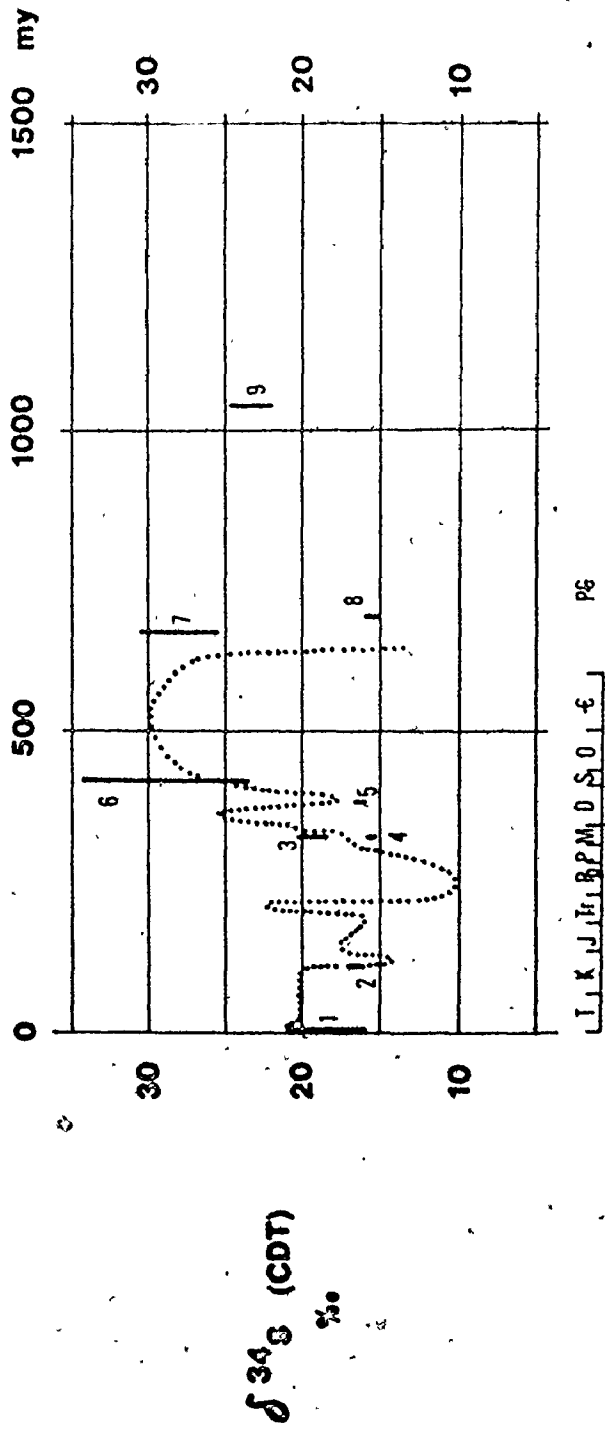
gypsification of these near surface rocks may have homogenized the deposit on this local scale.

The uniformity of the sulphur and oxygen  $\delta$  values of Permian evaporites suggests deep water deposition for the Zechstein and Castile rocks. The small sample size of the present study does not permit conclusions about the significance of slight isotopic differences within (vertically) and between basins.

### Secular Variation

Most of the sulphur isotope analyses in the present study are consistent with the published data. I have drawn Holser and Kaplan's (1966)  $\delta^{34}\text{S}$  versus time curve with the time scale extended into the Precambrian in Figure 8-26. The Precambrian formations shown (7, 8, 9) are not closely dated, and I have avoided the temptation to extend the secular curve. Nonetheless, it is apparent that temporal variation comparable to that of the Phanerozoic may also have taken place in the Precambrian. This is consistent with other evidence that indicates that the processes that regulate the sulphur isotope composition of seawater sulphate (bacterial sulphate reduction, evaporite deposition, shale formation) have been operating for at least 1000 million years.

The narrow range of  $\delta^{18}\text{O}$  of the Permian evaporites and their peculiar light value are strong evidence for the preservation of primary oxygen isotope compositions. However, there is little in Figure 8-27,



- 1 Abu Dhabi
  - 2 Guzsama Formation
  - 3 Middle Evaporite
  - 4 Late Enon Formation
  - 5 Prairie Evaporite
  - 6 Sabaa Evaporite
  - 7 Kilian Formation
  - 8 Mimio Inlet Formation
  - 9 Society Cliffs Formation
  - 10 Permian Evaporites
  - 11 Paradise Formation
- ..... HOLSER and KAPLAN (1966)

Figure 8-26: Evaporite Sulphur Delta Values versus Geological Time

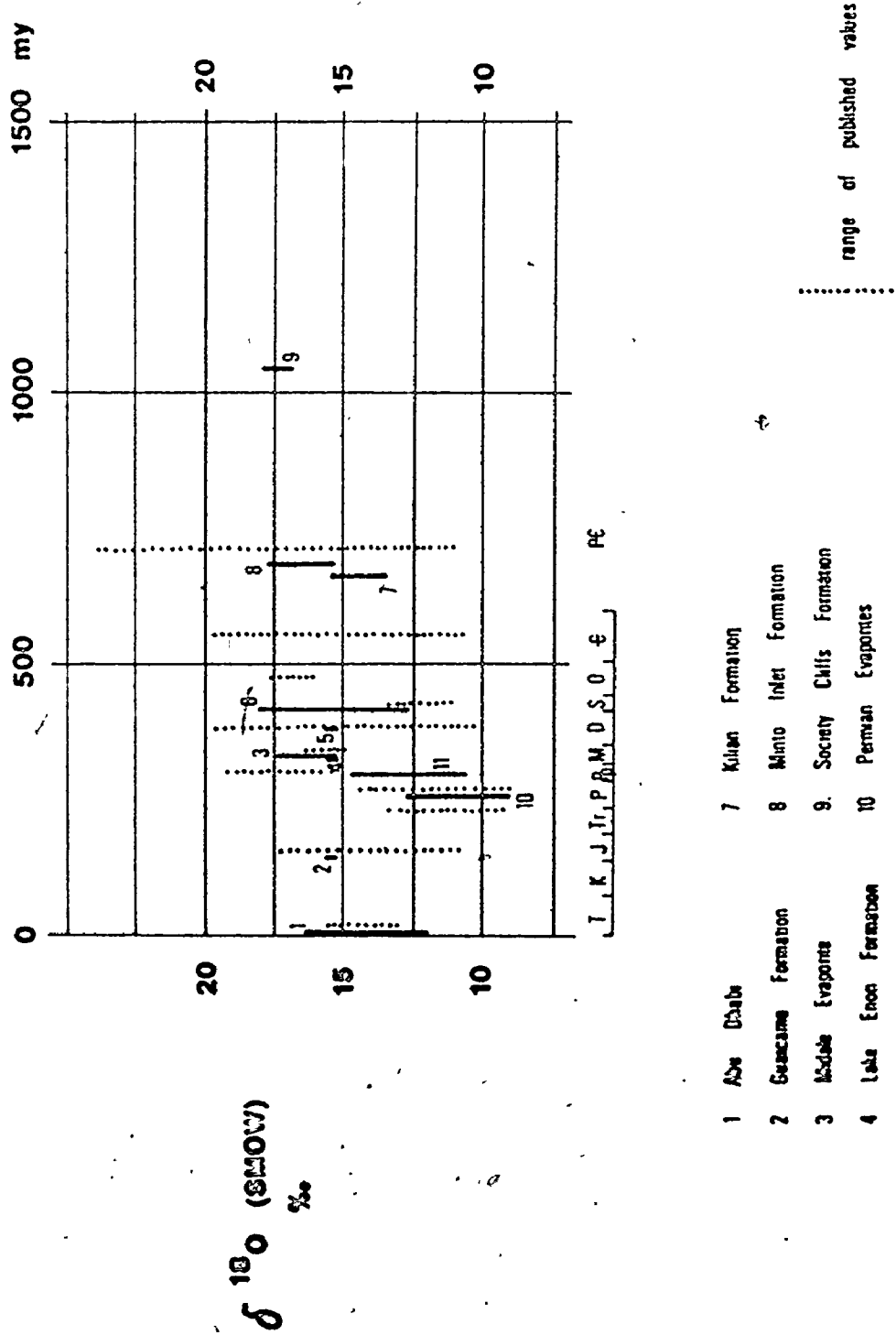


Figure 8-27: Evaporite Oxygen Del Values versus Geological Time

in which I have drawn the results of the present study and the range of published values for each period (Figure 3-3), to support the concept of secular variation of  $\delta^{18}\text{O}$  comparable to that for  $\delta^{34}\text{S}$ . Except for the Permian, there is no suggestion of characteristic  $\delta^{18}\text{O}$  values for any period.

The mechanisms that regulate  $\delta^{18}\text{O}$  and  $\delta^{34}\text{S}$  of seawater sulphate produced coincidental minima in the Permian. This is the only exception to the constancy of  $\delta^{18}\text{O}$  of seawater sulphate in the Phanerozoic and Precambrian. This suggests that the mode of deposition of the extensive Permian evaporites was different than in other periods.

Table 8-3: Isotopic Analyses of the Mississippian Midale Evaporite

LOCATION	DESCRIPTION		$\delta^{18}\text{O}$ (SMOW)	$\delta^{34}\text{S}$ (CDT)
1-10-5-5-W2 4443' LR24A	ANHYDRITE: buff and brown nodular	%INS: -0.5 $\text{SO}_4^{--}$ : 6.79 moles/kg	16.7	18.9
16-23-6-13-W2 4491' LR31A	ANHYDRITE: medium grey sucrosic massive	%INS: 5.0 $\text{SO}_4^{--}$ : 6.36 moles/kg	16.6	19.1
1-36-4-5-W2 4480' LR19B	ANHYDRITE: buff brown with purple mottle massive	XRD: AN %INS: 52.5 $\text{SO}_4^{--}$ : 2.38 moles/kg	16.8	19.0
3-26-4-5-W2 4612' LR18B	ANHYDRITE: buff brown with purple mottle	XRD: DO, AN %INS: 55.0 $\text{SO}_4^{--}$ : 1.80 moles/kg	17.2	19.0
13-5-5-6-W2 4687' LR25C	ANHYDRITE: buff brown with purple mottle	XRD: AN %INS: 47.0 $\text{SO}_4^{--}$ : 2.80 moles/kg	17.2	18.3



LOCATION	DESCRIPTION		$\delta^{18}\text{O}$ (SMOW)	$\delta^{34}\text{S}$ (CDT)
11-27-4-2-W2 4142' LR17A	ANHYDRITE: light buff grey with some red sucrosic	%INS: 5.6 $\text{SO}_4^{--}$ : 5.82 moles/kg	17.0	18.7
14-25-5-14-W2 4804' LR27C	ANHYDRITE: white nodule	%INS: 4.8 $\text{SO}_4^{--}$ : 6.08 moles/kg	16.0	19.8
14-25-5-14-W2 4827' LR27D	ANHYDRITE: medium buff brown massive with 1 mm black streaks	%INS: 20.8 $\text{SO}_4^{--}$ : 4.64 moles/kg XRD: AN	17.4	19.1
4-25-5-12-W2 4828' LR26F	ANHYDRITE: medium buff brown massive with dark grey mottle	%INS: 38.6 $\text{SO}_4^{--}$ : 4.46 moles/kg XRD: AN	16.0	19.6
7-21-4-6-W2 4783' LR20D	ANHYDRITE: buff grey with brown some purple mottle	XRD: AN %INS: 5.2 $\text{SO}_4^{--}$ : 5.48 moles/kg	17.2	19.7

LOCATION	DESCRIPTION		$\delta^{18}\text{O}$ (SMOW)	$\delta^{34}\text{S}$ (CDT)
1-35-3-3-W2 4468' LR12B	ANHYDRITE: banded (4 mm) buff and maroon	%INS: 0.2 $\text{SO}_4^{--}$ : 6.17 moles/kg	16.1	18.9
8-20-4-12-2 5110' LR21D	ANHYDRITE: light grey sucrosic mud stringers	%INS: 0.8 $\text{SO}_4^{--}$ : 6.75 moles/kg	15.9	18.4
8-20-4-12-2 5135' LR21E	ANHYDRITE: light grey massive with grey mottle	XRD: AN, DO %INS: 47.4 $\text{SO}_4^{--}$ : 2.86 moles/kg	17.2	18.9
8-27-4-14-W2 5173' LR22D	ANHYDRITE: white massive	XRD: AN %INS: -2.1 $\text{SO}_4^{--}$ : 6.94 moles/kg	16.7	20.3
4-8-3-5-W2 5070' LR13B	ANHYDRITE: medium buff grey with black patch	%INS: 5.6 $\text{SO}_4^{--}$ : 5.78 moles/kg	15.7	19.2
9-23-2-2-W2 4551' LR7B	ANHYDRITE: medium brown and maroon	XRD: AN %INS: 25.7 $\text{SO}_4^{--}$ : 4.84 moles/kg	16.4	19.9

LOCATION	DESCRIPTION		$\delta^{18}\text{O}$ (SMOW)	$\delta^{34}\text{S}$ (CDT)
16-12-2-5-W2 5158' LR8B	ANHYDRITE: medium grey massive with black streaks	XRD: AN, DO %INS: 43.2 $\text{SO}_4^{--}$ : 3.27 moles/kg	16.3	19.6
1-8-2-6-W2 5464' LR9	ANHYDRITE: medium grey massive with black streaks	XRD: AN %INS: 29.0 $\text{SO}_4^{--}$ : 3.96 moles/kg	16.4	19.4
7-20-3-15-W2 5872' LR15C	ANHYDRITE: medium grey massive	%INS: 9.2 $\text{SO}_4^{--}$ : 5.57 moles/kg	16.2	20.9
12-20-2-11-W2 5781' LR10E	ANHYDRITE: buff and grey	XRD: AN %INS: 45.5 $\text{SO}_4^{--}$ : 3.32 moles/kg	16.7	19.7
16-18-1-2-W2 5097' LR1E	ANHYDRITE: grey brown with 1 mm brown laminae also, dark grey nodule	XRD: AN %INS: 25.9 $\text{SO}_4^{--}$ : 4.83 moles/kg	15.5	19.3

LOCATION	DESCRIPTION	$\delta^{18}\text{O}$ (SMOW)	$\delta^{34}\text{S}$ (CDT)
12-29-1-5-W2 5536' LR32B	ANHYDRITE: white	%INS: 5.9	15.6
		$\text{SO}_4^{--}$ : 6.06 moles/kg	20.0

Table 8-4: Isotopic Analyses of Upper Silurian Salina Rocks

LOCATION	DESCRIPTION		$\delta^{18}\text{O}$ (SMOW)	$\delta^{34}\text{S}$ (CDT)
Elgin Lake Erie 1441-1442' A-2 An SALIA	ANHYDRITE: grey massive	XRD: AN %INS: 17.6 $\text{SO}_4^{--}$ : 6.50 moles/kg	14.7	26.2
Elgin Lake Erie 1443-1444' A-2 An SALIC	ANHYDRITE: grey white massive sharp contact with dolomite recrystallized	XRD: AN %INS: 1.3 $\text{SO}_4^{--}$ : 6.17 moles/kg	15.7	27.4
Elgin Lake Erie 1446' A-2 An SALID	ANHYDRITE: grey white with muddy stringers	%INS: 16.9 $\text{SO}_4^{--}$ : 5.58 moles/kg	15.7	29.3
Elgin Lake Erie 1450-1453' A-1 An SALIF	ANHYDRITE: grey irregular stringers in brown laminated dolomite	%INS: 29.5 $\text{SO}_4^{--}$ : 4.58 moles/kg	16.2	30.3

LOCATION	DESCRIPTION		$\delta^{18}\text{O}$ (SMOW)	$\delta^{34}\text{S}$ (CDT)
Elgin	ANHYDRITE:	%INS: 1.8	16.4	33.5
Lake Erie	dark brown	$\text{SO}_4^{--}$ : 4.54		
1450-1453'	brecciated	moles/kg		
A-1 An				
SAL1G				
Lambton	ANHYDRITE:	XRD: AN, HA	14.5	29.3
Moore 28 2	irregular fine	$\text{SO}_4^{--}$ : 5.86		
2065'	laminae	moles/kg		
B An?	halite vugs	%INS: 6.6		
SAL2A				
Lambton	ANHYDRITE:	%INS: 39.5	14.1	31.7
Moore 28 2	1 to 3 mm wavy	$\text{SO}_4^{--}$ : 2.62		
2065.5'	laminae	moles/kg		
B An?	halite vugs			
SAL2B				
Lambton	ANHYDRITE:	%INS: 18.7	14.0	27.3
Moore 28 2	grey with	$\text{SO}_4^{--}$ : 5.27		
2067'	brown dolomite	moles/kg		
B An?	in irregular			
SAL2C	laminae			
Lambton	ANHYDRITE:	%INS: 21.3	14.1	26.4
Moore 28 2	chickenwire	$\text{SO}_4^{--}$ : 5.92		
2288'	grey in brown	moles/kg		
A-1 Carb				
SAL2D				

LOCATION	DESCRIPTION		196	
			$\delta^{18}\text{O}$ (SMOW)	$\delta^{34}\text{S}$ (CDT)
Lambton Moore 28 2 2392'	ANHYDRITE: white massive	%INS: 16.7 $\text{SO}_4^{--}$ : 5.30 moles/kg	14.7	25.6
A-1 An SAL2F				
Essex Gosfield S 6 4 1126'	ANHYDRITE: white massive	%INS: 19.3 $\text{SO}_4^{--}$ : 5.05 moles/kg	15.5	28.1
A-1 An SAL3A				
Essex Gosfield S 6 4 1127'	ANHYDRITE: white massive	XRD: GY %INS: 6.4 $\text{SO}_4^{--}$ : 5.75 moles/kg	16.3	33.5
A-1 An SAL3B	in brecciated zone with brown dolomite			
Kent Lake Erie 1132'	ANHYDRITE: grey massive	%INS: 50.2 $\text{SO}_4^{--}$ : 2.70 moles/kg	15.4	27.8
A-2 An SAL4B	with brown stringers			

LOCATION	DESCRIPTION		$\delta^{18}\text{O}$ (SMOW)	$\delta^{34}\text{S}$ (CDT)
Kent	ANHYDRITE:	%INS: 31.3	15.9	26.2
Lake Erie	white	$\text{SO}_4^{--}$ : 4.32		
1138'	4 mm nodules	moles/kg		
A-2 An	in brown			
SAL4C	dolomite			
Lambton	ANHYDRITE:	XRD: CT, AN	15.4	27.1
Moore 10 2	brown with	$\text{SO}_4^{--}$ : 1.67		
1850'	calcite as	moles/kg		
A-2 An	irregular nodules	%INS: 72.3		
SAL5C	and stringers in grey dolomite			
Lambton	ANHYDRITE:	%INS: 28.4	15.5	-----
Moore 10 2	light grey	$\text{SO}_4^{--}$ : 4.50		
1861'	chickenwire	moles/kg		
A-2 An				
SAL5E				
Lambton	ANHYDRITE:	XRD: AN	14.9	31.9
Moore 19 6	grey in	%INS: 24.8		
2040'	wavy laminae	$\text{SO}_4^{--}$ : 3.92		
A-2 An	with halite	moles/kg		
SAL6A				



LOCATION	DESCRIPTION		$\delta^{18}\text{O}$ (SMOW)	$\delta^{34}\text{S}$ (CDT)
Lambton Moore 19 6 2041' A-2 An SAL6B	ANHYDRITE: grey massive with thin wavy parallel stringers	%INS: 30.3 $\text{SO}_4^{--}$ : 4.06 moles/kg	14.6	28.4
Lambton Moore 19 6 2043' A-2 An SAL6C	ANHYDRITE: white chickenwire with brown dolomite	%INS: 25.8 $\text{SO}_4^{--}$ : 4.33 moles/kg	14.6	27.1
Lambton Moore 19 10 2308' A-2 An SAL7A	GYPSUM: white with brown brecciated	%INS: 77.9 $\text{SO}_4^{--}$ : 0.35 moles/kg	17.1	34.6
Lambton Moore 19 10 2309' A-2 An SAL7B	GYPSUM: brown with brown brecciated	%INS: 47.5 $\text{SO}_4^{--}$ : 1.85 moles/kg	17.2	----
Lambton Sarnia 6 2 2152' A-1 An SAL8A	ANHYDRITE: with dolomite mottled brown and grey	%INS: 59.6 $\text{SO}_4^{--}$ : 1.83 moles/kg	14.8	28.9

LOCATION	DESCRIPTION		$\delta^{18}\text{O}$ (SMOW)	$\delta^{34}\text{S}$ (CDT)
Lambton Sarnia 6 2 2153' A-1 An SAL8B	ANHYDRITE: with dolomite brown and grey mottled	%INS: 17.4 $\text{SO}_4^{--}$ : 4.92 moles/kg	14.6	27.8
Lambton Sarnia 6 2 2155' A-1 An SAL8C	ANHYDRITE: grey with thin wavy brown stringers	XRD: AN %INS: 6.7 $\text{SO}_4^{--}$ : 4.70 moles/kg	15.0	28.7
Lambton Sombra 6 12 1807' A-2 An SAL9A	ANHYDRITE: grey finely laminated	XRD: DO, AN %INS: 48.8 $\text{SO}_4^{--}$ : 2.29 moles/kg	18.1	31.3
Lambton Sombra 6 12 1810' A-2 An SAL9B	ANHYDRITE: grey in contorted laminae dolomite	XRD: DO %INS: 92.3 $\text{SO}_4^{--}$ : 0.05 moles/kg	17.3	30.0
Lambton Sombra 6 12 1820' A-1 An SAL9E	ANHYDRITE: white vein in brown and grey laminated dolomite	%INS: 5.9 $\text{SO}_4^{--}$ : 5.98 moles/kg	16.3	28.1

LOCATION	DESCRIPTION		$\delta^{18}\text{O}$ (SMOW)	$\delta^{34}\text{S}$ (CDT)
Lambton	ANHYDRITE:	%INS: 34.6	14.7	30.0
Sombra 6 12	grey nodule	$\text{SO}_4^{--}$ : 3.63		
1823'	in brown	moles/kg		
A-1 An	dolomite			
SAL9F				
Lambton	ANHYDRITE:	%INS: 13.6	15.4	27.2
Warwick 13 3s	white stringers	$\text{SO}_4^{--}$ : 5.42		
1761'	in brown	moles/kg		
A-2 An	dolomite			
SAL10				
Huron	ANHYDRITE:	XRD: AN	15.0	29.9
Stephen 42 SB	light grey	%INS: 34.6		
1705'	with light brown	$\text{SO}_4^{--}$ : 3.48		
A-2 An	stringers	moles/kg		
SAL11A	recrystallized			
Huron	ANHYDRITE:	%INS: 36.8	14.7	27.3
Stephen 42 SB	light grey	$\text{SO}_4^{--}$ : 3.90		
1708'	mosaic	moles/kg		
A-2 An				
SAL11B				

LOCATION	DESCRIPTION		$\delta^{18}\text{O}$ (SMOW)	$\delta^{34}\text{S}$ (CDT)
Middlesex McGillivray 5 19 1338' in B Salt SAL13A	ANHYDRITE: grey laminae with brown dolomite contact with halite	XRD: AN %INS: 18.4 $\text{SO}_4^{--}$ : 4.23 moles/kg	13.6	26.7
Middlesex McGillivray 5 19 1373' B An SAL13B	ANHYDRITE: grey massive in brown laminated dolomite	%INS: 44.0 $\text{SO}_4^{--}$ : 4.58 moles/kg	16.0 (2)	27.0
Elgin Aldbrough 2 Gore 1650' A-2 An SAL14B	ANHYDRITE: grey nodules in wavy brown laminated dolomite	%INS: 3.2 $\text{SO}_4^{--}$ : 5.82 moles/kg	15.8	28.0
Elgin Aldbrough 2 Gore 1653' A-2 An SAL14C	ANHYDRITE: with dolomite fine wavy laminae	%INS: 22.7 $\text{SO}_4^{--}$ : 4.63 moles/kg	16.3	28.2

LOCATION	DESCRIPTION		$\delta^{18}\text{O}$ (SMOW)	$\delta^{34}\text{S}$ (CDT)
Elgin Aldbrough 2 Gore 1675' A-1 An SAL14E	ANHYDRITE: massive grey with irregular brown stringers	%INS: 3.4 $\text{SO}_4^{--}$ : 6.58 moles/kg	15.2	29.3
Norfolk Charlotte- ville 22 1 793' B An? SAL15N	ANHYDRITE: grey white nodular	%INS: 1.3 $\text{SO}_4^{--}$ : 7.13 moles/kg	13.7	----
Norfolk Charlotte- ville 22 1 817' A-2 An SAL15J	ANHYDRITE: grey white solution contact with very finely laminated dolomite	%INS: 1.4 $\text{SO}_4^{--}$ : 7.21 moles/kg	14.3 (2)	28.0
Norfolk Charlotte- ville 22 1 828' A-2 An SAL15H	ANHYDRITE: flattened nodules in wavy laminated brown dolomite	%INS: 11.6 $\text{SO}_4^{--}$ : 6.26 moles/kg	13.5	30.4

LOCATION	DESCRIPTION		$\delta^{18}\text{O}$ (SMOW)	$\delta^{34}\text{S}$ (CDT)
Norfolk- Charlotte- ville 22 1 843' A-2 An SAL15E	ANHYDRITE: grey massive sharp contact with finely laminated dolomite recrystallized	%INS: 10.5 $\text{SO}_4^{--}$ : 6.21 moles/kg	14.3	30.6
Norfolk- Charlotte- ville 22 1 889' A-1 An SAL15B	ANHYDRITE: grey massive sharp contact with laminated brown dolomite recrystallized	%INS: 9.3 $\text{SO}_4^{--}$ : 6.39 moles/kg	15.6	29.9
Michigan Montmorency Co basal A-1 Salt SAL16	ANHYDRITE: finely laminated with dolomite	%INS: 58.3 $\text{SO}_4^{--}$ : 1.52 moles/lg	13.9	28.5
Michigan Midland Co basal A-1 Salt SAL17	ANHYDRITE: finely laminated with dolomite	%INS: 58.6 $\text{SO}_4^{--}$ : 2.28 moles/kg	14.2 (2)	30.3

Domtar Construction Materials Limited, Mine  
near Caledonia, Ontario

Sample Number	$\delta^{18}\text{O}$ (SMOW)	$\delta^{34}\text{S}$ (CDT)
CA1	14.7 (3)	24.9 (1)
CA3	15.0 (2)	25.6 (1)
CA4	14.1 (2)	25.1 (1)
CA5	14.7 (2)	25.3 (1)
CA6	14.9 (2)	24.7 (1)
CA7	14.3 (2)	25.0 (1)
CA8	14.7 (2)	24.9 (1)
CA9	14.6 (2)	25.0 (1)
CA11	14.4 (2)	25.1 (1)
CA12	14.3 (2)	24.7 (1)
CA14	14.5 (3)	25.5 (1)
CA15	15.0 (2)	25.8 (1)
CA16	14.9 (2)	26.0 (1)
CA17	14.9 (3)	25.7 (1)
CA18	14.5 (3)	24.9 (1)
CA19	15.0 (2)	25.9 (1)
	<hr/>	<hr/>
MEAN	14.7	25.3
	$\pm 0.3$	$\pm 0.4$

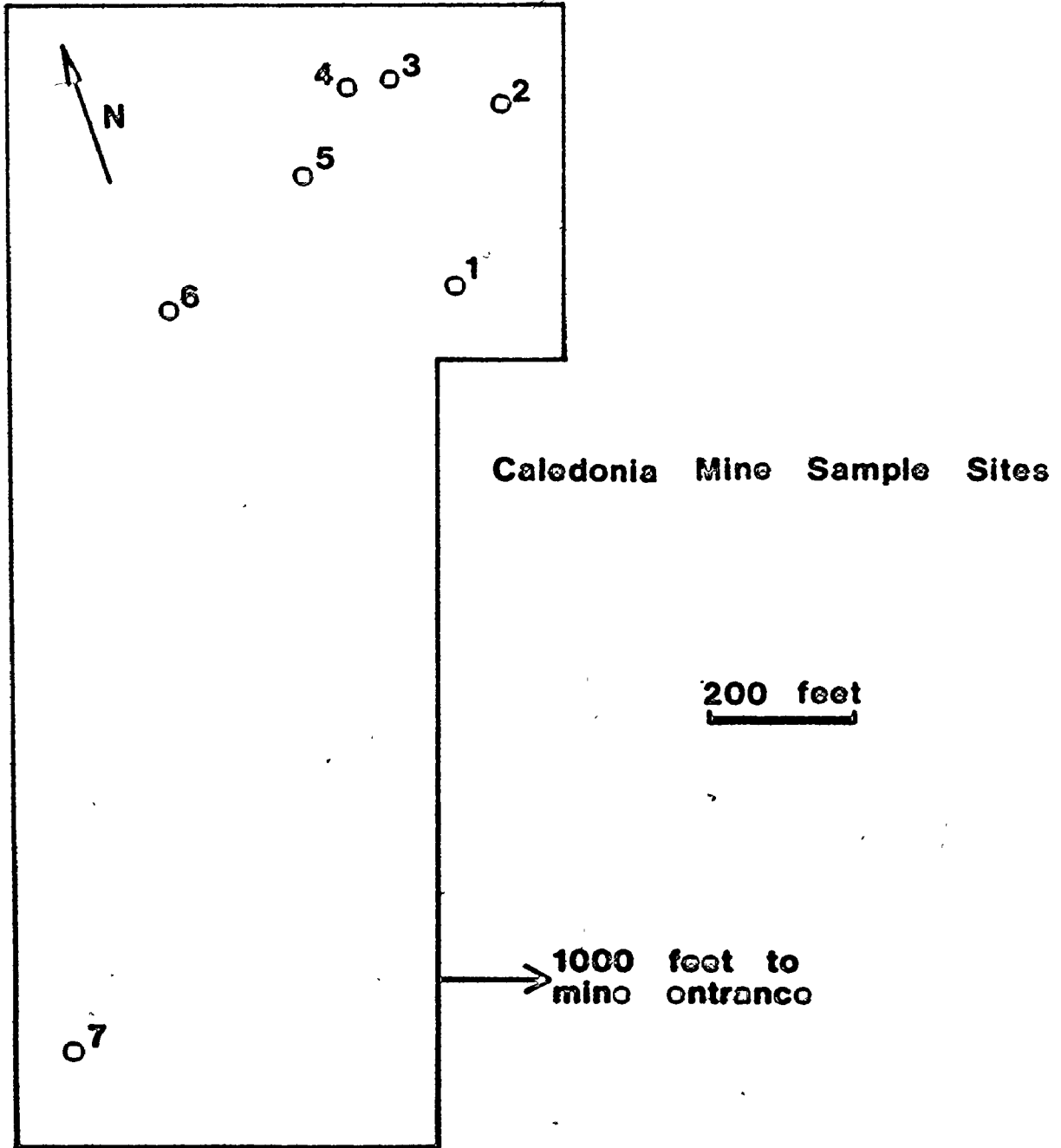
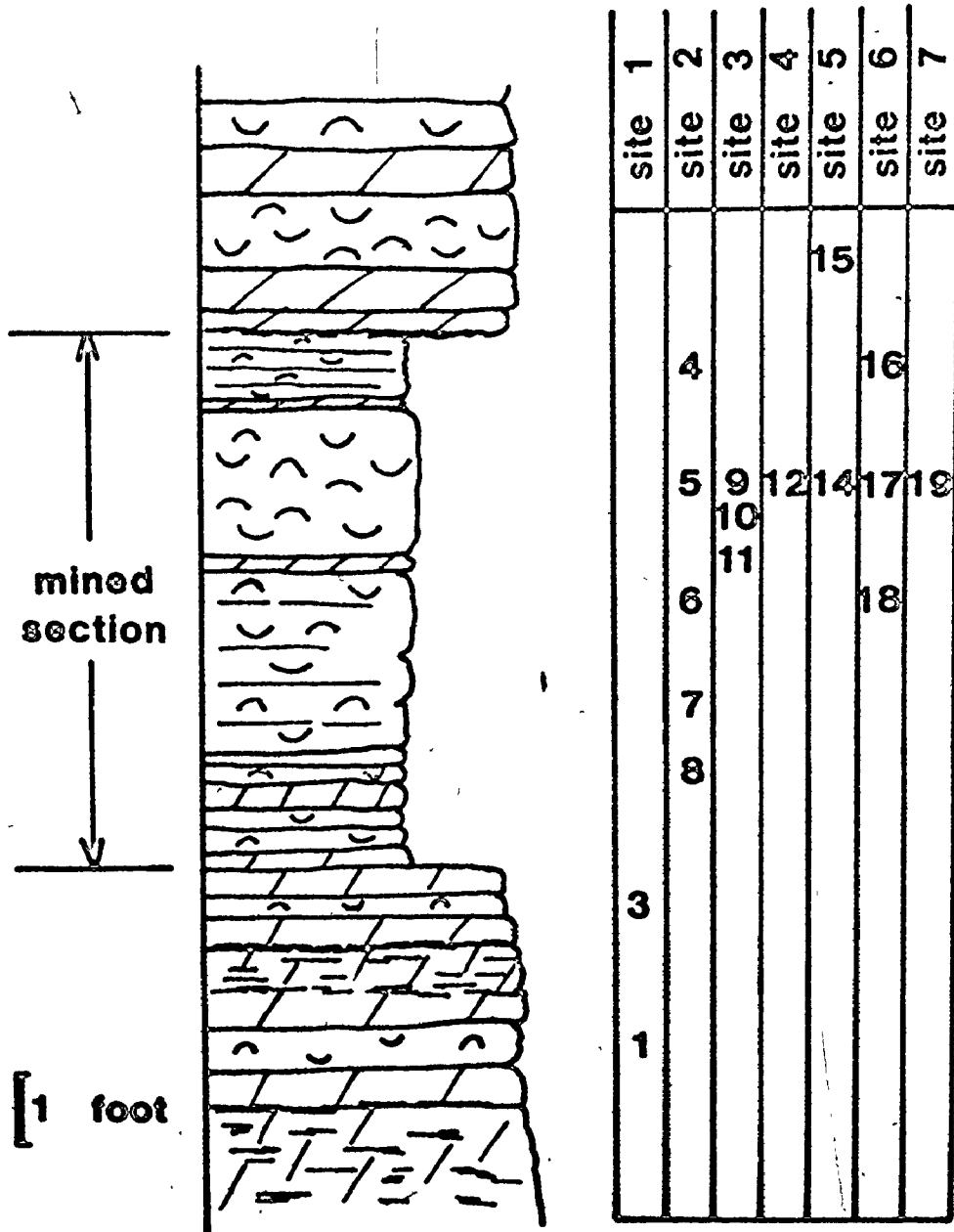


Figure 8-28: Caledonia Mine Sample Sites





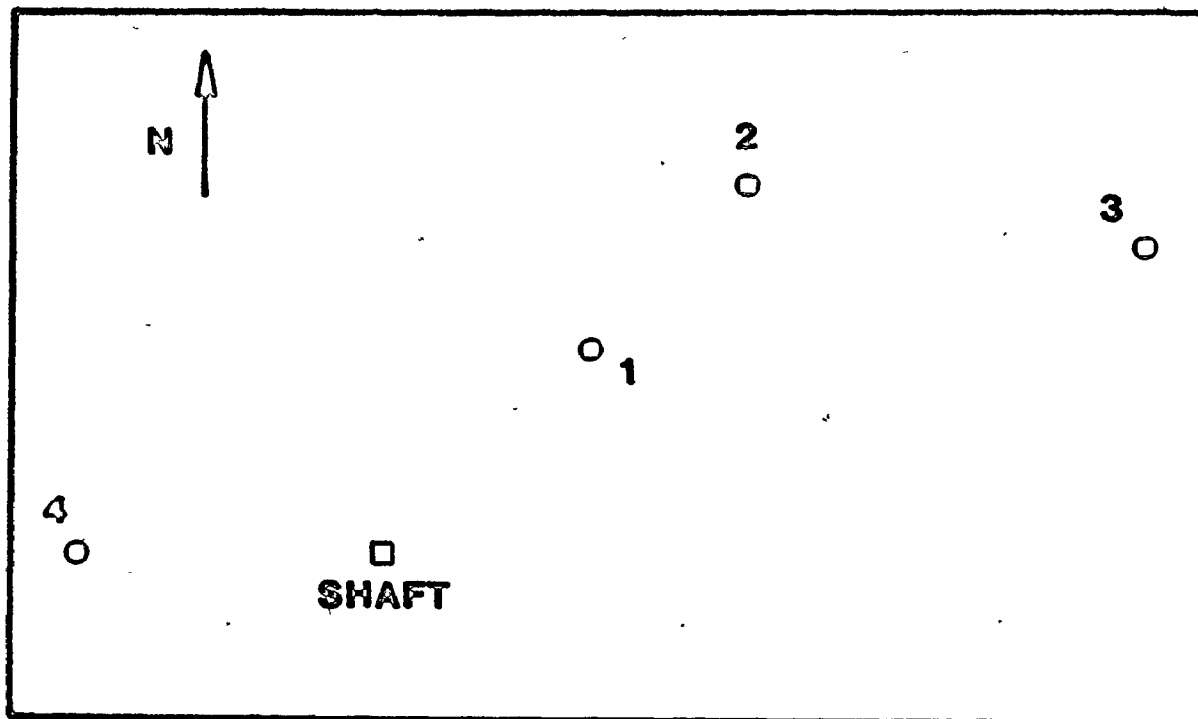
**Caledonia Mine  
Geological Section and Sample Locations**

Figure 8-29: Caledonia Mines Geological Section and Sample Locations (after Guillet, 1964)

Canadian Gypsum Company, Limited, Mine  
near Hagersville, Ontario

Sample Number	$\delta^{18}\text{O}$ (SMOW)	$\delta^{34}\text{S}$ (CDT)
HA1	13.5 (2)	24.5 (2)
HA2	12.9 (2)	24.6 (2)
HA3	14.1 (2)	24.9 (2)
HA4	13.4 (2)	24.7 (2)
HA6	14.4 (2)	24.4 (1)
HA7	13.9 (2)	23.7 (1)
HA9	14.8 (3)	24.2 (2)
HA11	15.0 (2)	24.3 (2)
HA13	14.1 (2)	24.9 (2)
HA14	14.5 (3)	24.5 (2)
HA16	15.3 (2)	24.1 (2)
	<hr/>	<hr/>
MEAN	14.2	24.4
	$\pm 0.7$	$\pm 0.3$

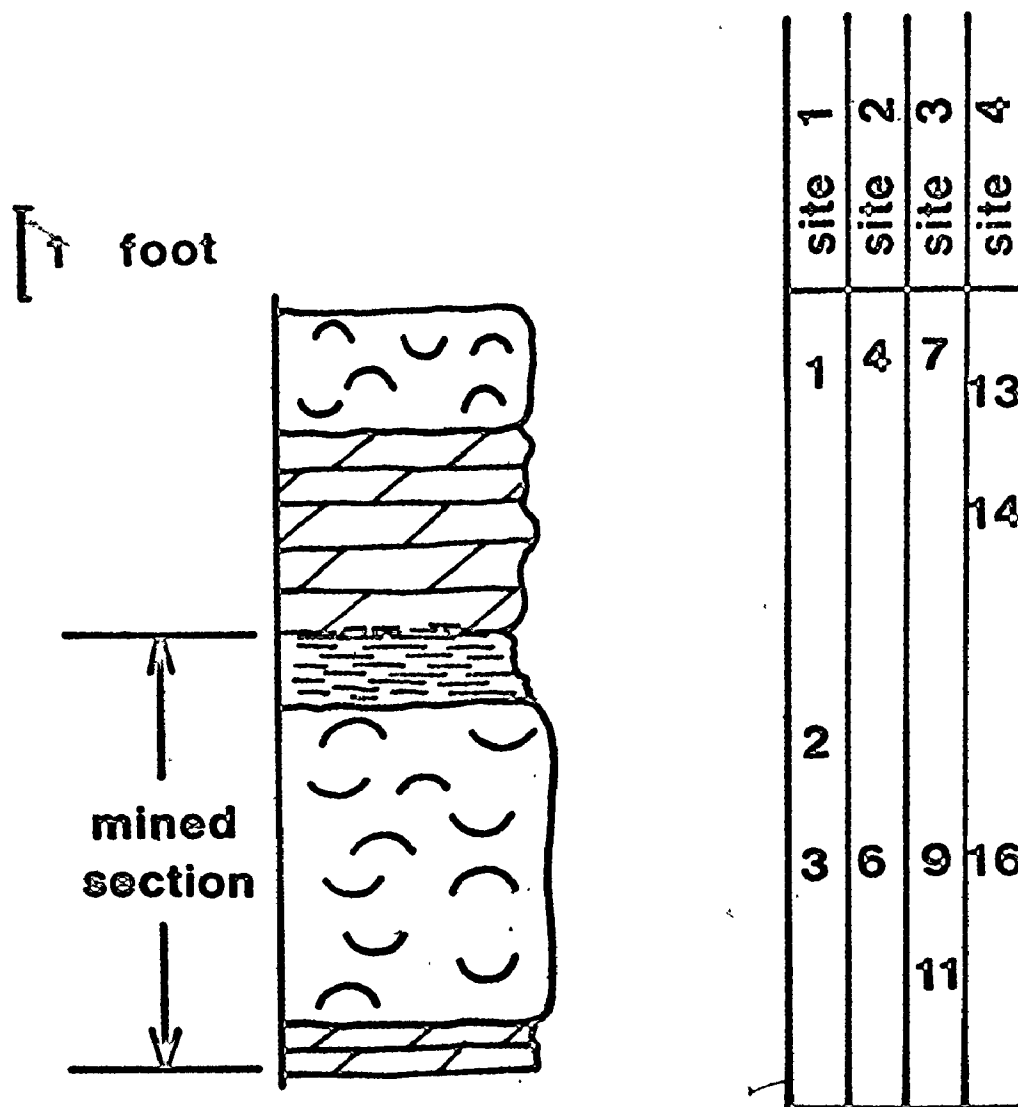
### Hagersville Mine Sample Sites



600 feet



Figure 8-30: Hagersville Mine Sample Sites



### Hagersville Mine

## Geological Section and Sample Locations

Figure 8-31: Hagersville Mine Geological Section and Sample Locations (after Guillet, 1964)

Table 8-5: Isotopic Analyses of some Permian Evaporites

Sulphur del values were measured by Jan Monster, and were summarized in Thode and Monster (1965). (Note Geographic Divisions.)

LOCATION	DESCRIPTION		$\delta^{18}\text{O}$ (SMOW)	$\delta^{34}\text{O}$ (CDT)
<u>UPPER PERMIAN GERMANY</u>				
stdl.	GYPSUM:	%INS: tr	11.7	11.4
Osterode	alabastine	$\text{SO}_4^{--}$ : 5.59		
Werra An		moles/kg		
A-1				
77-3				
Herste 17	GYPSUM:	%INS: 25.4	12.9	10.8
Werra An	white and grey	$\text{SO}_4^{--}$ : 4.41		
A-1	friable	moles/kg		
77-5				
Hameln 2	GYPSUM:	%INS: 7.8	13.0	10.8
Werra An	light grey	$\text{SO}_4^{--}$ : 5.86		
A-1	fine grained	moles/kg		
77-6	friable			
Gorleben	ANHYDRITE:	%INS: 15.6	11.3	10.6
Werra An	grey	$\text{SO}_4^{--}$ : 5.15		
A-1	massive	moles/kg		
77-8				
Suttrup	GYPSUM:	%INS: 16.1	12.8	12.1
Werra An	snow white	$\text{SO}_4^{--}$ : 5.33		
A-1	3 mm crystals	moles/kg		

LOCATION	DESCRIPTION		$\delta^{18}\text{O}$ (SMOW)	$\delta^{34}\text{S}$ (CDT)
oberlanger Tenge Basalanhydrit A-2 77-15	GYPSUM: white nodules with dark grey wrap	%INS: 60.9 $\text{SO}_4^{--}$ : 1.11 moles/kg	11.7	10.5
Herste 17 Basalanhydrit A-2 77-17	ANHYDRITE: grey with brown mottle massive	%INS: 53.4 $\text{SO}_4^{--}$ : 2.15 moles/kg	12.6	12.3
Böxlund Basalanhydrit A-2 77-18	ANHYDRITE: grey buff in flattened ellipsoids	%INS: 5.1 $\text{SO}_4^{--}$ : 6.14 moles/kg	11.8	11.7

LOCATION	DESCRIPTION		$\delta^{18}\text{O}$ (SMOW)	$\delta^{34}\text{S}$ (CDT)
Böxlund Hauptanhydrit A-3 77-20	ANHYDRITE: grey white massive with brown mud stringers	%INS: 34.5 $\text{SO}_4^{--}$ : 3.41 moles/kg	11.4	12.4
südliche Osterode Hauptanhydrit A-3 77-23	GYPSUM: alabastine with brown	%INS: tr $\text{SO}_4^{--}$ : 4.87 moles/kg	12.1	12.6
Vienenburg Pegmatiten- anhydrit A-4 77-24	ANHYDRITE: grey 1 to 2 mm crystals massive vuggy	%INS: 5.4 $\text{SO}_4^{--}$ : 5.70 moles/kg	11.7	12.3

LOCATION	DESCRIPTION		$\delta^{18}\text{O}$ (SMOW)	$\delta^{34}\text{S}$ (CDT)
<u>THE NETHERLANDS</u>				
Main Anhydrite 46-B1	ANHYDRITE: grey sucrosic	%INS: 4.9 $\text{SO}_4^{--}$ : 5.70 moles/kg	10.7	10.6
Roof Anhydrite 46-B2	ANHYDRITE: light grey massive	%INS: 33.2 $\text{SO}_4^{--}$ : 4.48 moles/kg	9.7	10.2
Basal Anhydrite 46-G1	ANHYDRITE: light grey with brown mottle	%INS: 49.7 $\text{SO}_4^{--}$ : 2.72 moles/kg	10.7	10.4
46-L1	ANHYDRITE: grey sucrosic	%INS: tr $\text{SO}_4^{--}$ : 6.29 moles/kg	12.9	10.6



LOCATION	DESCRIPTION		$\delta^{18}\text{O}$ (SMOW)	$\delta^{34}\text{S}$ (CDT)
<u>GREAT BRITAIN</u>				
Durham	ANHYDRITE:	%INS: 57.3	11.8	10.1
Anhydrite	medium grey	$\text{SO}_4^{--}$ : 1.93		
Mine	massive	moles/kg		
65-1				
Cumberland	GYPSUM:	%INS: n.d.	11.7	11.2
near Carlisle	grey white	$\text{SO}_4^{--}$ : 5.78		
Cocklakes	sucrosic	moles/kg		
Mine				
65-2				
Yorkshire	ANHYDRITE:	%INS: 24.1	10.3	10.2
Eskdale	buff with	$\text{SO}_4^{--}$ : 5.29		
North Riding	maroon mottle	moles/kg		
Upper				
Magnesian				
Limestone				
No. 4 boring				
4163'				
65-9				

LOCATION	DESCRIPTION		$\delta^{18}\text{O}$ (SMOW)	$\delta^{34}\text{S}$ (CDT)
<u>UNITED STATES</u>				
Reeves Co	GYPSUM?:	%INS: 35.6	11.0	11.1
15 C-3	drill cuttings	$\text{SO}_4^{--}$ : 3.20		
3800-3900'	1 mm grains	moles/kg		
132-1	grey			
Culbertson Co	GYPSUM?:	%INS: 44.7	11.2	11.0
12 59	drill cuttings	$\text{SO}_4^{--}$ : 2.48		
3100-3200'	0.5 to 2 mm	moles/kg		
132-3	grey and white			
Culbertson Co	GYPSUM?:	%INS: 66.0	10.9	10.7
10 6	drill cuttings	$\text{SO}_4^{--}$ : 0.89		
1100-1200'	1 mm	moles/kg		
132-4	medium grey			
Reeves Co	GYPSUM?:	%INS: 47.0	11.2	9.6
32 50	drill cuttings	$\text{SO}_4^{--}$ : 2.79		
5100-5200'	0.5 to 4 mm	moles/kg		
132-6	grey and white			
Reeves Co	GYPSUM?:	%INS: 18.0	10.7	10.8
31 51	drill cuttings	$\text{SO}_4^{--}$ : 4.63		
132-8	1 mm	moles/kg		
4300-4400'	buff			

## The Guaxcama Formation

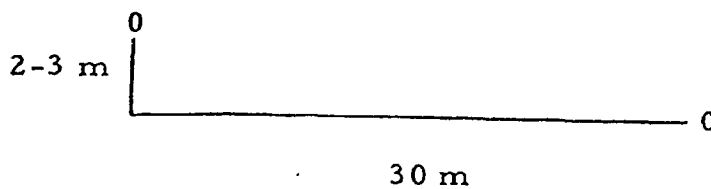
from Valles-San Luis Potosi Platform (North-Central Mexico)

obtained from John Fish, McMaster University

Age: Cretaceous (Aptian)

SAMPLE NUMBER	$\delta^{18}\text{O}$ (SMOW)	$\delta^{34}\text{S}$ (CDT)
JF1	16.1 (2)	16.6 (1)
JF2	16.3 (1)	15.8 (1)

NOTE: These are quarry samples



The Paradox Formation  
of the Paradox Basin of Colorado and Utah  
obtained from Jan Monster, McMaster University  
Age: Pennsylvanian (DesMoines Epoch)

SAMPLE	LOCATION	$\delta^{18}\text{O}$ (SMOW)	$\delta^{34}\text{S}$ (CDT)
PB1A	Sec. 22, T33N, R19W Montezuma County Colorado 6868-6872'	13.0	14.2*
PB1D	Sec. 22, T33N, R19W Montezuma County Colorado 6790-6795'	14.0	14.2*
PB1H	Sec. 22, T33N, R19W Montezuma County Colorado 7047-7052'	12.5	14.2*
PB2G	Sec. 19, T39N, R14W Montezuma County Colorado 5560-5561'	13.2	15.0*

SAMPLE	LOCATION	$\delta^{18}\text{O}$ (SMOW)	$\delta^{34}\text{S}$ (CDT)
PB2K	Sec. 19, T39N, R14W Montezuma County Colorado 5581-5582'	11.2	14.6**
PB3A	Sec. 15, T33 1/2 N, R20W Montezuma County Colorado 5958-5963'	11.8*	14.5**
PB5	No. Desert Creek No. 42-11 Utah 5429-5432'	13.4*	16.6**
	MEAN	12.7 ±1.0	14.7

\* These four oxygen isotope determinations have been normalized to correct for a systematic mass spectrometer error.

\*\* Sulphur isotope analyses performed by Jan Monster.

The Lake Énon Formation

of Nova Scotia

obtained from Paul Binney, Queen's University

Age: Mississippian

Sample	$\delta^{18}\text{O}$ (SMOW)	$\delta^{34}\text{S}$ (CDT)
EN110	15.6	15.5
EN116	15.2	15.1

The Prairie Evaporite Formation  
of Saskatchewan (from the shaft of the Sylvite Mine)  
obtained from the Sylvite Mine  
Age: Middle Devonian

	$\delta^{18}\text{O}$ (SMOW)	$\delta^{34}\text{S}$ (CDT)
SYL3	15.8	16.6

The Prairie Evaporite Formation  
of Saskatchewan

from the mined layer of Alwinsal Potash Mine, near Lanigan

Age: Middle Devonian

Note: these are not evaporites, but sulphate extracted from  
the insoluble seams that occur in the mined layer.

SAMPLE	(SO <sub>4</sub> <sup>2-</sup> ) moles/kg	δ <sup>18</sup> O (SMOW)	δ <sup>34</sup> S (CDT)
TE2	0.19	10.3 (2)	9.6 (2)
TD2	0.17	10.2 (2)	10.1
TC1	0.14	9.4 (2)	7.4



## The Shaler Group

of the Minto Arch area of Victoria Island, Canadian Arctic  
collected by Grant Young, University of Western Ontario

Age: Hadrynian

Note: all of the samples are gypsum; the mineralogy was determined  
using an X-ray diffractometer

SAMPLE	%INS	SO <sub>4</sub> <sup>--</sup> moles/kg	δ <sup>18</sup> O (SMOW)	δ <sup>34</sup> S (CDT)
KILLIAN FORMATION				
GY483	1.4	5.44	16.1	26.4
GY498	0.1	5.32	13.9	28.2
GY499	0.0	5.45	15.8	31.7
GY530	0.0	5.50	13.7	27.5
		MEAN, 1	14.9 ± 1.2	28.4 ± 2.3
MINTO INLET FORMATION				
GY220	11.3	5.22	16.2	15.2
GY227	12.1	4.83	16.2	15.4
GY229	11.3	5.30	16.0	15.2
GY235	11.3	5.34	17.6	15.3
		MEAN, 1	16.5 ± 0.7	15.3 ± 0.1
GORDON LAKE FORMATION				
GY000	87.2	0.80	14.6	15.6

## The Society Cliffs Formation

of Baffin Island

obtained from Reg Olson, University of British Columbia

Age: Helikian

SAMPLE	%INS	SO <sub>4</sub> <sup>--</sup> moles/kg	$\delta^{18}\text{O}$ (SMOW)	$\delta^{34}\text{S}$ (CDT)
SC2WG	9.4	4.95	17.3 (2)	23.7
SC2EG	10.8	4.79	18.2	23.7
SC1WG	1.4	5.56	17.7	23.2
SC1EG	1.2	4.91	17.4	23.7
OG	1.9	4.70	17.3	24.5
		MEAN, $1\sigma$	17.5 $\pm$ 0.4	23.7 $\pm$ 0.4

## CONCLUSIONS

It has been shown that in general  $\delta^{18}\text{O}(\text{SO}_4^{--})$  of evaporites is not significantly correlated with  $\delta^{34}\text{S}(\text{SO}_4^{--})$  of evaporite rocks. At the outset, it was expected that the variation of  $\delta^{18}\text{O}$  might be independent because the oxygen in sulphate is not permanently linked to the sulphur cycle. It is apparent from the present results and the published work of Mizutani and Rafter (1973) that sulphate may exchange oxygen with water during sulphate reduction. However, it is not possible to relate  $\delta^{18}\text{O}(\text{SO}_4^{--})$  variation to that of  $\delta^{18}\text{O}(\text{H}_2\text{O})$  of seawater beyond the general statement that  $\delta^{18}\text{O}(\text{SO}_4^{--})$  appears to have been roughly constant ( $\pm 2\text{‰}$ ) and this may be the limit of the variation of  $\delta^{18}\text{O}(\text{H}_2\text{O})$  of seawater back to about  $10^9$  years ago.

### Abu Dhabi Sabkha

Gypsum is precipitating in the interstices of the carbonate sediment of the upper intertidal algal marine zone of the sabkha at Abu Dhabi. The isotopic equilibrium fractionations between gypsum and dissolved sulphate are  $\Delta^{34}\text{S} = 1.5\text{‰}$  and  $\Delta^{18}\text{O} = 3.5\text{‰}$ . The fractionation for oxygen is larger than published kinetic values but is comparable to the experimental results obtained in this work. Sulphate reduction

results in increase of sulphur and oxygen  $\delta$  values in the central sabkha where gypsum and anhydrite are not accumulating. The brine in the landward regime contains dissolved sulphate with light sulphur  $\delta$  values (ca. +16‰) and as a result the sulphate minerals of the landward portion of the sabkha are acquiring a lighter  $\delta^{34}\text{S}$ . It is not clear how much of the sabkha will experience this isotopic shift, but it is evident that some portion of the sabkha will ultimately have  $\delta^{34}\text{S}$  that is 3 to 4‰ lighter than the primary values of the marine regime. It is unlikely that a landward regime could have had quantitative significance on the larger scale of ancient evaporite formation.

#### Ancient Evaporites

It has been demonstrated that  $\delta^{18}\text{O}$  of seawater sulphate has not varied over geological time within the limits of measurement on ancient evaporites, with the exception of a pronounced minimum in the Permian. This coincides in time with a minimum in  $\delta^{34}\text{S}$  of seawater sulphate.

The large range of sulphur and oxygen  $\delta$  values of the Upper Silurian rocks may be attributed to a sabkha origin for the sulphate minerals deposited away from the basin centre. There is a weak correlation between these variables with a slope such as might have been produced by bacterial reduction of sulphate. The small range of sulphur and oxygen  $\delta$  values of the Permian evaporites suggests deep water deposition. The isotopic uniformity of the Mississippian Midale Evaporite is not consistent with evidence for a sabkha origin but may be due to postdepositional

homogenization. The large range of sulphur  $\delta$  values reported for some geological periods (the "noise" on the secular curve) may be primary depositional variation.

### Future Work

It has been shown that seawater sulphate is not in isotopic equilibrium with seawater, and that a satisfactory model for  $\delta^{18}\text{O}$  of seawater sulphate has not been developed. Calculations on the flux of sulphur in the biomass indicate that photosynthetic activity may be quantitatively significant in determining  $\delta^{18}\text{O}$  of seawater sulphate. Thus an important future study must be to determine the isotopic character and quantitative importance of the sulphur flux in plants.

The isotopic measurements on the Otto Fiord Evaporite (Davies and Nassichuk, 1975) have not been described in detail sufficient to establish their significance. If it can be shown for several anhydrite beds that  $\delta^{34}\text{S}$  gradually decreases from the base to the top by 4‰, then such variation will have to be modelled and similar evaporites should be examined to test the general validity of the model.

## REFERENCES

- Alling, H. L. and L. I. Briggs, Jr., 1961. Stratigraphy of Upper Silurian Cayugan Evaporites. Am. Assoc. Petroleum Geologists Bull., V. 45, pp. 515-547.
- Anderson, R., Y. and D. W. Kirkland, 1966. Intrabasin Varve Correlation. Geol. Soc. America Bull., V. 77, pp. 241-255.
- Beards, R. J., 1967. Guide to the Subsurface Paleozoic Stratigraphy of Southern Ontario. Ontario Department of Energy and Resources Management, Paper 67-2, 19 p.
- Bennett, C. A. and N. L. Franklin, 1954. Statistical analysis in chemistry and the chemical industry. John Wiley and Sons. New York 724 p.
- Berry, W. B. N. and A. J. Boucot, 1970. Correlation of the North American Silurian rocks. Geol. Soc. Amer. Spec. Paper. No. 120, 289 p.
- Betts, R. H. and R. H. Voss, 1970. The Kinetics of Oxygen exchange between the sulphite ion and water. Can. Jour. Chem., V. 48, pp. 2035-2041.
- Blout, C. W. and F. W. Dickson, 1973. Gypsum-Anhydrite Equilibria in Systems  $\text{CaSO}_4\text{-H}_2\text{O}$  and  $\text{CaSO}_4\text{-NaCl-H}_2\text{O}$ . Amer. Miner., V. 58, pp. 323-331.

- Borchert, H. and R. O. Muir, 1964. Salt Deposits - the Origin, Metamorphism and Deformation of Evaporites. D. van Nostrand Ltd., Toronto, 339 p.
- Braitsch, O., 1971. Salt Deposits, Their Origin and Composition. Springer-Verlag, New York, 297 p.
- Branson, E. B., 1915. Origin of thick gypsum and salt deposits. Geol. Soc. Amer. Bull., V. 26, pp. 231-242.
- Briggs, L. I. Jr., 1958. Evaporite Facies. Jour. Sed. Petrology, V. 28, pp. 46-56.
- Butler, G. P., 1969. Modern evaporite deposition and geochemistry of co-existing brines, the sabkha, Trucial Coast, Arabian Gulf. Jour. Sed. Petrology, V. 39, pp. 70-81, 89 (SIC)
- \_\_\_\_\_, 1970. Recent Gypsum and Anhydrite of the Abu Dhabi sabkha, Trucial Coast: an alternative explanation of origin in Third Symposium on Salt, V. 1, J. L. Rau and L. F. Dellwig (eds.), N. Ohio Geol. Soc., Cleveland, pp. 120-152.
- \_\_\_\_\_, Krouse, R. H. and R. Mitchell, 1973. Sulphur-Isotope Geochemistry of an Arid Supratidal Environment, Trucial Coast in The Persian Gulf, B. H. Purser (ed.), pp. 453-467.
- Chase, C. G. and E. C. Perry Jr., 1972. The Oceans: Growth and Oxygen Isotope Evolution. Science V. 171, pp. 992-994.
- Clarke, F. W., 1924. The Data of Geochemistry. Fifth Ed., U. S. Geol. Surv. Bull., 770, 841 p.

- Claypool, G. E., Holser, W. T., Kaplan, I. R., Sakai, H., and I. Zak, 1972. Sulphur and Oxygen Isotope Geochemistry of Evaporite Sulphates, *Abstr. Geol. Soc. America Abstracts*, V. 4, p. 473.
- Coomer, P. G. and E. R. Olson, 1974. Conversion of Sulphides to  $\text{SO}_2$  for Sulphur Isotope Analysis Using the CuO Method. McMaster University Department of Geology Technical Memorandum No. 75-5 (unpublished report) 9p.
- Cortecci, G., 1973. Oxygen-Isotope variations in sulphate ions in the water of some Italian lakes. *Geochim. Cosmochim. Acta*, V. 37, pp. 1531-1542
- \_\_\_\_\_ and A. Longinelli, 1968. Oxygen Isotope Measurements of Sulphate Ions Separated from Diluted Solutions. *Earth Plan. Sci. Letters*, V. 4, pp. 325-327.
- Craig, H., 1961. Standard for reporting concentrations of deuterium and oxygen - 18 in natural waters. *Science*, V. 133, pp. 1833-1834.
- Dansgaard, W., 1964. Stable Isotopes in Precipitation. *Tellus*, V. 16, pp. 436-468.
- Davies, G. R. and W. W. Nassichuk, 1975. Subaqueous evaporites of the Carboniferous Otto Fiord Formation, Canadian Arctic Archipelago: A summary. *Geology*, V. 3, pp. 273-278.
- Dean, W. E., Davies, G. R., and R. Y. Anderson, 1975. Sedimentological significance of nodular and laminated anhydrite. *Geology*, V. 3, pp. 367-372.



- Dellwig, L. F., 1955. Origin of the Salina Salt of Michigan. Jour. Sed. Petr., V. 25, pp. 83-110.
- Epstein, S., Buchsbaum, R. Lowenstam, H. A. and H. C. Urey, 1953. Revised carbonate-water isotopic temperature scale. Geol. Soc. Am. Bull. V. 64, pp. 1315-1325.
- \_\_\_\_\_ and T. K. Mayeda, 1953. Variation of the  $^{18}\text{O}/^{16}\text{O}$  ratio in natural waters. Geochim. Cosmochim. Acta. V. 4, pp. 213-224.
- Evans, C. C., 1950. Underground hunting in the Silurian of southwestern Ontario. Geol. Assoc. Can., V. 3, pp. 55-85.
- Fontes, J. C., 1966. Fractionnement Isotopique dans l'Eau de Crystallisation du Sulfate de Calcium. Geol. Rundschau, V. 55, pp. 172-178.
- Fritz, P., Drimmie, R. J. and V. K. Nowicki, 1974. Preparation of sulphur dioxide for mass spectrometer analysis by combustion of sulphides with copper oxide. Anal. Chem. V. 46, pp. 164-166.
- Fuller, S. G. C. M., 1956. Mississippian Rocks and Oilfields in south eastern Saskatchewan. Saskatchewan Dept. Mineral Resources, Rpt. No. 19, 72p.
- Fuzesy, L. M., 1960. Correlation and Subcrops of the Mississippian Strata in Southeastern and Sout-Central Saskatchewan. Saskatchewan Dept. Mineral Resources, Rpt. No. 51, 63p.
- \_\_\_\_\_, 1973. Petrology and Hydrocarbon Potential of Mississippian Ratcliffe Beds in South-Central Saskatchewan. Canada. Abst. Amer. Assoc. Petrol. Geol., V. 57 p. 956.
- Gieskes, J. M., 1973. Interstitial Water Studies, Leg 15-Alkalinity, pH, Mg, Ca, Si,  $\text{PO}_4$  and  $\text{NH}_y$  in Initial Reports of the Deep Sea Drilling Project. V. 20, pp. 813-829.

- Gill, D. 1974. Cyclic Deposition of Silurian Carbonates and Evaporites in Michigan Basin: Discussion. Amer. Assoc. Petrol. Geol. Bull. V. 59, pp. 535-538.
- Goldhaber, M. B. and I. R. Kaplan, 1974. The Sulphur Cycle in The Sea, V. 5, E. D. Goldberg (ed.), pp. 569-655.
- Gonfiantini, R. and J. C. Fontes, 1963. Oxygen Isotopic Fractionation in the Water of Crystallization of Gypsum. Nature, V. 200, pp. 644-646
- Guillet, G. R., 1964. Gypsum in Ontario. Ontario Department of Mines Industrial Mineral Report No. 18, 126 p.
- Hardie, L. A., 1967. The gypsum-anhydrite equilibrium at 1 atm. pressure. Amer. Min., V. 52, pp. 121-200.
- Harrison, A. G. and H. G. Thode, 1958. Mechanism of the bacterial reduction of sulphate from isotope fractionation studies. Trans. Faraday Soc., V. 54. pp. 84-92.
- Holland, H. D., 1973. Systematics of the isotopic composition of sulphur in the oceans during the Phanerozoic and its implications for atmospheric oxygen. Geochim. Cosmochim. Acta. V. 37. pp. 2605-2616.
- Holser, W. T. and I. R. Kaplan, 1966. Isotope Geochemistry of Sedimentary Sulphates. Chem. Geol. V. 1, pp. 93-135
- Holter, M. E., 1969. The Middle Devonian Prairie Evaporite of Saskatchewan. Saskatchewan Dept. Mineral Resources, Report No. 123. 133 p.

- Hsu, K. J., 1972. Origin of saline giants: A critical review after discovery of the Mediterranean Evaporite. *Earth Science Review.*, V. 8, pp. 371-396.
- \_\_\_\_\_, Cita, M. B. and W. B. F. Ryan, 1973. The Origin of the Mediterranean Evaporites. in *Initial Reports of the Deep Sea Drilling Project. V. XIII Pt. 2*, pp. 1203-1231.
- Jacka, A. D. and L. A. Franco, 1974. Deposition and Diagenesis of Permian Evaporites and Associated Carbonates and Clastics on Shelf Areas of the Permian Basin, Fourth Symp. on Salt, N. Ohio Geol. Soc, Cleveland, Alan H. Cooper (ed.) pp. 67-87.
- Kaplan, I. R. and S. C. Rittenberg, 1964. Microbiological fractionation of Sulphur Isotopes. *Jour. Gen. Microbiol.*, V. 34, pp. 195-212.
- Kassler, P. 1973. The Structural and Geomorphic Evolution of the Persian Gulf, in *The Persian Gulf*, B. H. Purser (ed.), pp. 11-32.
- Kemp, A. L. W. and H. G. Thode, 1968. The mechanism of the bacterial reduction of sulphate and sulphite from isotope fractionation studies. *Geochim. Cosmochim. Acta*, V. 32, pp. 71-91.
- King, R. H., 1947. Sedimentation in Permian Castile Sea. *Am. Assoc. Petroleum Geologists Bull.*, V. 31, pp. 470-477.
- Kinsman, D. J. J., 1966. Gypsum and Anhydrite of Recent Age, Trucial Coast, Persian Gulf, in *Second Symposium on Salt*, V. 1, J. L. Rau (ed.). N. Ohio Geol. Soc., Cleveland, pp. 302-326.

- Kinsman, D. J. J., 1969. Modes of formation, sedimentary association, and diagnostic features of shallow-water and supratidal evaporites. Bull. Amer. Assoc. Petrol. Geol., V.53, pp. 830-840.
- \_\_\_\_\_, 1974. Calcium Sulphate Minerals of Evaporite Deposits; Their Primary Mineralogy and Diagenetic History. Fourth Symp. Salt, N. Ohio Geol. Soc., Cleveland, pp. 343-348.
- Knauth, L. P., 1973. Oxygen and Hydrogen Isotope Ratios in Chert and Related Rocks. Ph.D. Thesis, Cal. Inst., Tech., Pasadena, 379 p.
- Koblentz-Mischke, O. O., Volkovinsky, V. V. and J. G. Kabanova, 1970. Plankton Primary Production of the World Ocean. in Scientific Exploration of the South Pacific. W. S. Wooster (ed.) National Acad. Sci., Washington, D.C. 1. 183-193.
- Landes, K. K., 1945. The Salina and Bass Island rocks in the Michigan Basin Basin. U.S. Geol. Survey Oil and Gas Inv., Prelim. Map 40.
- Lawrence, J. R., 1973. Interstitial Water Studies Leg 15 - Stable Oxygen and Carbon Isotope Variations in Water Carbonates and Silicates from the Venezuela Basin (Site 149) and the Aves Ridge (148). in Initial Reports of the Deep Sea Drilling Project, V. 20 pp. 891-899.
- Lloyd, R. M., 1966. Oxygen isotope enrichment of sea water by evaporation, Geochim. Cosmochim. Acta., V. 30, pp. 801-814.
- \_\_\_\_\_, 1967. Oxygen-19 Composition of Oceanic Sulphate. Science V. 156, pp. 1228-1231.

- Lloyd, R. M., 1968. Oxygen Isotope Behaviour in the Sulphate-Water System, Jour. Geoph. Res., V. 73, p. 6099-6110.
- \_\_\_\_\_, 1973. Interstitial Water Studies, Leg 15 -  $O^{18}$  in Sulphate Ion in Initial Reports of the Deep Sea Drilling Project V. 20, pp. 887-889.
- Longinelli, A., 1968. Oxygen Isotopic Composition of Sulphate Ions in Water from Thermal Springs. Earth Plan. Sci. Letters. V. 4, pp. 206-210.
- \_\_\_\_\_, and H. Craig, 1967. Oxygen-18 Variations in Sulphate Ions in Sea Water and Saline Lakes. Science V. 156, pp. 56-59.
- \_\_\_\_\_ and G. Cortecci, 1970. Isotopic Abundance of Oxygen and Sulphur in Sulphate Ions from River Water. Earth Plan. Sci., Letters. V. 7, pp. 376-380.
- MacDonald, G. J. F., 1953. Anhydrite-gypsum equilibrium relations. Amer. Jour. Sci., V. 251, pp. 884-898.
- Matthews, R. D. and G. C. Egleson, 1974. The Origin and Implications of a Mid-Basin Potash Facies in the Salina Salt of Michigan. Fourth Symp. Salt, N. Ohio Geol. Soc., Cleveland A. H. Coogan (ed.) pp. 14-34.
- McKenzie, J. A. and K. J. Hsu, 1974. Isotope Hydrology of the Coastal sabkha of Abu Dhabi - Site of Recent Dolomitization (abstr.). Geol. Soc. Am. Abstr with Programs, V. 6. p. 864.
- Mesolella, K. J., Robinson, J. D., McCormick, I. M. and A. R. Ormiston, 1974. Cyclic Deposition of Silurian Carbonates and Evaporites in Michigan Basin. Amer. Assoc. Petrol. Geol. Bull., V. 58 pp. 34-62.

- Mizutani, Y., 1971. An improvement in the carbon-reduction method for the oxygen isotopic analysis of sulphates. *Geochem. Jour.*, V. 5, pp. 69-77.
- \_\_\_\_\_ and T. A. Rafter, 1969a. Oxygen Isotopic Composition of Sulphates - Part 3, Oxygen Isotopic Fractionation in the Bisulphate Ion-Water System. *N. Z. Jour. Sci.*, V. 12, pp. 54-59.
- \_\_\_\_\_ and \_\_\_\_\_, 1969b. Oxygen Isotopic Composition of Sulphates - Part 4, Bacterial Fractionation of Oxygen Isotopes in the Reduction of Sulphate and in the Oxidation of Sulphur. *N. Z. Jour. Sci.*, V. 12, pp 60-68.
- \_\_\_\_\_ and \_\_\_\_\_, 1973. Isotopic behaviour of sulphate oxygen in the bacterial reduction of sulphate. *Geochem. Jour.* V. 6, pp. 183-191.
- Monster, J., 1973. Preparation of SO<sub>2</sub> samples for Mass-spectrometry using Copper Oxide as an Oxydant. McMaster University Department of Chemistry, Report No. 97 (unpublished report) 26 p.
- Murray, R. C., 1964. Origin and Diagenesis of Gypsum and Anhydrite. *Jour. Sed. Petr.* V. 34, pp. 512-523.
- Nielsen, H., 1966. Schwefelisotope im Marinen Kreislauf und das <sup>34</sup>S der Früheren Meere. *Geol. Rundschau*, V. 55, pp. 160-172.
- Northrop, D. A. and R. N. Clayton, 1966. Oxygen Isotope Fractionations in Systems Containing Dolomite. *Jour. Geol.* V. 74, pp. 174-196.
- Olson, E. R., 1970. Anomalies in the Alwinal Mine Potash Layer. Bachelor's Thesis, University of Saskatchewan, 31 p.

- Olson, E. R., 1973. Manual for Graphite Reduction of Sulphate. McMaster University Department of Geology, Technical Memorandum No. 73-7, (unpublished report), 15 p.
- Patterson, R. J., 1972. Hydrology and Carbonate Diagenesis of a Coastal sabkha in the Persian Gulf. Ph.D. Thesis, Princeton University, 473 p.
- Perry, E. C. and F. C. Tan, 1972. Significance of oxygen and carbon isotope determinations in early Precambrian cherts and carbonate rocks of southern Africa. Geol. Soc. Amer. Bull., V. 83, pp. 647-664.
- Persian Gulf, 1973. Holocene Carbonate Sedimentation and Diagenesis in a Shallow Epicontinental Sea. B. H. Purser (ed.), Springer-Verlag, New York, 471 p.
- Pilot, J., Röser, H. J. and P. Müller, 1972. Zur geochemischen Entwicklung des Meerwassers und mariner Sedimente im Phanerozoikum mittels Untersuchungen von S- O- und C- Isotopen. Neue Bergbautechnik, 2Jg., H. 3, pp. 161-168.
- Posnjak, E., 1940. Deposition of calcium sulphate from seawater. Amer. Jour. Sci., V. 238, pp. 559-568.
- Purser, B. H. and G. Evans, 1973. Regional Sedimentation along the Trucial Coast, SE Persian Gulf in The Persian Gulf, B. H. Purser (ed.) pp. 211-222.
- \_\_\_\_\_ and E. Seibold, 1973. The Principal Environmental Factors Influencing Holocene Sedimentation and Diagenesis in the Persian Gulf in The Persian Gulf, B. H. Purser (ed.), pp. 1-10.

- Rafter, T. A., 1967. Oxygen Isotopic Composition of Sulphates - Part I, A method for the Extraction of Oxygen and its Quantitative Conversion to Carbon Dioxide for Isotopic Ratio Measurement. N. Z. Jour. Sci., V. 10, pp. 493-510.
- \_\_\_\_\_ and Y. Mizutani, 1967. Oxygen Isotopic Composition of Sulphates - Part 2, Preliminary Results to their Environment and to their  $\delta^{34}\text{S}$  values. N. Z. Jour. Sci. V. 10, pp. 816-840.
- Rees, C. E., 1970. The sulphur isotope balance of the ocean. An improved model. Earth Plan. Sci. Letters, V. 7, pp. 366-370.
- \_\_\_\_\_ 1973. A steady state model for sulphur isotope fractionation in bacterial reduction processes. Geochim. Cosmochim. Acta, V. 37, pp. 1141-1162.
- Richter-Bernburg, G., 1955. Über saline sedimentation. Deutsch. Geol. Gesell. Zeitschur, V. 105, pp. 593-645.
- Roliff, W. A., 1949. Salina-Guelph fields of Southwestern Ontario. Amer. Assoc. Petrol. Geol. Bull., V. 33, pp. 153-188.
- Sakai, H., 1972. Oxygen Isotope Ratios of some evaporites from Precambrian to recent ages. Earth Plan. Sci. Letters, V. 15, pp. 201-205.
- \_\_\_\_\_ and H. R. Krouse, 1971. Elimination of Memory Effects in  $^{18}\text{O}/^{16}\text{O}$  determinations in Sulphates. Earth Plan. Sci., Letters, V. 11, pp. 369-373.
- Schmalz, R. F., 1969. Deep-water evaporite deposition; a genetic model. Amer. Assoc. Petrol. Bull., V. 53, pp. 789-823.



- Schwarcz, H. P., 1974. Oxygen Isotope Fractionation between Sulphate Crystals and Liquid during Evaporation of Sea Water. (unpubl. Report) 22p.
- \_\_\_\_\_ and G. Cortecchi, 1974. Isotopic Analyses of Spring and Stream Water Sulphate from the Italian Alps and Apennines. *Chem. Geol.* V. 13, pp. 285-294.
- Seibold, E. Di ester, L., Fütterer, D., Lange, H., Muller, P. and Werner, F., 1973. Holocene Sediments and Sedimentary Processes in the Iranian Part of the Persian Gulf. in *The Persian Gulf*, B. H. Purser (ed.) pp. 57-80.
- Sloss, L. L., 1969. Evaporite deposition from layered solutions. *Amer. Assoc. Petrol. Geol. Bull.*, V. 53, pp. 776-789.
- Sofer, Z., 1975. Isotopic composition of hydration water in gypsum. Ph.D. Thesis, Feinberg graduate school, The Weizman Institute of Science, Rehovot. (not seen)
- \_\_\_\_\_ and J. R. Gat, 1972. Activities and concentrations of oxygen-18 in concentrated aqueous salt solutions: analytical and geophysical implications. *Earth Plan. Sci. Letters.* V. 15, pp. 232-238.
- \_\_\_\_\_ and \_\_\_\_\_, 1975. The Isotopic Composition of Evaporating Brines: Effect of the Isotopic Activity Ratio in Saline Solutions. *Earth Plan. Sci. Letters* V. 26, pp. 179-186.
- Solomon, M., Rafter, T. A. and K. C. Durham, 1971. Sulphur and oxygen isotope studies in the northern Pennines in relation to ore genesis. *Trans. Inst. Min. Metall.* V. 80, pp. B259-B275.
- Stewart, F. H., 1963. Marine Evaporites. Chapter Y in *Data of Geochemistry.* Sixth Ed., U. S. Geol. Survey Prof. Paper 440-Y pp. Y1-Y52.

- Strickland, J. D. H., 1966. Measuring the Production of Marine Phytoplankton. Canada Fisheries Research Board Bulletin, No. 122, 172 p.
- Thode, H. G. and J. Monster, 1965. Sulphur Isotope Geochemistry of Petroleum, Evaporites and Ancient Seas, in Fluids in Subsurface Environments, a Symposium. Am. Assoc. Petroleum Geologists Memoir No. 4., pp. 367-377.
- Teis, R. V., 1957. Isotopic Composition of oxygen in natural sulphates. Geochemistry, USSR, n. 3, pp. 257-263.
- Treesh, M. I. and G. M. Friedman, 1974. A new Interpretation of the Salina Group (Upper Silurian) of New York. Fourth Symp. Salt, N. Ohio Geol. Soc., Cleveland A. H. Coogan (ed.) pp. 35-46.
- Truesdell, A. H., 1974. Oxygen Isotope Activities and Concentrations in Aqueous Salt Solutions at Elevated Temperatures: Consequences for Isotope Geochemistry. Earth Plan. Sci. Letters, V. 23, pp. 387-396.
- Urey, H. C., 1974. The thermodynamic properties of isotopic substances. Jour. Chem. Soc., pp. 1562-1581.
- \_\_\_\_\_, Lowenstam, H. A., Epstein, S., and C. R. McKinney, 1951. Measurement of Paleotemperatures and Temperatures of the Upper Cretaceous of England, Denmark, and the Southeastern United States. Geol. Soc. Amer. Bull., V. 62, pp. 399-416.
- Usiglio, J., 1849. Analyse de l'eau de la Méditerranéan sur les côtes de France Annales de Chimie et de Physique, sér. 3, V. 27, pp. 92-107.

- van't Hoff, H. H., 1912. Untersuchungen über die Bildungsverhältnisse der ozeanischen Salzablagerungen, insbesondere des Stassfurter Salzlagers, Precht und Cohen, Leipzig, 374 p.
- Wagner, C. W. and C. van der Togt, 1973. Holocene Sediment Types and Their Distribution in the southern Persian Gulf, in The Persian Gulf, B. H. Purser (ed.) pp. 123-156.
- Wardlaw, N. C. and D. L. Christie, 1975. Sulphates of Submarine Origin in Pennsylvanian Otto Fiord Formation of Canadian Arctic. Bull. Can. Petrol. Geol., V. 23, pp. 149-171.
- Yeremenko, N. A. and R. G. Pankina, 1971. Variation of  $\delta S^{34}$  in the Sulphates of Modern and Ancient Marine Basins of the Soviet Union. Geochem. Int., V. 8. pp. 45-54.
- Zen, E-An., 1965. Solubility Measurements in the System  $CaSO_4$ -NaCl- $H_2O$  at  $35^\circ$ ,  $50^\circ$  and  $70^\circ C$  and one atmosphere Pressure. Jour. Petr., V. 6, pp. 124-164.

## APPENDIX

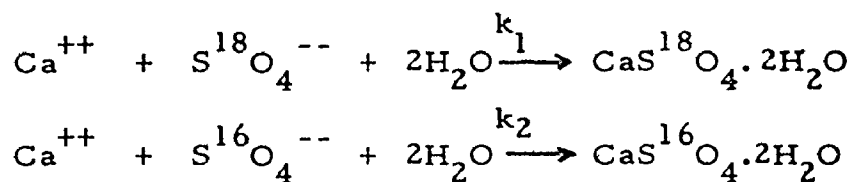
### Exchange Experiments

Experiments were carried out to determine the oxygen isotope equilibrium fractionation factor between crystalline gypsum and dissolved sulphate ( $\Delta_{c-s}$ ). Lloyd (1968) has reported a value of 2‰ for the precipitation of gypsum during the progressive evaporation of a solution of calcium sulphate in water. Schwarcz (1974) has found an initial fractionation of 2‰ between gypsum and dissolved sulphate for the precipitation of gypsum from seawater; the fractionation decreased during the course of the experiments. Lloyd (1968) has measured the isotope composition of natural mineral-brine pairs and has determined the average difference ( $\Delta_{c-s}$ ) to be 3.5‰. Schwarcz (1974) has found the same fractionations (3.5‰ average) for gypsum forming in evaporating pans. In Chapter 7 of this work, the fractionation between gypsum and interstitial brine for the intertidal regime at Abu Dhabi is shown to be about 3.5‰.

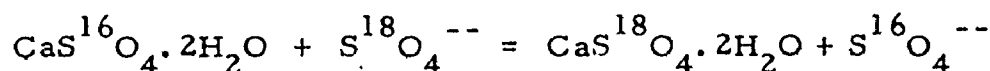
Schwarcz (1974) has suggested that in nature brines and crystal remain in contact for some time after crystal formation thus affording an opportunity for postprecipitation exchange, whereas his laboratory

experiments and those of Lloyd (1968) were designed to minimize such effects.

The experiments reported here differ from those of Lloyd (1968) and Schwarcz (1974) in that there is no net precipitation but rather the balanced exchange of sulphate anions between the crystal phase and the solution (see Equation 9-1 and 9-2).



$$a = k_1/k_2 \quad 9-1$$



$$a = \frac{\text{CaS}^{18}\text{O}_4 \cdot 2\text{H}_2\text{O}}{\text{CaS}^{16}\text{O}_4 \cdot 2\text{H}_2\text{O}} \bigg/ \frac{\text{S}^{18}\text{O}_4^{--}}{\text{S}^{16}\text{O}_4^{--}} \quad 9-2$$

The present experiments were designed to be in chemical equilibrium throughout, and to be suitable for analysis according to the partial exchange method of Northrop and Clayton (1966). Saturated solutions of calcium sulphate either isotopically enriched or depleted with respect to  $^{18}\text{O}$  were prepared. Sized crystalline gypsum of normal isotopic composition was added to the solutions which were then sealed with a layer of light oil to prevent evaporation. The glass reaction flasks were maintained at  $25^\circ\text{C}$  in a waterbath. After 25 days an aliquot of the

solution plus solid was extracted. The remaining mixture was permitted to exchange for an additional 172 days. The isotopic composition of the separated phases and the fractionations are presented in Table 9-1, and plotted on Figure 9-1.

A graph of initial fractionation versus initial minus final fractionation for isochemical experiments should intersect the initial fractionation axis at the equilibrium fractionation (Northrop and Clayton, 1966). Figures 9-2, 9-3, 9-4 and 9-5 are such plots for 0.000 mNaCl and 2.024 mNaCl solutions. They indicate that  $\Delta_{c-s} = 1.7 \pm 0.55\%$  and  $3.7 \pm 0.25\%$  respectively for the exchange in the last 172 days, and  $\Delta_{c-s} = 5.4 \pm 0.25\%$  and  $2.6 \pm 0.25\%$  for the exchange in the first 25 days. The average of the four fractionations is  $3.35\%$ .

Some details of the experiments suggest that the 2.024 mNaCl solutions should provide a better estimate of  $\Delta_{c-s}$ . The attempt to control the grain size and grain size distribution of the gypsum resulted in non-equilibrium at the beginning of the experiments. The sized gypsum had been dried in acetone; in the 0.000 mNaCl solutions (Experiments 30 and 31) the gypsum soon recrystallized into a continuous sheet of selenite on the bottom of the reaction flasks. This may have been due in part to the too fine grain size (-200, +270 mesh) but was probably also a result of the acetone drying (J. R. Kramer, personal communication). The selenite was subsequently broken up using the teflon coated magnets that were already in the flasks, but the resulting

Table 9-1. Isotopic Data on Saturated Solutions of Calcium Sulphate

			←-----0-----*	-----25d-----*	-----200d-----*			
	mNaCl	*	$\delta XL_o$	$\delta SOLN_o$	$\delta XL_i$	$\delta SOLN_i$	$\delta XL_f$	$\delta SOLN_f$
30	0.000	1.9 (1.5)	13.97	-8.31	4.85	-3.15	3.41	-2.51
31	0.000	1.9 (1.8)	13.97	41.17	30.41	30.34	30.21	29.57
32	2.024	1.9 (1.3)	13.97	-8.06	3.22	-1.49	2.44	-1.26
33	2.024	1.9 (1.5)	13.97	41.13	30.16	30.99	32.29	30.05

$$* \frac{\text{moles } [SO_4] \text{ solution}}{\text{moles } [SO_4] \text{ crystal}}$$

parentheses = after 25 d

(ALL AT 25°C IN WATERBATH)

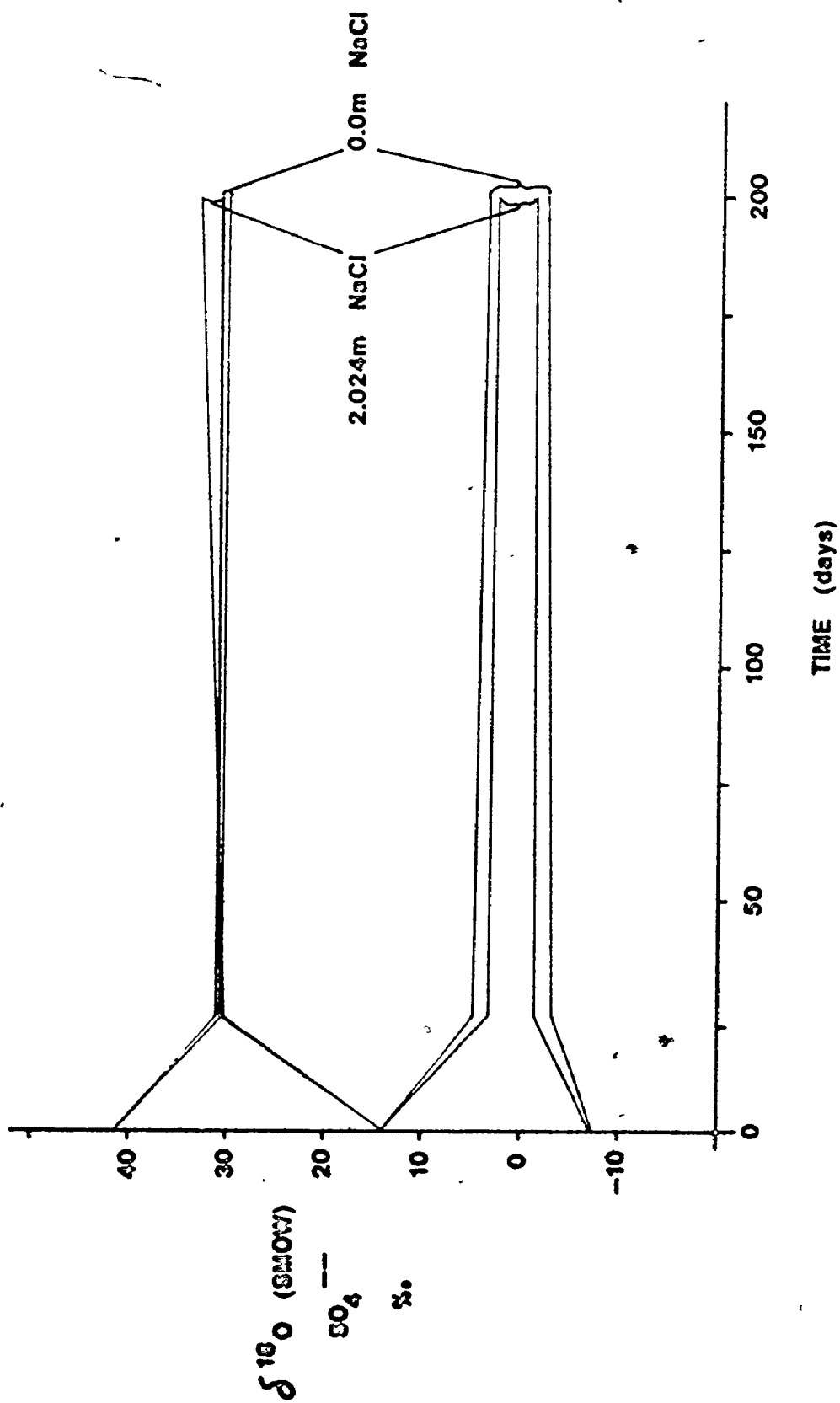
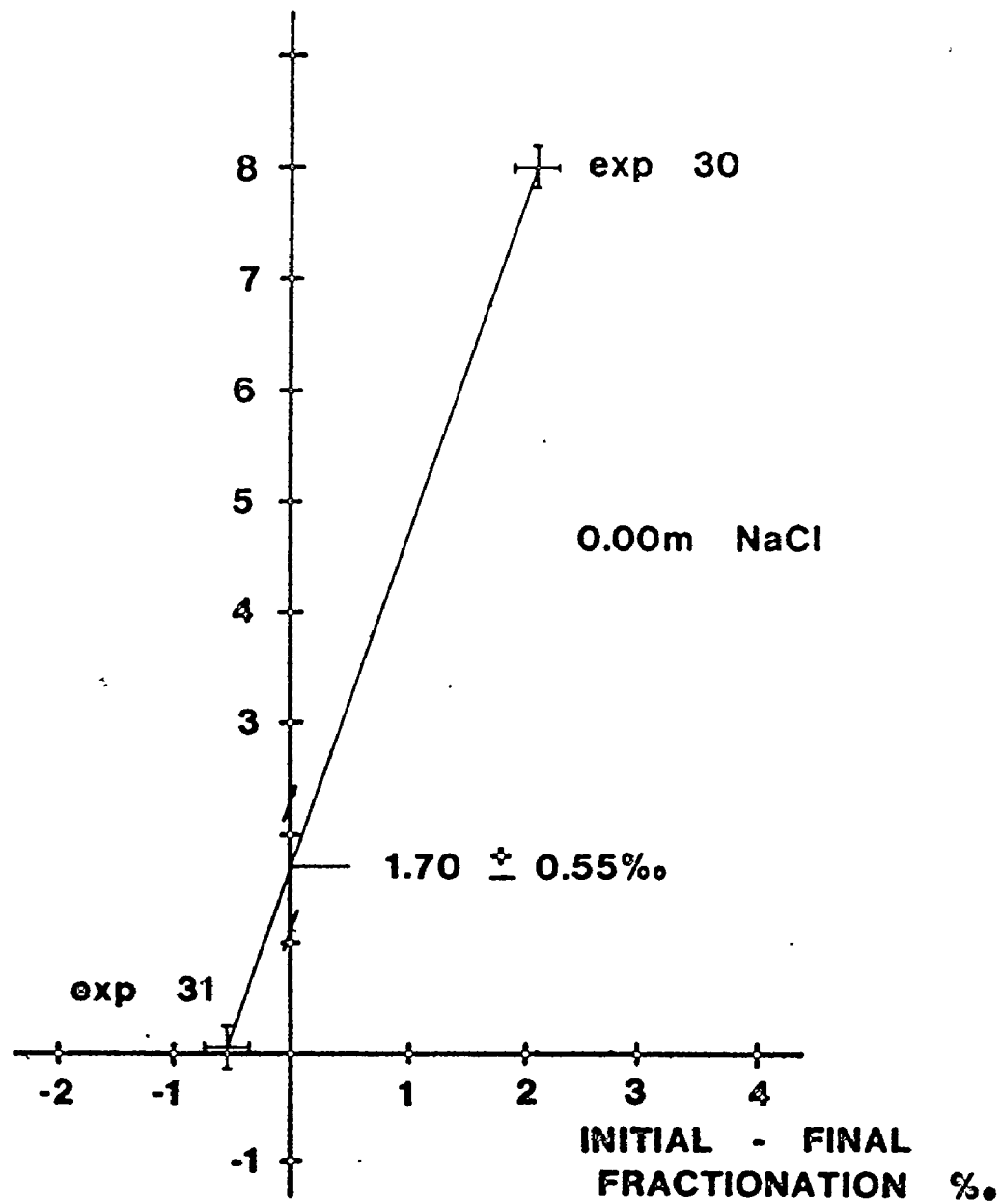


Figure 9-1: Oxygen Del Values versus time Exchange Experiments



INITIAL FRACTIONATION ‰



estimated analytical error

Figure 9-2: Northrop/Clayton Plot for Experiments 30 and 31, last 172 days (Initial fractionation =  $\Delta_i$ ; Initial Final fractionation =  $(\alpha_f - 1)10^3$ )

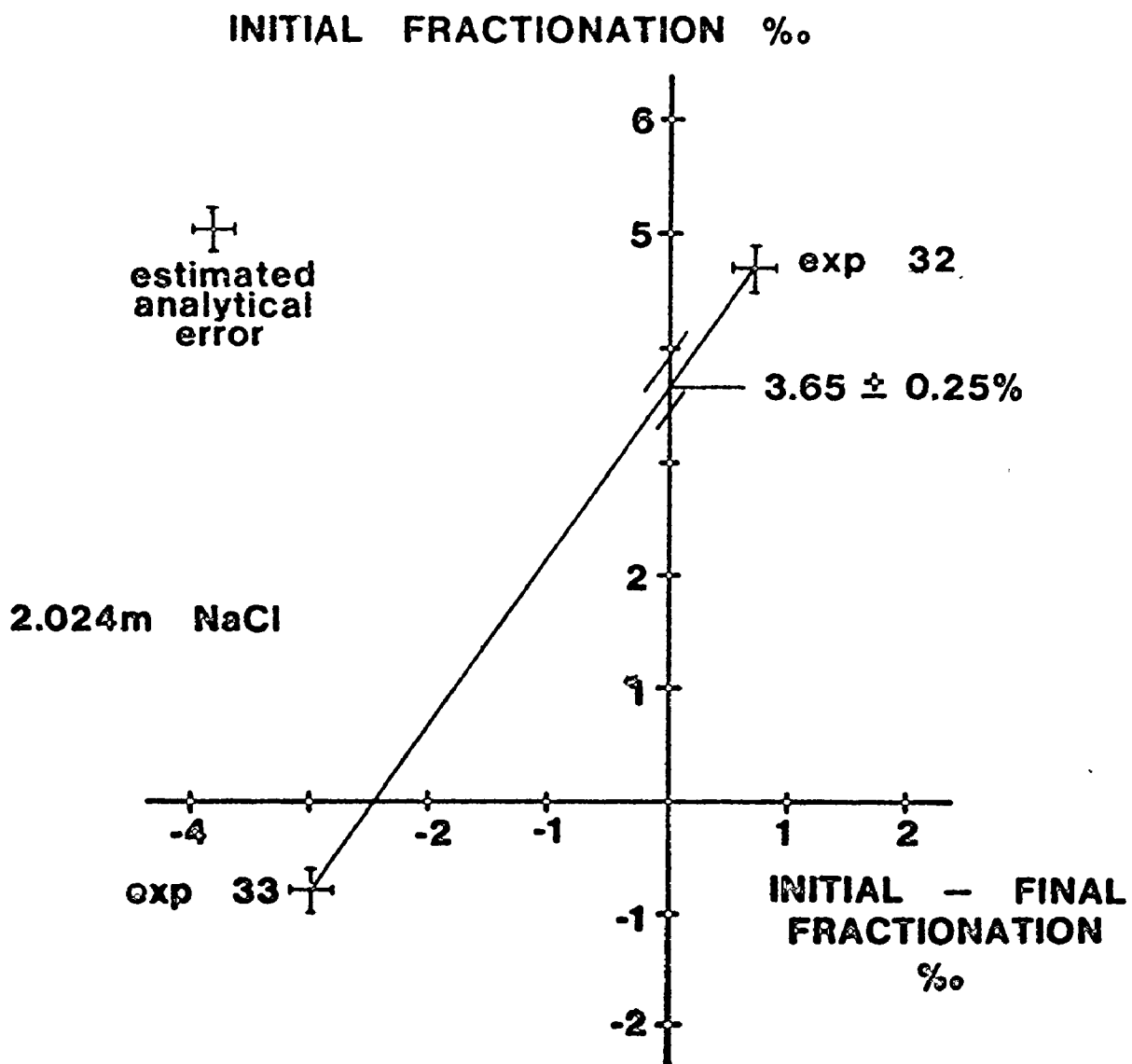


Figure 9-3: Northrop/Clayton Plot for Experiments 32 and 33, last 172 days (Initial fractionation =  $\Delta_i$ ; Initial Final fractionation =  $(\alpha_f - 1)10^3$ )

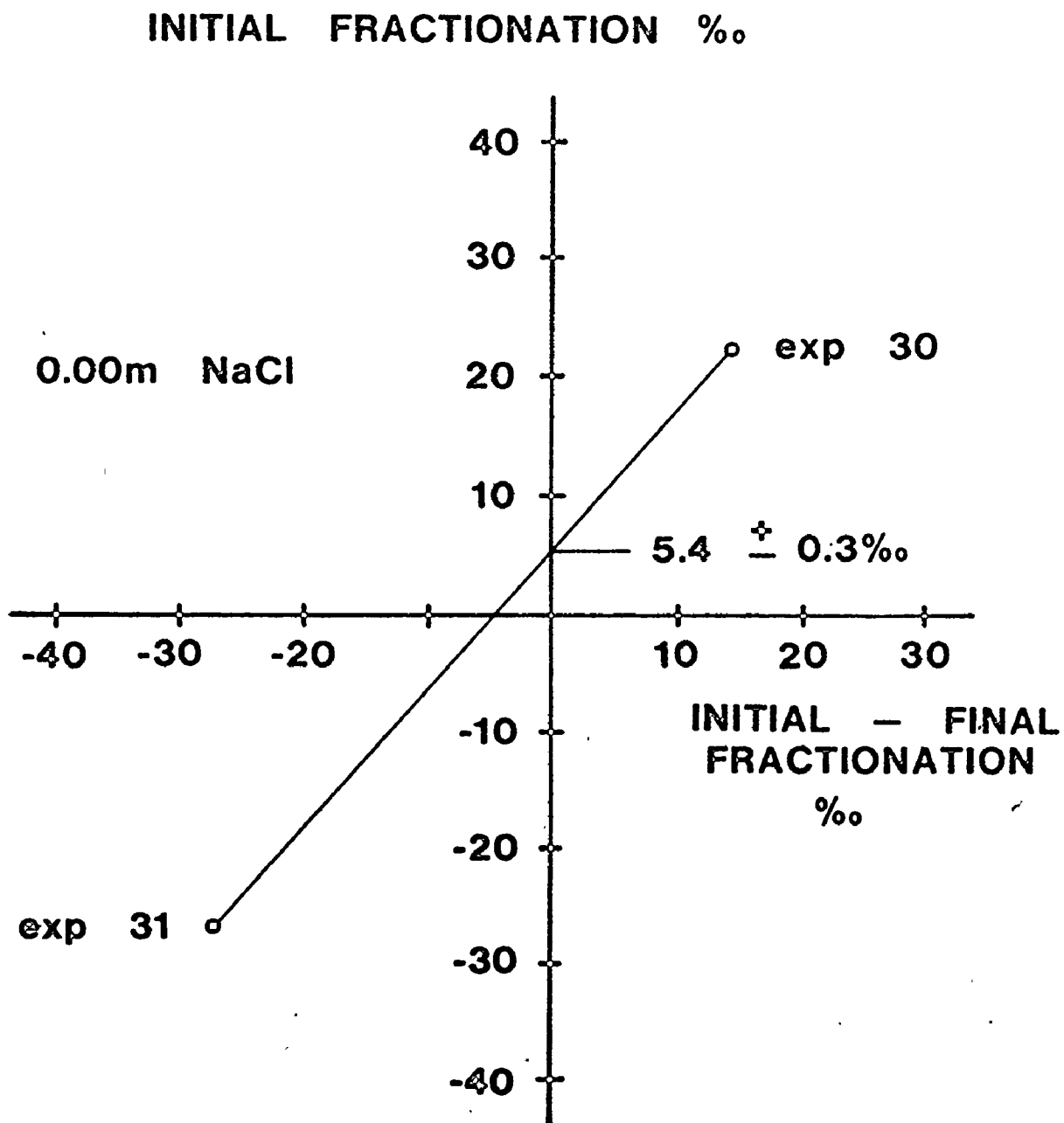


Figure 9-4: Northrop/Clayton Plot for Experiments 30 and 31, first 25 days (Initial fractionation  $\Delta_i$ ; Initial Final fractionation =  $(a_f - 1)10^3$ )

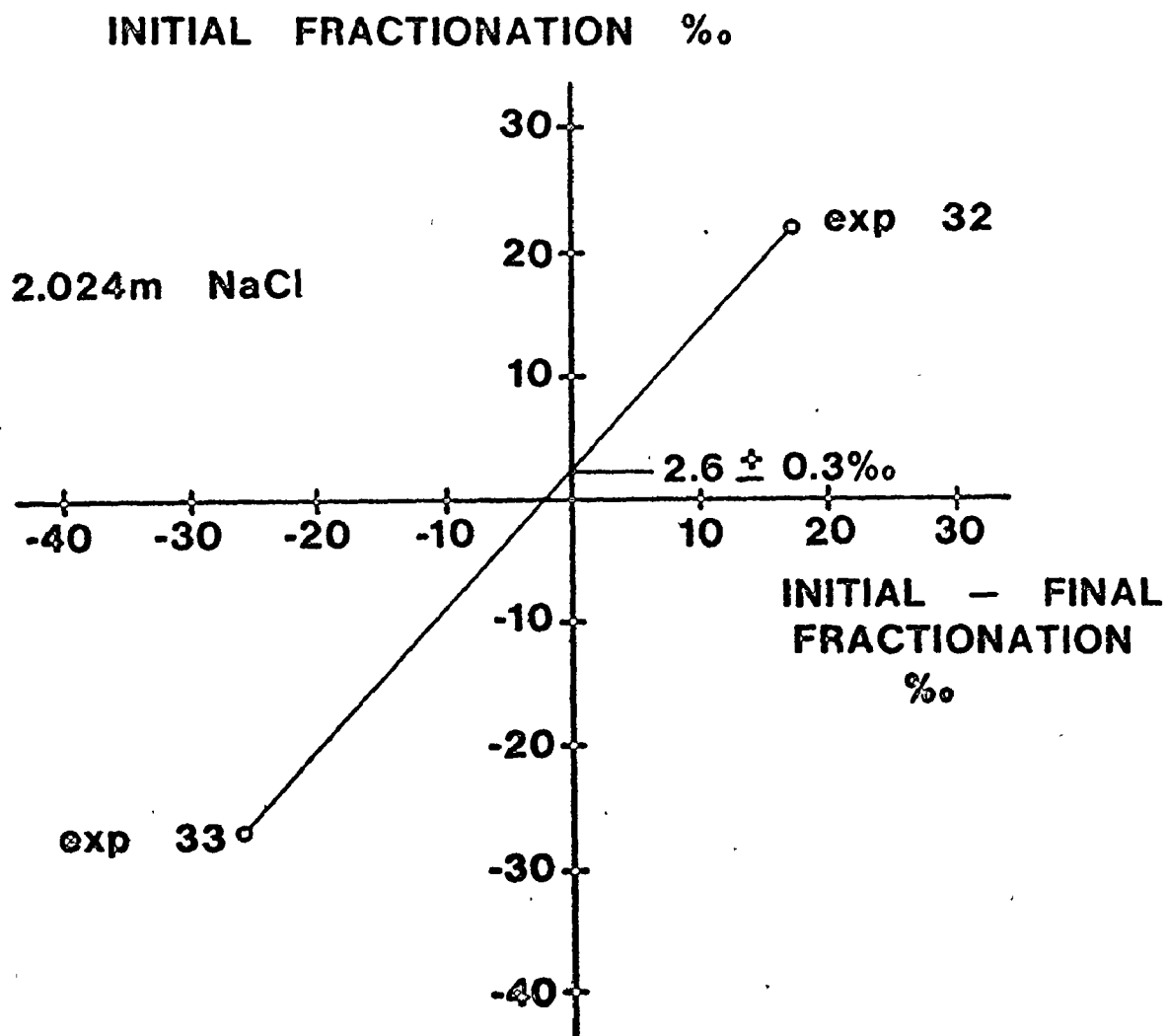


Figure 9-5: Northrop/Clayton Plot for Experiments 32 and 33, first 25 days (Initial fractionation -  $\Delta_i$ ; Initial Final Fractionation =  $(\alpha_f - 1)10^3$ )

grain size was much coarser and less well sorted than the starting gypsum. Both the recrystallization and the breaking up of the gypsum occurred in the first week of the experiments, so that equilibrium should have been established well within the first 25 days. It is apparent from Figures 9-4 and 9-5 that the first isotopic shifts may be interpreted as approaching equilibrium. Gross recrystallization was not observed in the 2.024 mNaCl solutions (Experiments 32 and 33); presumably it was inhibited by the high salinity. For this reason, the data from the more saline experiments are preferred; they indicate  $\Delta_{c-s} = 3.2\text{‰}$ .

The problem described above could be avoided in future experiments by adding the crystalline gypsum in a wet slurry. Although the mixing of the slurry solution and the bulk of the brine would have to be accounted for, the initial chemical disequilibrium would be circumvented.

The paucity of data produced here is regrettable; it does not reflect the effort made, but it is consistent with the experimental intractability of gypsum (see Chapter 6). The preceding twenty-nine experiments did not provide consistent estimates of the equilibrium fractionation; problems with the starting materials were indicated.

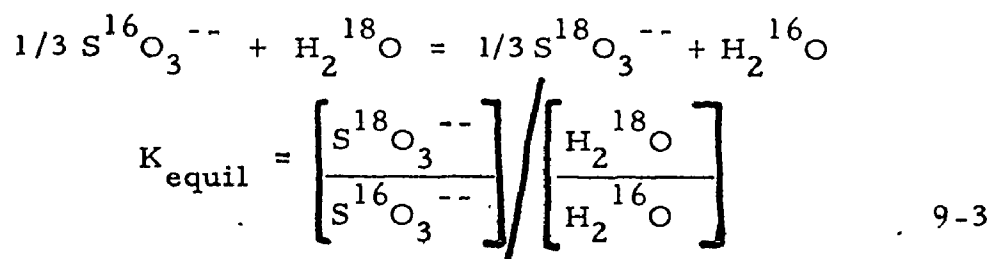
The present experiments have yielded an equilibrium fractionation ( $\Delta_{c-s} \approx 3.2\text{‰}$ ) that is significantly greater than the kinetic fractionation determined by Lloyd (1968) and by Schwarcz (1974). The excellent agreement of the present experimental result with data for natural systems suggests that, as Schwarcz (1974) proposed, the larger  $\Delta_{c-s}$

values in natural brine pans may be accounted for by postcrystallization equilibration.

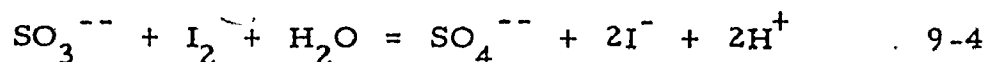
### Labelled Gypsum

Gypsum enriched in  $^{18}\text{O}$  was prepared in the following way. Sulphite was dissolved in water enriched in  $^{18}\text{O}$ , during which it exchanged oxygen isotopes with water (Betts and Voss, 1970). The sulphite was then oxidized to sulphate using a solution of iodine and potassium iodide. Calcium chloride was added to the solution and gypsum precipitated. Gypsum depleted in  $^{18}\text{O}$  was prepared in an analogous manner with isotopically light water. A graph of  $\delta^{18}\text{O}$ -GYPSUM versus  $\delta^{18}\text{O}$ -WATER is presented in Figure 9-6; a good linear fit to a slope of almost unity is apparent.

The sulphate produced has an oxygen del value that is governed by two steps, both involving the oxygen in water. The first step is equilibrium isotope exchange between sulphite and water.



The second step is the oxidation of sulphite by iodine; water oxygen is incorporated into the sulphate.



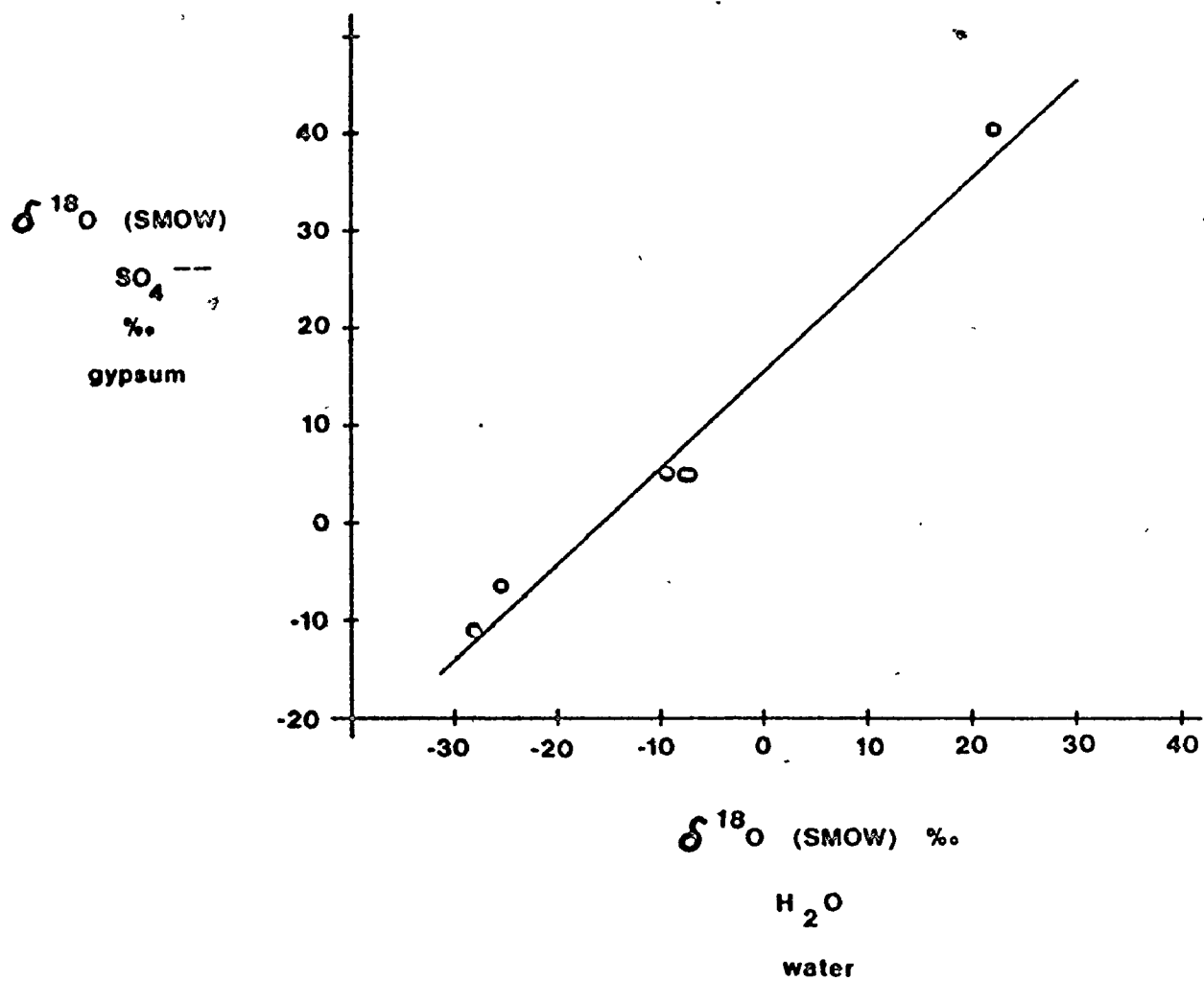


Figure 9-6: Oxygen-Labelled Sulphate from Sulphite Exchange with Oxygen-Labelled Water, at 25°C

Table 9-2:  $^{18}\text{O}$ -Labelled Gypsum via Sulphide/Water Exchange

EXP	NOTES	$\delta^{18}\text{O-H}_2\text{O}$	$\delta^{18}\text{O-SO}_4$
TWS		- 7.20(1)	11.14(3)
TWS2	boiled	- 7.20(1)✓	4.87(2)
NWS		- 9.23(2)✓	4.89(2)
NWS3	$\text{N}_2$ bubbling (2 hrs.)	- 9.23(2)	3.36(1)
MDWIA	bubbled $\text{N}_2$   LOW YIELDS	- 7.34(2)	4.89(2)
MDWIB		- 7.34(2)	5.25(1)
MDWIIA		- 7.34(2)✓	4.85(1)
MDWIIB	0°C	- 7.34(2)	7.25(1)
LIG	bubbled $\text{N}_2$   LOW YIELD	-28.08(2)	-14.36(1)
LIIG	bubbled $\text{N}_2$ successive supernatants were -8.0, -8.7, -8.7	-28.08(2)✓	-11.05(2)
HIG		22.07(1)✓	39.95(3)
LIIG	bubbled $\text{N}_2$	-25.45(1)✓	- 6.47(3)

✓ = used for figure

others rejected for low yields or not at 25°C



The simplest interpretation of the straight line shown in Figure 9-6 is that the equilibrium fractionation between sulphite and water is 1.020 (Equation 9-3), and that on the oxidation to sulphate step, water oxygen is incorporated without fractionation. If there is a fractionation on the second step, then neither it nor the equilibrium fractionation between sulphite and water can be estimated from the data here.

The oxidation of sulphite by the strong oxydant iodine may not be comparable to oxidation in natural systems, and the results here shown may not be applied to natural systems without considerable further research. They do emphasize the probable importance of intermediate sulphite in determining the oxygen isotope composition of sulphate.

2